Application of Plasma Phenomena

Po-Yu Chang

Institute of Space and Plasma Sciences, National Cheng Kung University

Lecture 9

2025 fall semester

Thursday 9:00-12:00

Materials:

https://capst.ncku.edu.tw/PGS/index.php/teaching/

Online courses:

https://reurl.cc/ZlG6k6

2025/11/26 updated

Diagnostics

- Single/double Langmuir probe – n_e, T_e
- Interferometer – n_e
- Schlieren – dn_e/dx
- Faraday rotator – B
- Bdot probe – B
- Charged particle – B
- Spectroscopy – T_e, n_e
- Thomson scattering – T_e, n_e, T_i, n_i
- Faraday cup – dn_i/dt
- Retarding Potential Analyzer - v_i
- Intensified CCD – 2D image
- Framing camera – 2D image
- Streak camera – 1D image
- VISAR – shock velocity
- Neutron time of flight (NToF)
  - Neutron yield, T_i
- Thomson parabola – e/m
- Data analysis using Pulse Shaping
- Stimulated Brillouin scattering
  - Laser pulse compression

Electromagnetic wave can be used to measure the density or the magnetic field in the plasma

- **Nonmagnetized isotropic plasma (interferometer needed):**

$$n^2 = 1 - \frac{X\left(1-X\right)}{1-X-\frac{1}{2}Y^2\sin^2\theta \pm \left[\left(\frac{1}{2}Y^2\sin^2\theta\right)^2 + \left(1-X\right)^2 Y^2\cos^2\theta\right]^{1/2}}$$

$$= 1 - X = 1 - \frac{\omega_{\mathrm{p}}^2}{\omega^2} = 1 - \frac{n_{\mathrm{e}}}{n_{\mathrm{cr}}} \qquad \left(\boldsymbol{Y \equiv \frac{\Omega}{\omega} \equiv 0}\right)$$

Note: $\omega_{\mathrm{p}}^2 = \dfrac{n_{\mathrm{e}}e^2}{\epsilon_0 m_{\mathrm{e}}}$ $\quad n_{\mathrm{cr}} = \dfrac{\epsilon_0 m_{\mathrm{e}}\omega^2}{e^2}$

- **Magnetized isotropic plasma (Polarization detected needed):**

Parallel to B_0

$$n^2 = 1 - \frac{\omega_{\mathrm{p}}^2}{\omega\left(\omega \pm \Omega\right)} \qquad \frac{E_{\mathrm{x}}}{E_{\mathrm{y}}} = \pm i \qquad \Omega \equiv \frac{eB_0}{m_{\mathrm{e}}}$$

Faraday rotation: linear polarization rotation caused by the difference between the speed of LHC and RHC polarized wave.

Electromagnetic wave can be used to measure the density or the magnetic field in the plasma

- **Nonmagnetized isotropic plasma (interferometer needed):**

$$n^2 = 1 - \frac{X(1-X)}{1 - X - \frac{1}{2}Y^2\sin^2\theta \pm \left[\left(\frac{1}{2}Y^2\sin^2\theta\right)^2 + (1-X)^2 Y^2\cos^2\theta\right]^{1/2}}$$

$$= 1 - X = 1 - \frac{\omega_p^2}{\omega^2} = 1 - \frac{n_e}{n_{cr}} \qquad \left(\boldsymbol{Y \equiv \frac{\Omega}{\omega} \equiv 0}\right)$$

Note: $\omega_p^2 = \frac{n_e e^2}{\epsilon_0 m_e}$ $n_{cr} = \frac{\epsilon_0 m_e \omega^2}{e^2}$

- **Magnetized isotropic plasma (Polarization detected needed):**

Parallel to B_0

$$n^2 = 1 - \frac{\omega_p^2}{\omega(\omega \pm \Omega)} \qquad \frac{E_x}{E_y} = \pm i \qquad \Omega \equiv \frac{eB_0}{m_e}$$

Faraday rotation: linear polarization rotation caused by the difference between the speed of LHC and RHC polarized wave.

There are two main style of interferometer

Michelson interferometer

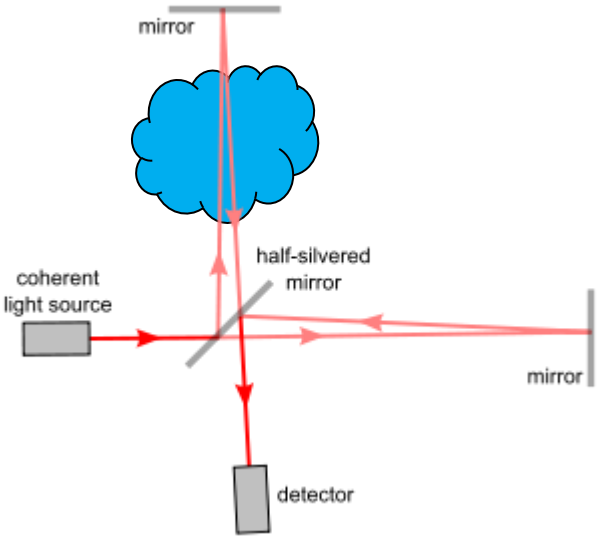

Mach-zehnder interferometer

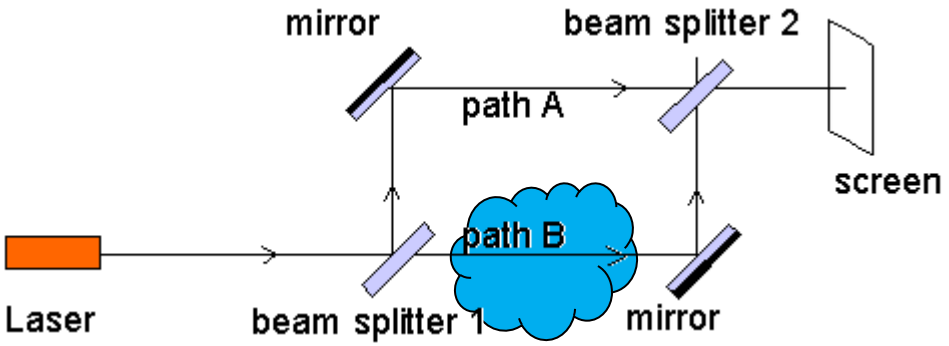

Interference pattern are due to the phase difference between two different path

$$E_1 = E_1 \exp(-i\omega t)$$

$$E_2 = E_2 \exp(-i\omega t + i\phi)$$

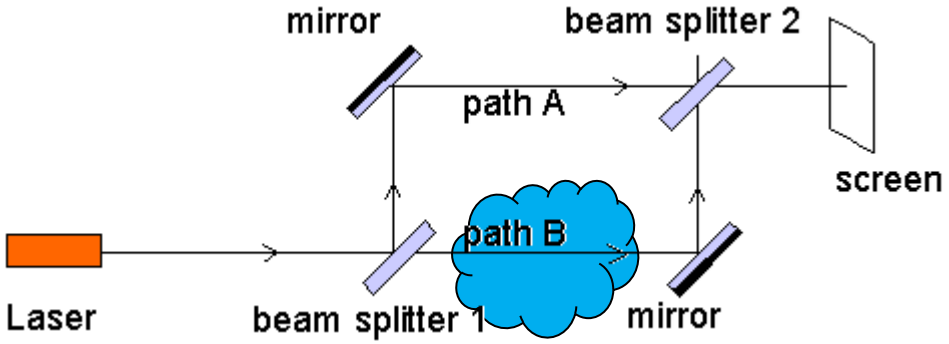

$$E = E_1 + E_2 = [E_1 + E_2 \exp(i\phi)] \exp(-i\omega t)$$

$$\begin{aligned} I &= |E|^2 = E^* E = [E_1 + E_2 \exp(-i\phi)] \exp(i\omega t) [E_1 + E_2 \exp(i\phi)] \exp(-i\omega t) \\ &= E_1^2 + E_2^2 + E_1 E_2 \exp(i\phi) + E_1 E_2 \exp(-i\phi) \\ &= E_1^2 + E_2^2 + 2E_1 E_2 \cos\phi \\ &= (E_1^2 + E_2^2)\left(1 + \frac{2E_1 E_2}{E_1^2 + E_2^2} \cos\phi\right) \end{aligned}$$

The intensity on screen depends on the phase different between two paths

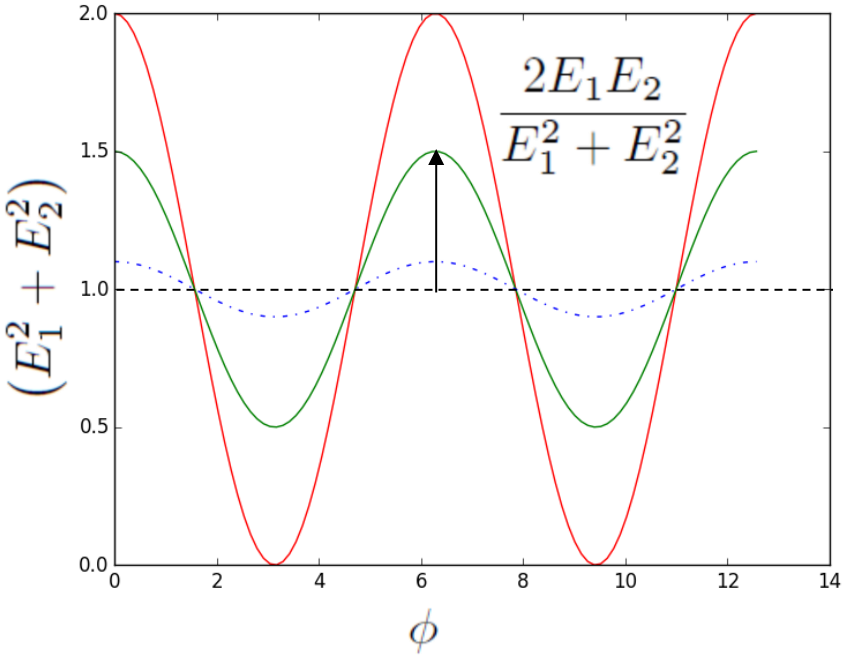

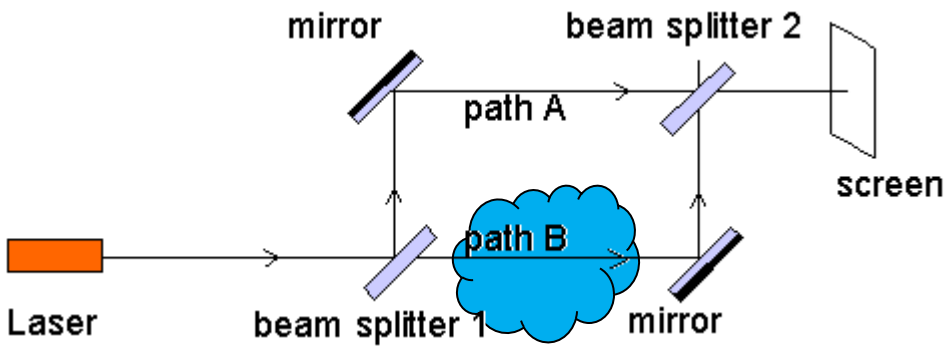

$$I = (E_1^2+E_2^2)\left(1+\frac{2E_1E_2}{E_1^2+E_2^2}\cos\phi\right)$$

The phase different depends on the line integral of the electron density along the path

$$\phi = \int k dl = \int n \frac{\omega}{c} dl$$

$$n^2 = 1 - \frac{n_e}{n_{cr}} \qquad n_{cr} = \frac{\epsilon_0 m_e \omega^2}{e^2}$$

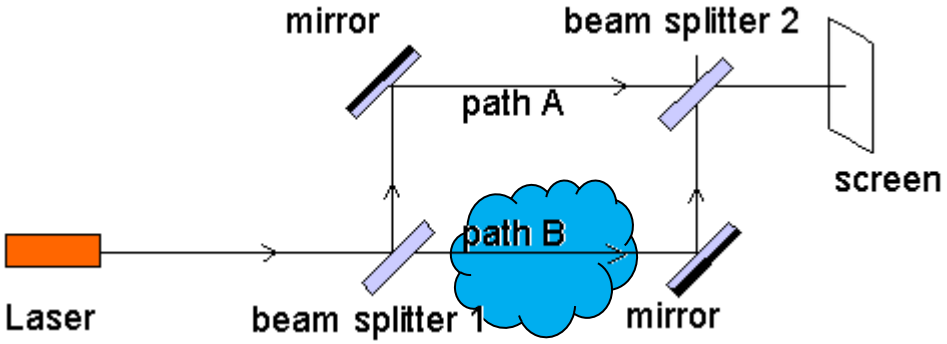

$$\begin{aligned}
\Delta\phi &= \int (k_{\text{plasma}} - k_0)\, dl = \frac{\omega}{c} \int (n-1)\, dl \\
&= \frac{\omega}{c} \int \left(\sqrt{1 - \frac{n_e}{n_c}} - 1 \right) dl \approx \frac{\omega}{c} \int \left(1 - \frac{1}{2}\frac{n_e}{n_c} - 1 \right) dl \\
&= -\frac{\omega}{2cn_c} \int n_e dl
\end{aligned}$$

Note that $n_e << n_{cr}$ **is assumed,** $\sqrt{1 - \frac{n_e}{n_{cr}}} \approx 1 - \frac{1}{2}\frac{n_e}{n_{cr}}$

The phase is determined by comparing to the pattern without the phase shift

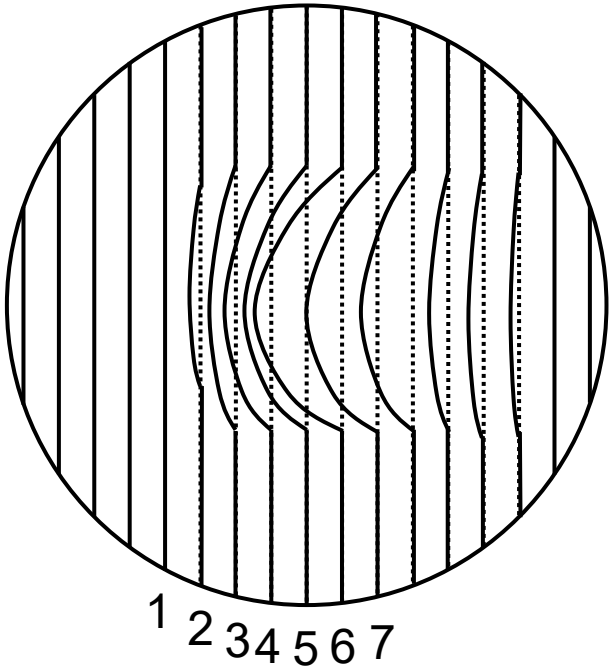

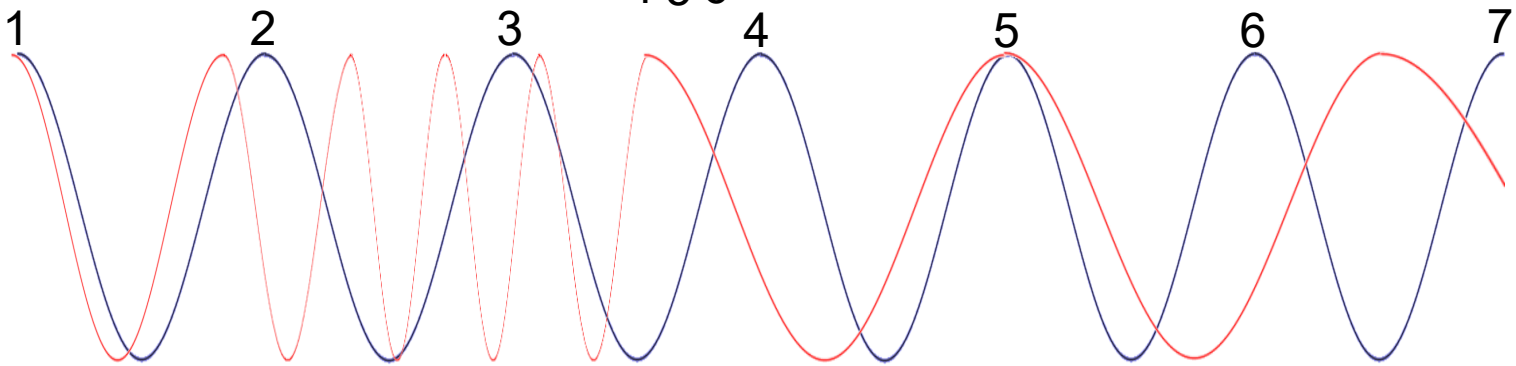

Fourier transform can be used to retrieve the data from the interferometer image

$$\mathbf{I}(x,y) = I_0(x,y) + m(x,y)\cos[2\pi\nu_0 x + \phi(x,y)] \qquad \cos(x) = \frac{e^{ix} + e^{-ix}}{2}$$

$$= I_0(x,y) + \frac{1}{2}m(x,y)\left(e^{i[2\pi\nu_0 x+\phi(x,y)]} + e^{-i[2\pi\nu_0 x+\phi(x,y)]}\right)$$

$$= I_0(x,y) + \frac{1}{2}m(x,y)e^{i\phi(x,y)}e^{i2\pi\nu_0 x} + \frac{1}{2}m(x,y)e^{-i\phi(x,y)}e^{-i2\pi\nu_0 x}$$

$$= I_0(x,y) + c(x,y)e^{i2\pi\nu_0 x} + c^*(x,y)e^{-i2\pi\nu_0 x}$$

$$c(x,y) \equiv \frac{1}{2}m(x,y)e^{i\phi(x,y)} \qquad \phi(x,y) = \tan^{-1}\left(\frac{\mathrm{Im}[c(x,y)]}{\mathrm{Re}[c(x,y)]}\right)$$

$$\hat{g}(f_x, y) \equiv \mathrm{FT}[g(x,y)]$$

$$\hat{g}(f_x - \nu_0, y) = \mathrm{FT}\left[g(x,y)e^{i2\pi\nu_0 x}\right]$$

$$\hat{I}(f_x, y) = \hat{I}_0(f_x, y) + \hat{c}(f_x - \nu_0, y) + \hat{c}^*(f_x + \nu_0, y)$$

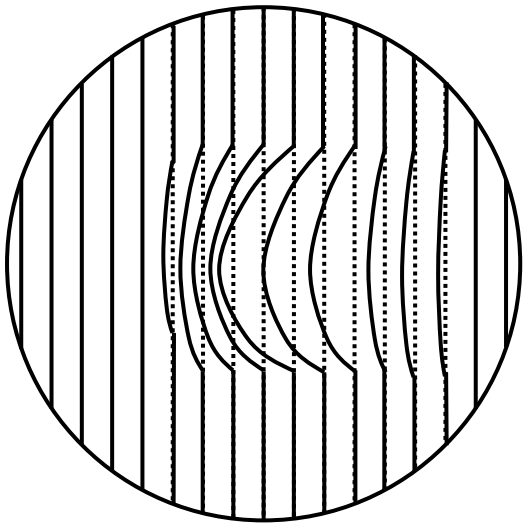

M. Hipp etc., *Measurement* **36** (2004), 53.

Basic knowledge of Fourier transform

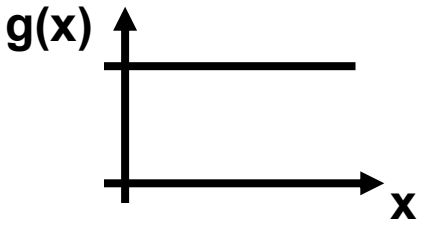

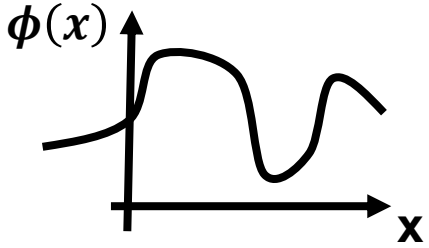

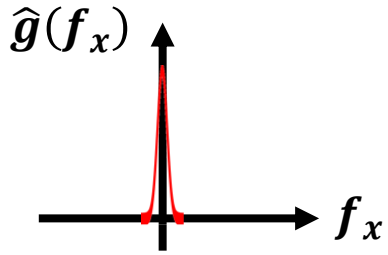

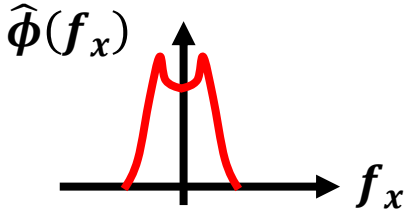

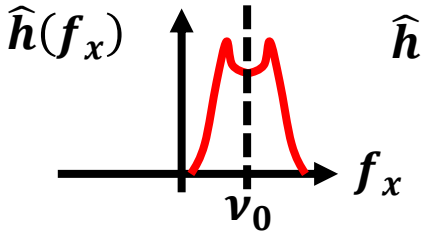

$$\mathbf{h}(x) = \phi(x) \times e^{\mathrm{i}2\pi\nu_0 x}$$

$$\hat{h}(f_x) = \mathrm{FT}\left[\phi(x)e^{\mathrm{i}2\pi\nu_0 x}\right] = \hat{\phi}(f_x - \nu_0)$$

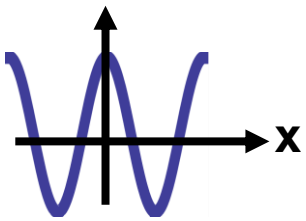

$$\mathbf{g}(x) = cos(2\pi\nu_0 x) = \frac{e^{\mathrm{i}2\pi\nu_0 x} + e^{-\mathrm{i}2\pi\nu_0 x}}{2}$$

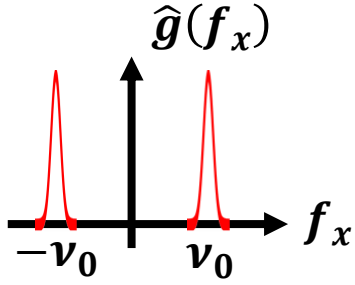

Procedure of retrieving data

$$I(x) = I_0(x) + m(x)\cos[2\pi\nu_0 x + \phi(x)] = I_0(x) + c(x)e^{i2\pi\nu_0 x} + c^*(x)e^{-i2\pi\nu_0 x}$$

$$\hat{I}(f_x) = \hat{I}_0(f_x) + \hat{c}(f_x - \nu_0) + \hat{c}^*(f_x + \nu_0)$$

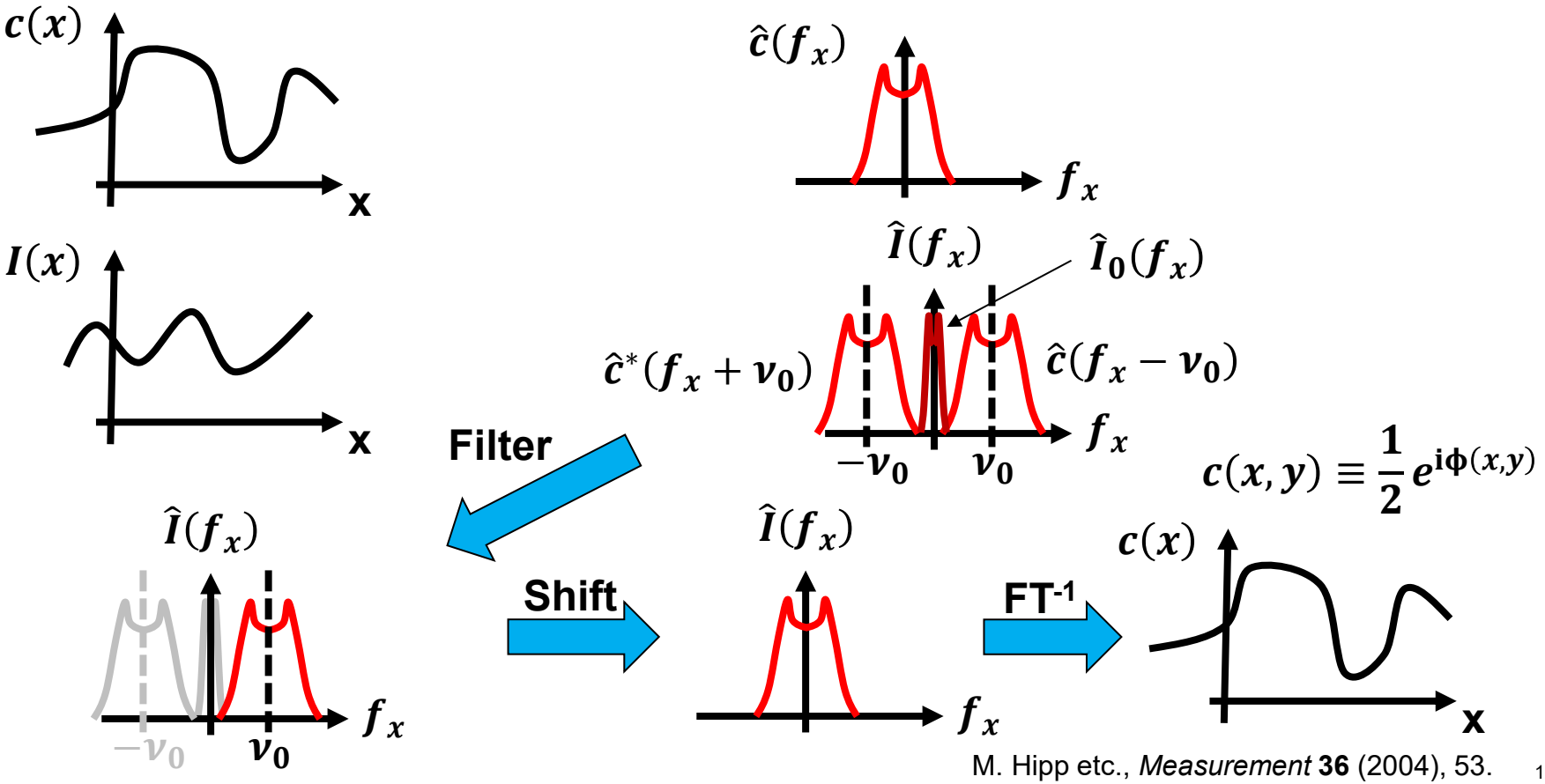

M. Hipp etc., *Measurement* **36** (2004), 53.

Example of retrieving data from 1D interferometer

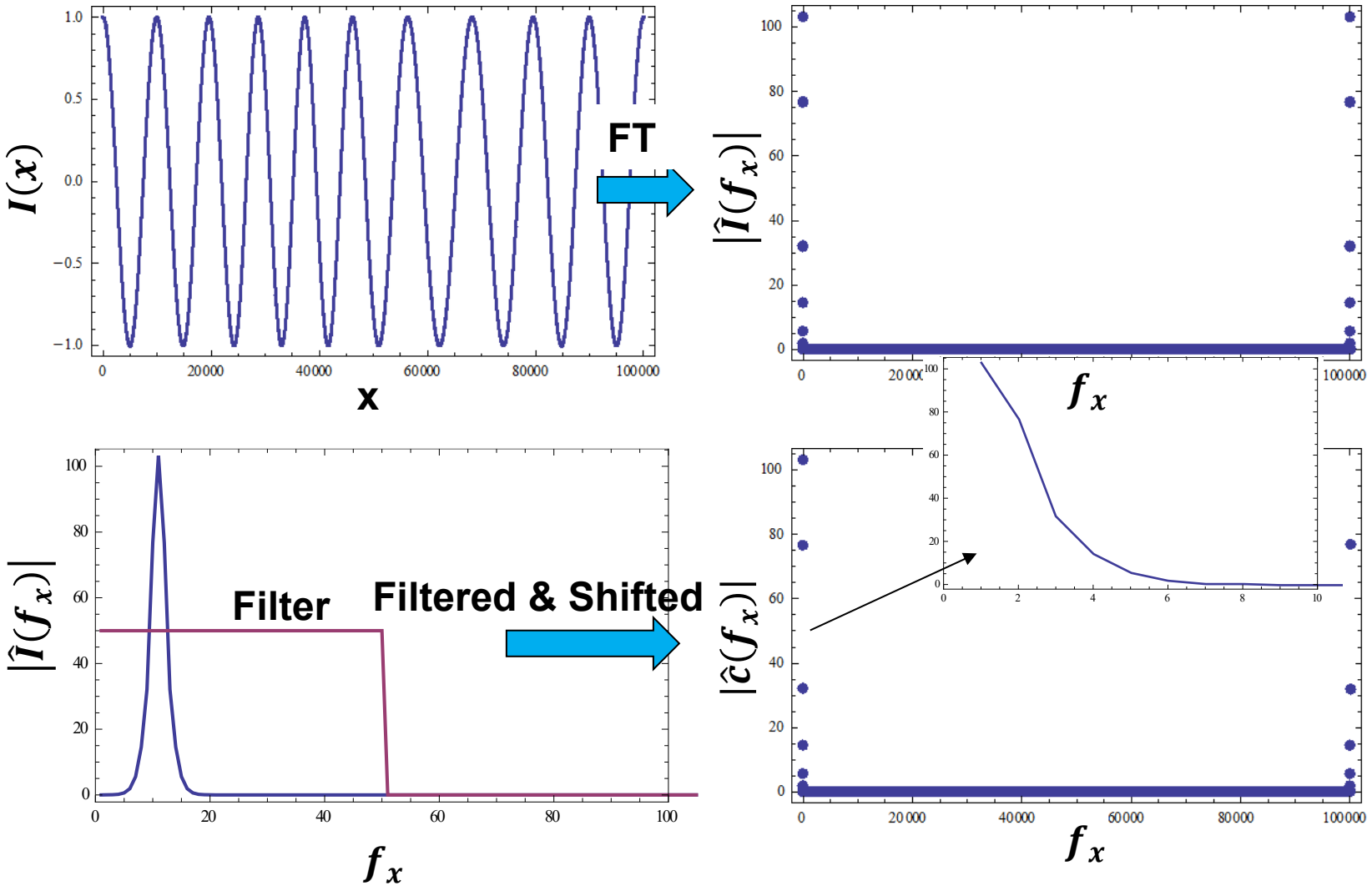

The retrieved data need to be modified if the phase change is too much

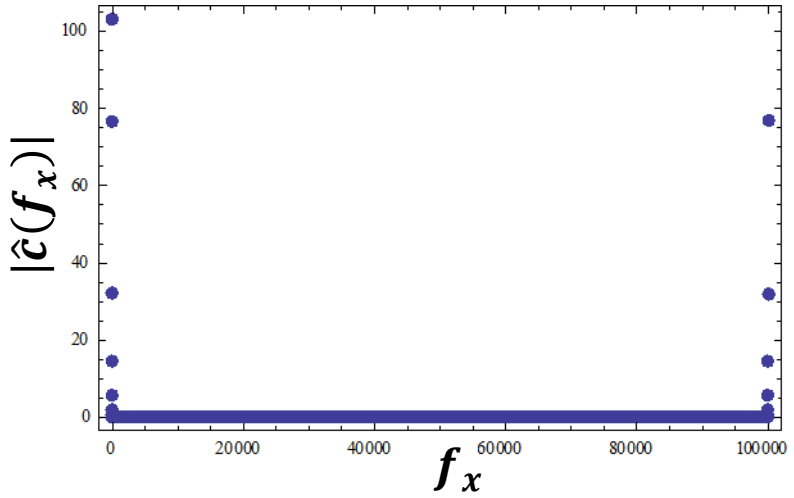

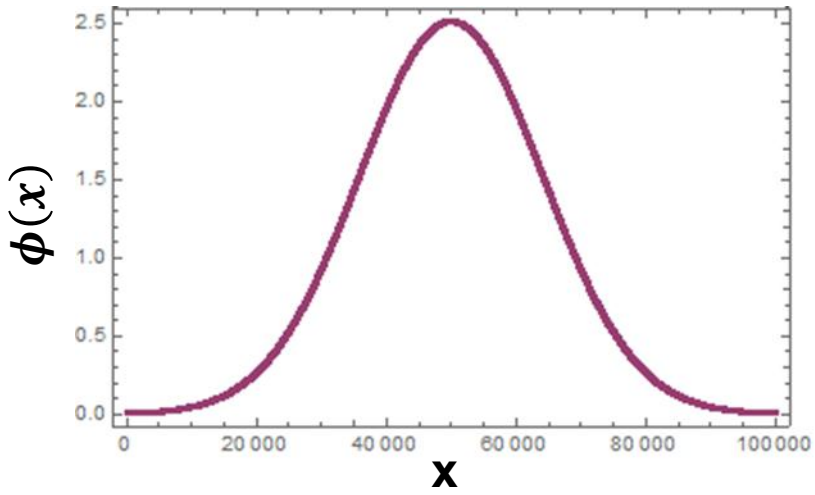

FT^{-1}& $\phi(x) = tan^{-1}\left(\frac{Im[c(x)]}{Re[c(x)]}\right)$

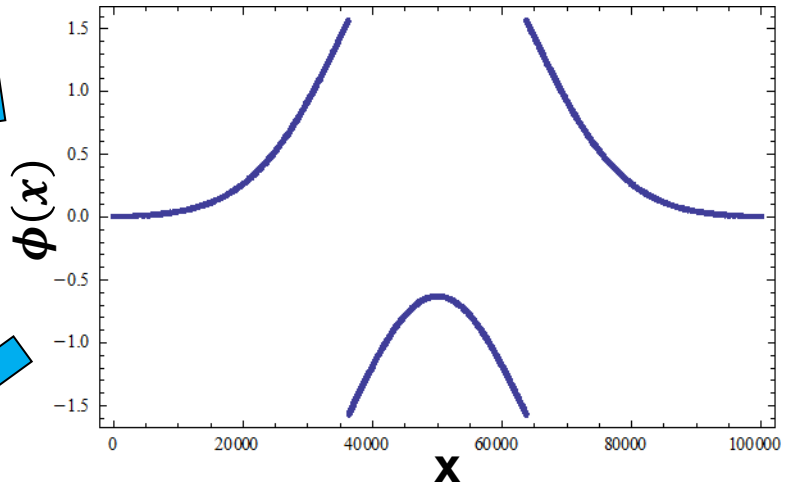

The final phase difference needs to be determined manually since it may exceeds 2π

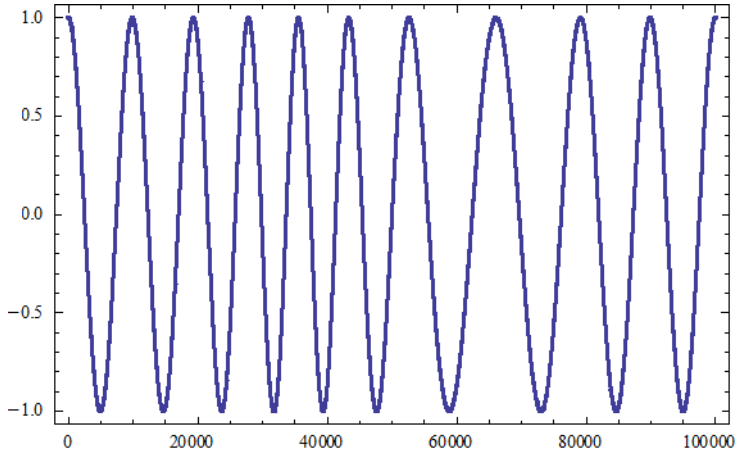

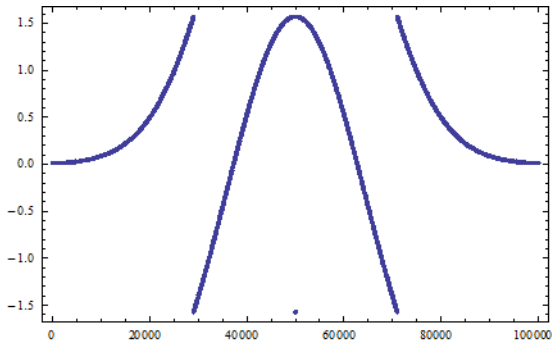

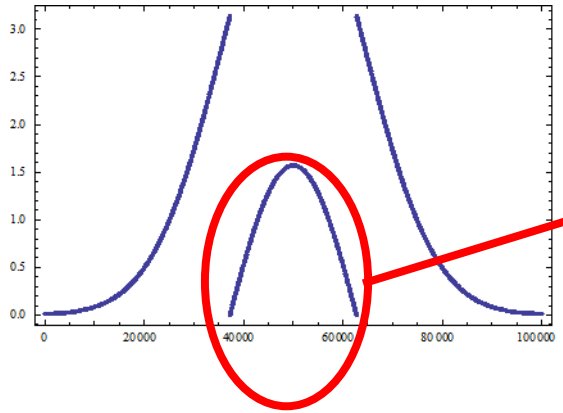

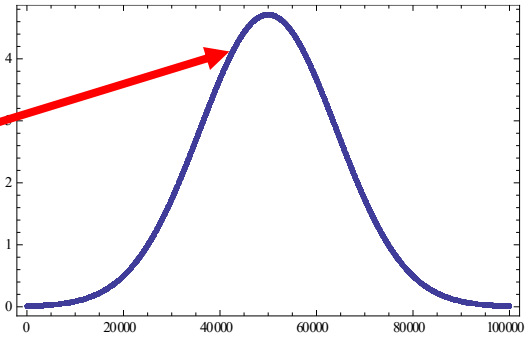

Example of retrieving data from 2D interferometer

$$\mathbf{I}(x,y) = \cos[2\pi\nu_0 x + \phi(x,y)]$$

$$\hat{I}(f_x, y) = \hat{c}(f_x - \nu_0, y) + \hat{c}^*(f_x + \nu_0, y)$$

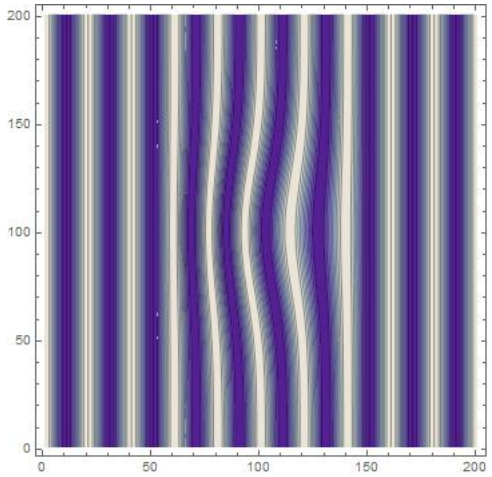

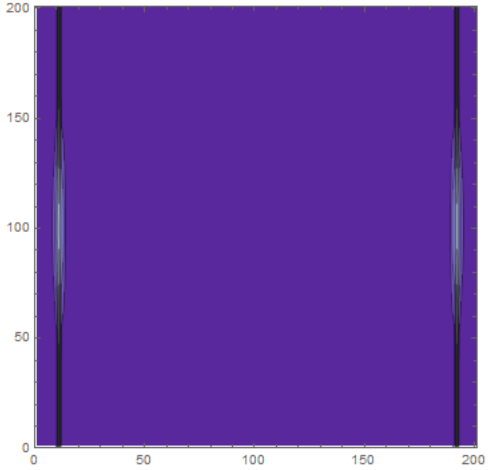

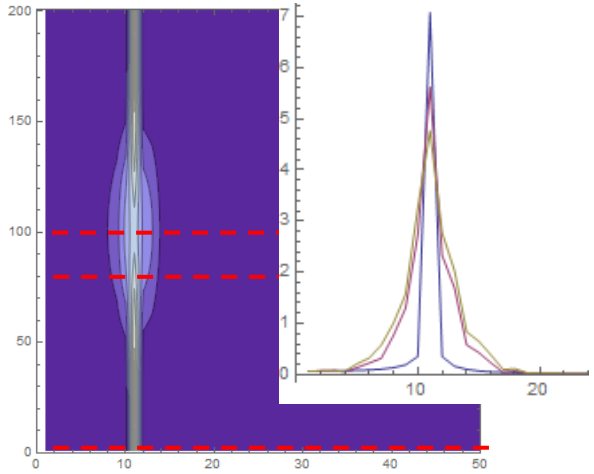

Filter

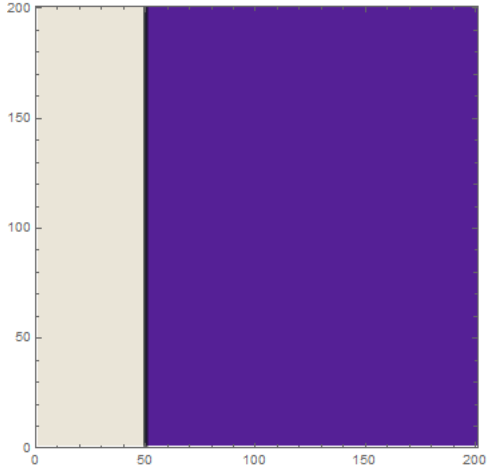

Filtered & Shifted

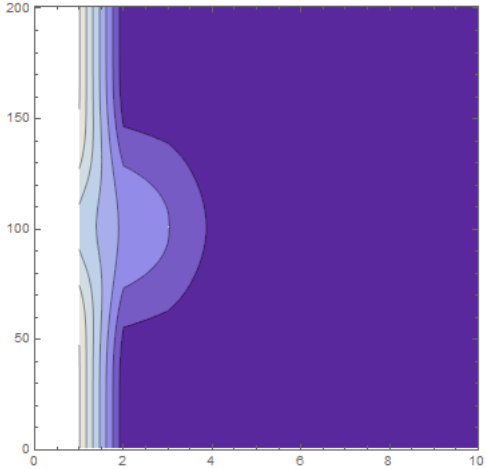

Retrieved data

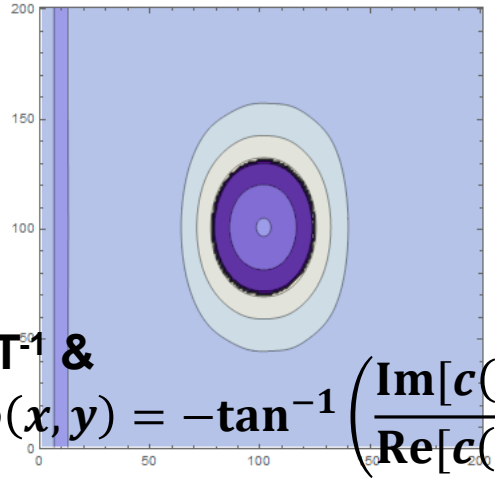

FT^{-1} &

$$\phi(x,y) = -\tan^{-1}\left(\frac{\mathrm{Im}[c(x,y)]}{\mathrm{Re}[c(x,y)]}\right)$$

The retrieved data may need to be modified if the phase change is too large

Retrieved data

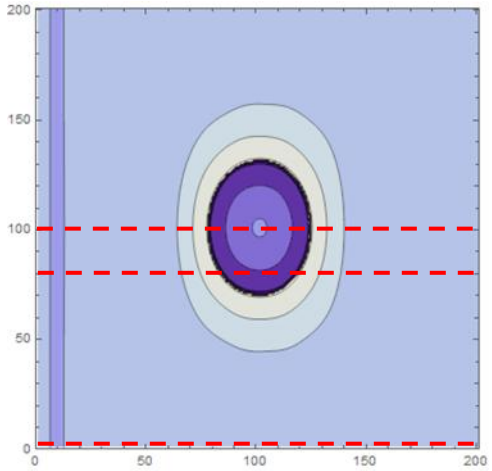

1D profile

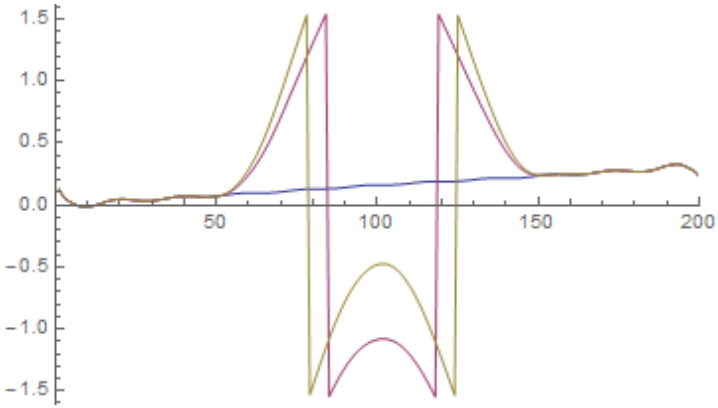

Modified result

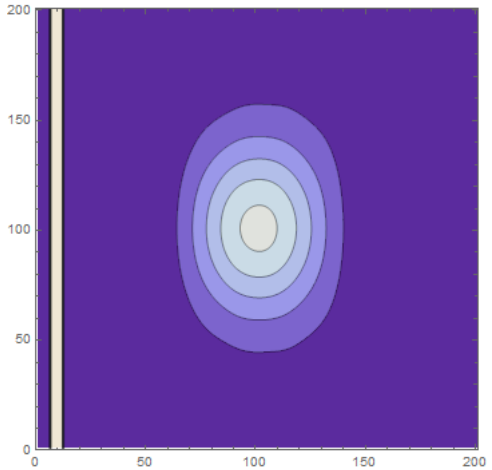

- **Noise came from low spatial resolution.**

Schlieren imaging system can detect density gradient

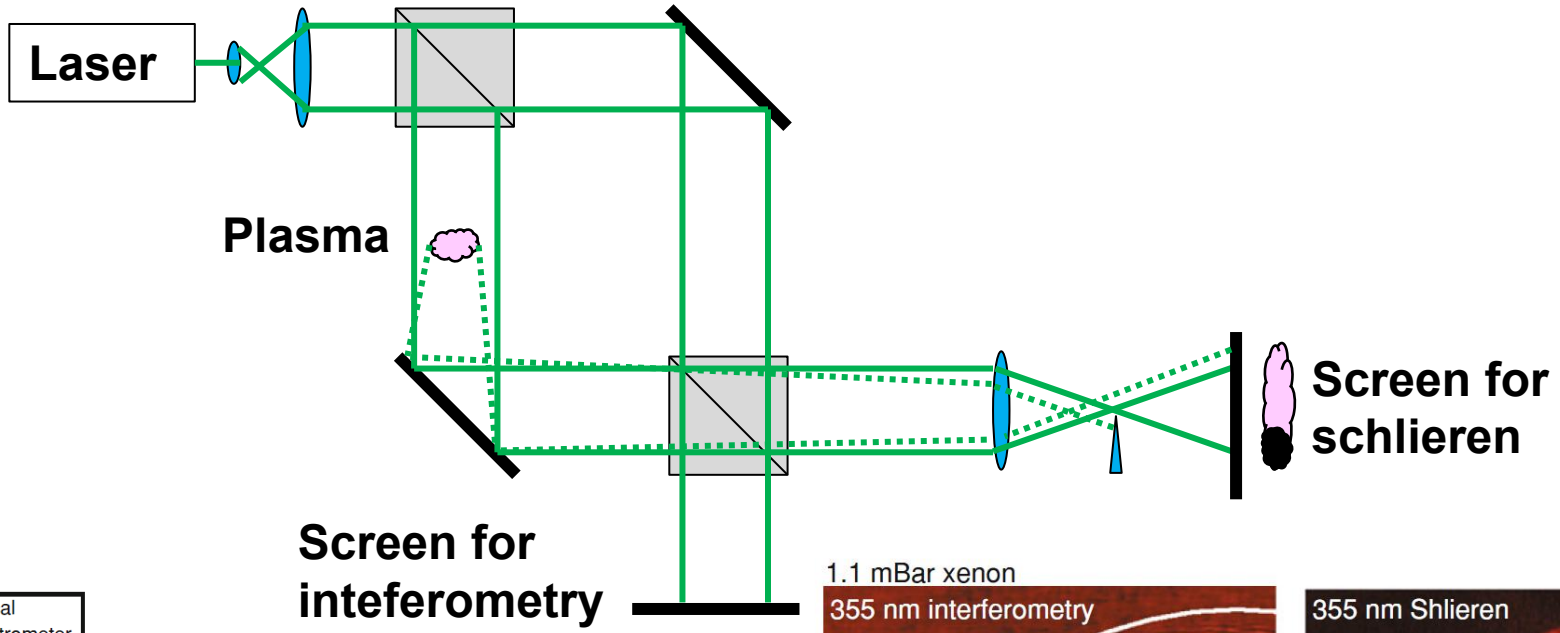

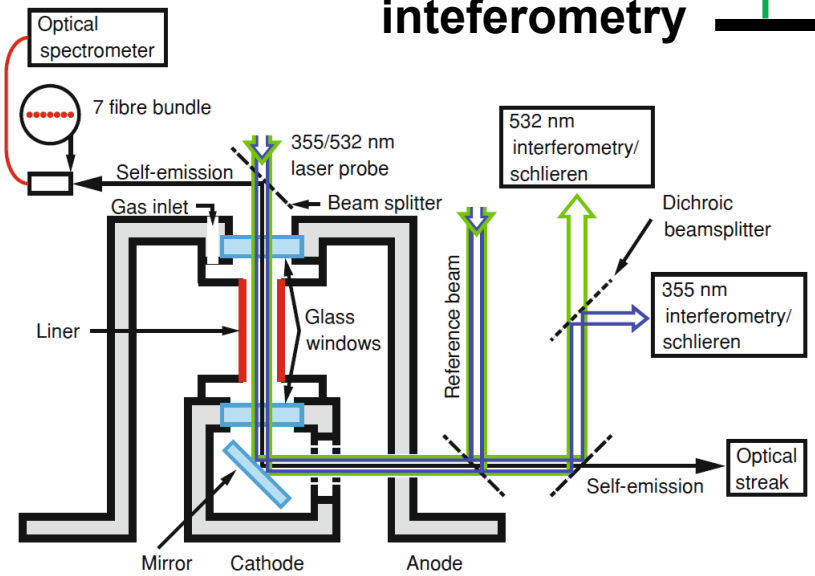

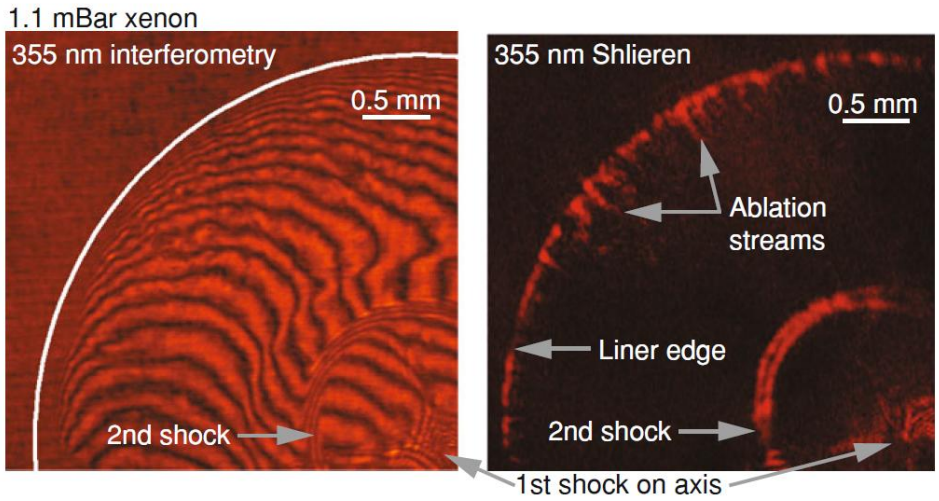

G. C. Burdiak, Cylindrical liner z-pinches as drivers for converging strong shock experiments

Angular spectrum of plane waves can be used for diagnostic

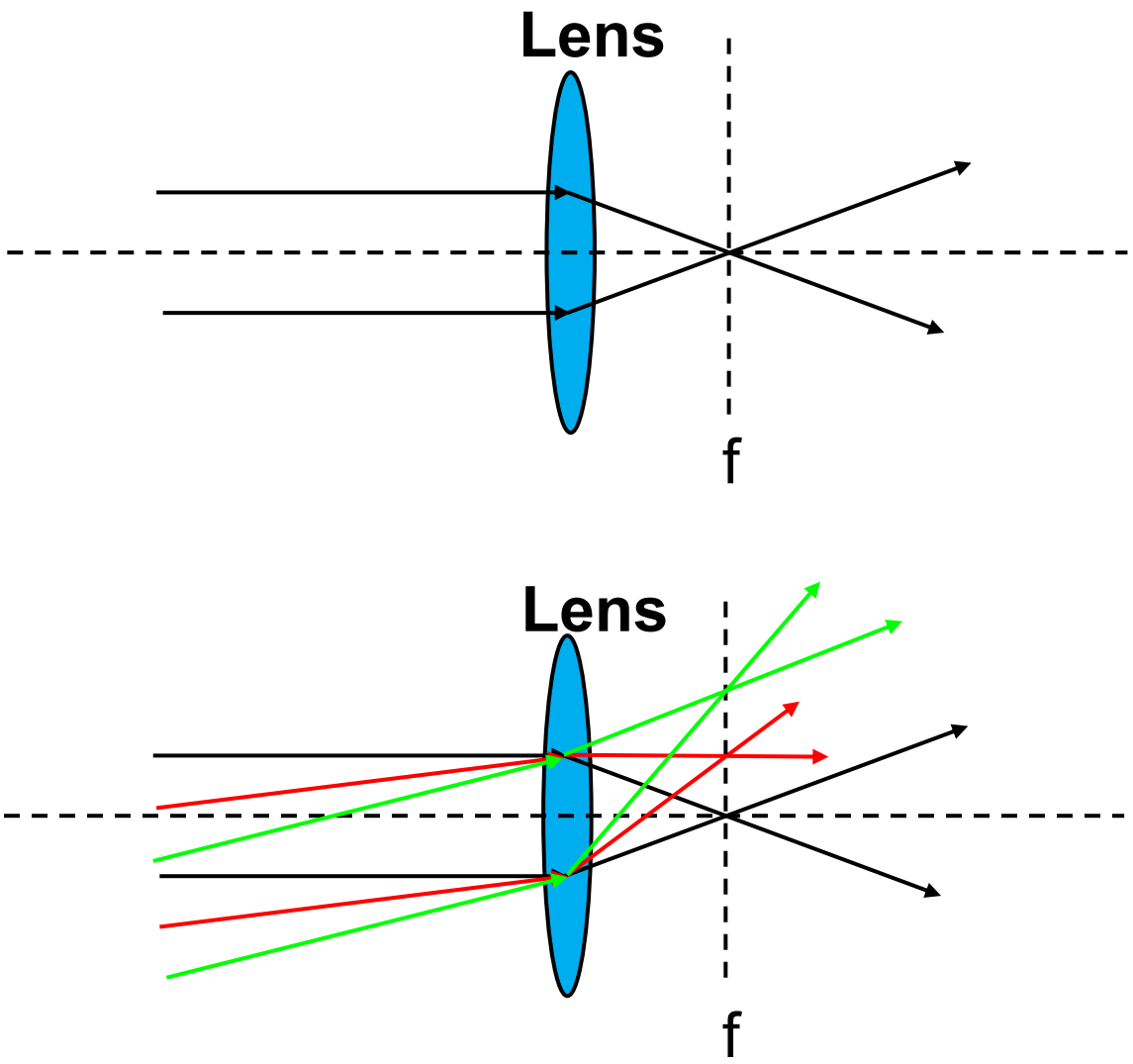

Rays with different angles go through different focal points on the focal points

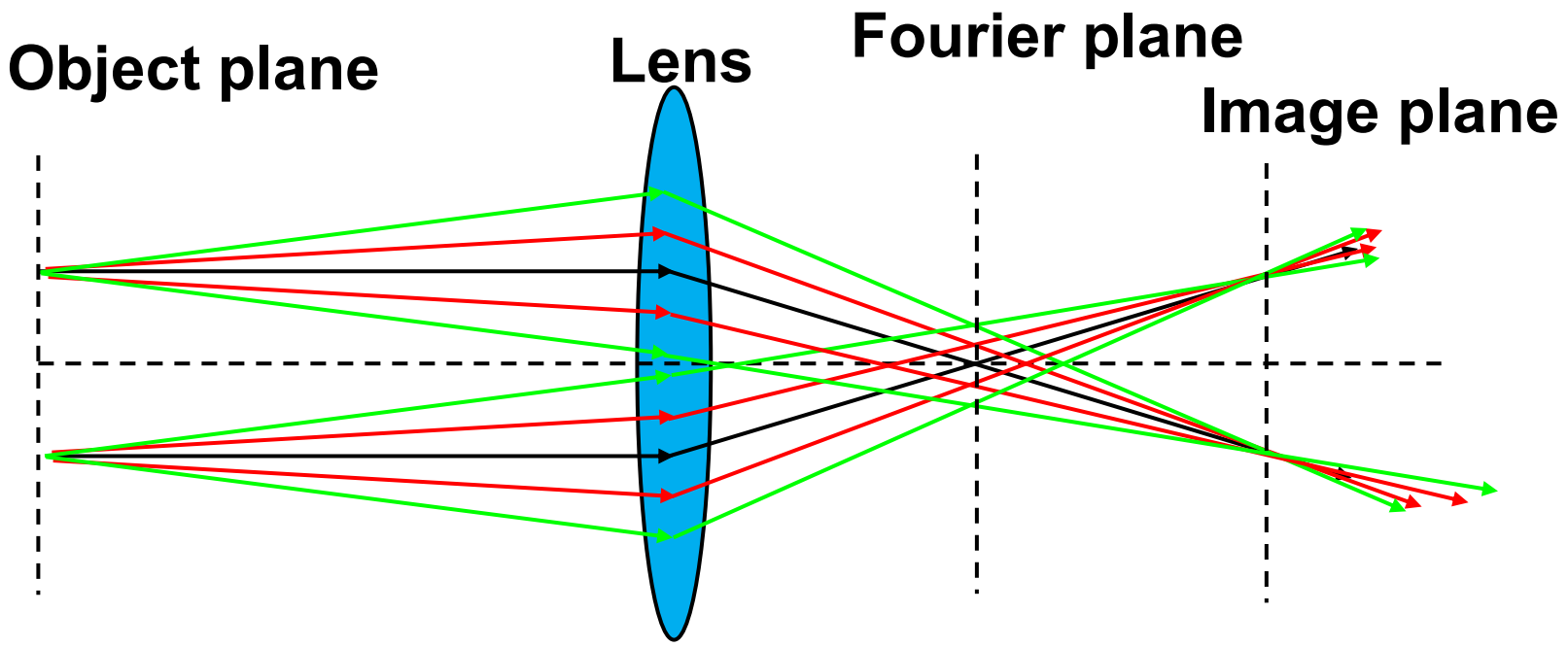

Parallel beams are deflected to different angles with grating with different spatial frequencies

- Grating with low spatial frequency

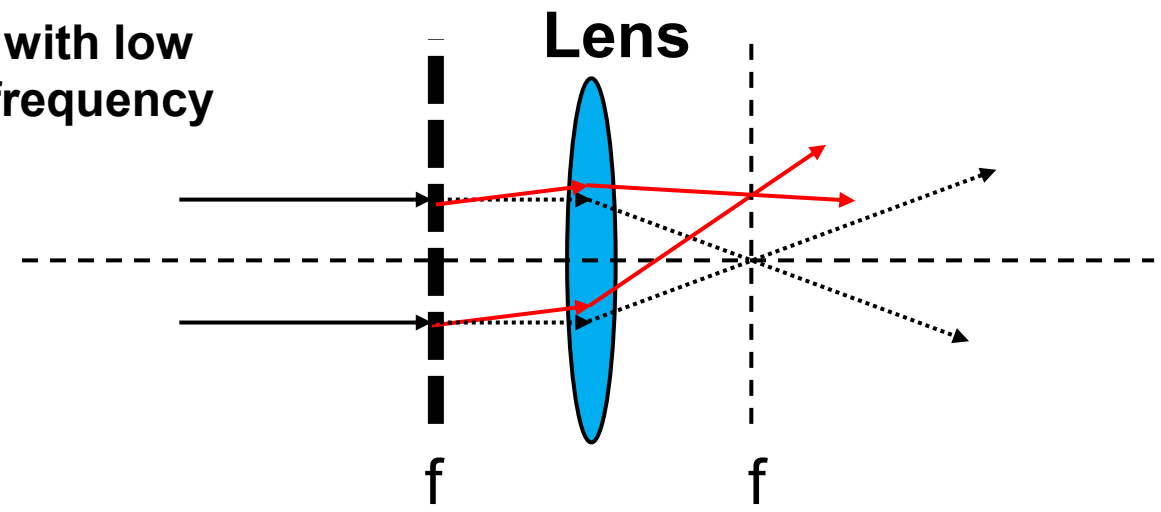

- Grating with high spatial frequency

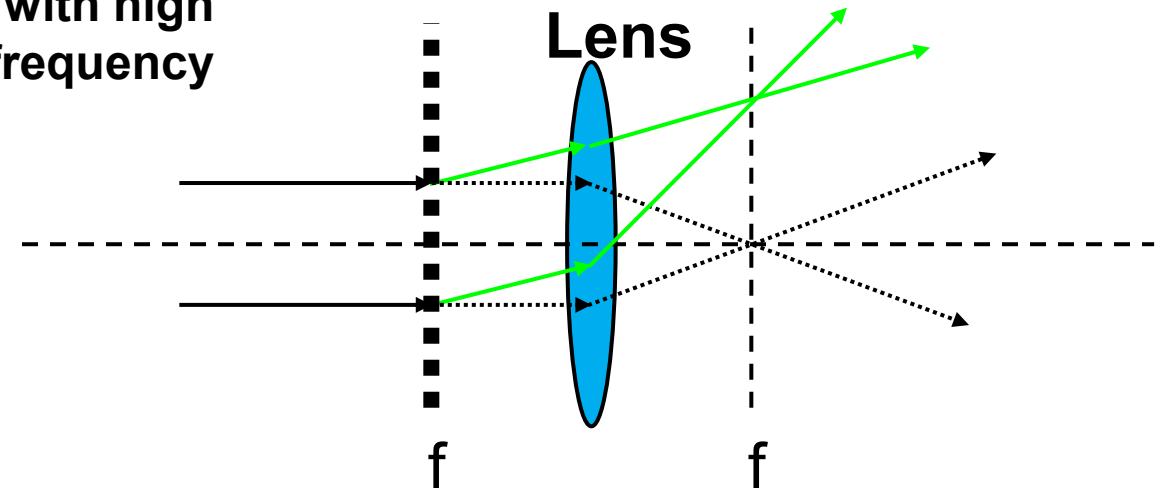

A pinhole or a dot acts like a low-pass / high-pass filter

- **Using pinhole:**
  Low-pass filter

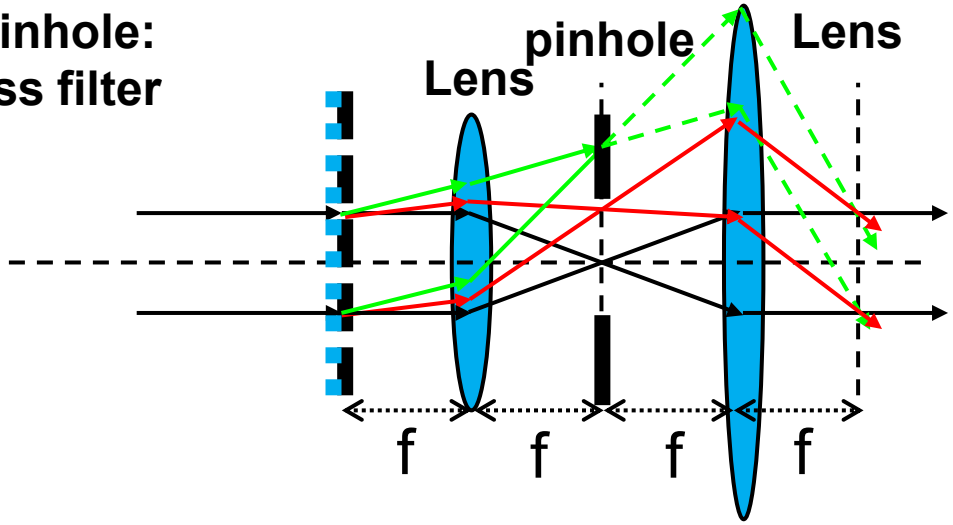

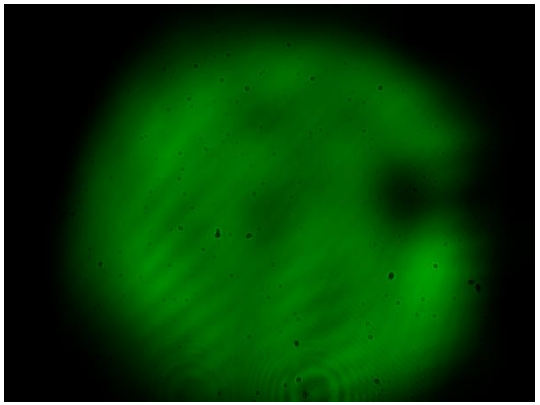

- **Using dot:**
  High-pass filter

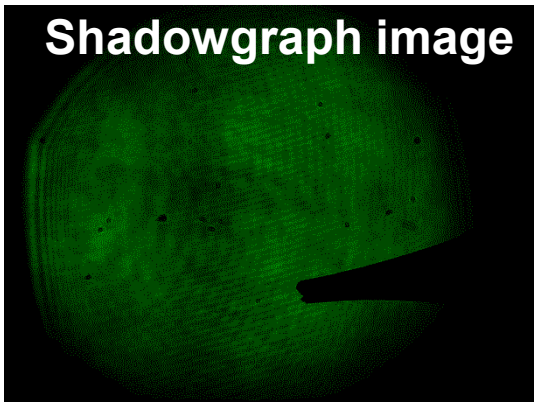

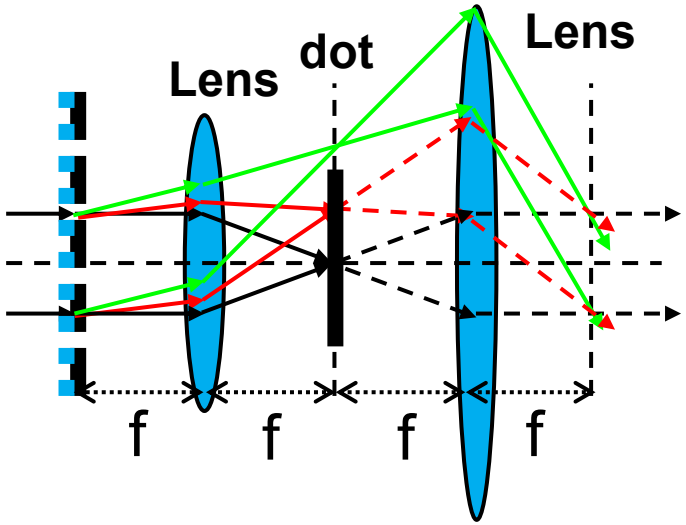

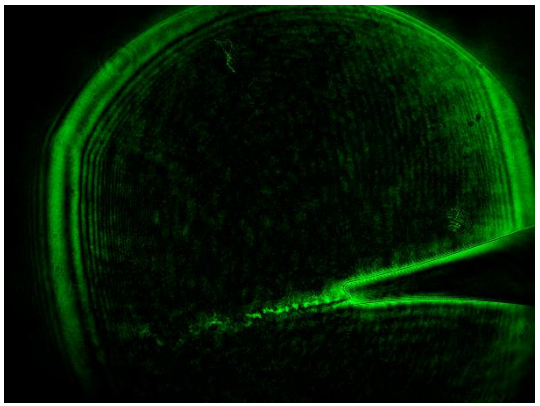

A symmetric Schlieren image can be obtained if the knife edge is replaced by a “floating dot”

- Knife edge

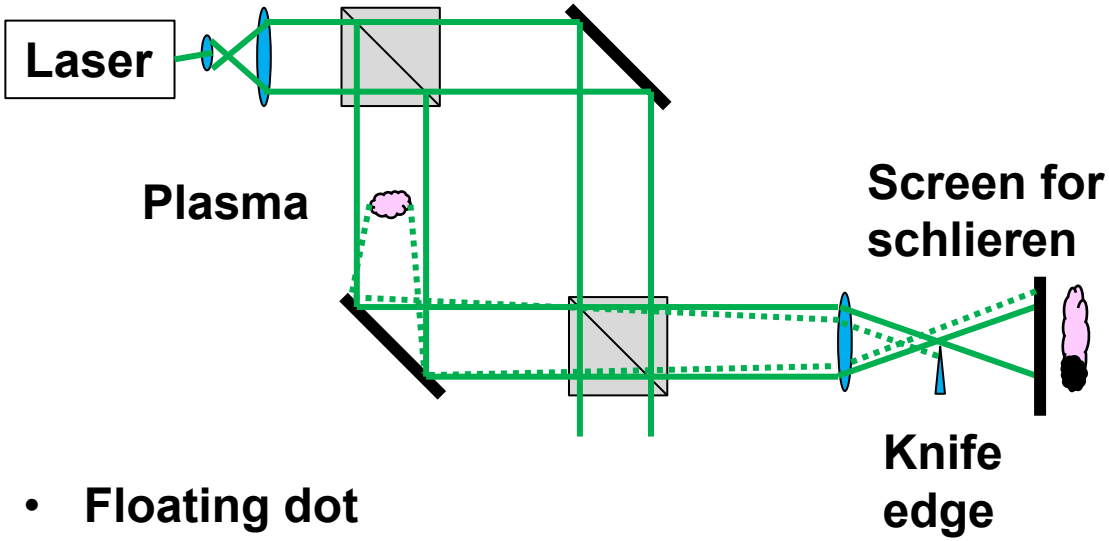

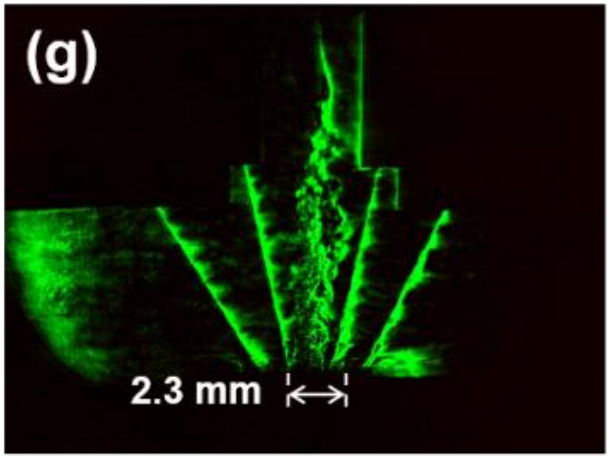

- Floating dot

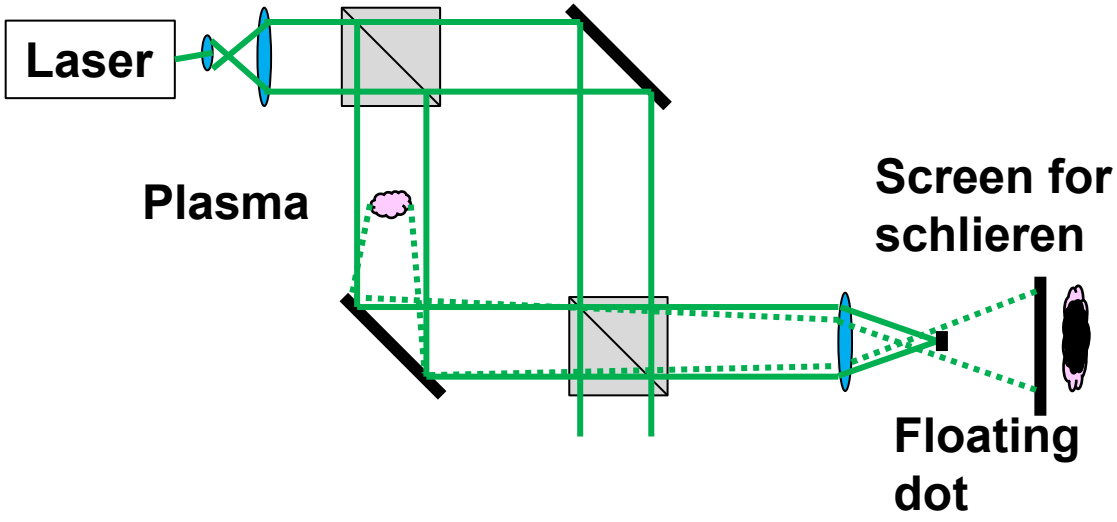

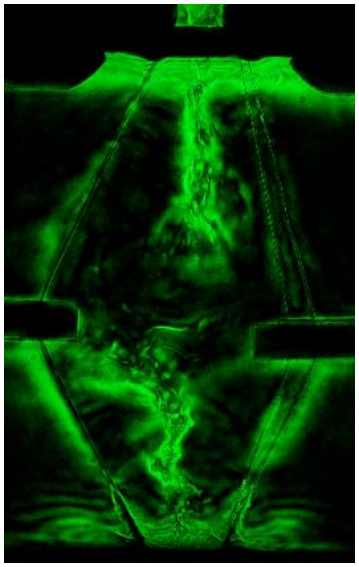

Angular filter refractometry (AFR) maps the refraction of the probe beam at TCC to contours in the image plane

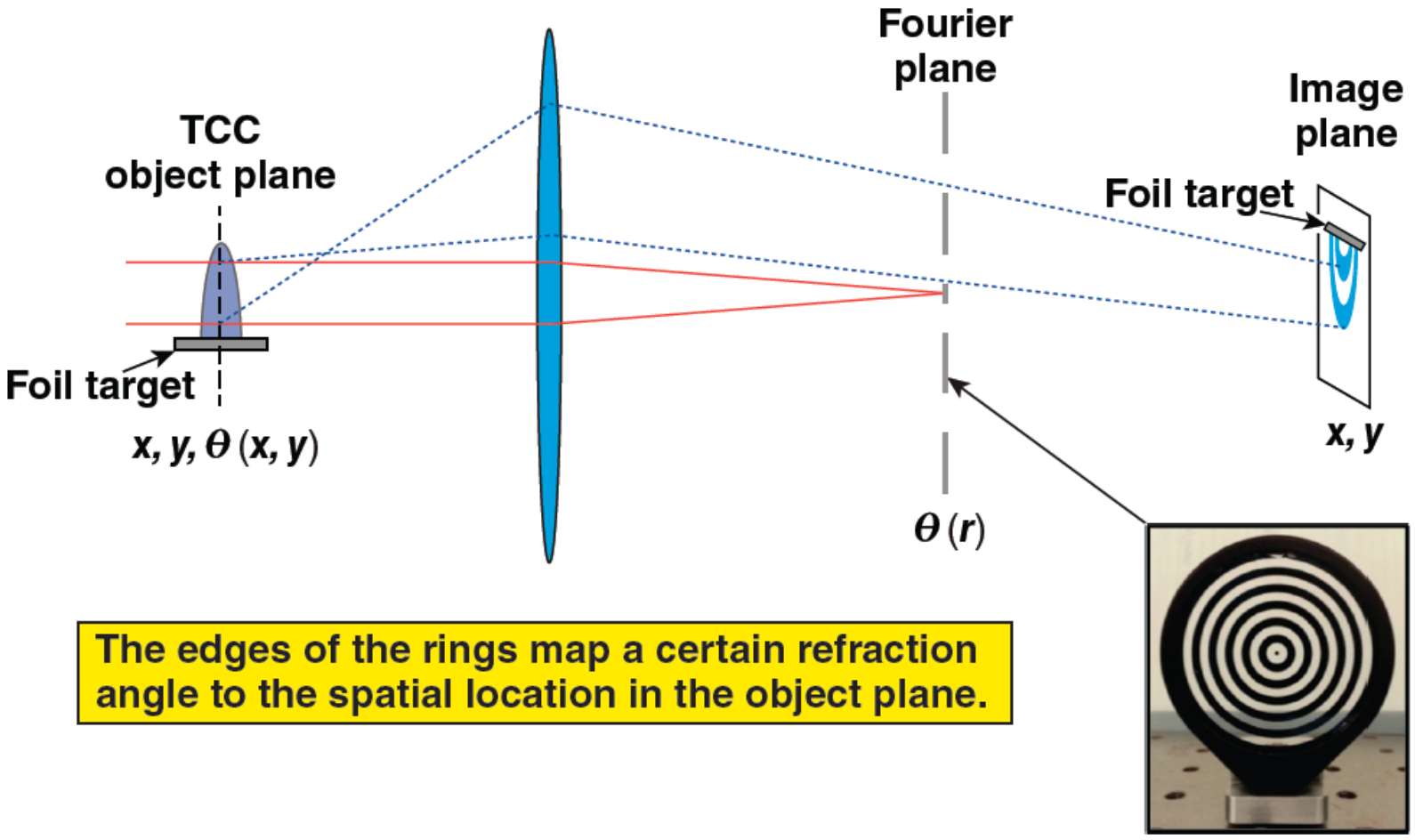

The edges of the rings map a certain refraction angle to the spatial location in the object plane.

Angular spectrum of plane waves can be used for diagnostic

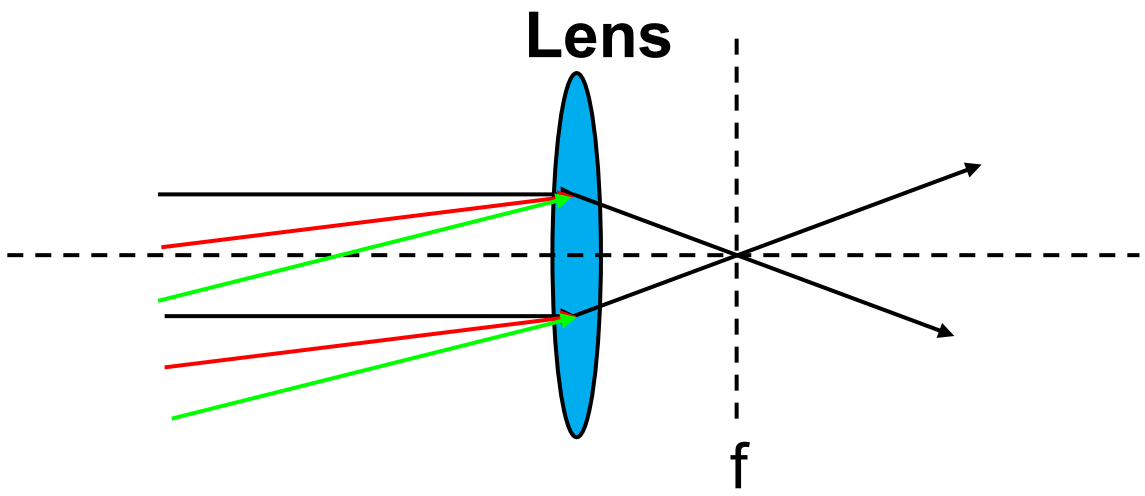

Angular spectrum of plane waves can be used for diagnostic

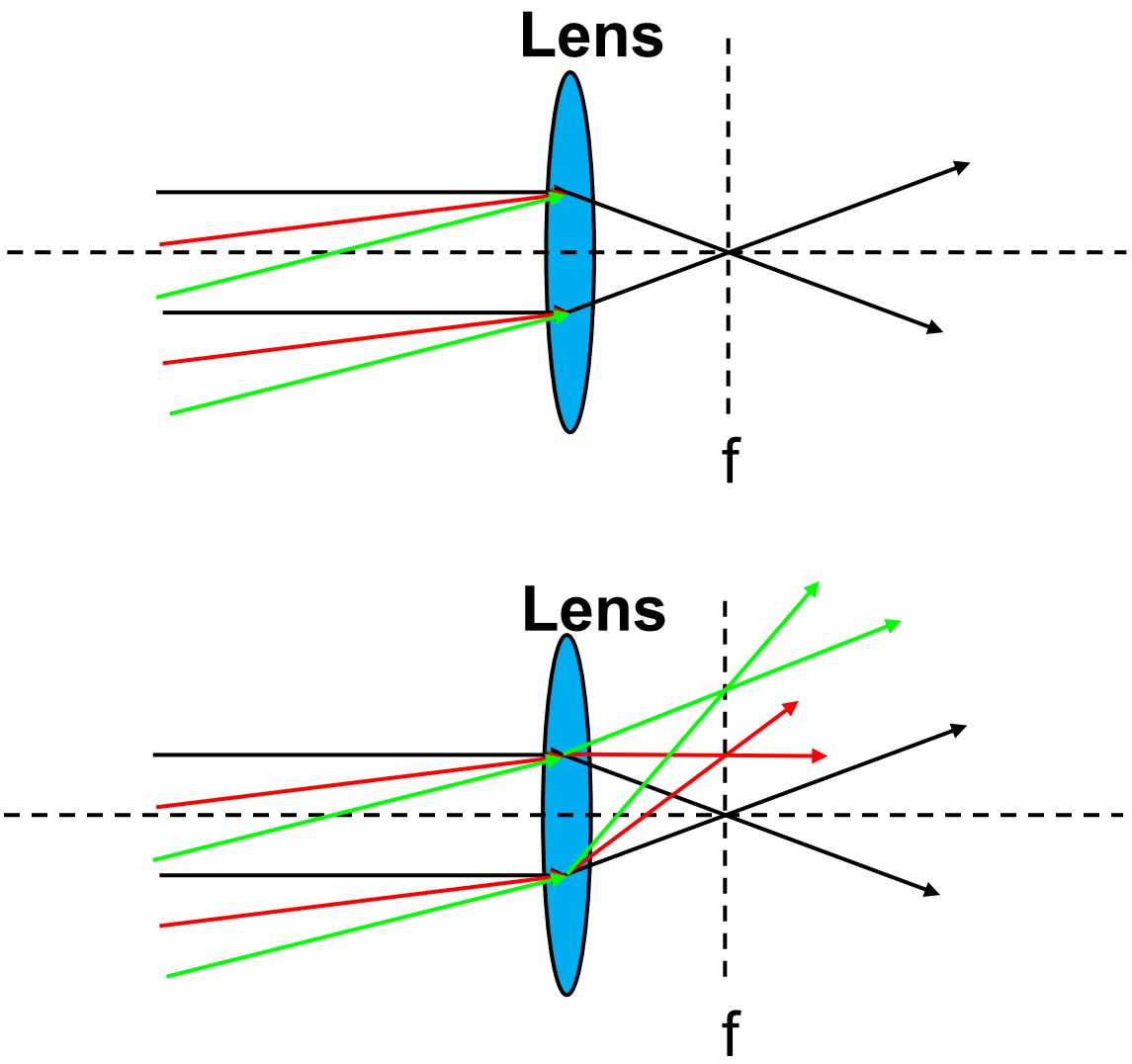

Rays with different angles go through different focal points on the focal points

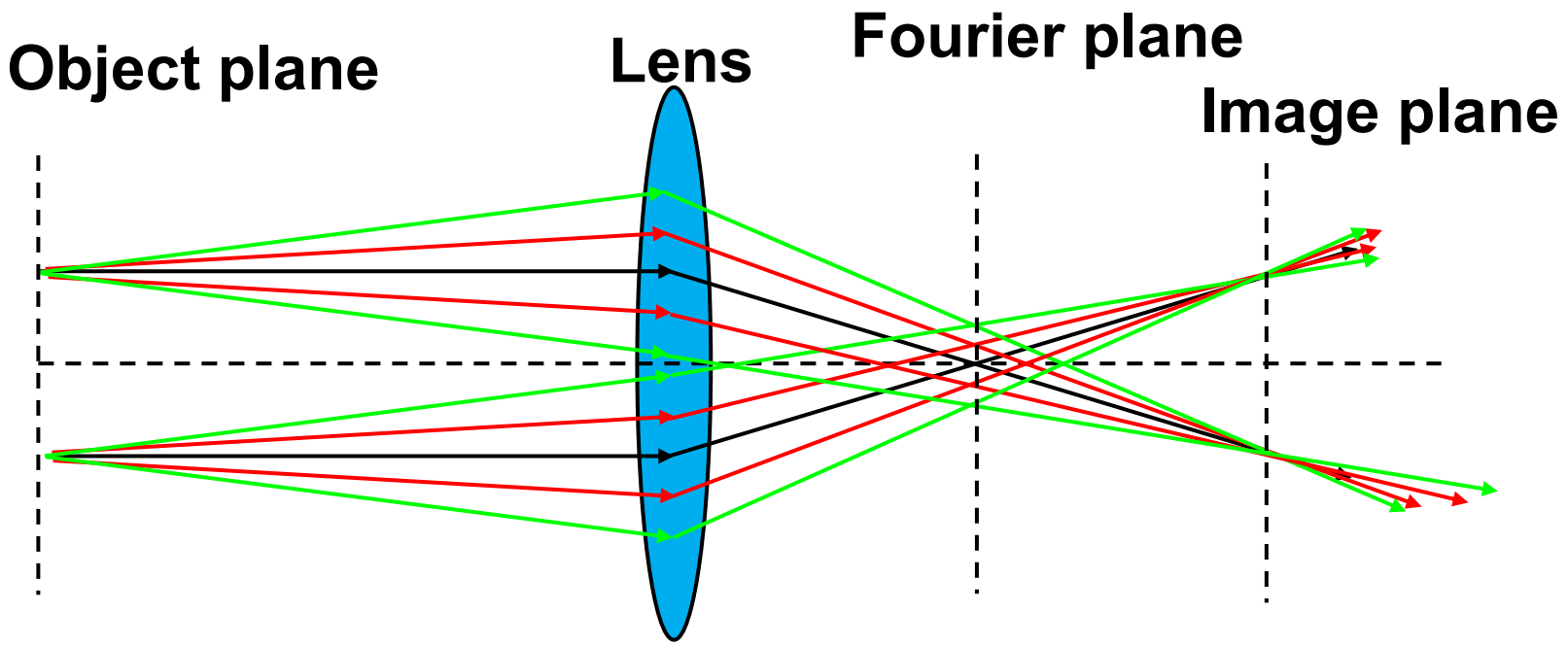

Rays with different angles can be selected by blocking different focal points

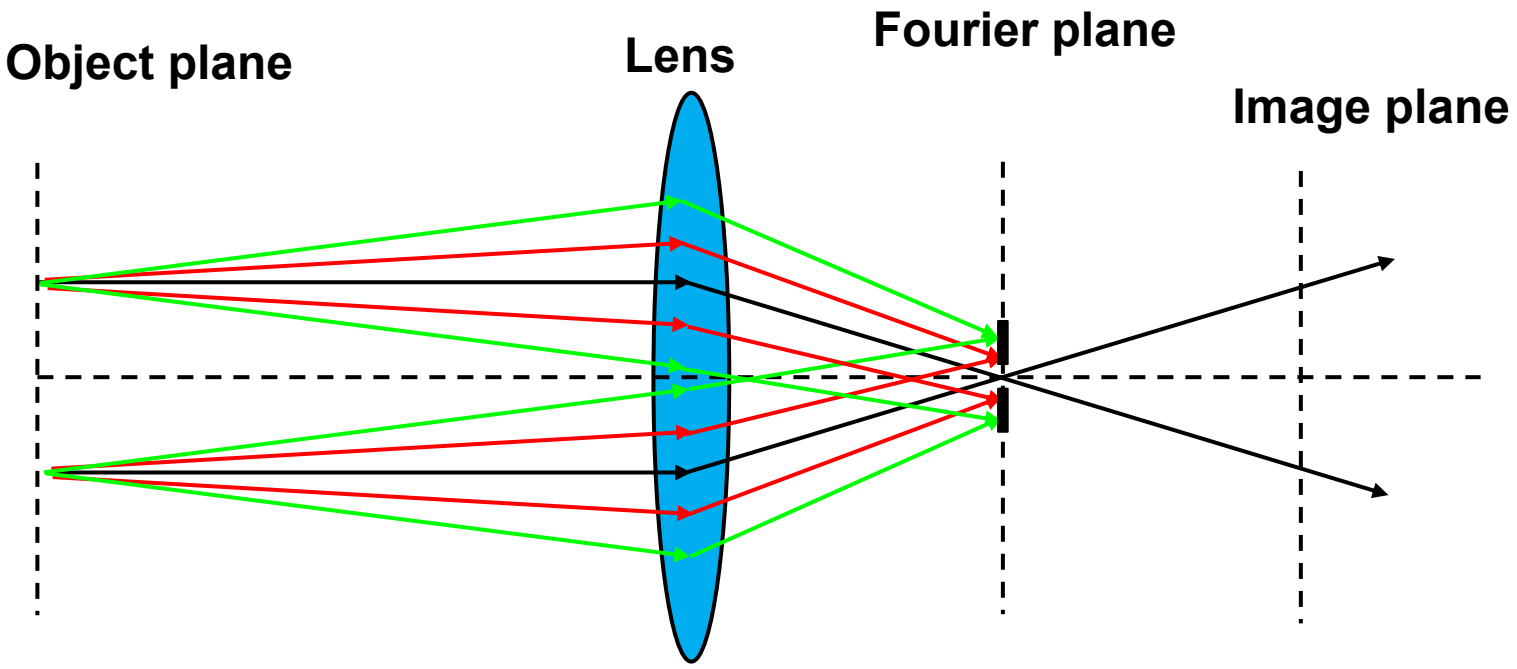

Rays with different angles go through different focal points on the focal points

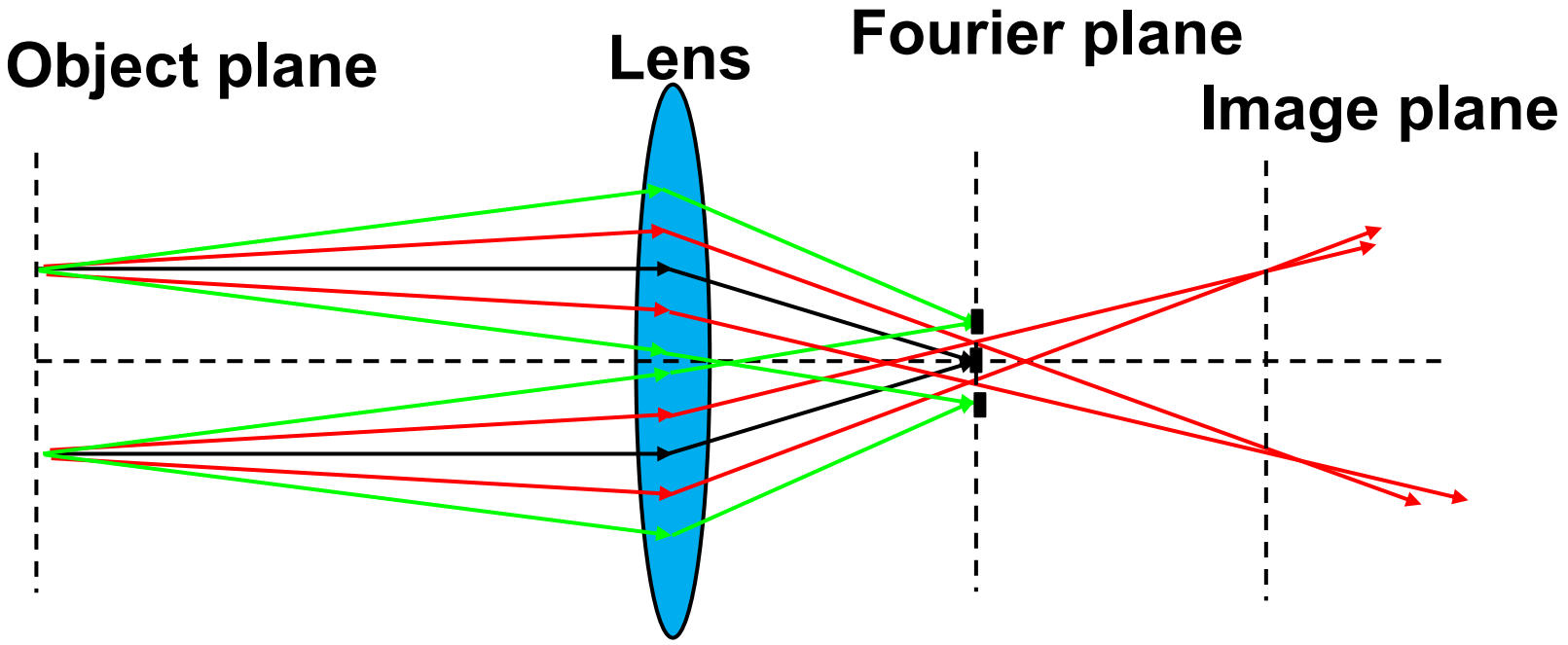

Rays with different angles go through different focal points on the focal points

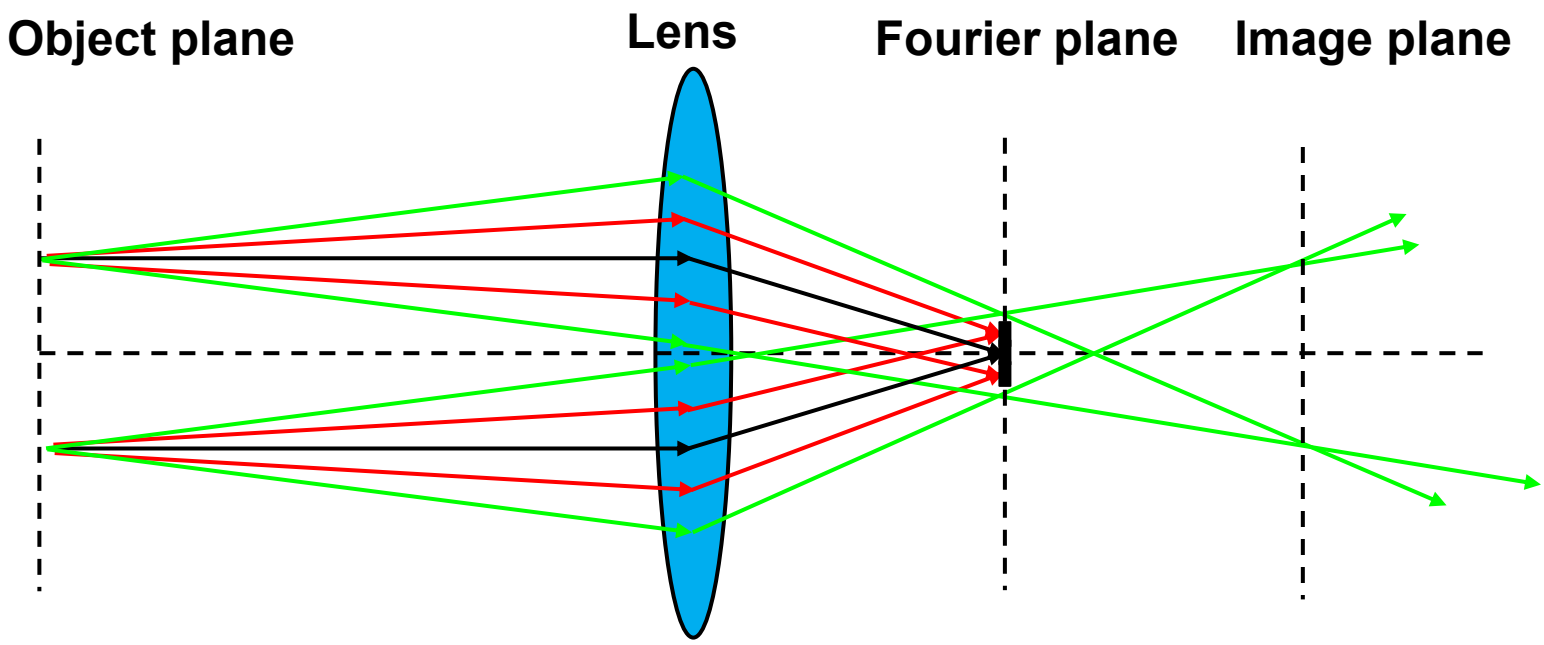

Angular filter refractometry (AFR) maps the refraction of the probe beam at TCC to contours in the image plane

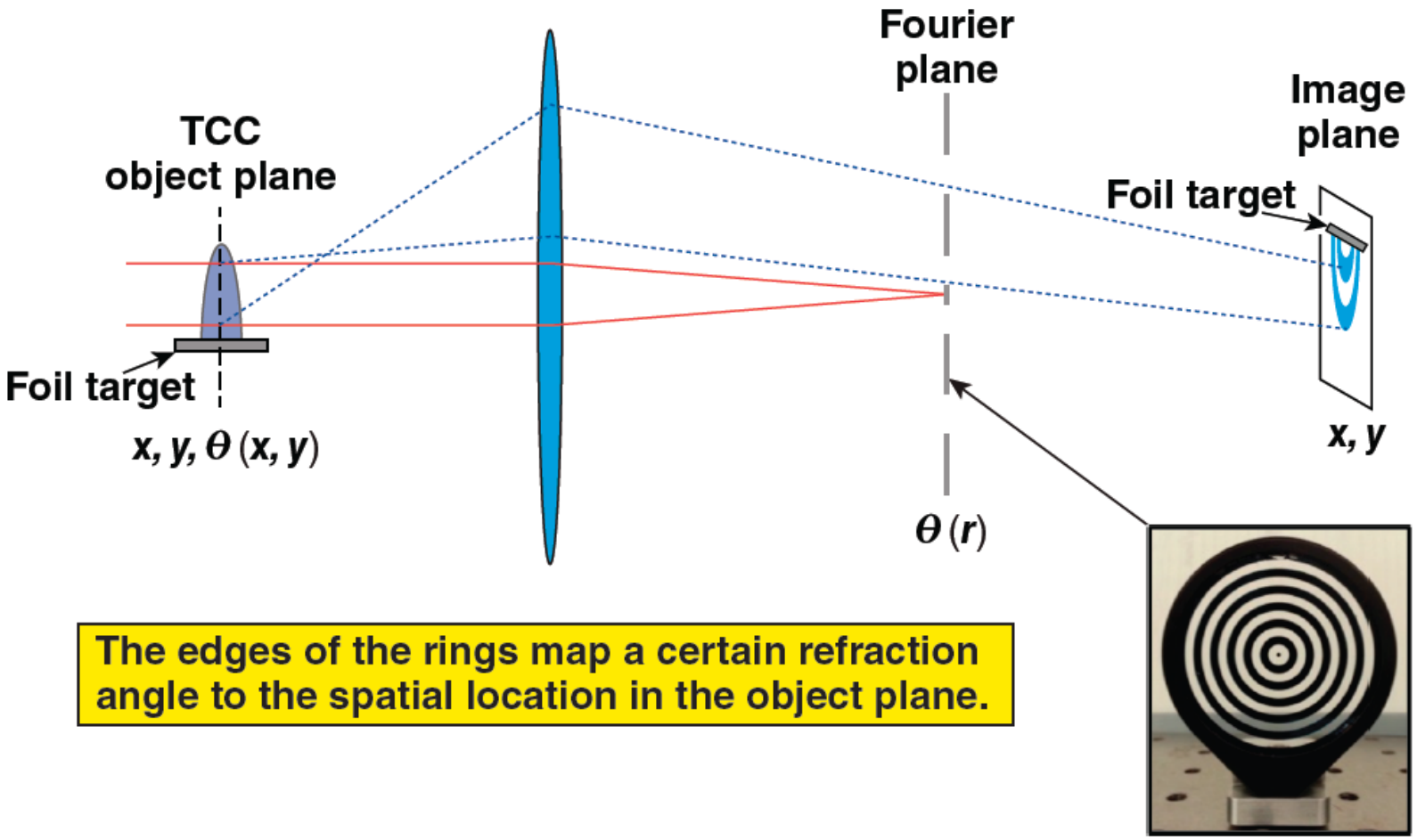

The edges of the rings map a certain refraction angle to the spatial location in the object plane.

Channeling of multi-kilojoule high-intensity laser beams in an inhomogeneous plasma was observed using AFR

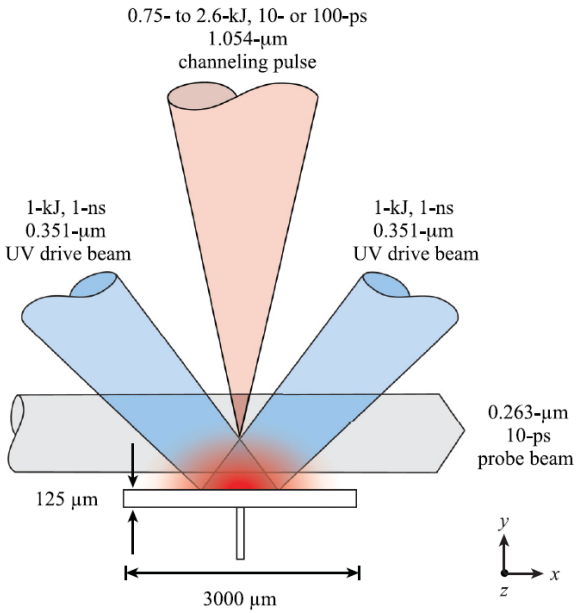

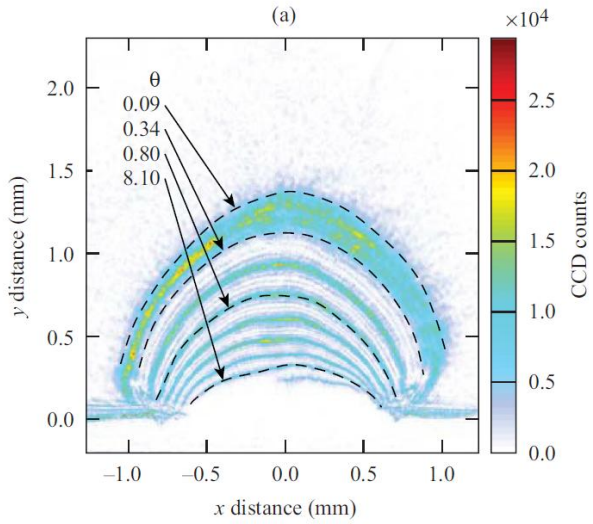

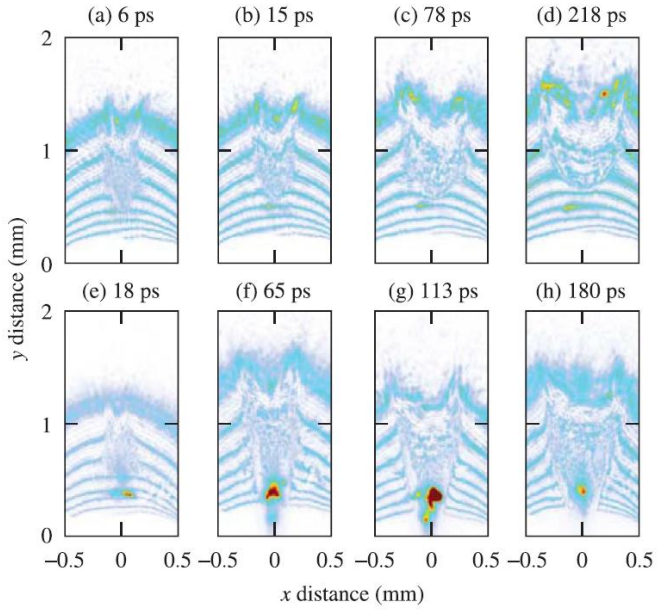

S. Ivancic *et al.*, Phys. Rev. E 91 , 051101 (2015)

Electromagnetic wave can be used to measure the density or the magnetic field in the plasma

- Nonmagnetized isotropic plasma (interferometer needed):

$$n^2 = 1 - \frac{X\left(1-X\right)}{1-X-\frac{1}{2}Y^2\sin^2\theta \pm \left[\left(\frac{1}{2}Y^2\sin^2\theta\right)^2 + \left(1-X\right)^2 Y^2\cos^2\theta\right]^{1/2}}$$

$$= 1 - X = 1 - \frac{\omega_{\mathrm{p}}^2}{\omega^2} = 1 - \frac{n_{\mathrm{e}}}{n_{\mathrm{cr}}} \qquad \left(Y \equiv \frac{\Omega}{\omega} \equiv 0\right)$$

Note: $\omega_{\mathrm{p}}^2 = \frac{n_{\mathrm{e}}e^2}{\epsilon_0 m_{\mathrm{e}}}$ $n_{\mathrm{cr}} = \frac{\epsilon_0 m_{\mathrm{e}}\omega^2}{e^2}$

- **Magnetized isotropic plasma (Polarization detected needed):**

Parallel to B_0

$$n^2 = 1 - \frac{\omega_{\mathrm{p}}^2}{\omega\left(\omega \pm \Omega\right)} \qquad \frac{E_{\mathrm{x}}}{E_{\mathrm{y}}} = \pm i \qquad \Omega \equiv \frac{eB_0}{m_{\mathrm{e}}}$$

Faraday rotation: linear polarization rotation caused by the difference between the speed of LHC and RHC polarized wave.

Circular polarization

$$E_x = E_0 \exp(-i\omega t)$$

$$E_y = iE_x = iE_0 \exp(-i\omega t) = E_0 \exp\left(i\frac{\pi}{2}\right) \exp(-i\omega t) = E_0 \exp\left[-i\left(\omega t - \frac{\pi}{2}\right)\right]$$

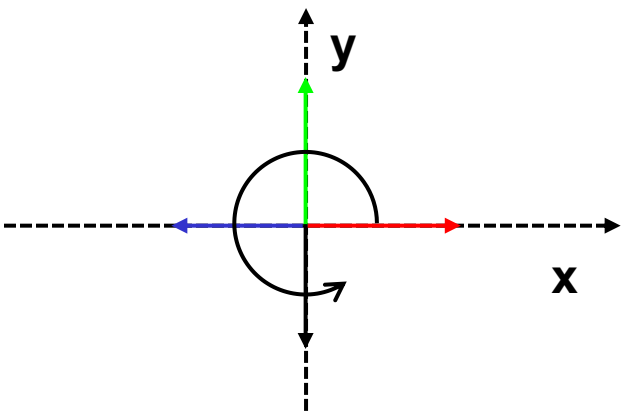

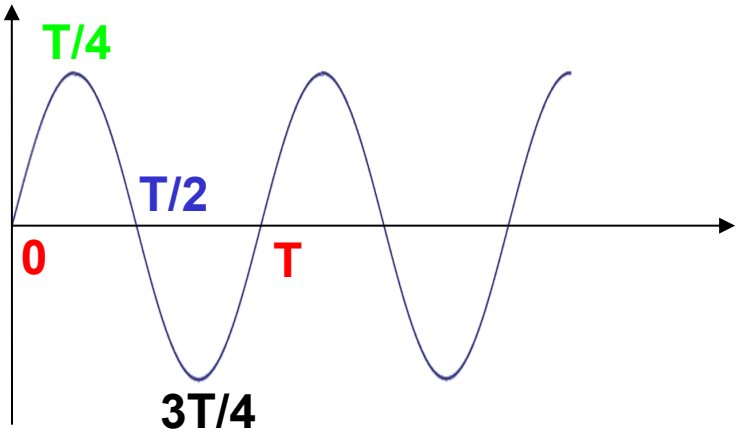

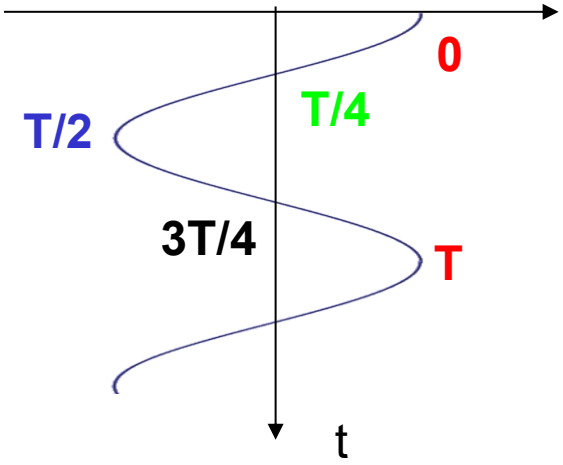

Linear polarization rotates as the wave propagates with different speed in LHC and RHC polarization

$$\vec{E} = E_0\hat{x} = \frac{E_0}{2}\left[(\hat{x}+i\hat{y})+(\hat{x}-i\hat{y})\right] \qquad \vec{E}(z) = \vec{E}\exp(i\phi) \qquad \phi_{\mathrm{R}} \neq \phi_{\mathrm{L}}$$

$$\vec{\boldsymbol{E}}(\boldsymbol{z}) = \frac{\boldsymbol{E_0}}{\boldsymbol{2}}\left[(\hat{\boldsymbol{x}}+\boldsymbol{i}\hat{\boldsymbol{y}})\boldsymbol{e}^{\mathbf{i}\boldsymbol{\phi}_R}+(\hat{\boldsymbol{x}}-\boldsymbol{i}\hat{\boldsymbol{y}})\boldsymbol{e}^{\mathbf{i}\boldsymbol{\phi}_L}\right] \qquad \bar{\phi} \equiv \frac{\phi_{\mathrm{R}}+\phi_{\mathrm{L}}}{2} \quad , \quad \Delta\phi = \frac{\phi_{\mathrm{R}}-\phi_{\mathrm{L}}}{2}$$

$$= \frac{\boldsymbol{E_0}}{\boldsymbol{2}}\left[\hat{\boldsymbol{x}}\left(\boldsymbol{e}^{\mathbf{i}\boldsymbol{\phi}_R}+\boldsymbol{e}^{\mathbf{i}\boldsymbol{\phi}_L}\right)+\hat{\boldsymbol{y}}\boldsymbol{i}\left(\boldsymbol{e}^{\mathbf{i}\boldsymbol{\phi}_R}-\boldsymbol{e}^{\mathbf{i}\boldsymbol{\phi}_L}\right)\right]$$

$$= \frac{\boldsymbol{E_0}}{\boldsymbol{2}}\left[\hat{\boldsymbol{x}}\left(\boldsymbol{e}^{\boldsymbol{i}\left(\bar{\boldsymbol{\phi}}+\frac{\boldsymbol{\Delta\phi}}{\boldsymbol{2}}\right)}+\boldsymbol{e}^{\boldsymbol{i}\left(\bar{\boldsymbol{\phi}}-\frac{\boldsymbol{\Delta\phi}}{\boldsymbol{2}}\right)}\right)+\hat{\boldsymbol{y}}\boldsymbol{i}\left(\boldsymbol{e}^{\boldsymbol{i}\left(\bar{\boldsymbol{\phi}}+\frac{\boldsymbol{\Delta\phi}}{\boldsymbol{2}}\right)}-\boldsymbol{e}^{\boldsymbol{i}\left(\bar{\boldsymbol{\phi}}-\frac{\boldsymbol{\Delta\phi}}{\boldsymbol{2}}\right)}\right)\right]$$

$$= \boldsymbol{E_0}\boldsymbol{e}^{\boldsymbol{i}\bar{\boldsymbol{\phi}}}\left[\hat{\boldsymbol{x}}\left(\frac{\boldsymbol{e}^{\boldsymbol{i}\frac{\boldsymbol{\Delta\phi}}{\boldsymbol{2}}}+\boldsymbol{e}^{-\boldsymbol{i}\frac{\boldsymbol{\Delta\phi}}{\boldsymbol{2}}}}{\boldsymbol{2}}\right)+\hat{\boldsymbol{y}}\boldsymbol{i}\left(\frac{\boldsymbol{e}^{\boldsymbol{i}\frac{\boldsymbol{\Delta\phi}}{\boldsymbol{2}}}-\boldsymbol{e}^{-\boldsymbol{i}\frac{\boldsymbol{\Delta\phi}}{\boldsymbol{2}}}}{\boldsymbol{2}}\right)\right]$$

$$= \boldsymbol{E_0}\boldsymbol{e}^{\boldsymbol{i}\bar{\boldsymbol{\phi}}}\left[\hat{\boldsymbol{x}}\cos\left(\frac{\boldsymbol{\Delta\phi}}{\boldsymbol{2}}\right)\mathbf{Cos}+\hat{\boldsymbol{y}}\sin\left(\frac{\boldsymbol{\Delta\phi}}{\boldsymbol{2}}\right)\right]$$

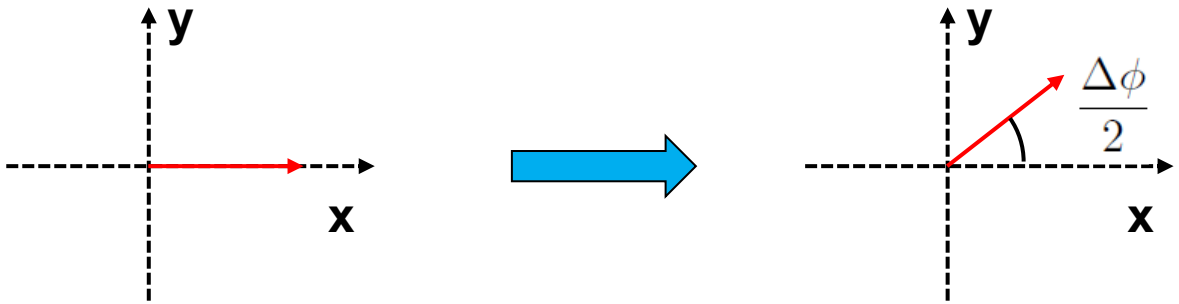

A linear polarized wave can be decomposed into one left-handed circular polarized wave and a righ-handed circular polarized wave

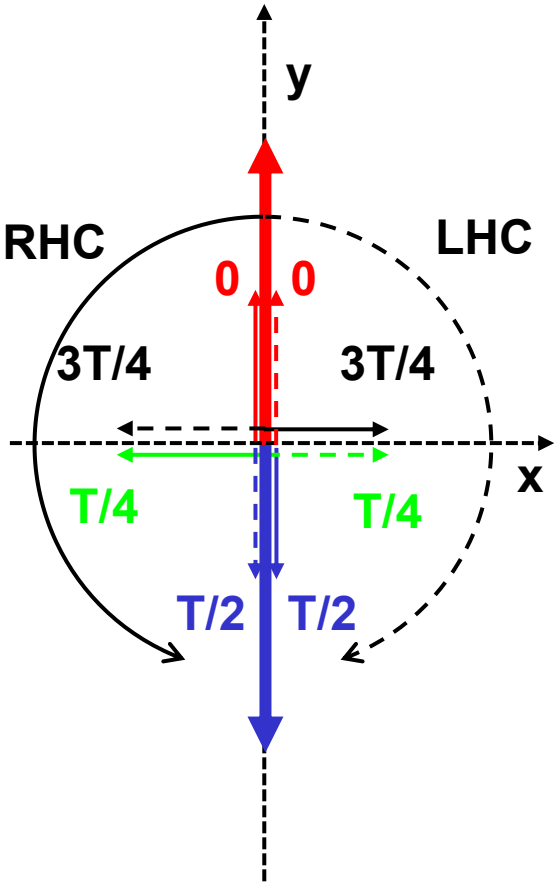

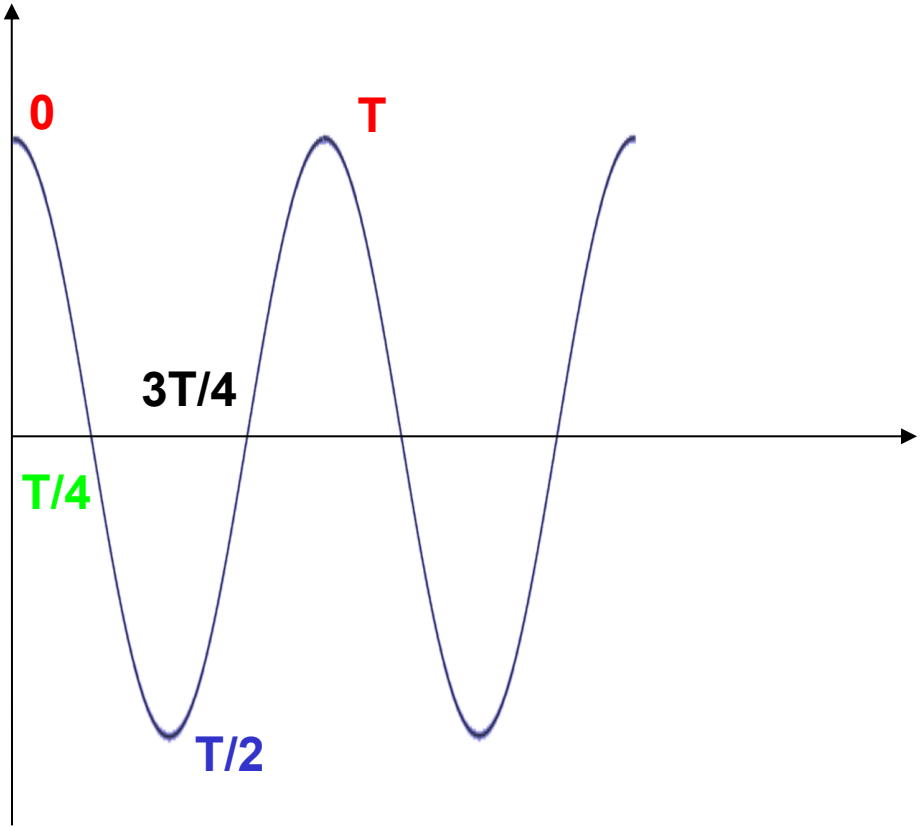

The rotation angle of the polarization depends on the linear integral of magnetic field and electron density

$$\phi = \int k dl = \int n \frac{\omega}{c} dl \qquad \alpha = \frac{\Delta\phi}{2} = \frac{\omega}{2c} \int (n_{\mathrm{R}} - n_{\mathrm{L}})\, dl$$

$$n_{\mathrm{R}} = \sqrt{1 - \frac{X}{1+Y}} \sim 1 - \frac{1}{2}\frac{X}{1+Y} \qquad X, Y << 1$$

$$n_{\mathrm{L}} \sim 1 - \frac{1}{2}\frac{X}{1-Y} \qquad \frac{X}{1 \pm Y} << 1$$

$$n_{\mathrm{R}} - n_{\mathrm{L}} \sim \frac{X}{2}\left(\frac{1}{1-Y} - \frac{1}{1+Y}\right) = \frac{XY}{1-Y^2} \sim XY$$

$$\alpha \sim \frac{\omega}{2c} \int XY\, dl = \frac{\omega}{2c} \int \frac{\omega_{\mathrm{p}}^2}{\omega^2}\frac{\Omega}{\omega} dl = \frac{1}{2c} \int \frac{n_{\mathrm{e}}}{n_{\mathrm{cr}}}\frac{eB}{m_{\mathrm{e}}} dl$$

$$= \frac{e}{2cm_{\mathrm{e}}n_{\mathrm{cr}}} \int n_{\mathrm{e}} B dl$$

The rotation angle of the polarization depends on the linear integral of magnetic field and electron density

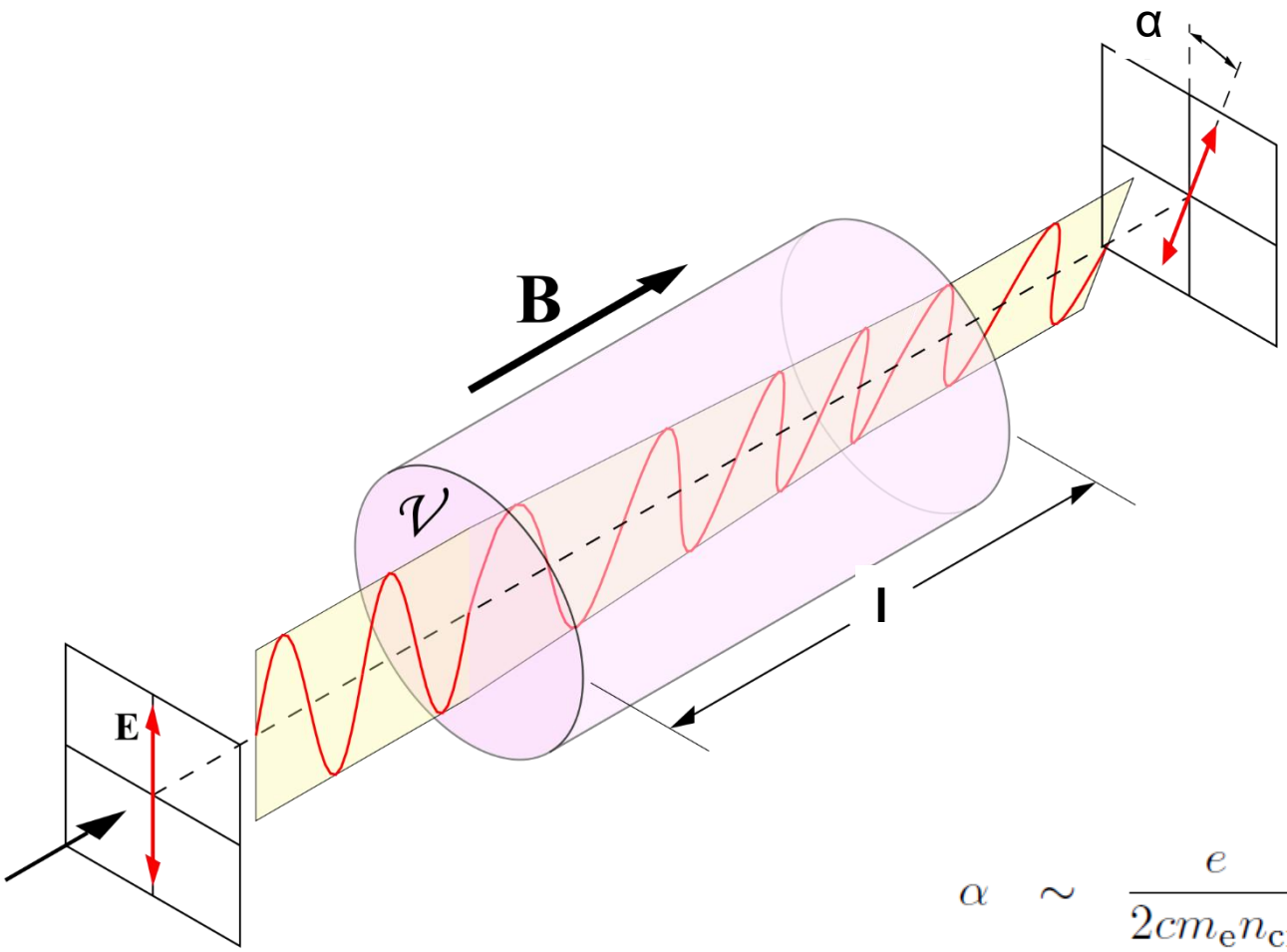

$$\alpha \sim \frac{e}{2cm_e n_{cr}} \int n_e B dl$$

Magnetic field can be generated when the temperature and density gradients are not parallel to each other

$$\frac{\partial \vec{B}}{\partial t} = \nabla \times \left[\underbrace{\vec{u} \times \vec{B}}_{\text{Convection term}} + \underbrace{\frac{1}{\sigma \mu_0} \nabla \times \vec{B}}_{\text{Diffusion term}} + \underbrace{\frac{\nabla p_\mathrm{e}}{n_\mathrm{e} e}}_{\text{self generated field}} \underbrace{- \frac{1}{\mu_0} \left(\frac{\nabla \times \vec{B}}{n_\mathrm{e} e} \times \vec{B} \right)}_{\text{Hall term}} \right]$$

$$\nabla \times \frac{\nabla p_\mathrm{e}}{n_\mathrm{e} e} = -\frac{k_\mathrm{B}}{e} \frac{\nabla n_\mathrm{e} \times \nabla T_\mathrm{e}}{n_\mathrm{e}}$$

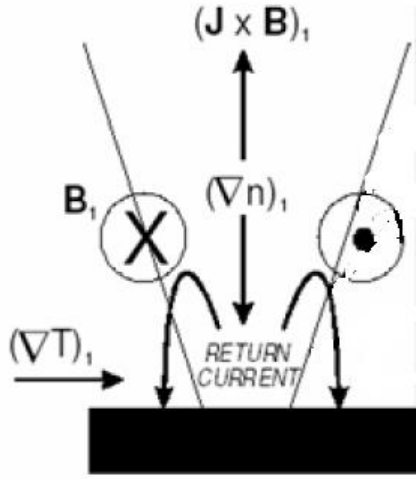

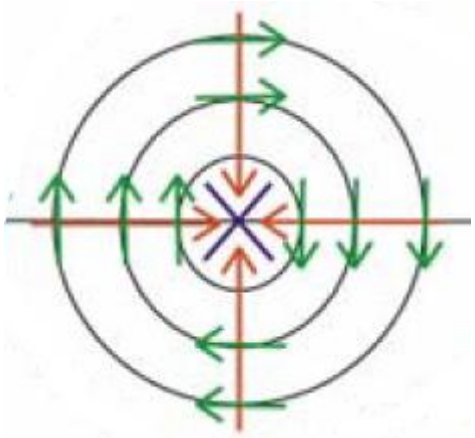

(grad n_e) ✕ (grad T_e) ⟶ B field ⟶

P M Nilson *et al.*, Central Laser Facility Annual Report 2004/2005

Polarimetry diagnostic can be used to measure the magnetic field

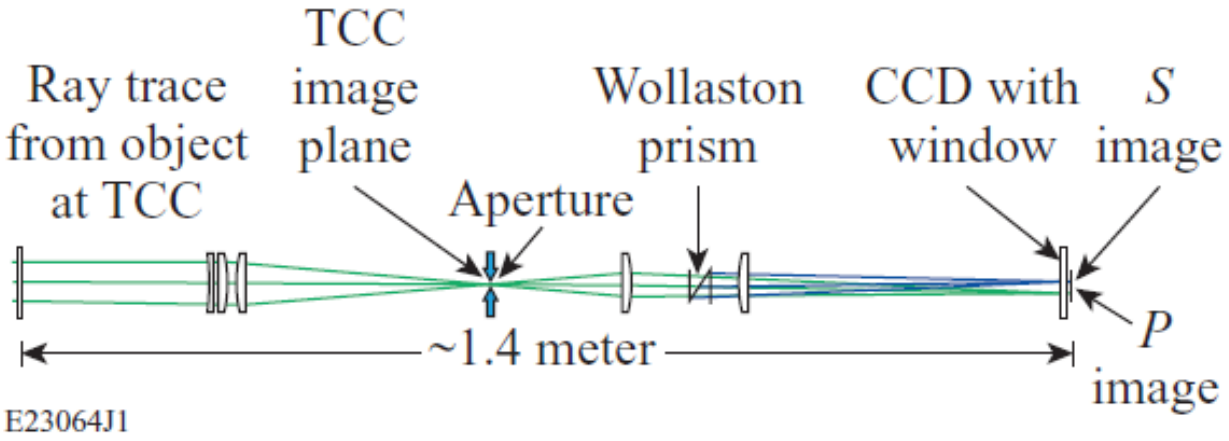

Wollaston prism

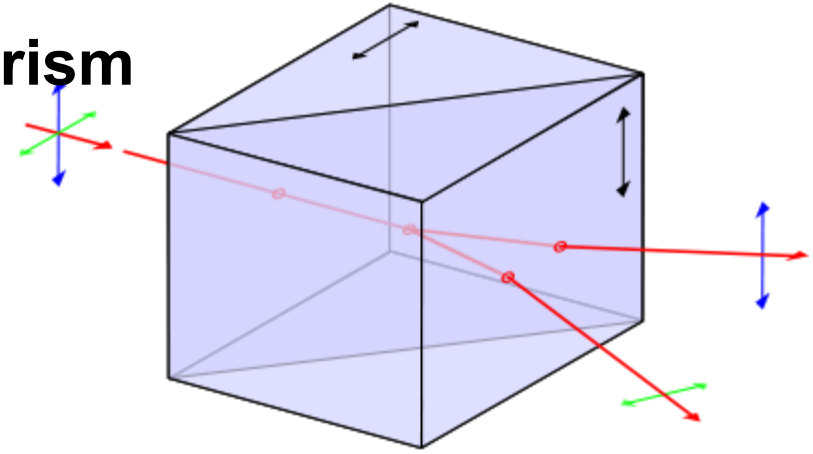

A. Davies *et al.*, Rev. Sci. Instrum. **85**, 11E611 (2014)

Self-generated field was suggested when multi-kilojoule high-intensity laser beams illuminated on an inhomogeneous plasma

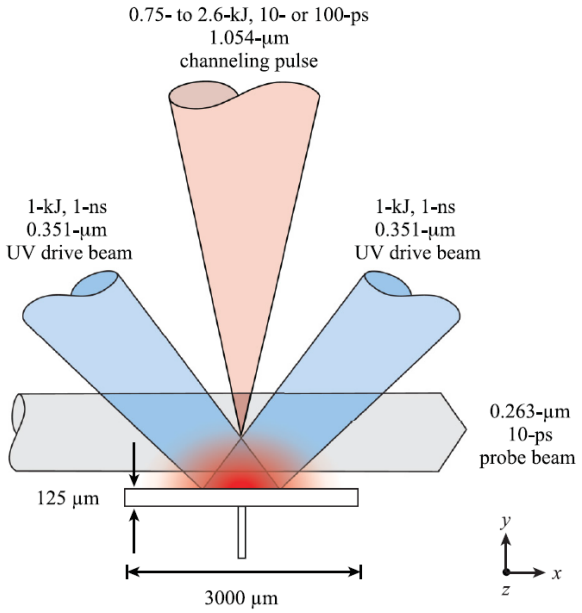

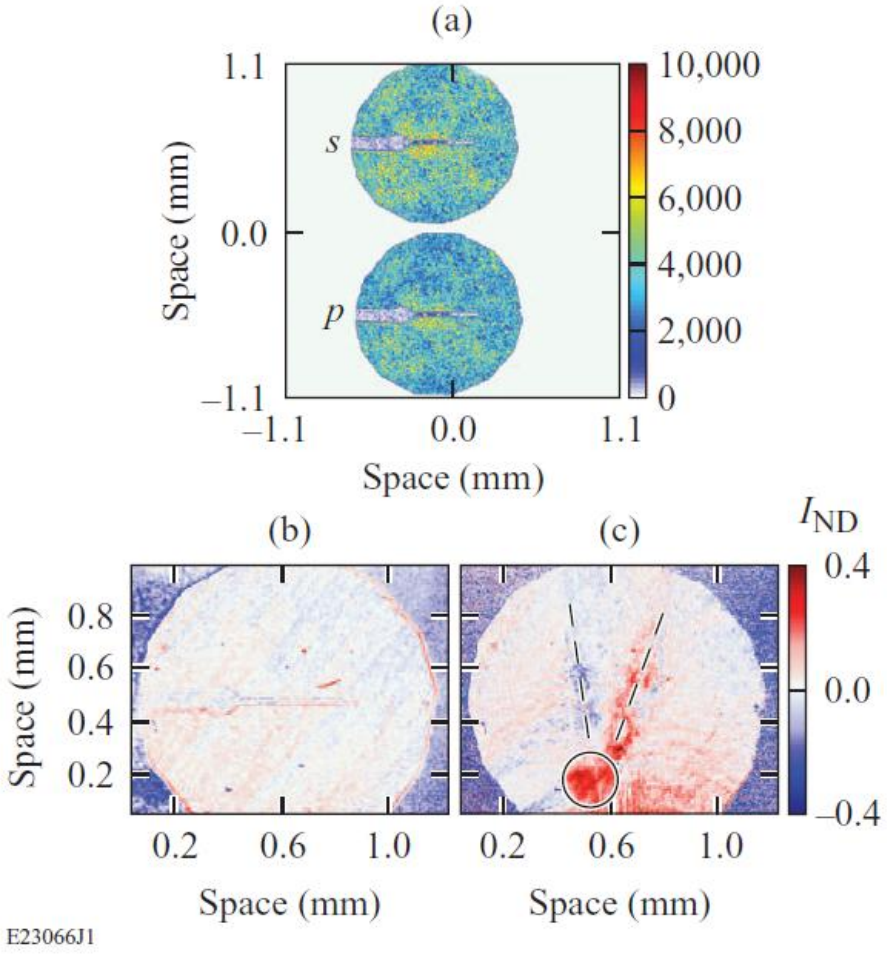

Time-resolved imaging system with temporal resolution in the order of nanoseconds was implemented

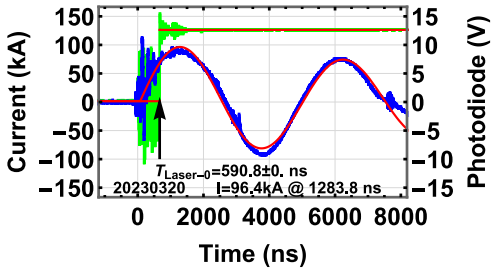

Timing determination

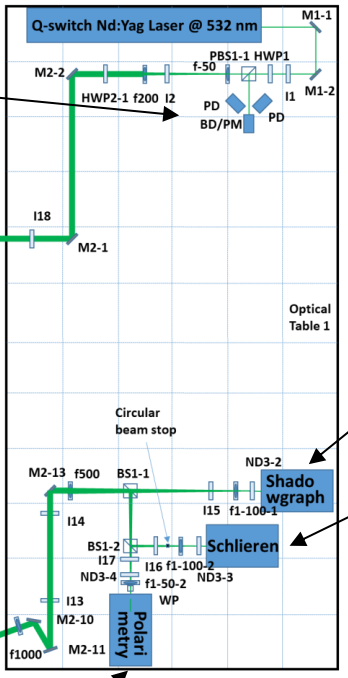

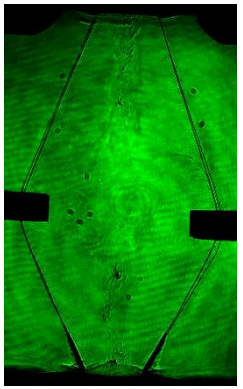

Plasma image

Plasma edge detection

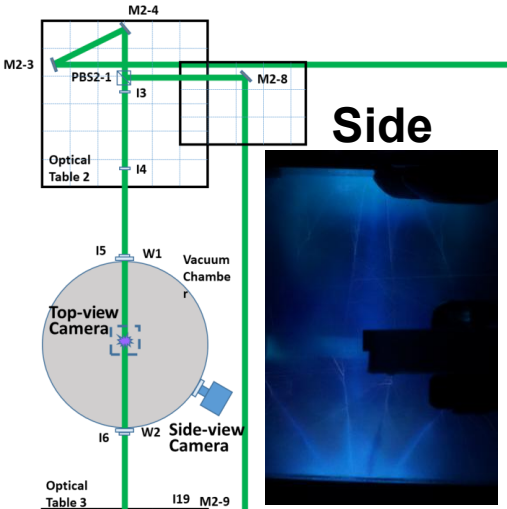

Side

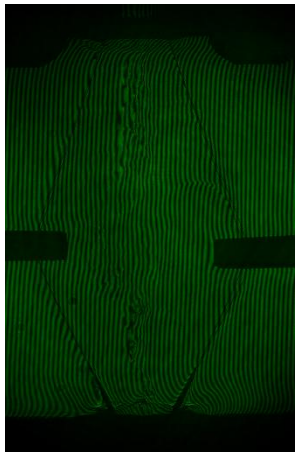

Density measurement

B field measurement

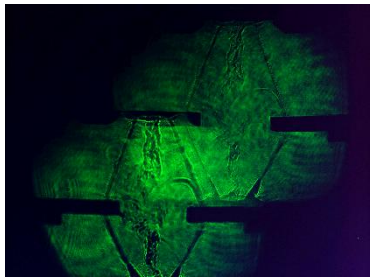

The magnetic field can be measured by measuring the deflected angle of charged particles

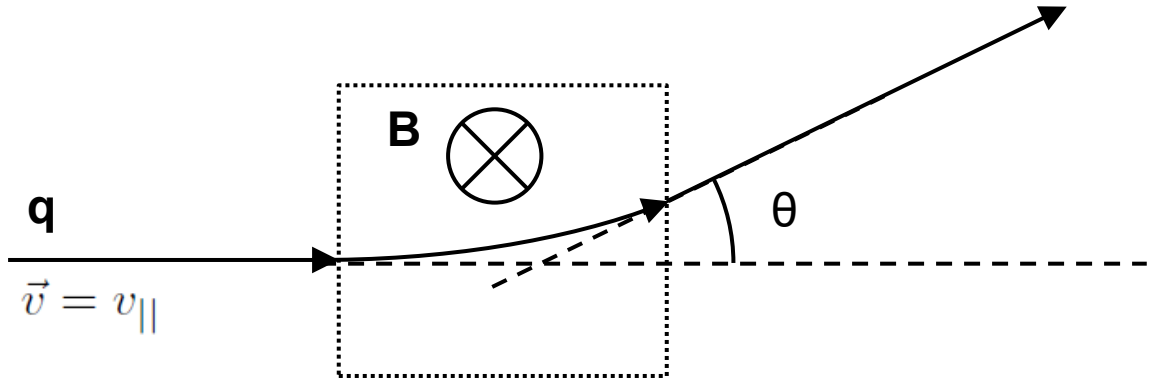

$$F_\perp = q\vec{v} \times \vec{B} = qv_{||}B = m\frac{dv_\perp}{dt}$$

$$v_\perp = \int \frac{qv_{||}B}{m}dt = \frac{qv_{||}}{m}\int Bdt\frac{dx}{dx} = \frac{qv_{||}}{m}\int \frac{B}{v_{||}}dx = \frac{q}{m}\int Bdx$$

$$\tan\theta = \frac{v_\perp}{v_{||}} = \frac{q}{mv_{||}}\int Bdx = \frac{q}{\sqrt{2mE}}\int Bdx \qquad \int Bdx = \frac{\sqrt{2mE}}{q}\tan\theta$$

Magnetic field was measured using protons

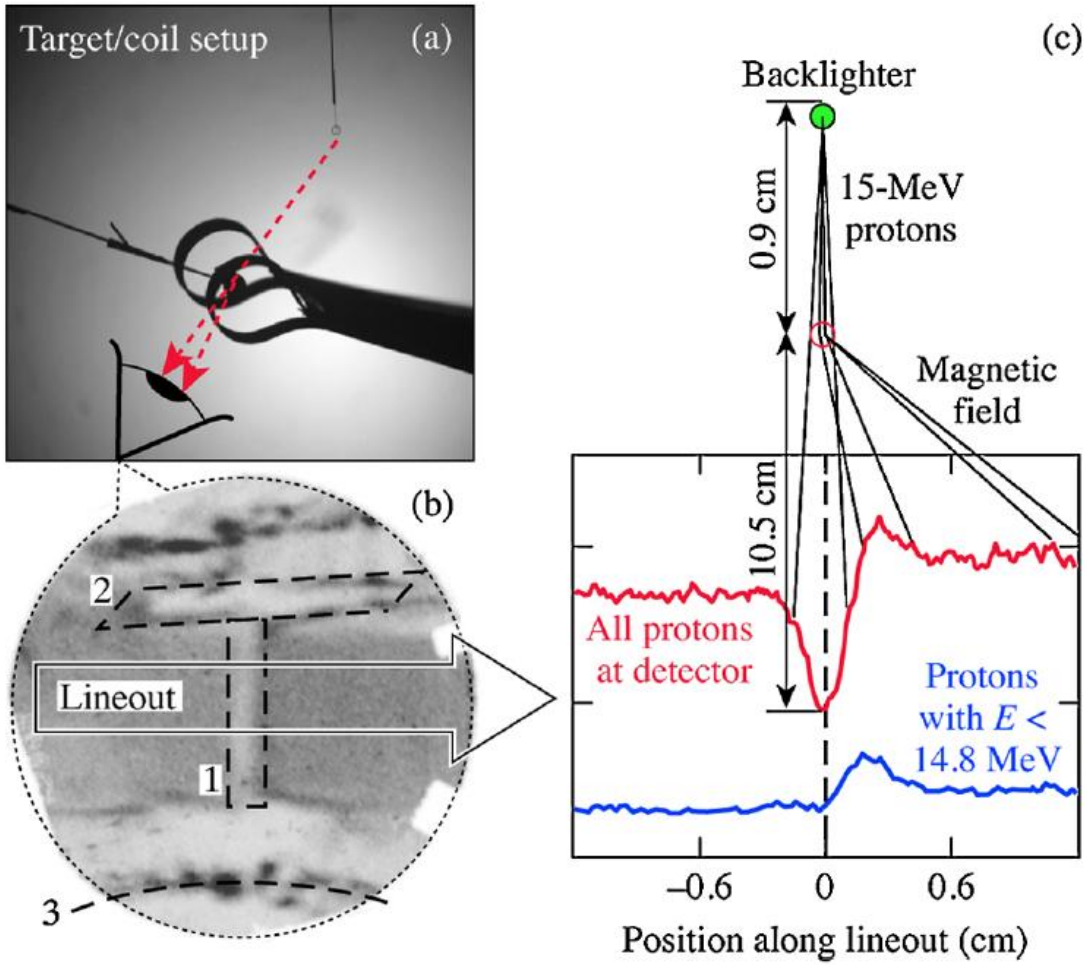

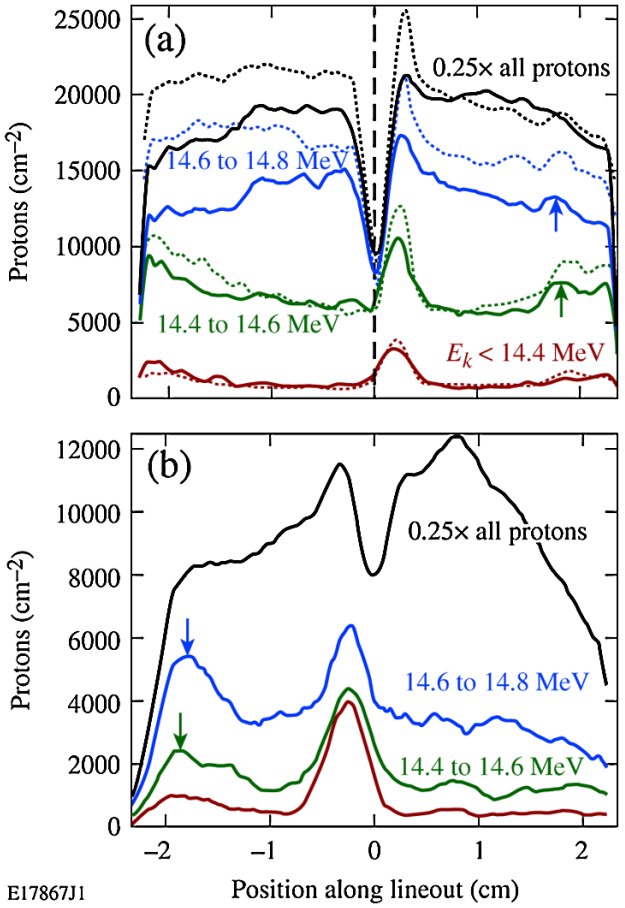

O. V. Gotchev *et al.*, Phys. Rev. Lett. **103**, 215004 (2009)

Protons can be generated from fusion product or copper foil illuminated by short pulse laser

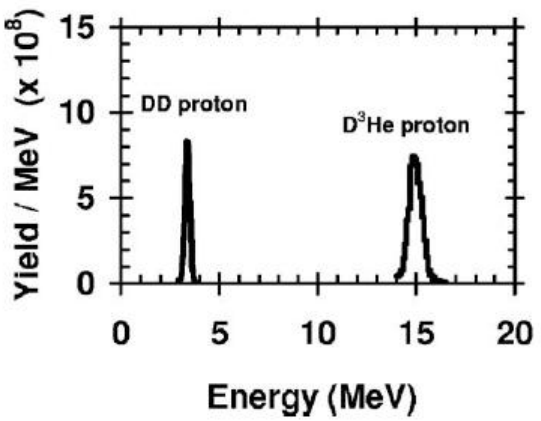

$$D + D \longrightarrow T(1.01\text{MeV}) + p(3.02\text{MeV})$$

$$D + \text{He}^3 \longrightarrow \text{He}^4(3.6\text{MeV}) + p(14.7\text{MeV})$$

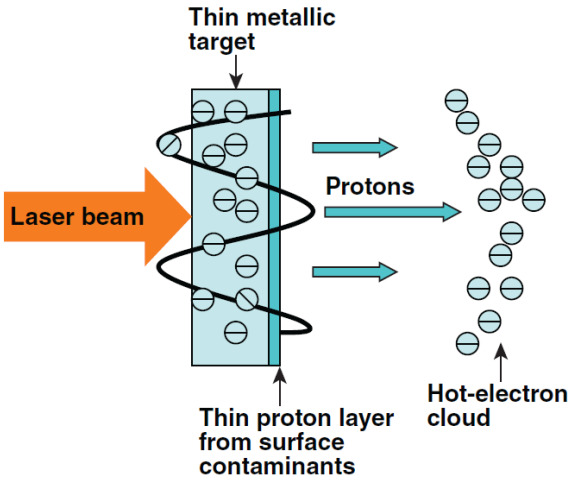

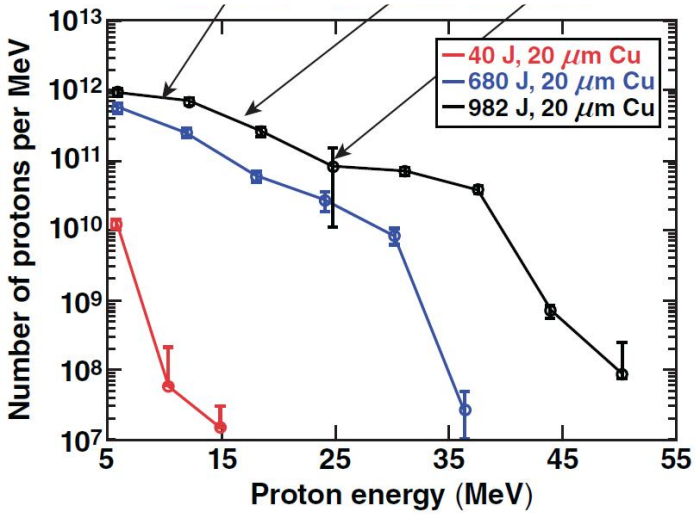

Target normal sheath acceleration (TNSA)

C. K. Li *et al.*, Rev. Sci. Instrum. **77**, 10E725 (2006)
L. Gao, PhD Thesis

Protons can leave tracks on CR39 or film

CR 39

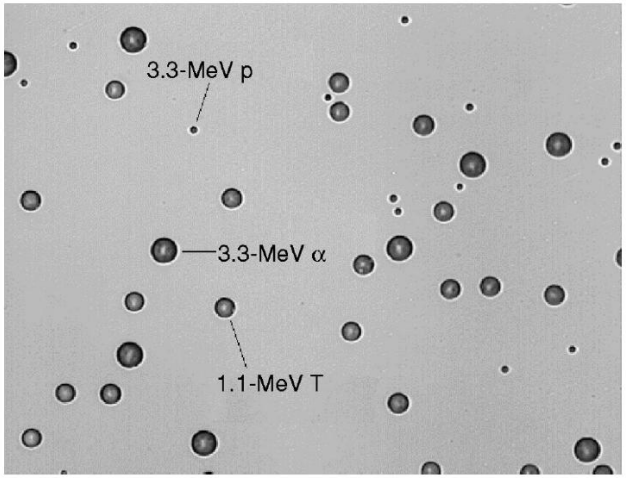

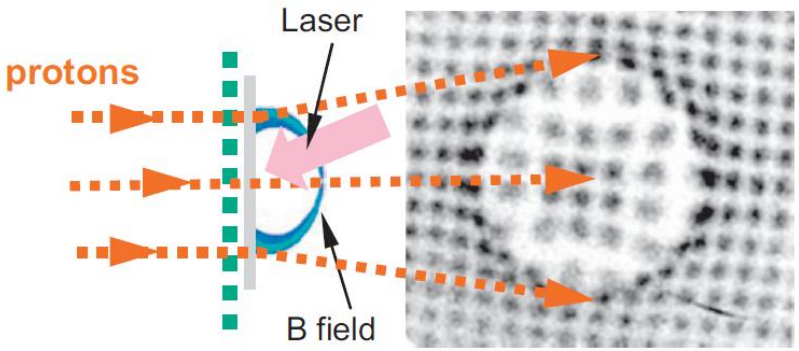

Radiochromic film pack

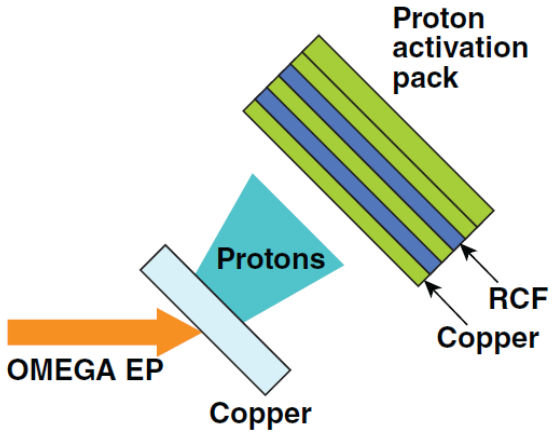

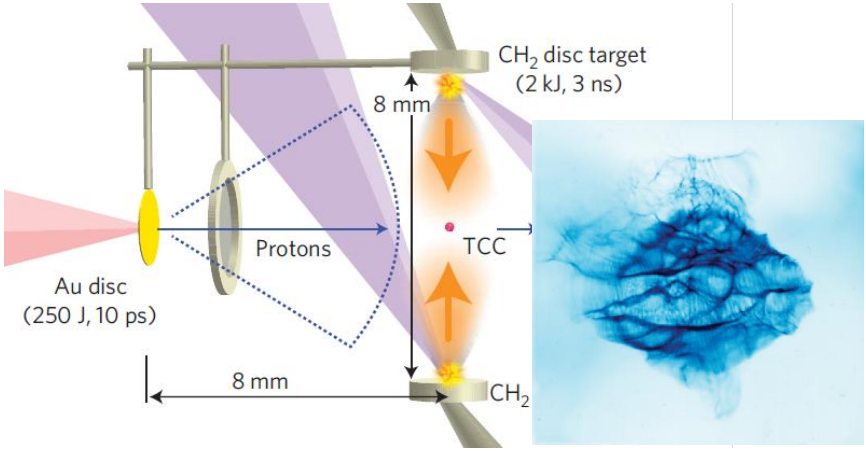

F. H. Seguin *et al.*, Rev. Sci. Instrum. **74**, 975 (2003)
C. K. Li *et al.*, Phys. Plasmas **16**,056304 (2009)
L. Gao, PhD Thesis
N. L. Kugland et al., Nature Phys. B, 809 (2012)

Track diameter on the CR39 is depended on the particle energy that incidents

CR 39

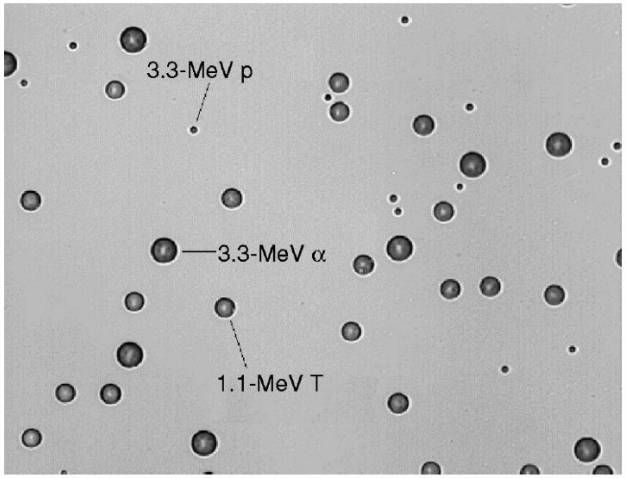

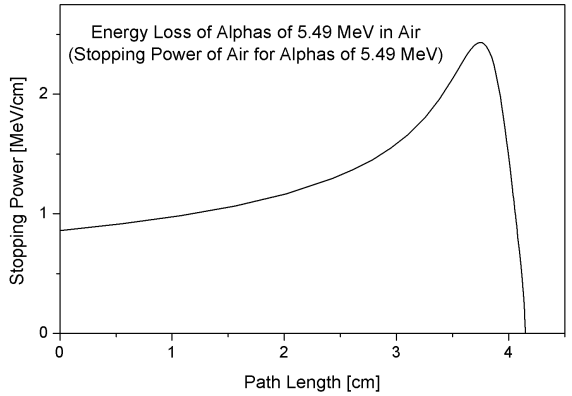

Low energy particle

Etched with NaOH with different etching time.

High energy particle

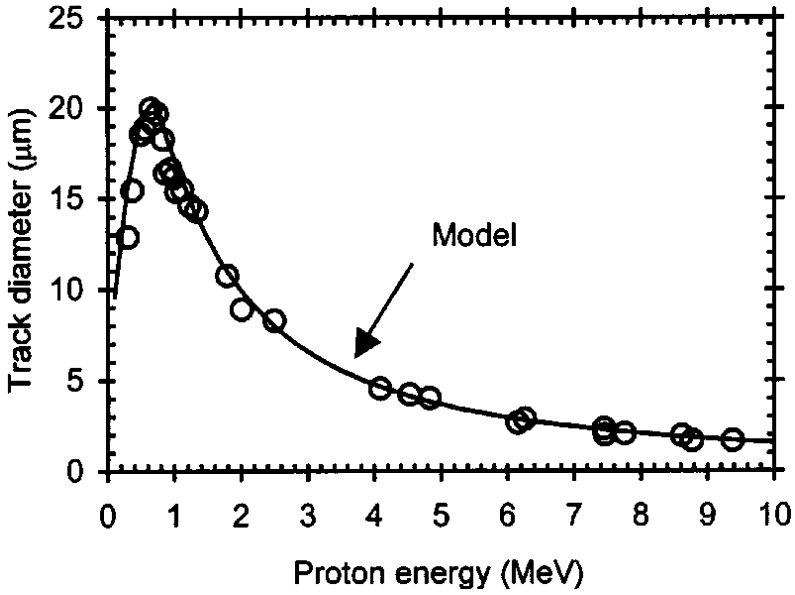

F. H. Seguin *et al.*, Rev. Sci. Instrum. **74**, 975 (2003)

Time dependent magnetic field can be measured using B-dot probe

$$\vec{B} = \vec{B}(t) \qquad \nabla \times \vec{E} = -\frac{\partial \vec{B}}{\partial t}$$

$$\int d\vec{A}\, \nabla \times \vec{E} = \oint \vec{E}\, d\vec{l} = V = -\int d\vec{A}\, \frac{\partial \vec{B}}{\partial t}$$

$$V \sim -A\frac{\partial B}{\partial t} \qquad B = -\int \frac{V}{A} dt \sim -\frac{1}{A}\int V dt$$

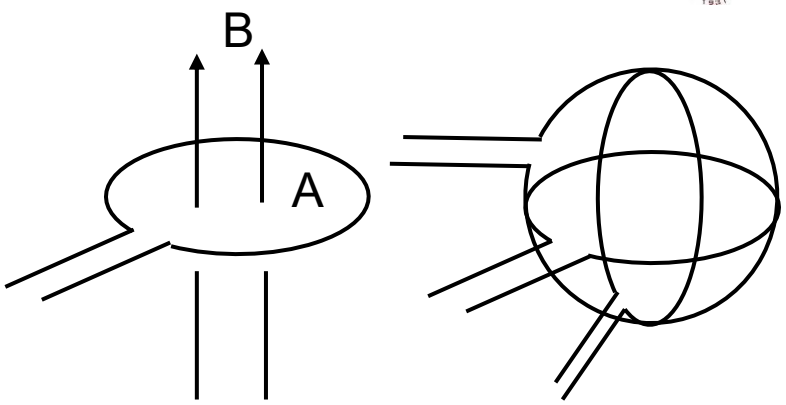

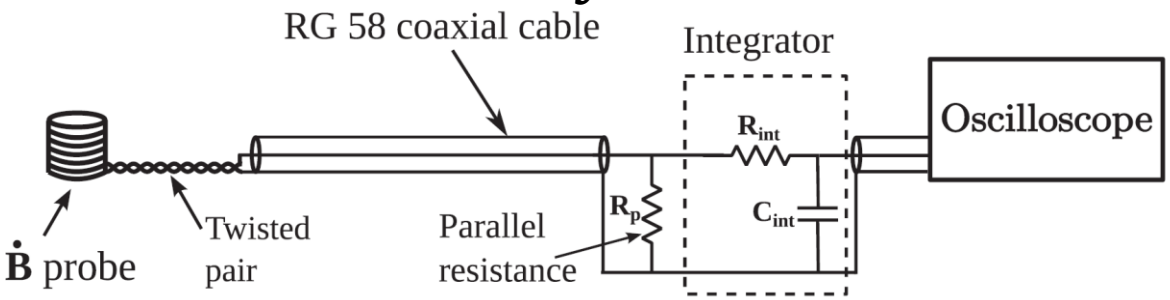

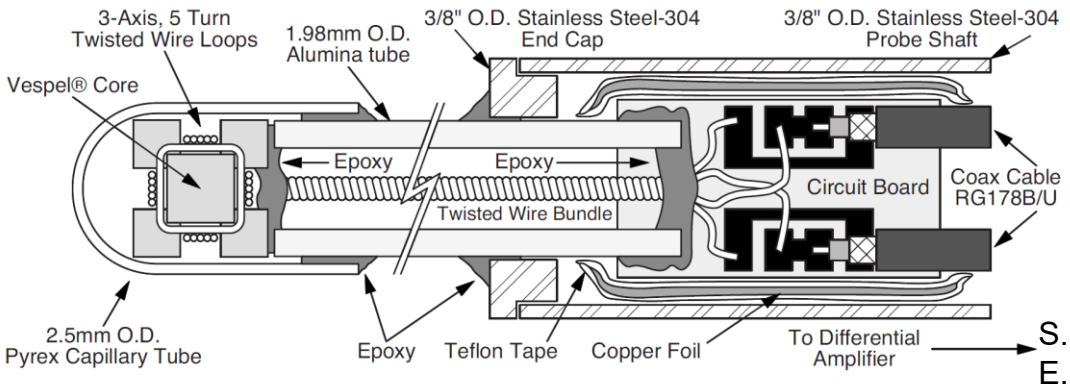

S. Bose *et al.*, Eur. J. Phys. **40**, 015803 (2019)
E. T. Everson *et al.*, Rev. Sci. Instrum. **80**, 113505 (2009)

Time dependent magnetic field can be measured using B-dot probe

$$\vec{B} = \vec{B}(t) \qquad \nabla \times \vec{E} = -\frac{\partial \vec{B}}{\partial t}$$

$$\int d\vec{A}\, \nabla \times \vec{E} = \oint \vec{E}\, d\vec{l} = V = -\int d\vec{A}\, \frac{\partial \vec{B}}{\partial t}$$

$$V \sim -A\frac{\partial B}{\partial t} \qquad B = -\int \frac{V}{A} dt \sim -\frac{1}{A}\int V dt$$

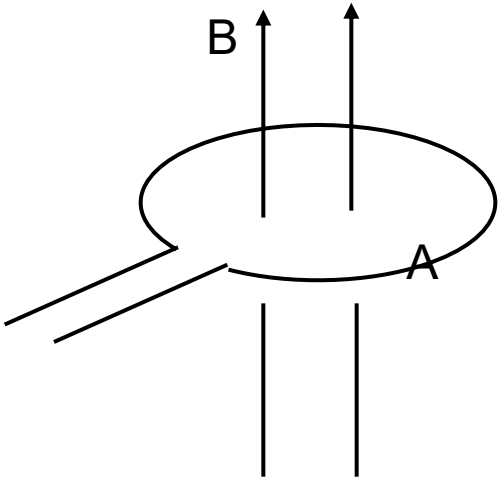

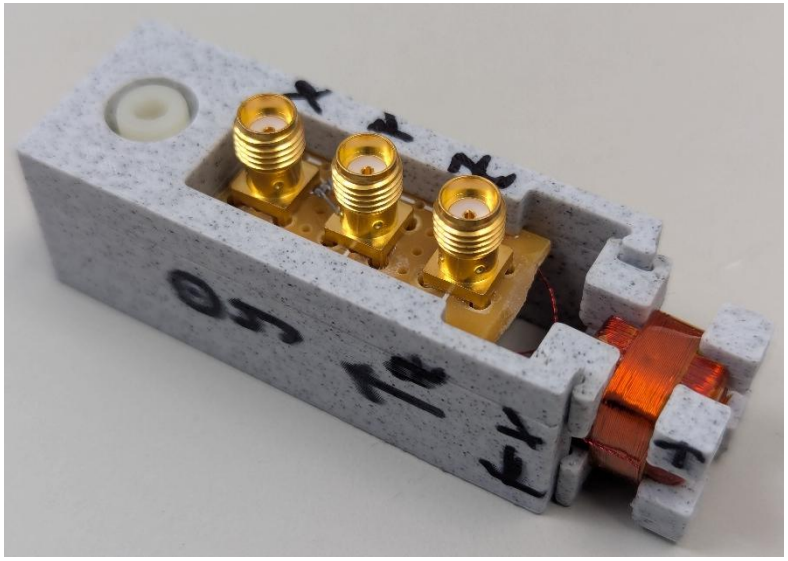

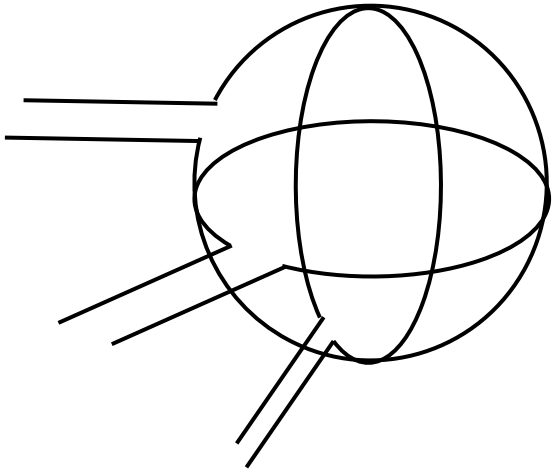

Courtesy by 林耕宇.

The signal from the B-dot probe is integrated and amplified

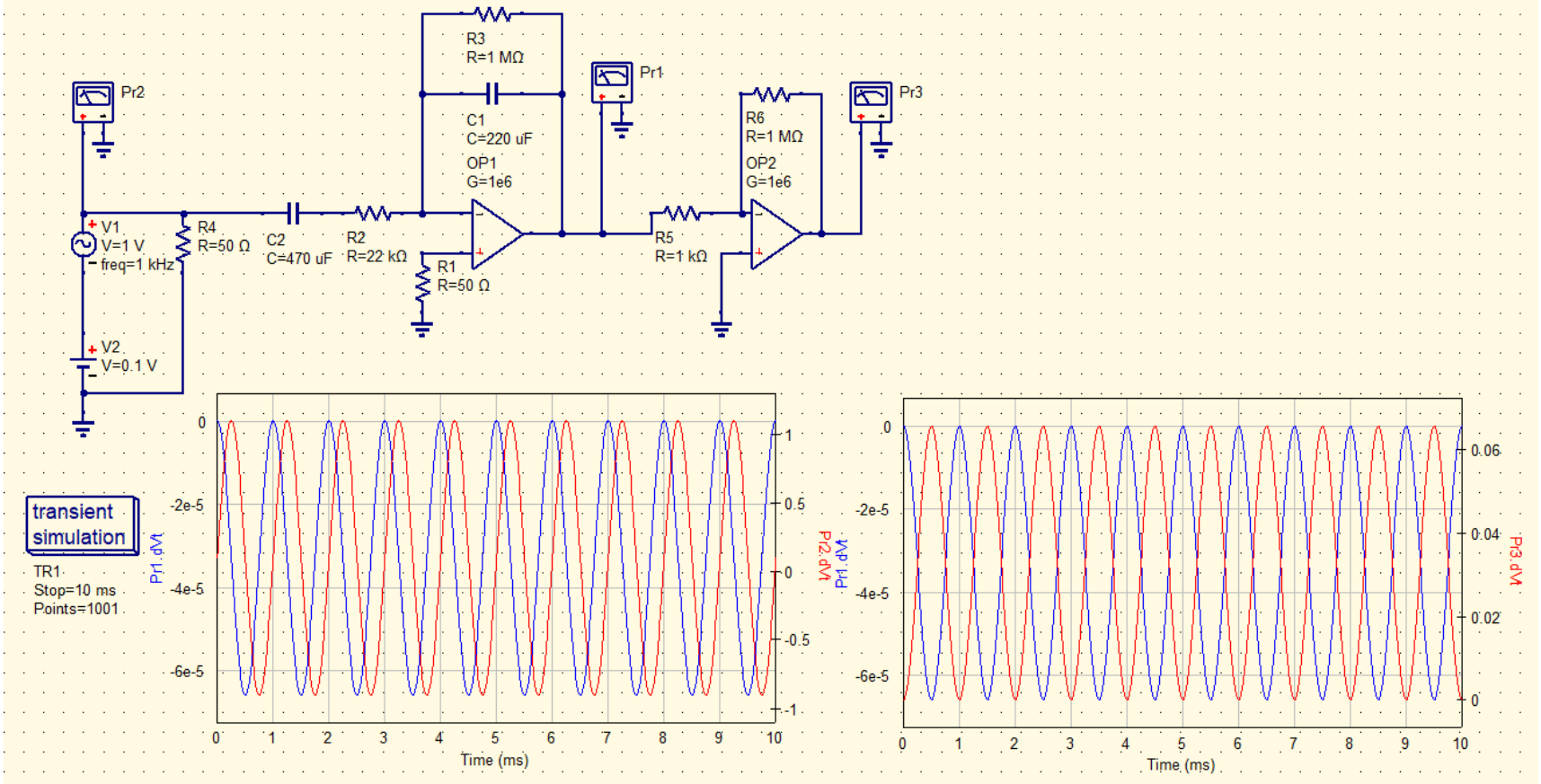

Courtesy by 柯智瀚.

B-dot probe experiments

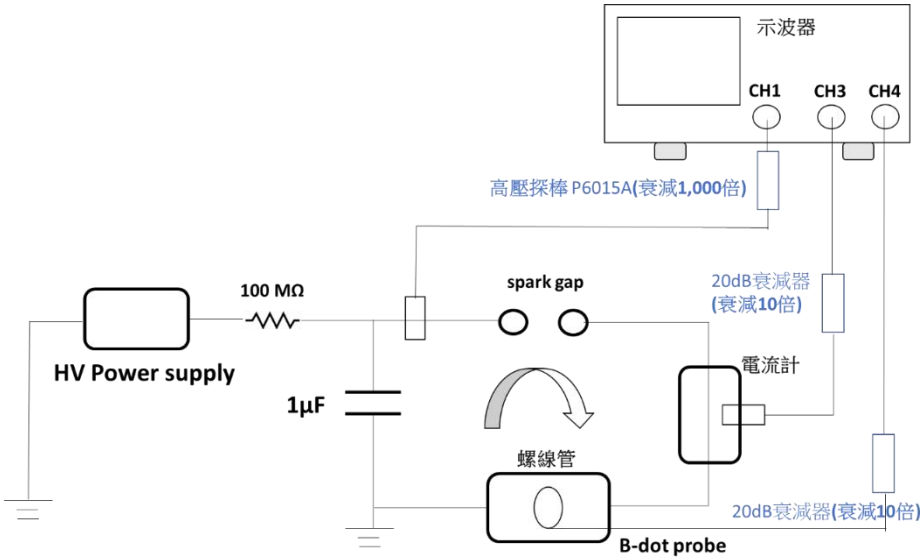

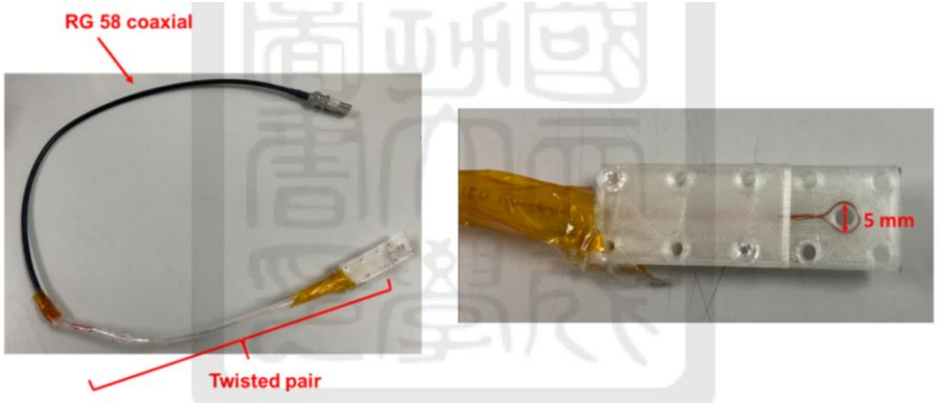

- **Without integrator**

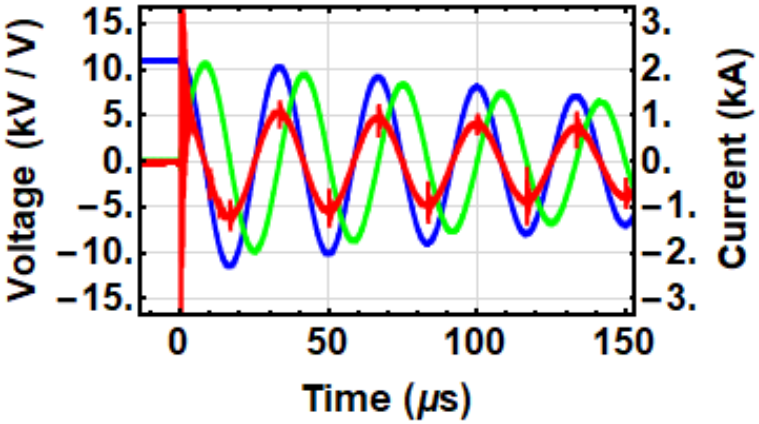

- **With integrator**

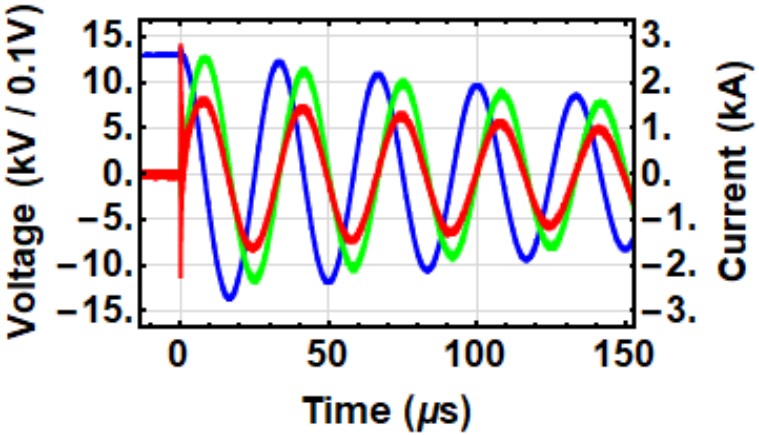

Cheng-Han Du's experimental report.

A Thomson parabola uses parallel electric and magnetic fields to deflect particles onto parabolic curves that resolve q/m

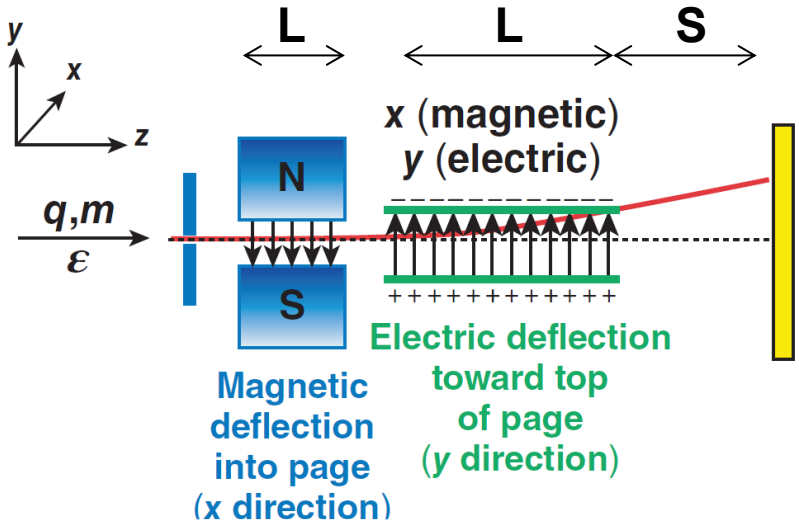

- Deflection caused by magnetic field ~q/p
- Deflection caused by electric field ~q/KE
- Ion traces form parabolic curves on detector plane

$$y = \frac{m}{q}\frac{E}{B^2SL}x^2$$

$$F_x = qv_{||}B = m\frac{dv_x}{dt}$$

$$v_x = \frac{q}{m}v_{||}B\Delta t = \frac{q}{m}v_{||}B\frac{L}{v_{||}} = \frac{qBL}{m}$$

$$\tan\theta_x = \frac{v_x}{v_{||}} = \frac{qBL}{mv_{||}} = \frac{qBL}{\sqrt{2m\epsilon}}$$

$$F_y = qE = m\frac{dv_y}{dt}$$

$$v_y = \frac{q}{m}E\Delta t = \frac{q}{m}E\frac{L}{v_{||}} = \frac{qEL}{mv_{||}}$$

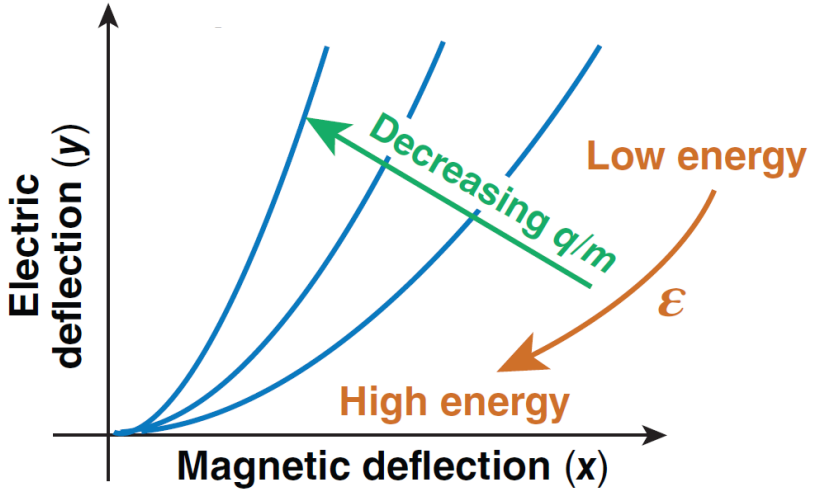

$$\tan\theta_y = \frac{v_y}{v_{||}} = \frac{qEL}{mv_{||}^2} = \frac{qEL}{2\epsilon}$$

E16717b

A faraday cup measures the flux of charge particles

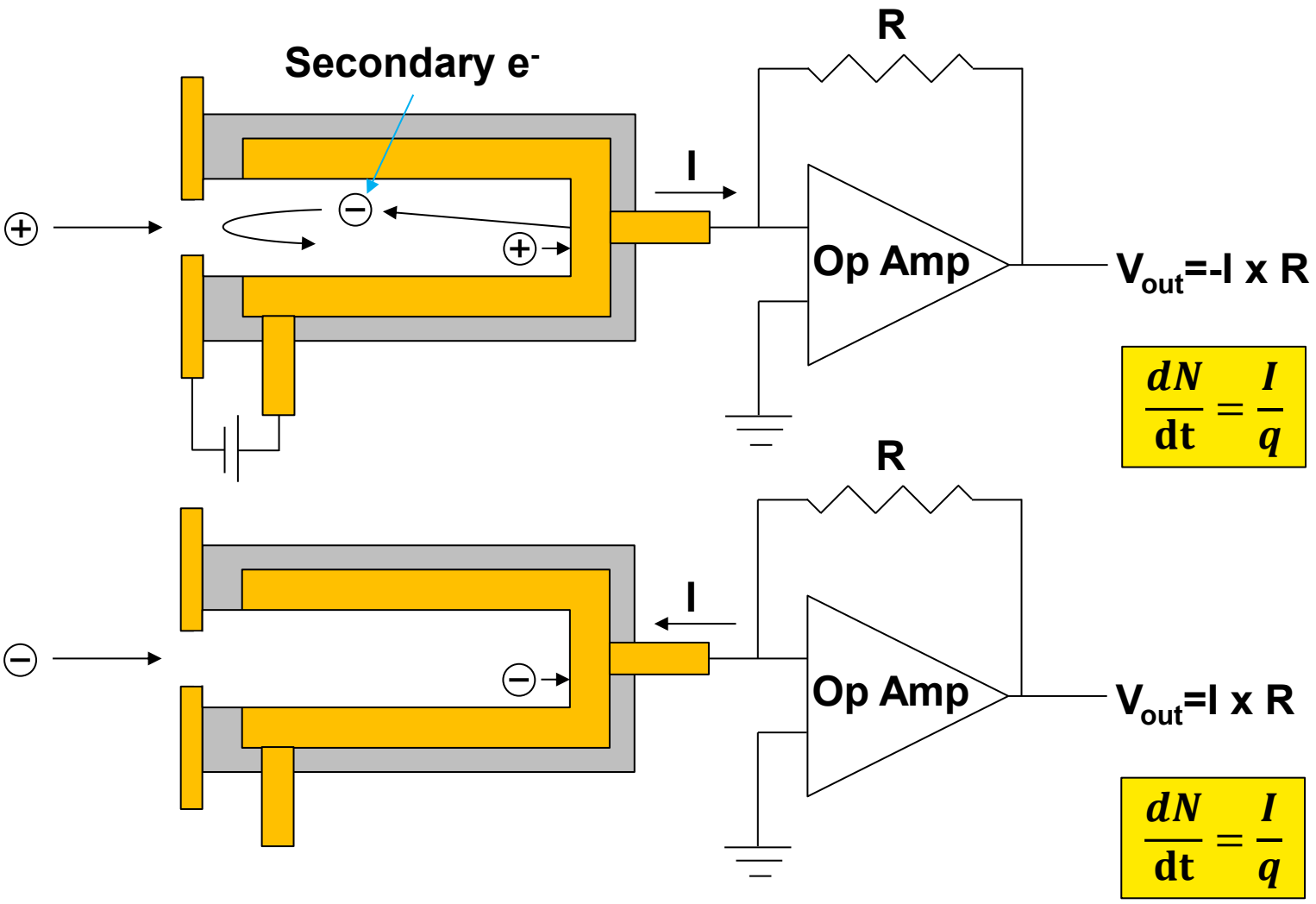

Retarding potential analyzer measures the energy / velocity distribution function

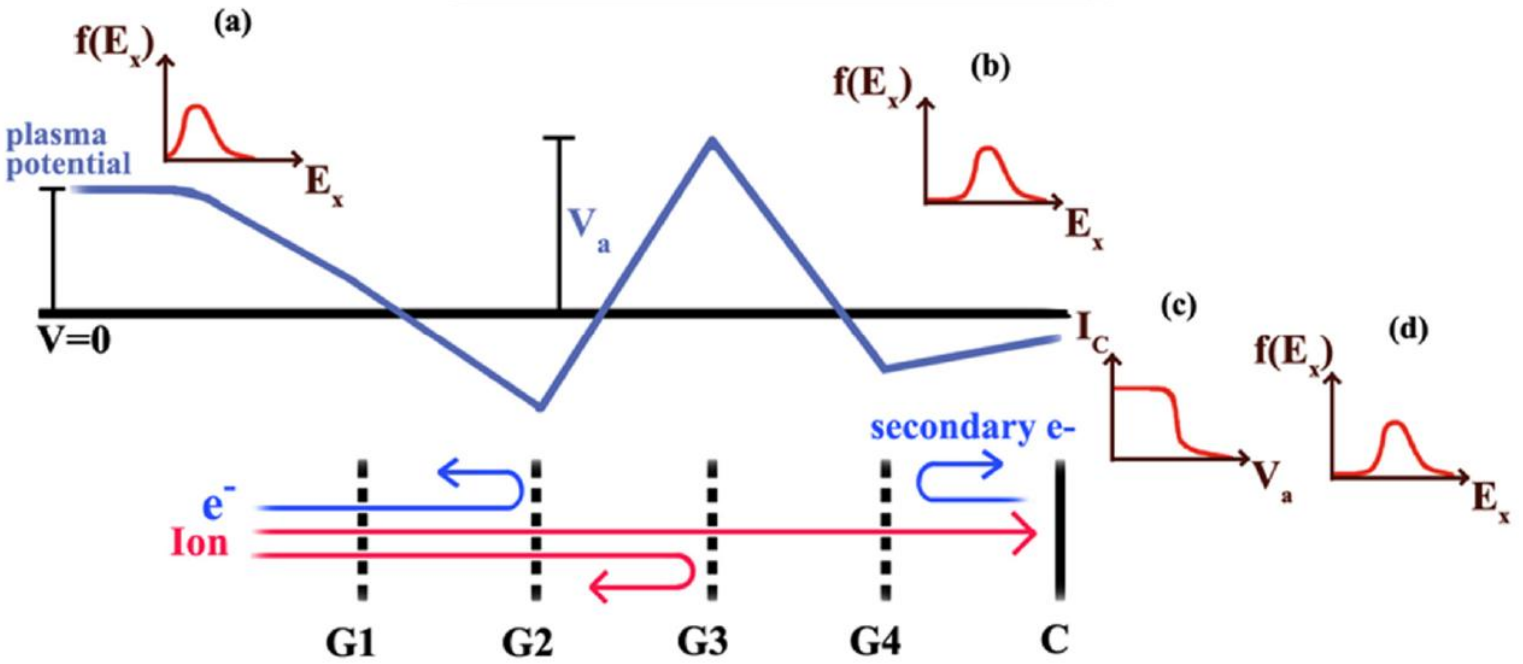

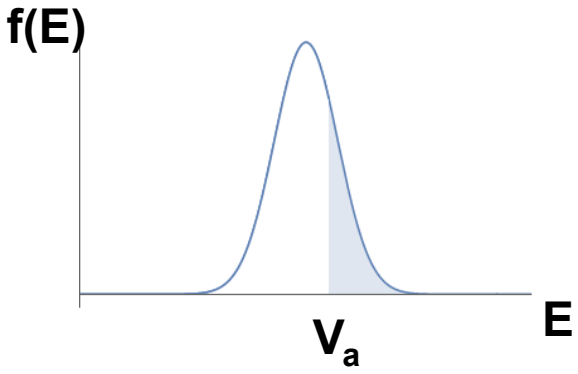

H.-K. Fang, 2015 NCKU Ph. D. Thesis, Ion measurements of ionosphere plasma in space plasma operation chamber

The photon energy spectrum provides valuable information

- Plasma conditions can be determined from the photon spectrum
  - visible light: absorption and laser-plasma interactions
  - x rays: electron temperature, density, plasma flow, material mixing
- There are three basic tools for determining the spectrum detected
  - filtering
  - grating spectrometer
  - Bragg spectrometer

Spectrum can be obtained using grating

- **Grating is used to disperse the light**

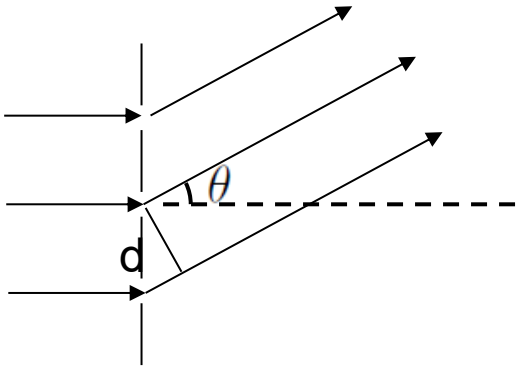

$$d\sin\theta = m\lambda$$

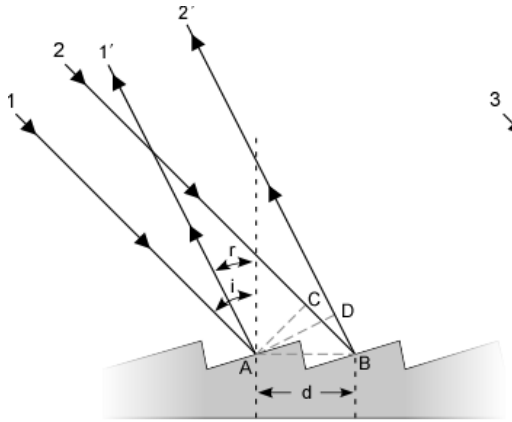

nλ = d(sin(i) + sin (r))

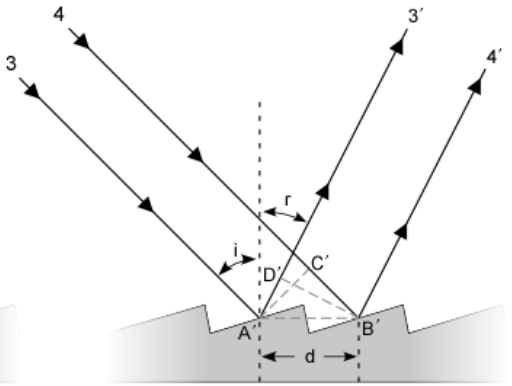

nλ = d(sin(i) - sin (r))

- **Bragg condition in the crystal is used for X-ray.**

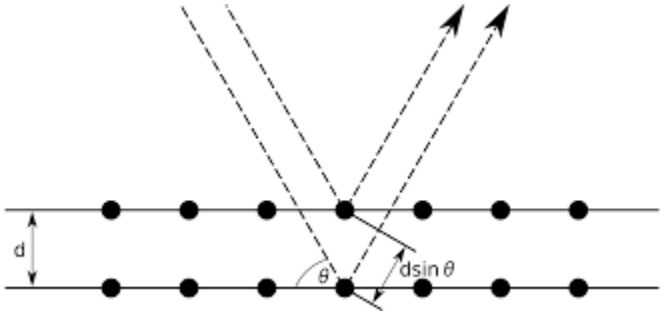

$$2d\sin\theta = m\lambda$$

Temperature and density can be obtained from the emission

Line emission

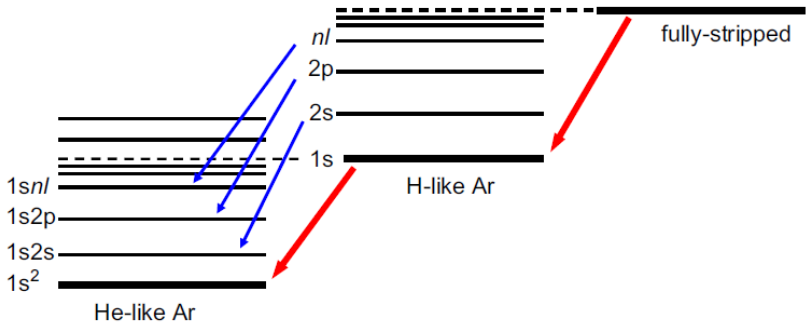

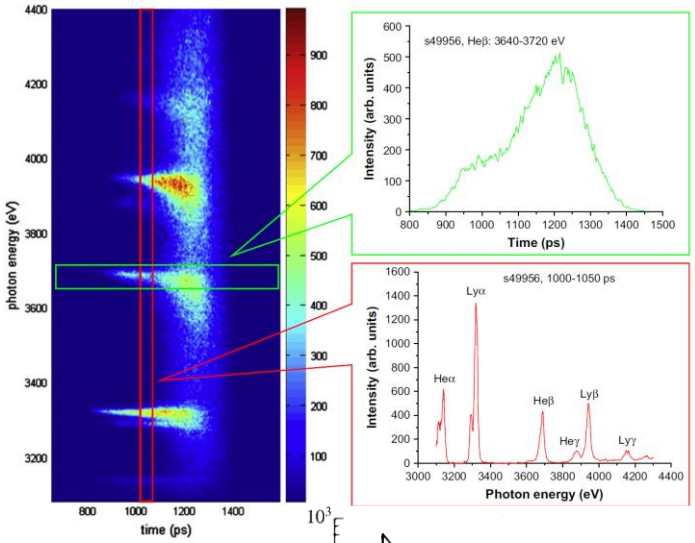

Bremsstrahlung emission

$$\eta_\nu = \frac{16\pi}{3\sqrt{6\pi}} \frac{e^6}{m_e^2 c^3} \frac{Z_i^2 n_e}{\sqrt{k_B T_e / m_e} A m_p} \exp\left(-\frac{h\nu}{k_B T_e}\right)$$

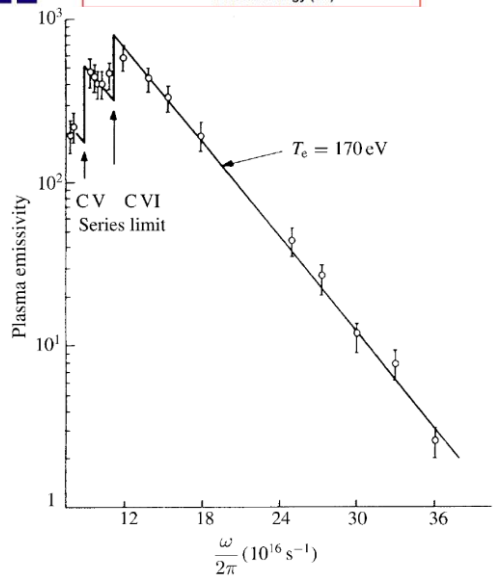

R. Florido *et al.*, High Energy Dens. Phys. **6**, 70 (2010)

Information of x-ray transmission or reflectivity over a surface can be obtained from the Center for X-Ray Optics

- **http://henke.lbl.gov/optical_constants/**

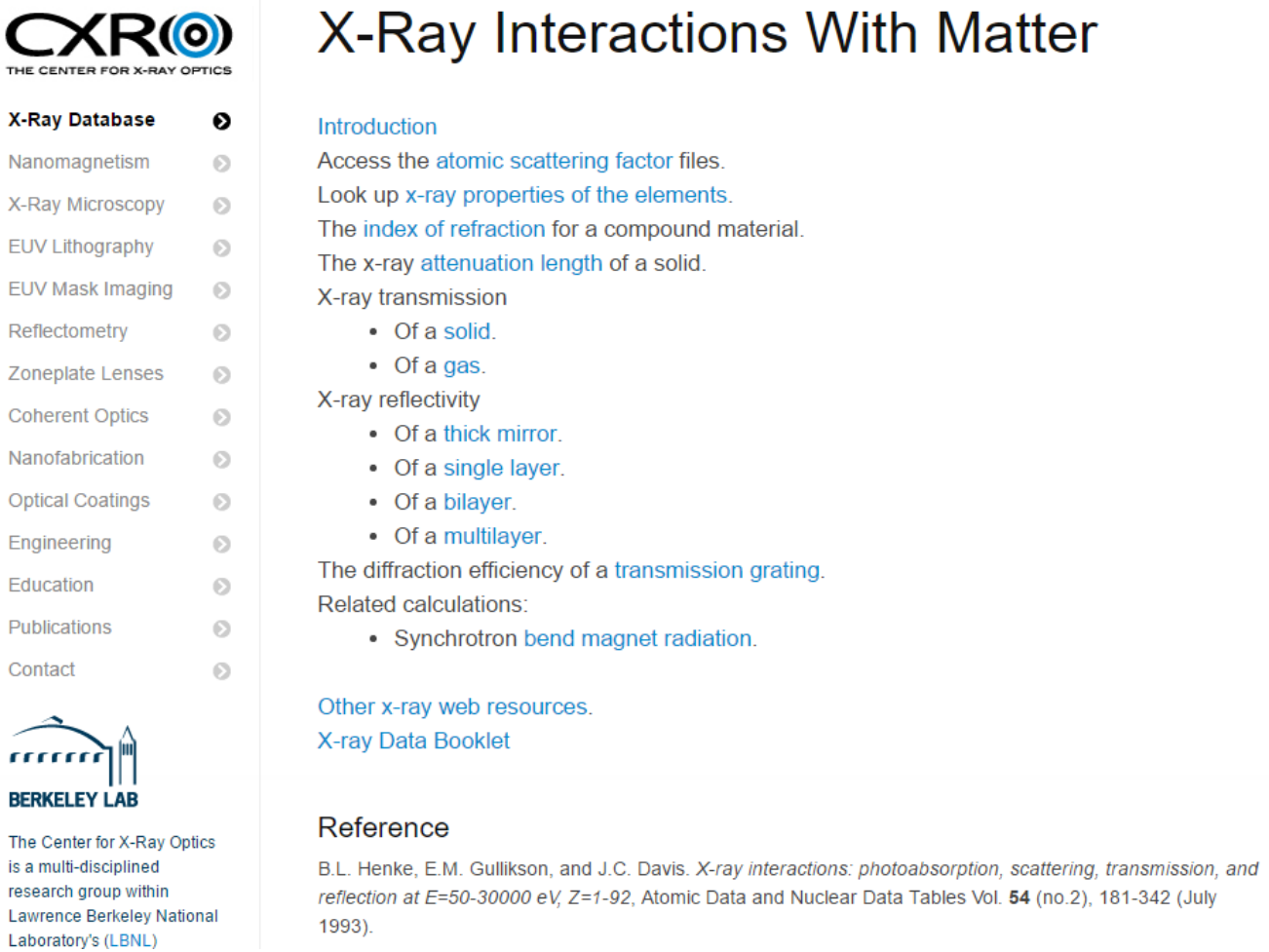

A band pass filter is obtained by combing a filter and a mirror

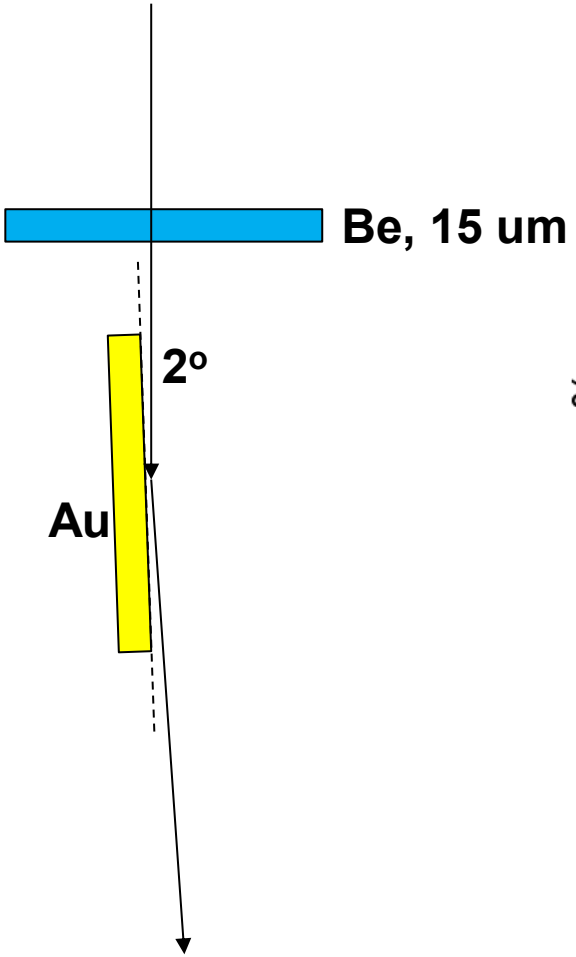

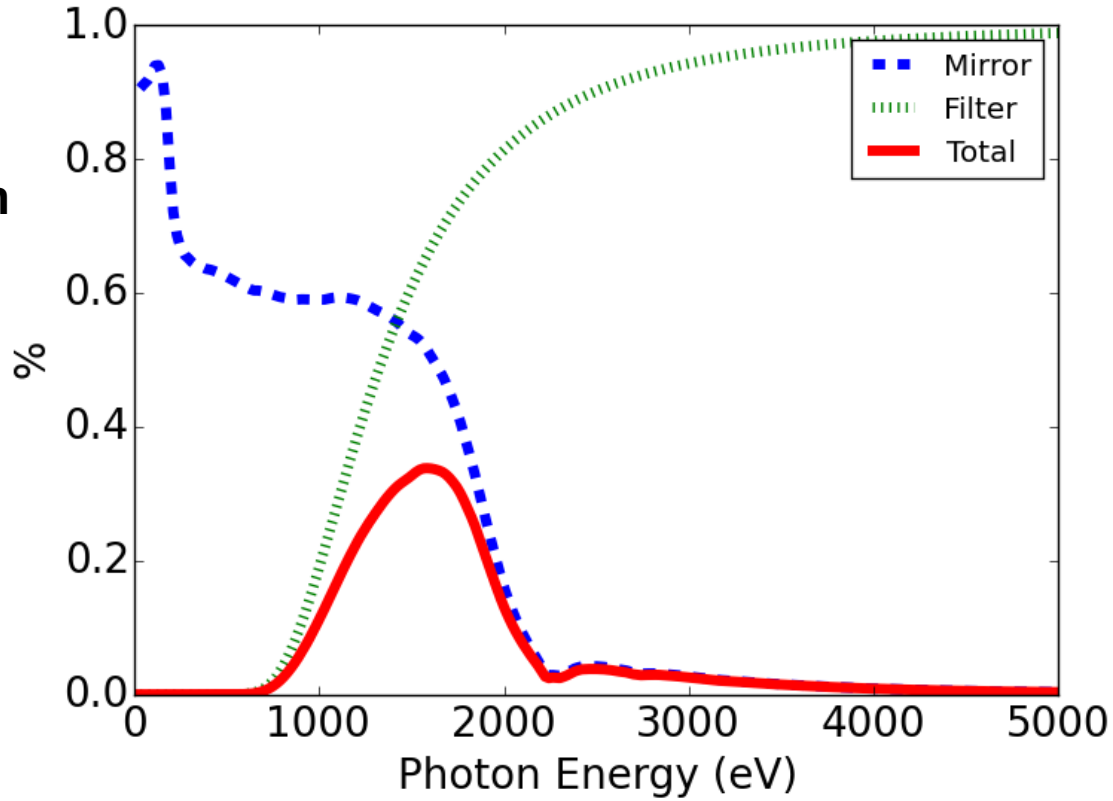

X rays can not be concentrated by lenses

- X-ray refractive indices are less than unity, $n \lesssim 1$
- For those with lower refractive indices, the absorption is also strong
- X-ray mirrors can be made through
  - Bragg reflection
  - External total reflection with a small grazing angle

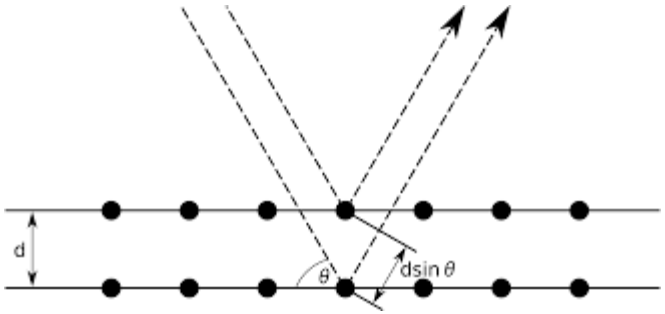

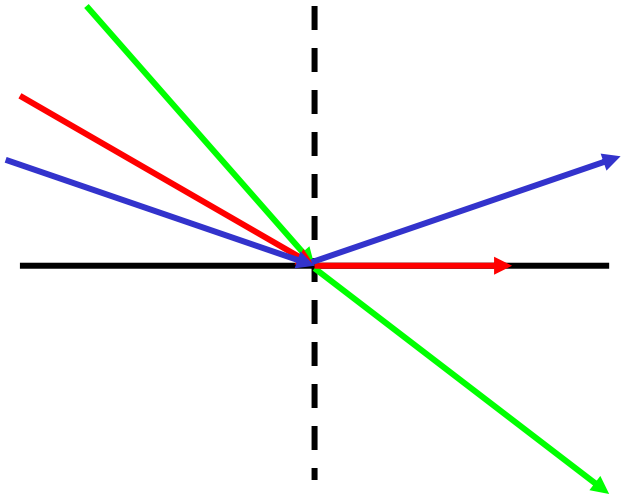

The simplest imaging device is a pinhole camera

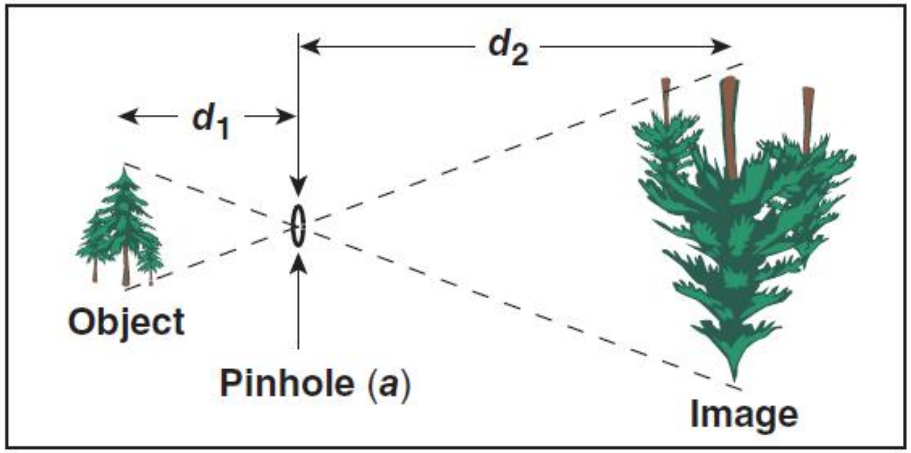

Kodak Brownie camera

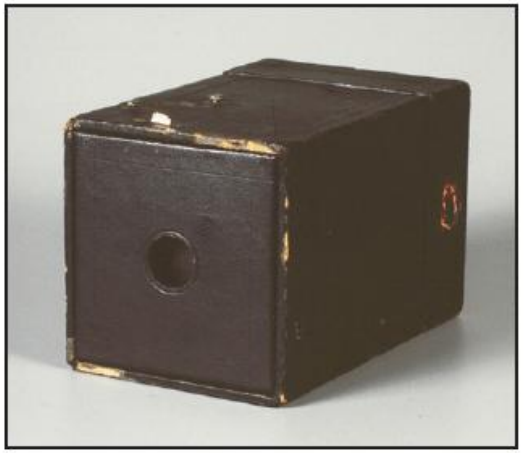

- Magnification = $\frac{d_2}{d_1}$
- Infinite depth of field (variable magnification)
- Pinhole diameter determines
  - resolution ~a
  - light collection: $\Delta\Omega = \frac{\pi}{4}\frac{a^2}{d_1^2}$

Imaging optics (e.g., lenses) can be used for higher resolutions with larger solid angles.

E13982a

2D images can be taken using charge injection device (CID) or charge coupled device (CCD)

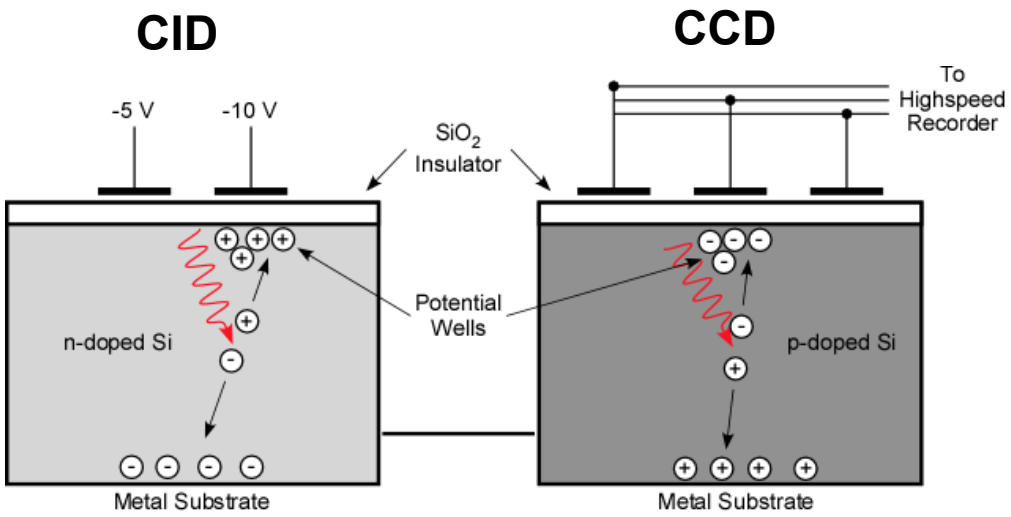

- **Color mask is used for color image**

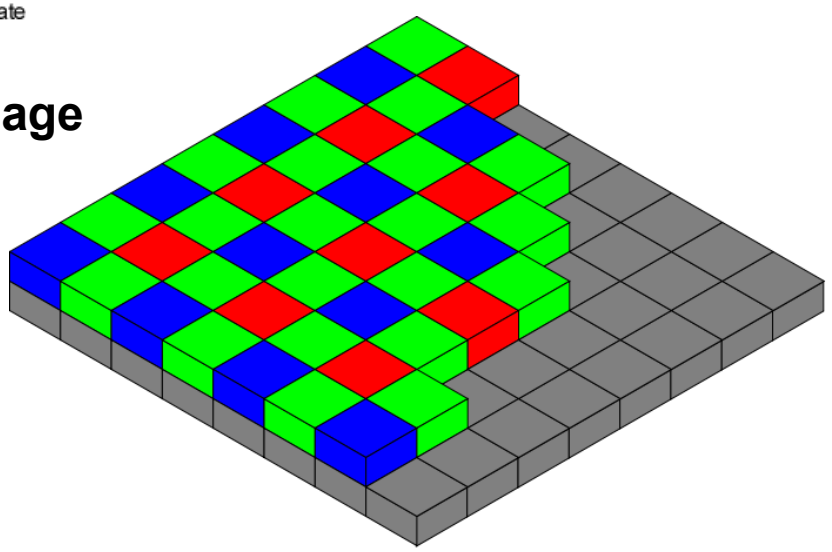

http://people.whitman.edu/~dunnivfm/FAASICPMS_Ebook/CH2/2_2_9.html
https://en.wikipedia.org/wiki/Charge-coupled_device

Charges are transferred along the array for readout in CCD

CCD readout:

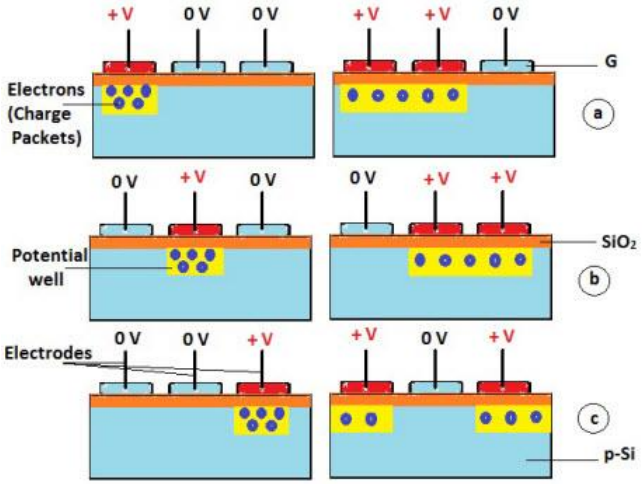

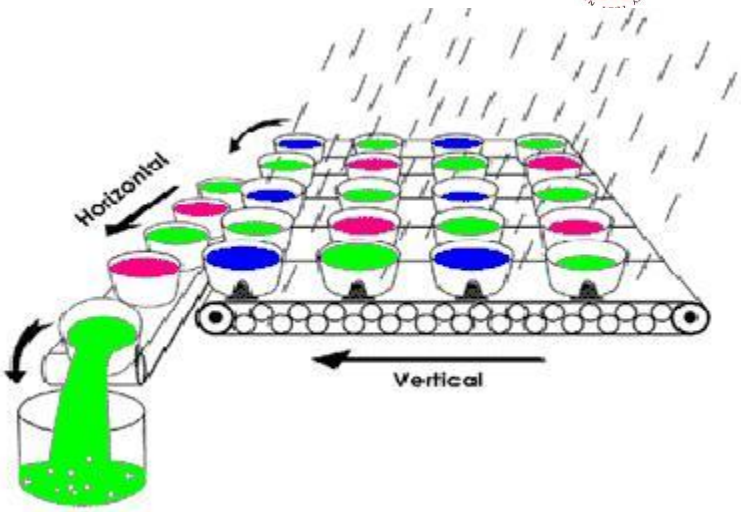

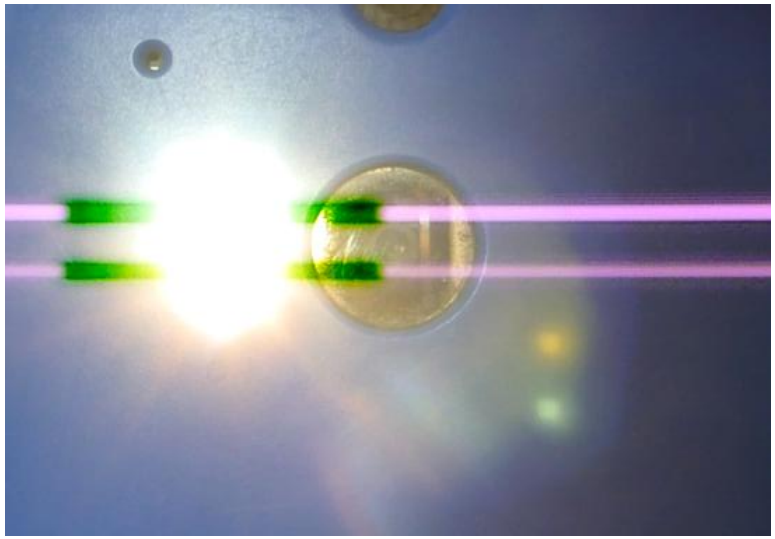

https://www.elprocus.com/know-about-the-working-principle-of-charge-coupled-device/
http://www.siliconimaging.com/ARTICLES/CMOS%20PRIMER.htm

Signal is readout individually in CMOS sensor

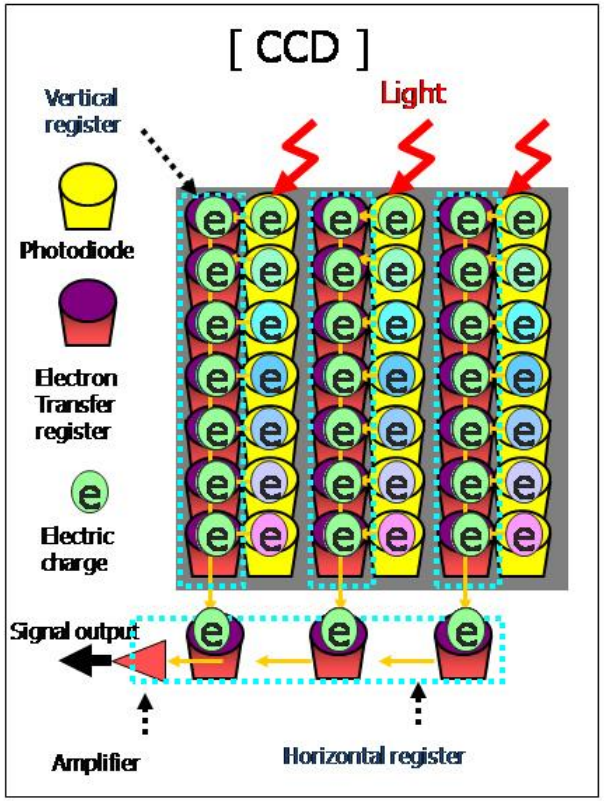

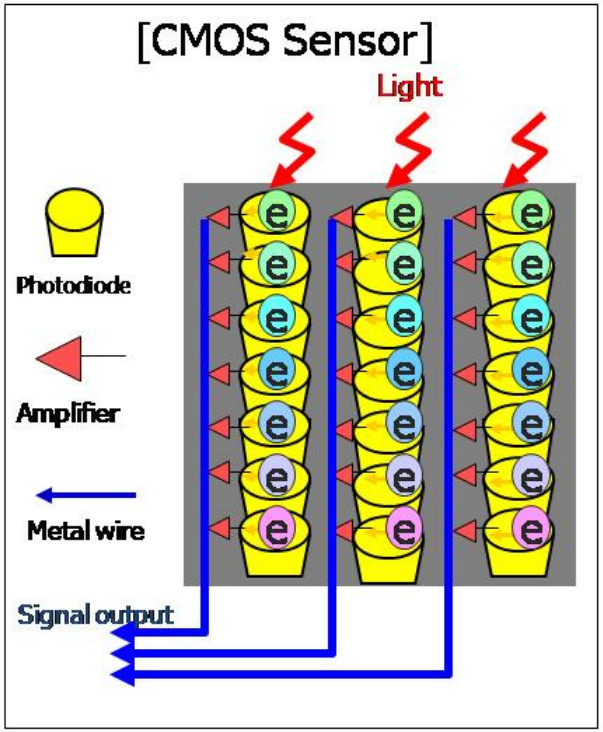

http://www.digitalbolex.com/global-shutter/

Electronic detectors provide rapid readout

- Electronic detectors are typically semiconductors or ionization-based stacks (e.g., photomultipliers)

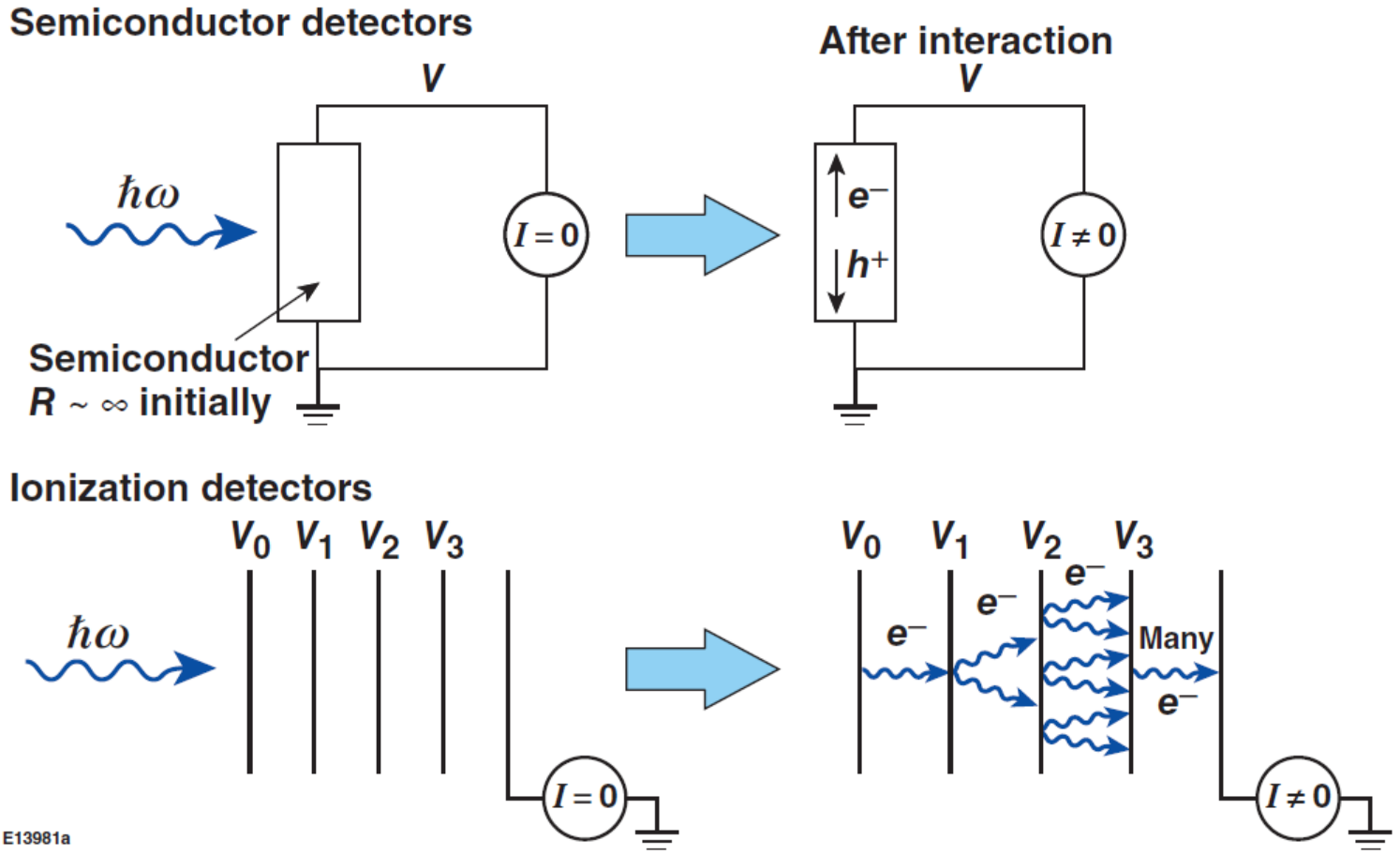

The number of electrons can be increased through photomultipliers or microchannel plate (MCP)

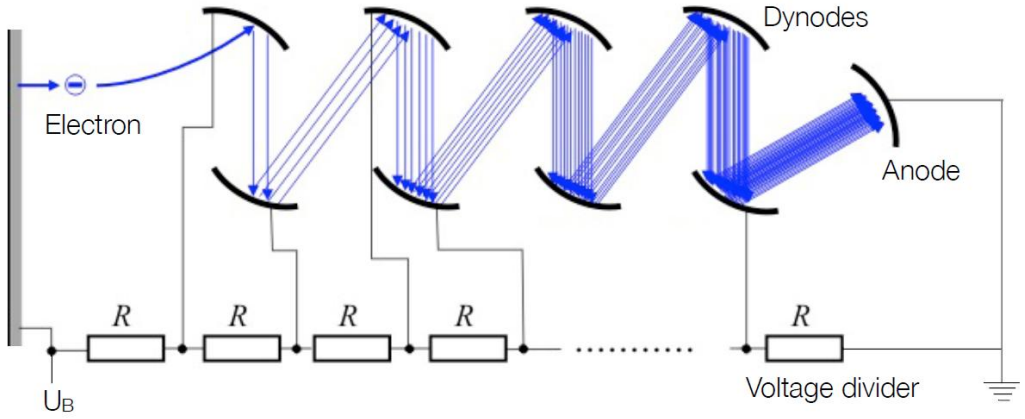

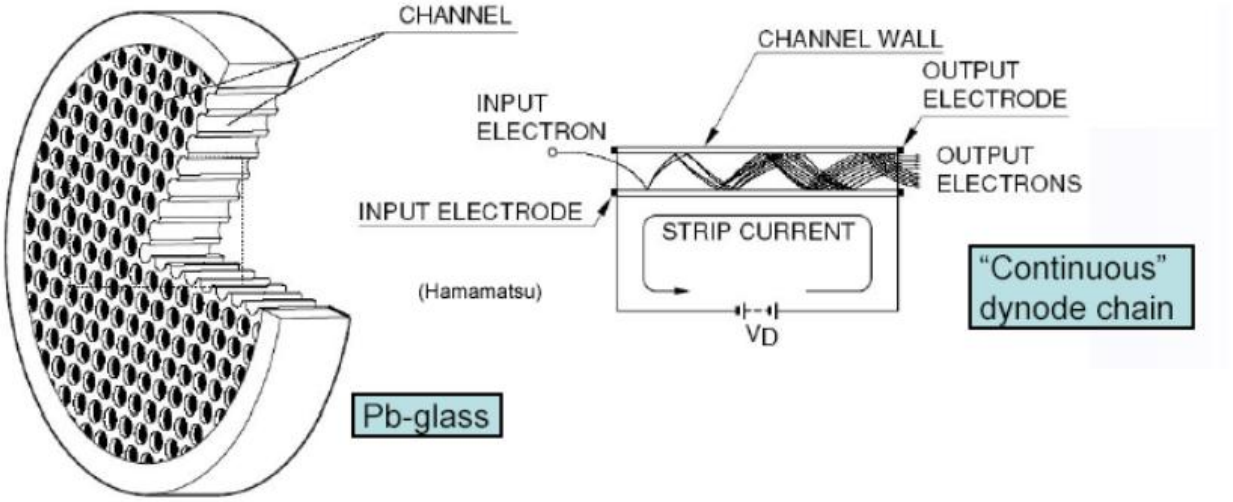

X-rays are imaged using photocathode, MCP, phosphor, and CCD

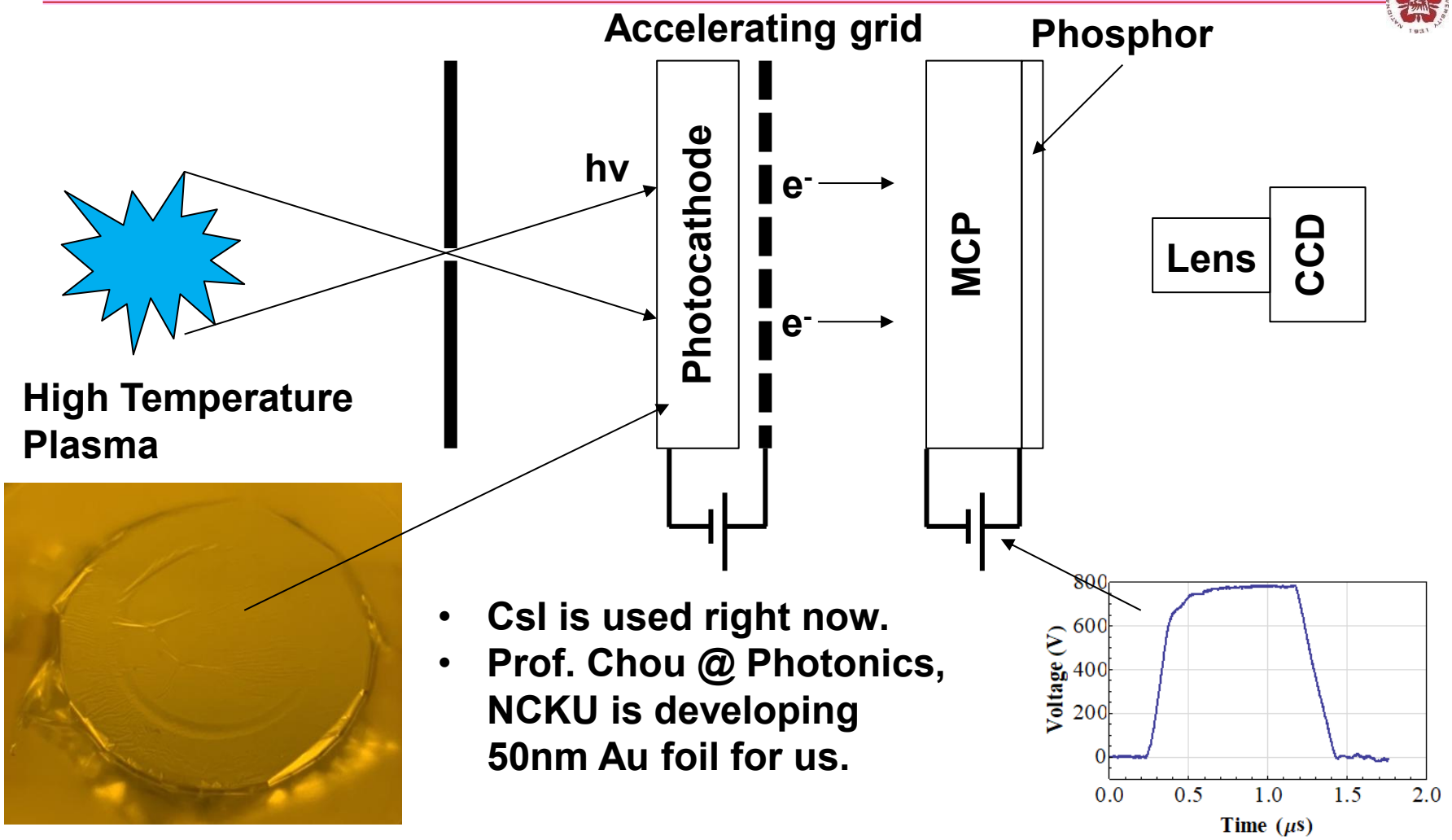

- CsI is used right now.
- Prof. Chou @ Photonics, NCKU is developing 50nm Au foil for us.

- Images can be gated using fast high voltage pulses.

A negative high-voltage pulse is used in our x-ray pinhole camera

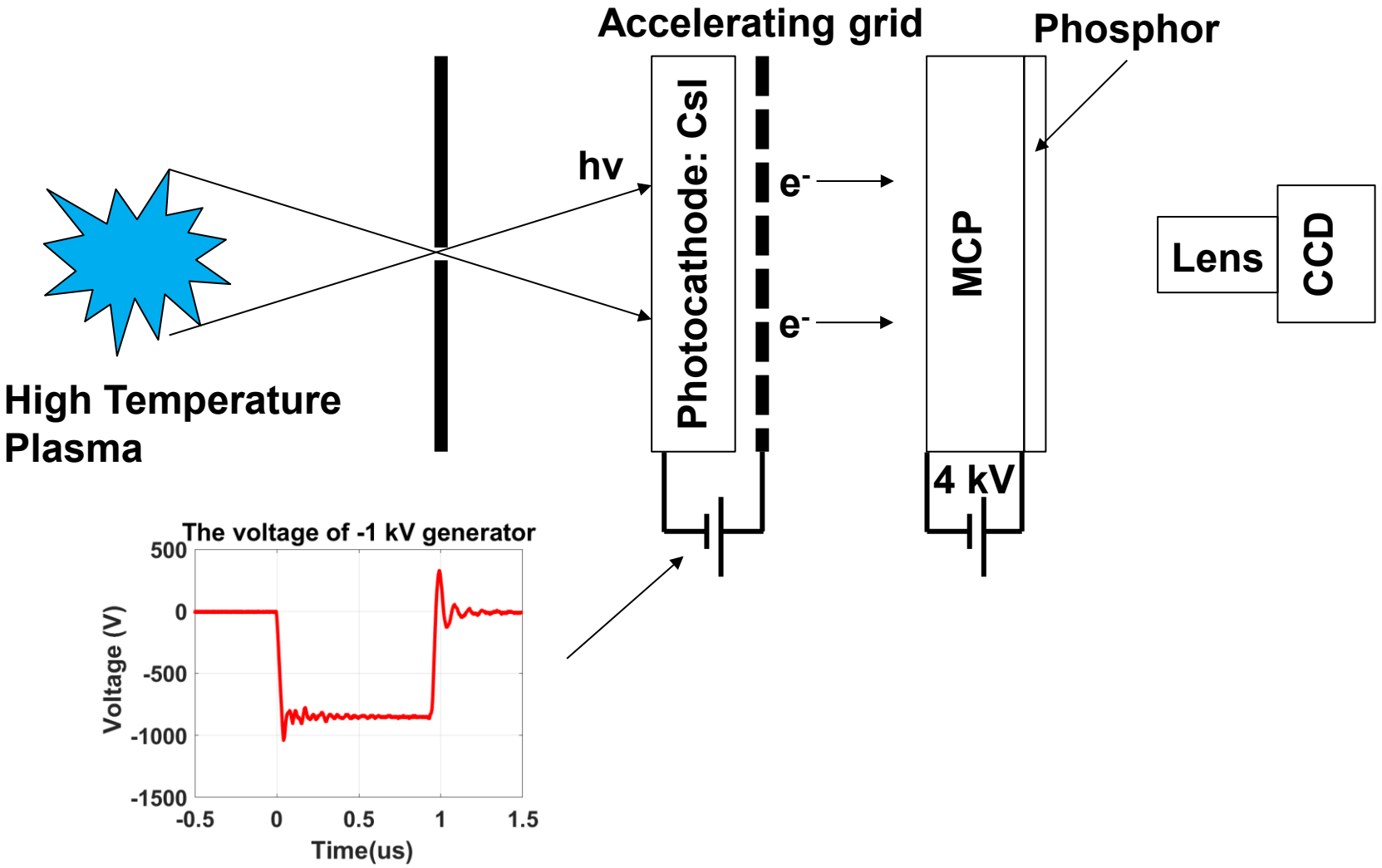

- **The x-ray camera with a shutter opening time of ≤ 10 ns will be built.**

Response of components of ICCDs

■Spectral Response Characteristics

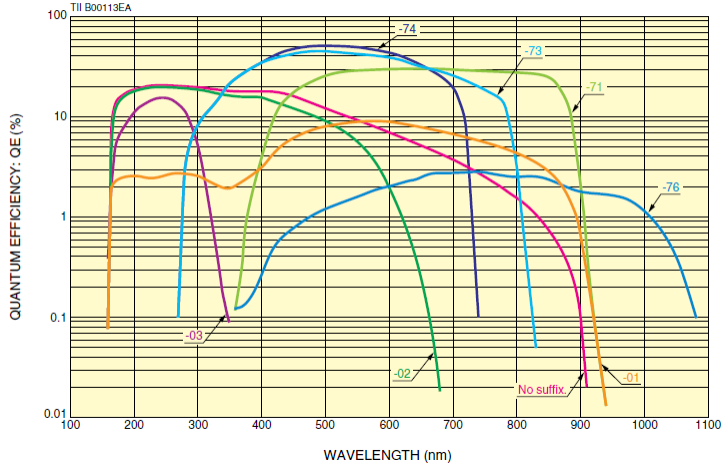

Suffix	Photo Cathode	Input Window
-71	GaAs	Borosilicate Glass
-73	Extended Red GaAsP	Borosilicate Glass
-74	GaAsP	Borosilicate Glass
-76	InGaAs	Borosilicate Glass
Non	Multialkali	Synthetic Silica
-01	Extended Red Multialkali	Synthetic Silica
-02	Bialkali	Synthetic Silica
-03	Cs-Te	Synthetic Silica

The sensitivity at short wavelengths charges with typical transmittance of window materials. Please refer to figure 4 (P6).

NOTE: For Gen II, gate operation types may have slightly lower sensitivity in the ultraviolet region.

An FOP is made up of a bundle of 50 million optical fibers.

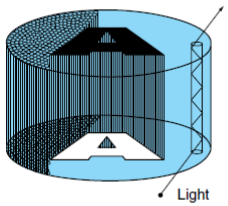

Each individual optical fiber transmits light and this light can be received as an image.

INPUT WINDOWS

Figure 4: Typical Transmittance of Window Materials

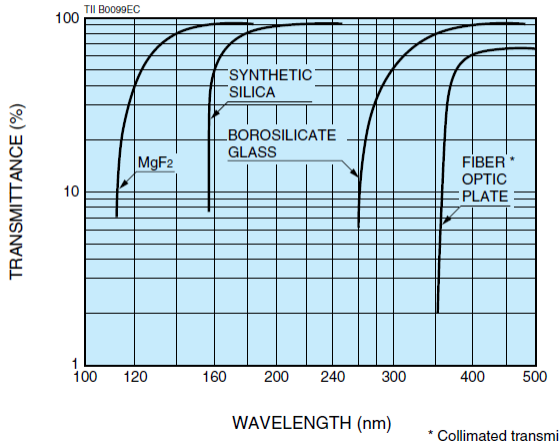

* Collimated transmission

Figure 5: Typical Phosphor Spectral Emission Characteristics

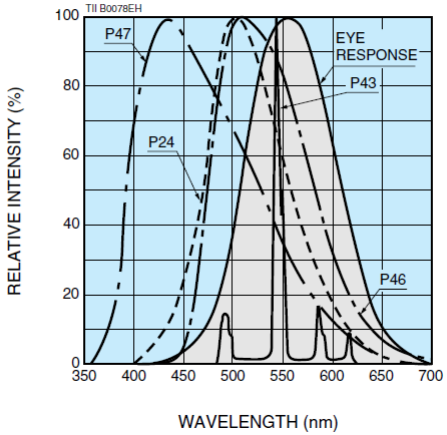

Figure 6: Typical Decay Characteristics

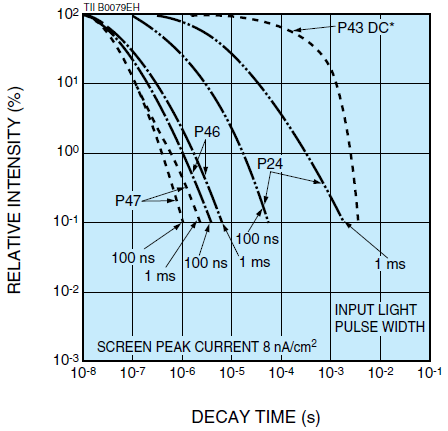

* Decay time obtained following to the continuous input light removal.

Hamamatsu Images Intensifiers brochure

A pinhole camera was designed and was built

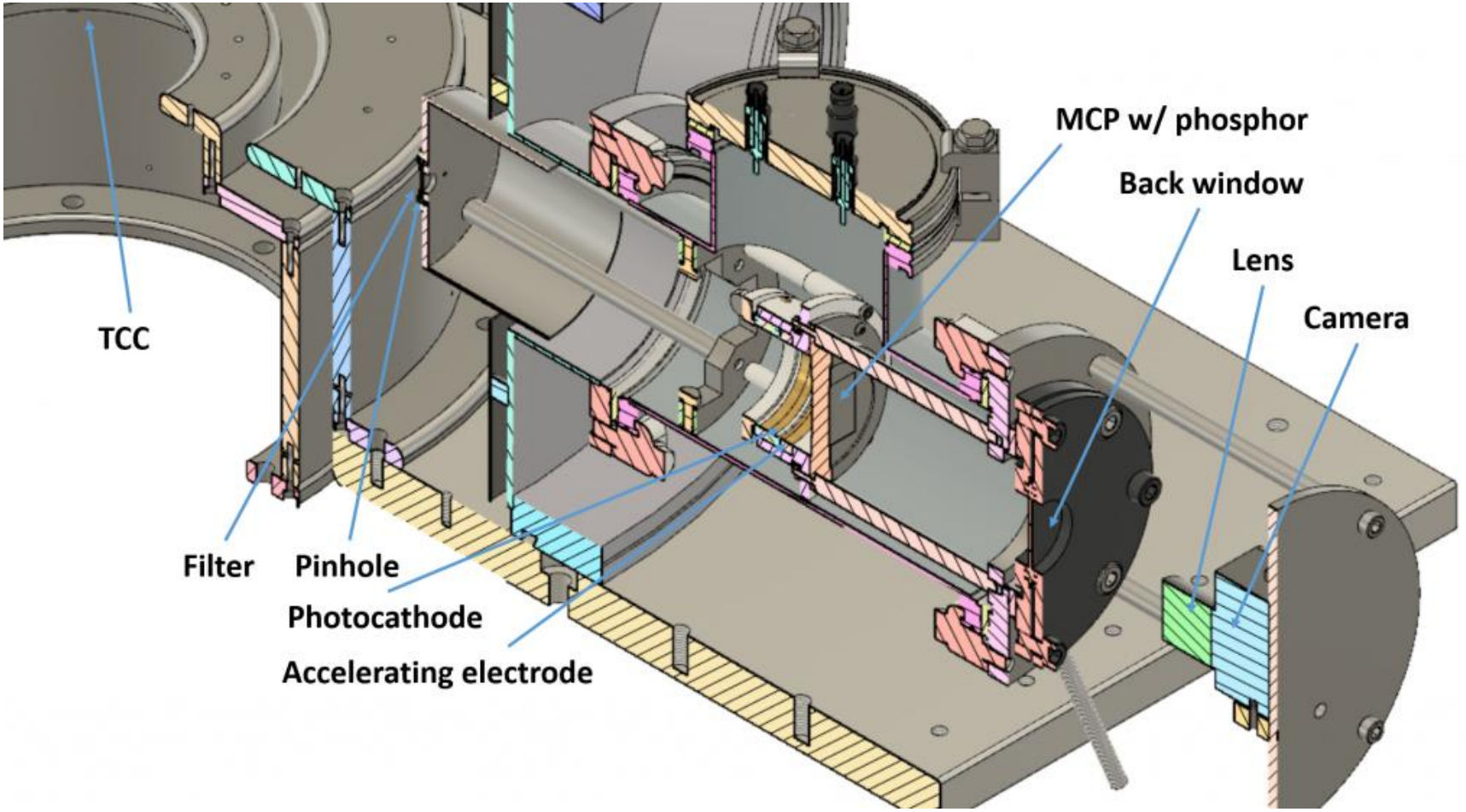

We demonstrated using x-ray pinhole camera to capture the radiation from an imploded x pinch

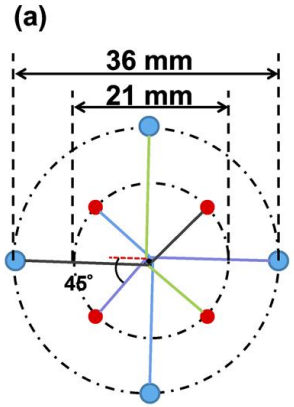

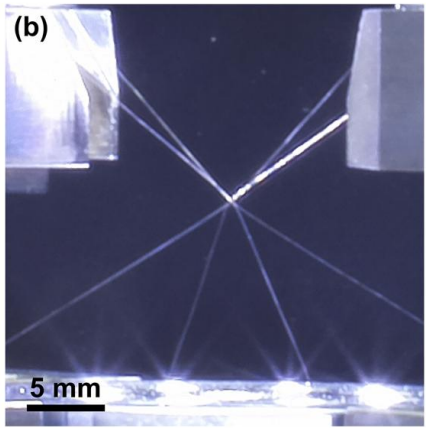

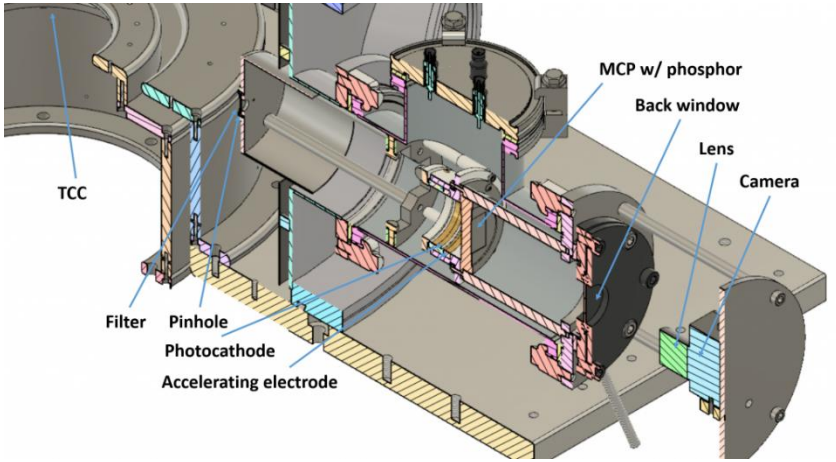

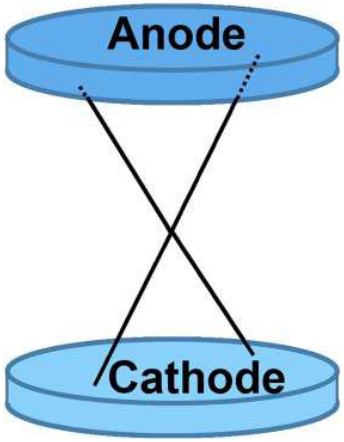

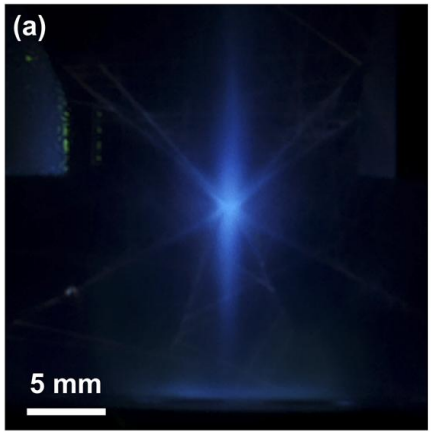

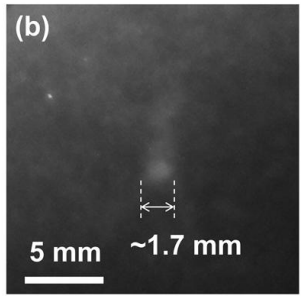

P.-Y. Chang *et al.*, Rev. Sci. Instrum **93**, 043505 (2022)

Electronic detectors provide rapid readout

- Electronic detectors are typically semiconductors or ionization-based stacks (e.g., photomultipliers)

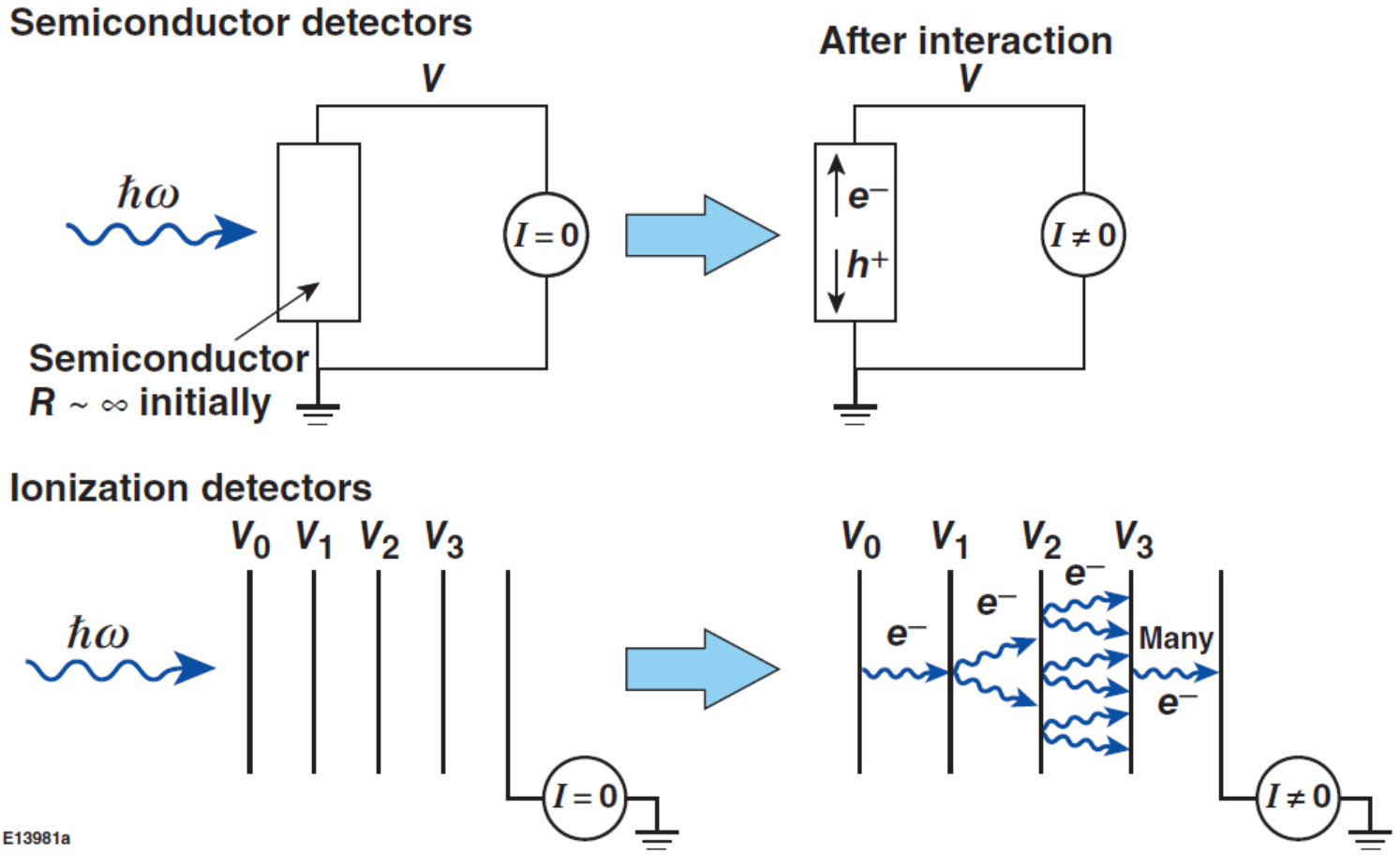

A framing camera provides a series of time-gated 2-D images, similar to a movie camera

- The building block of a framing camera is a gated microchannel-plate (MCP) detector
- An MCP is a plate covered with small holes, each acts as a photomultiplier

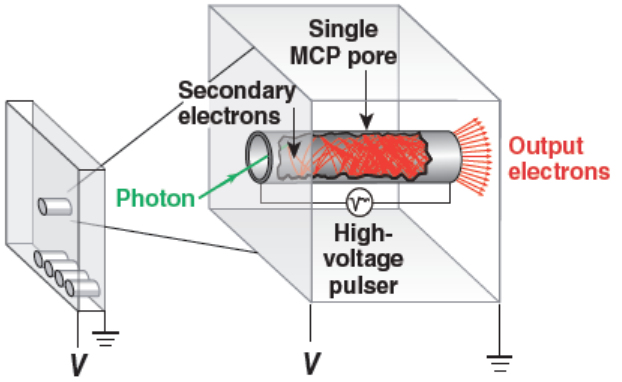

Multiple electrons are produced each time an electron or photon hits the wall

- A voltage pulse is sent down the plate, gating the detector

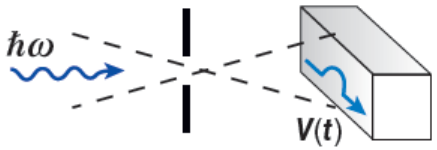

The detector is only on when the voltage pulse is present

E13986b

A framing camera detector consists of a microchannel plate (MCP) in front of a phosphor screen

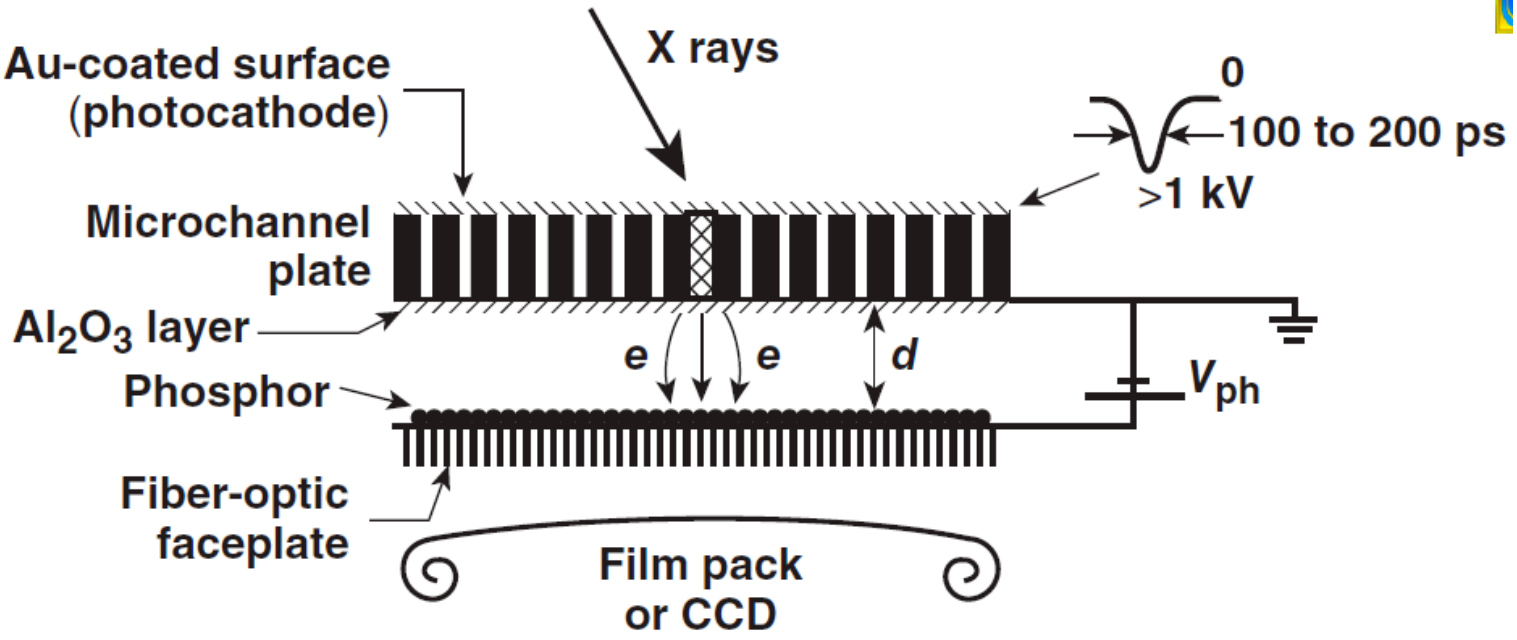

- Electrons are multiplied through MCP by voltage V_c
- Images are recorded on film behind phosphor
- Insulating Al_2O_3 layer allows for V_{ph} to be increased, thereby improving the spatial resolution of phosphor

E7795b

Two-dimensional time-resolved images are recorded using x-ray framing cameras

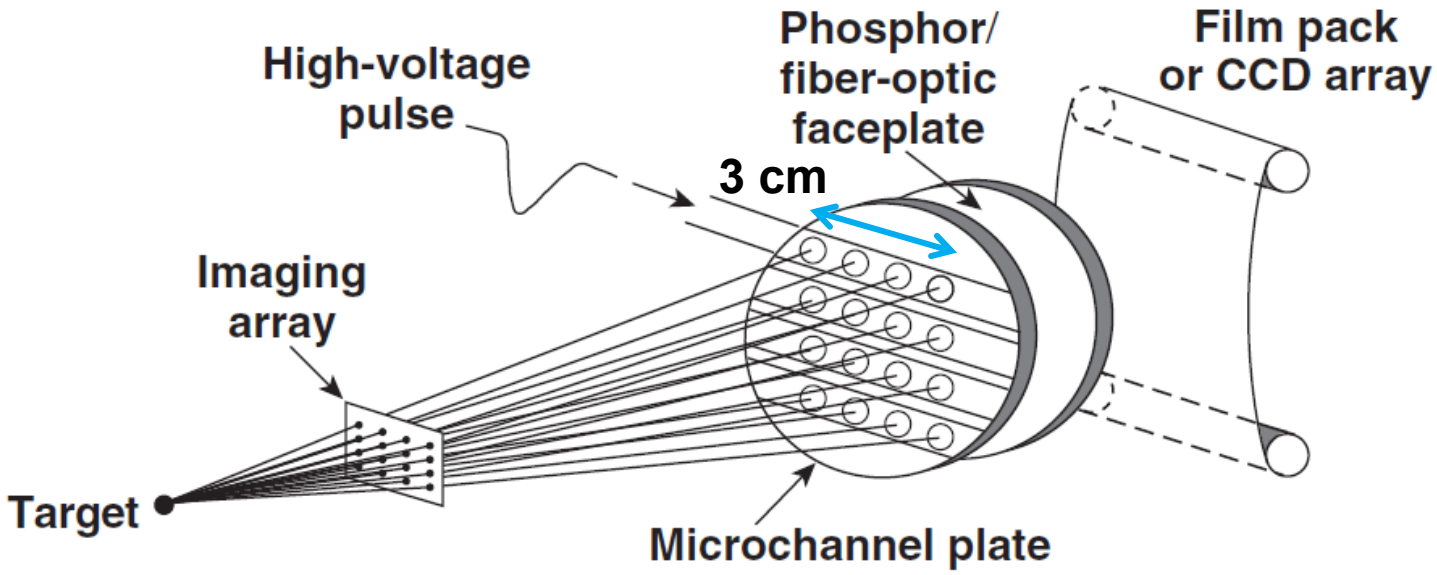

- Temporal resolution = 35 to 40 ps
- Imaging array: Pinholes: 10- to 12-μm resolution, 1 to 4 keV
- Space-resolved x-ray spectra can be obtained by using Bragg crystals and imaging slits

E7105b

Ex: $\Delta t = \dfrac{3\ \text{cm}/3}{3 \times 10^{10}\ \text{cm/s}} = 33\ \text{ps}$

X-ray framing cameras for recording two-dimensional time-resolved images will be built by the end of 2021

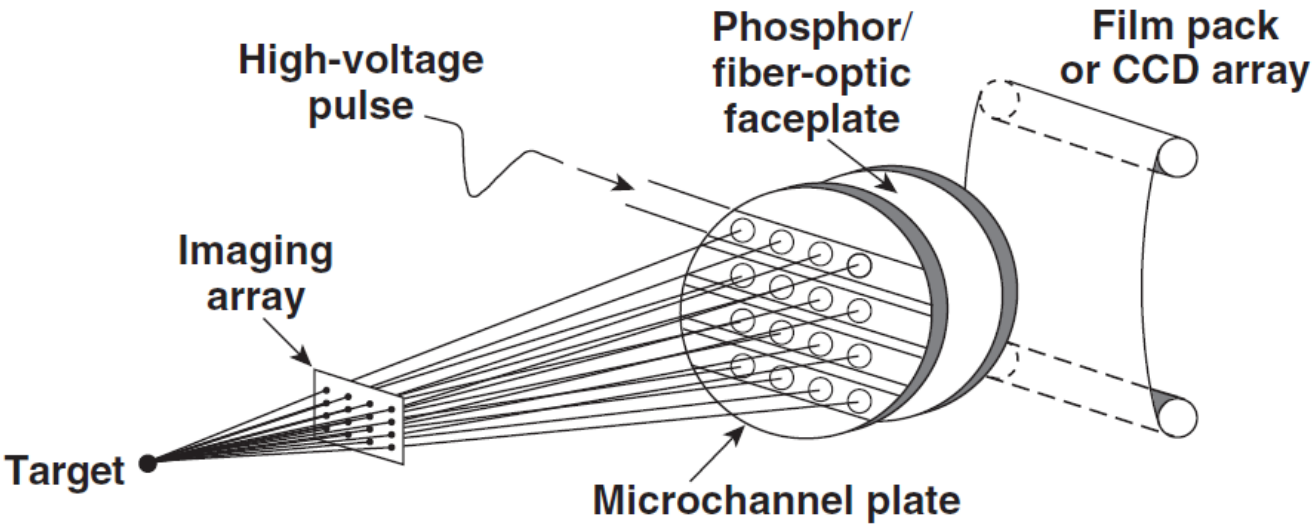

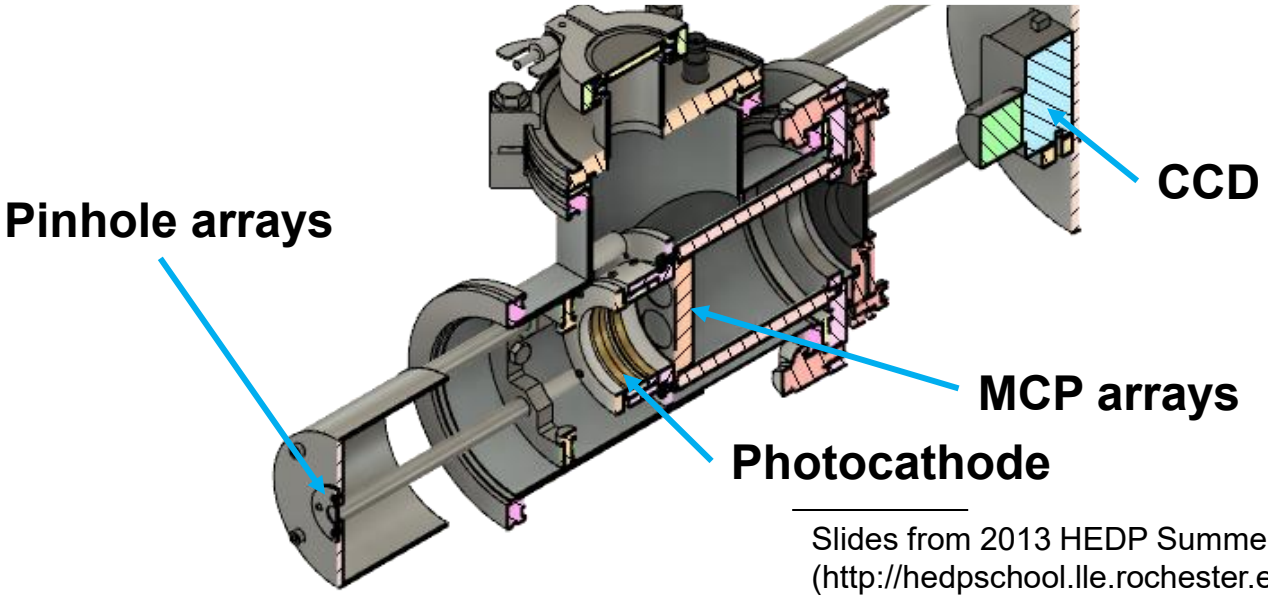

Slides from 2013 HEDP Summer School
(http://hedpschool.lle.rochester.edu/1000_proc2013.php)

Each pinhole camera will be triggered separately

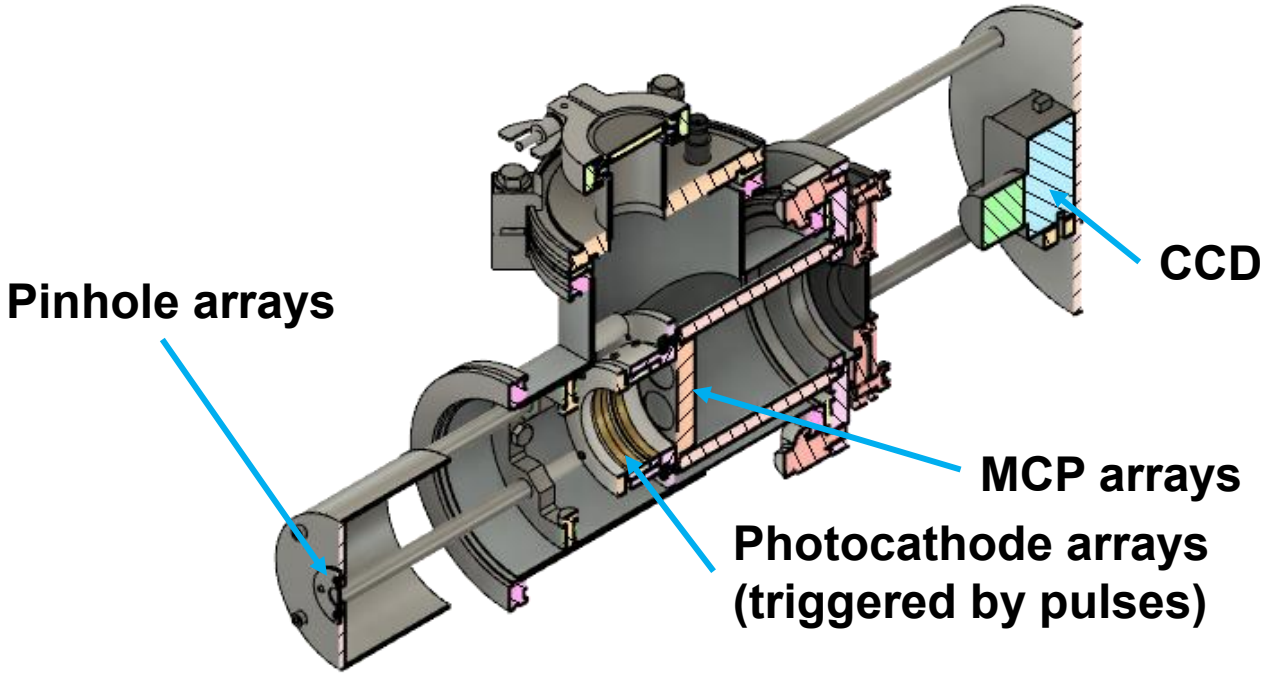

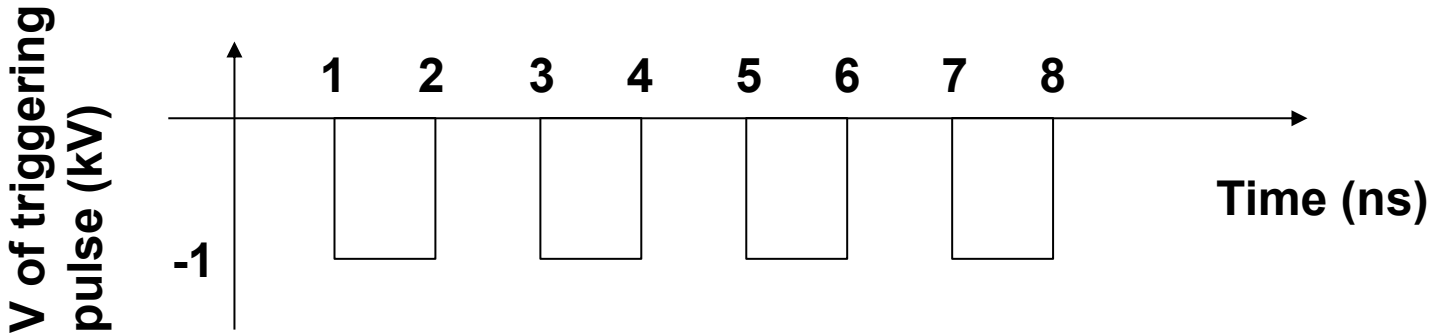

A streak camera provides temporal resolution of 1-D data

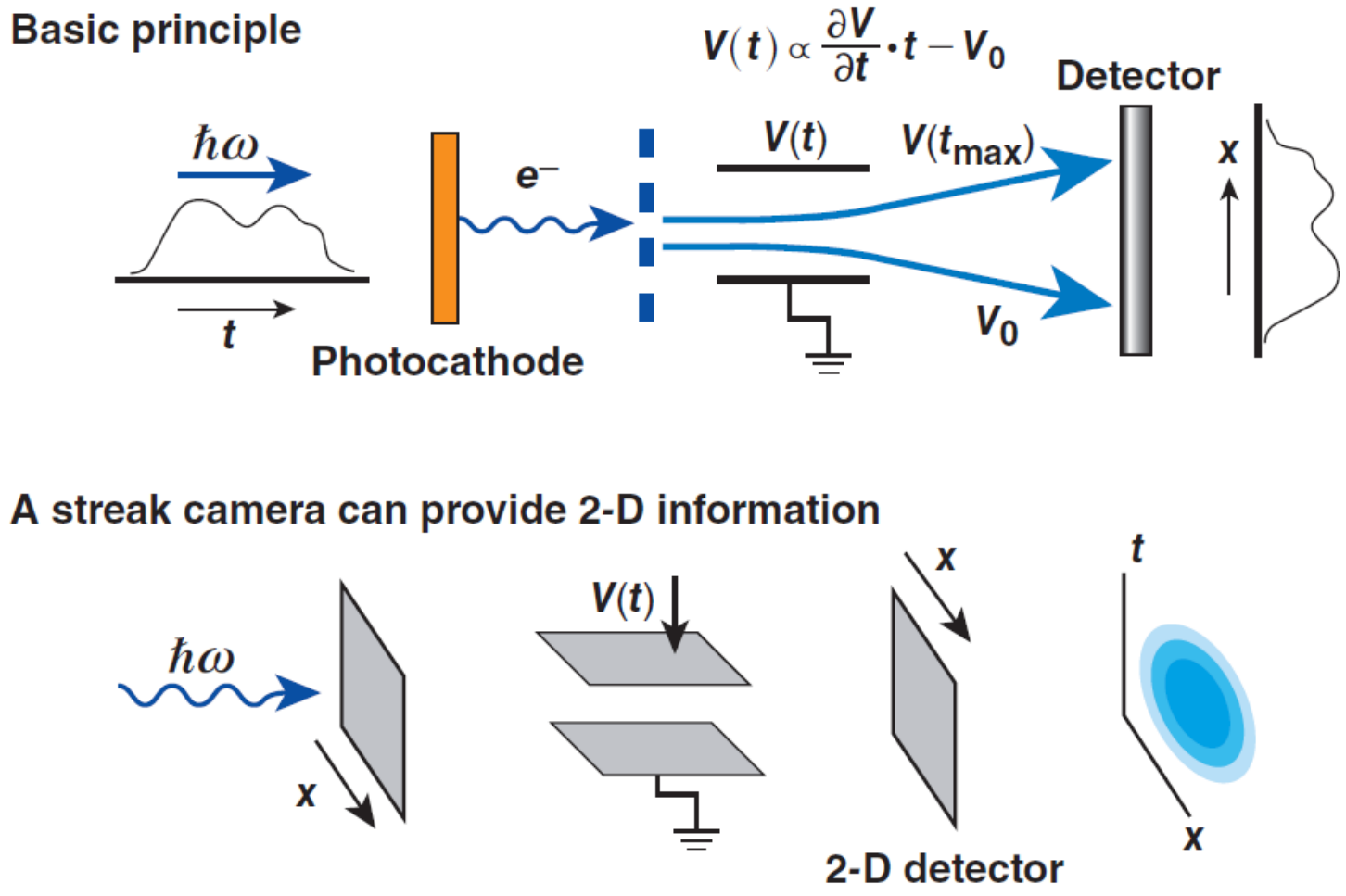

A slit is to prevent spatial information at different times interfering with each other

Imaging system
- **Visible light: regular lens**
- **X rays: pinhole**

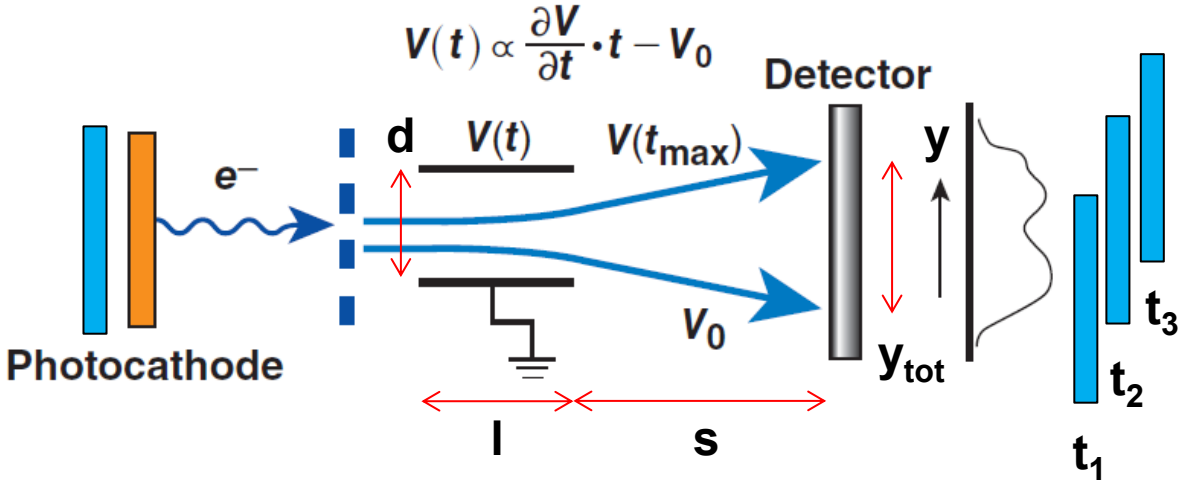

Imaging system
- **Visible light: regular lens**
- **X rays: pinhole**

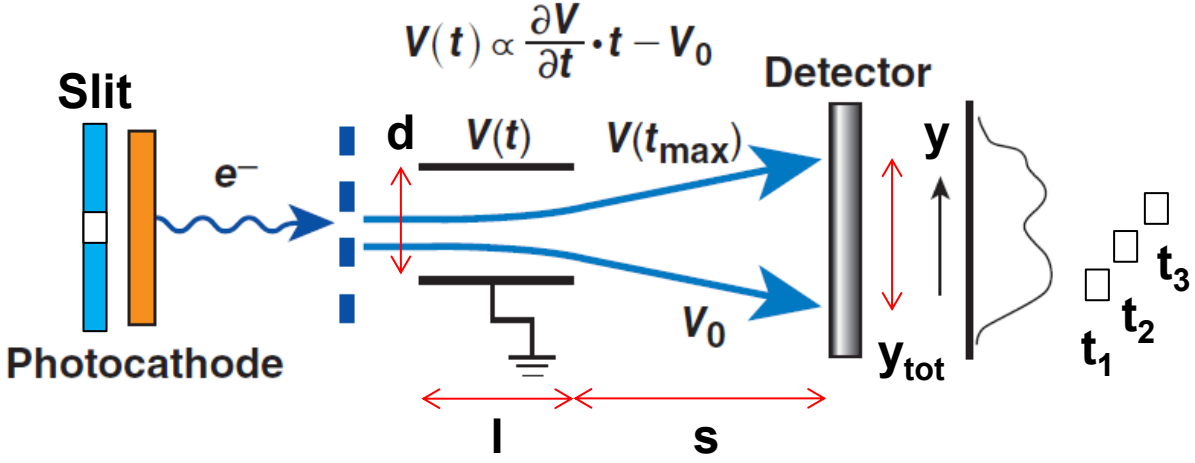

A temporal resolution higher than 15 ps is expected

Imaging system
- **Visible light: regular lens**
- **X rays: pinhole**

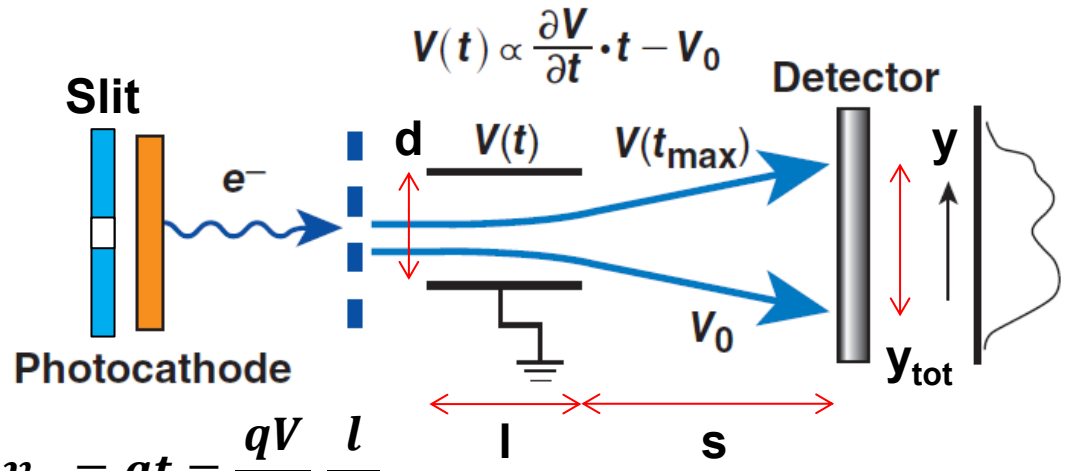

$$a = \frac{F}{m} = \frac{qE}{m} = \frac{qV}{md} \qquad v_{\perp} = at = \frac{qV}{md}\frac{l}{v_{||}}$$

$$y = s\,\mathrm{Tan}\theta = s\frac{V_{\perp}}{V_{||}} = \frac{1}{2E_k}\frac{l}{d}sqV = \frac{1}{2E_k}\frac{l}{d}sq(V_0 + V't)$$

- **Let d=10 mm, l=20 mm, s=50 mm, E_k=1 keV, V=-200 ~ 200 V**

$$V' \equiv \frac{V_{tot}}{t_{tot}} = 0.06\,\mathrm{kV/ns} \qquad y_{tot} = 15\mathrm{mm} \qquad y_{tot} = 15\mathrm{mm}$$

- **Temporal resolution:**

$$\delta t = \delta y \frac{2E_k d}{lsqV'} = 15\,\mathrm{ps} \quad \text{for} \quad \delta y = 45\mu\mathrm{m}$$

- **δt will be adjusted by changing E_k.**

A streak camera with temporal resolution of 15 ps has been developed

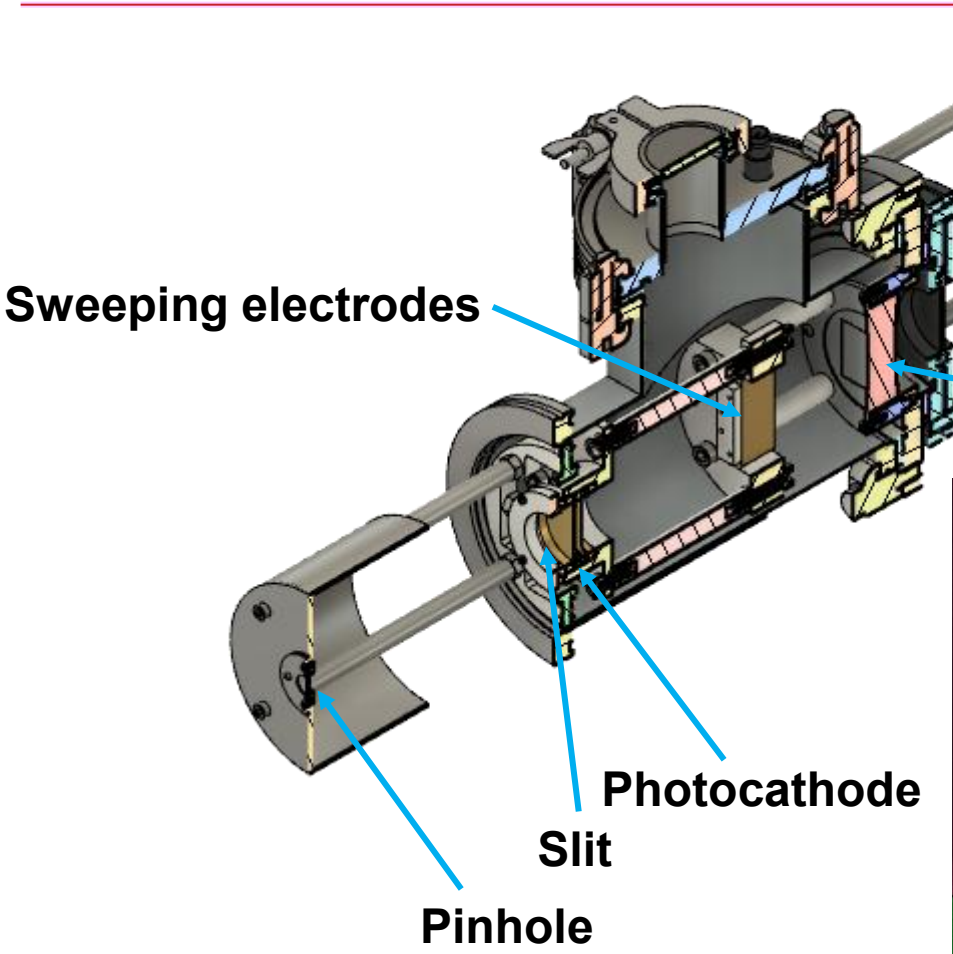

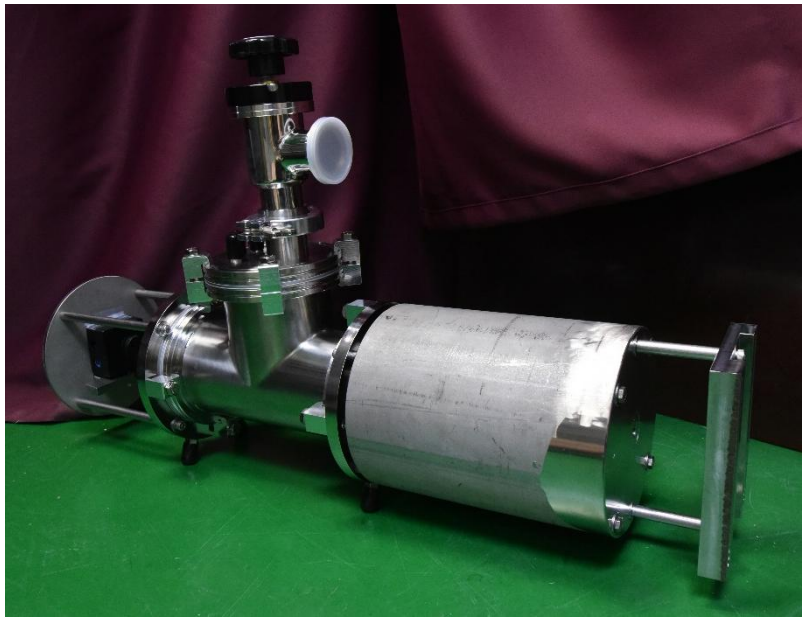

Shell trajectories can be measured using framing camera or streak camera

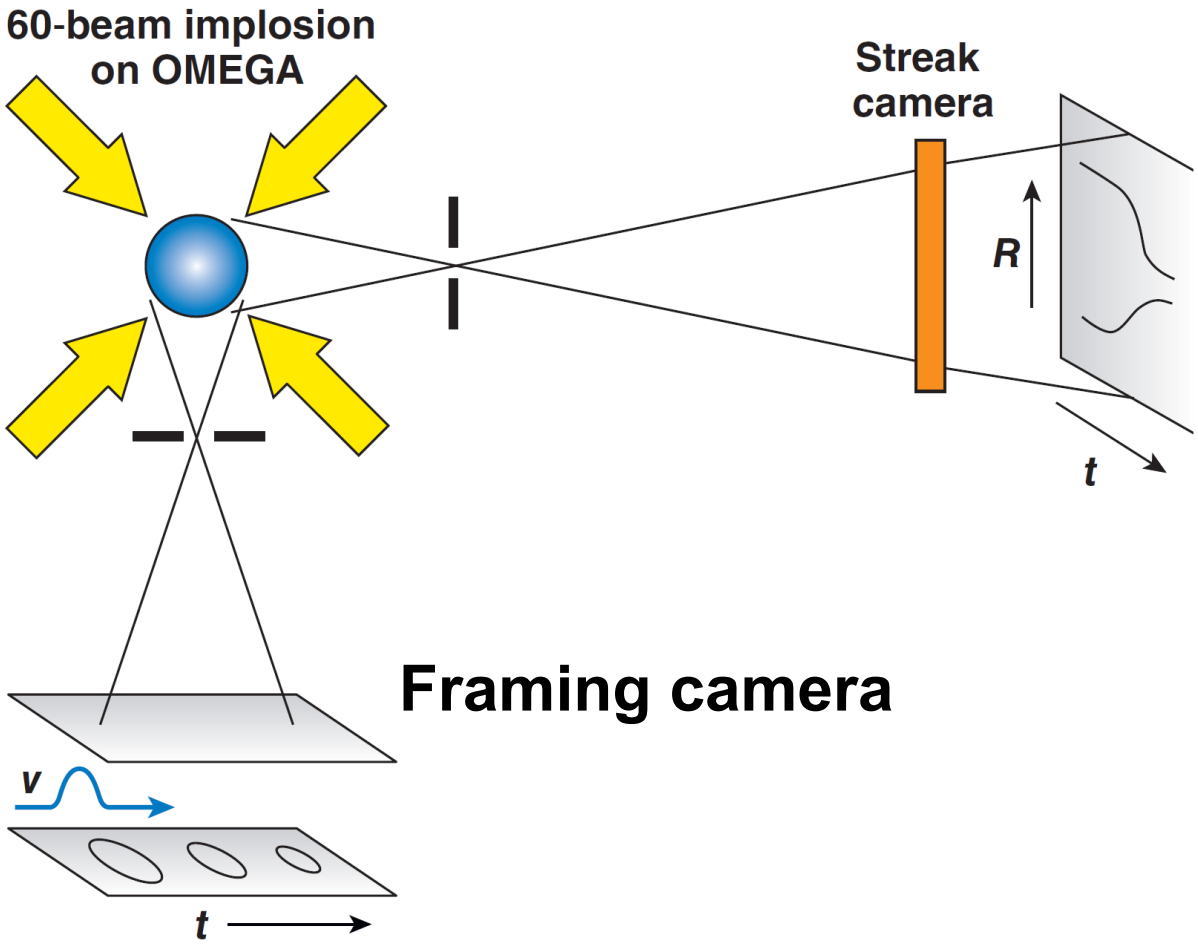

Comparison of images from framing camera versus streak camera

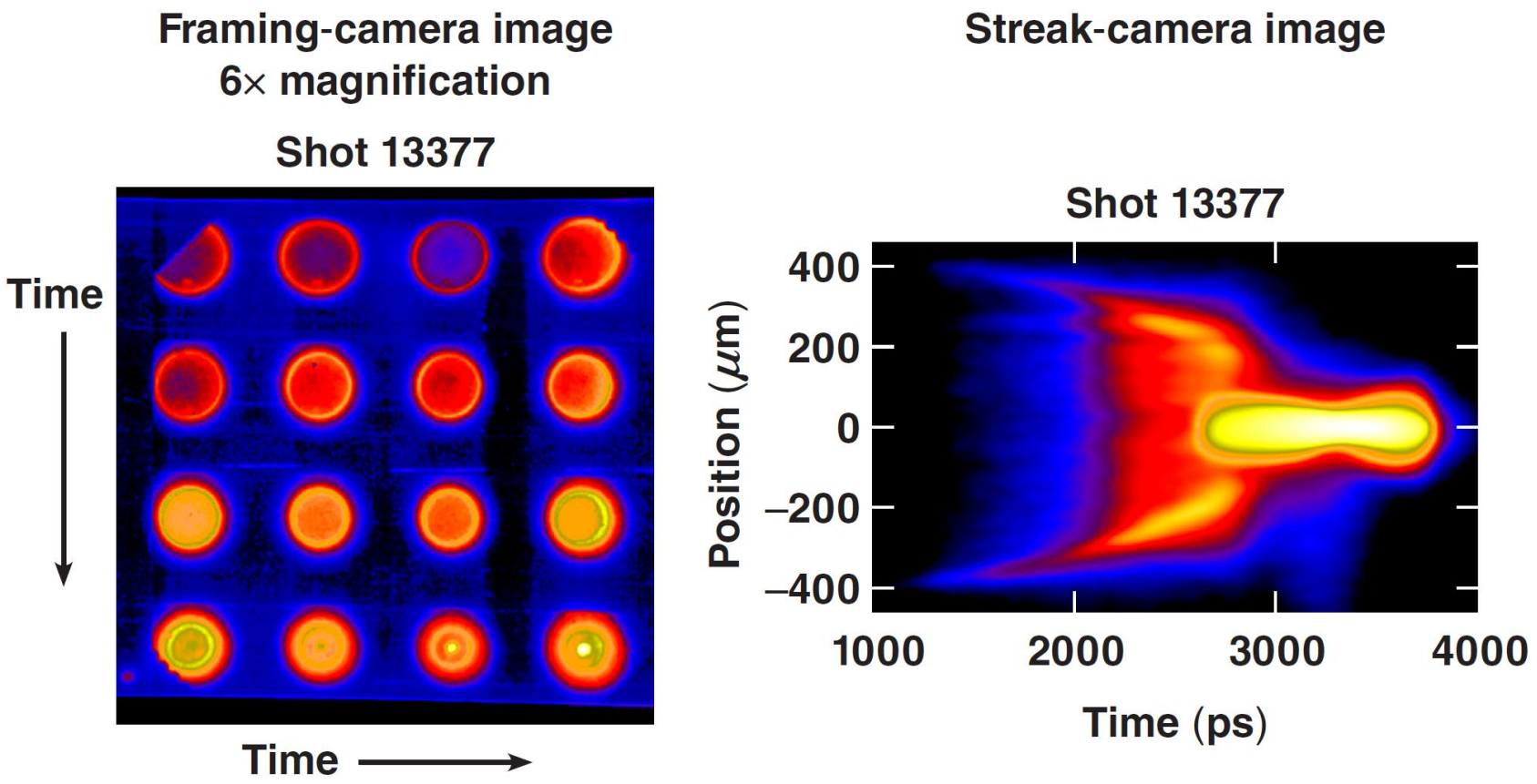

The optical density can be measured using the absorption of a backlighter

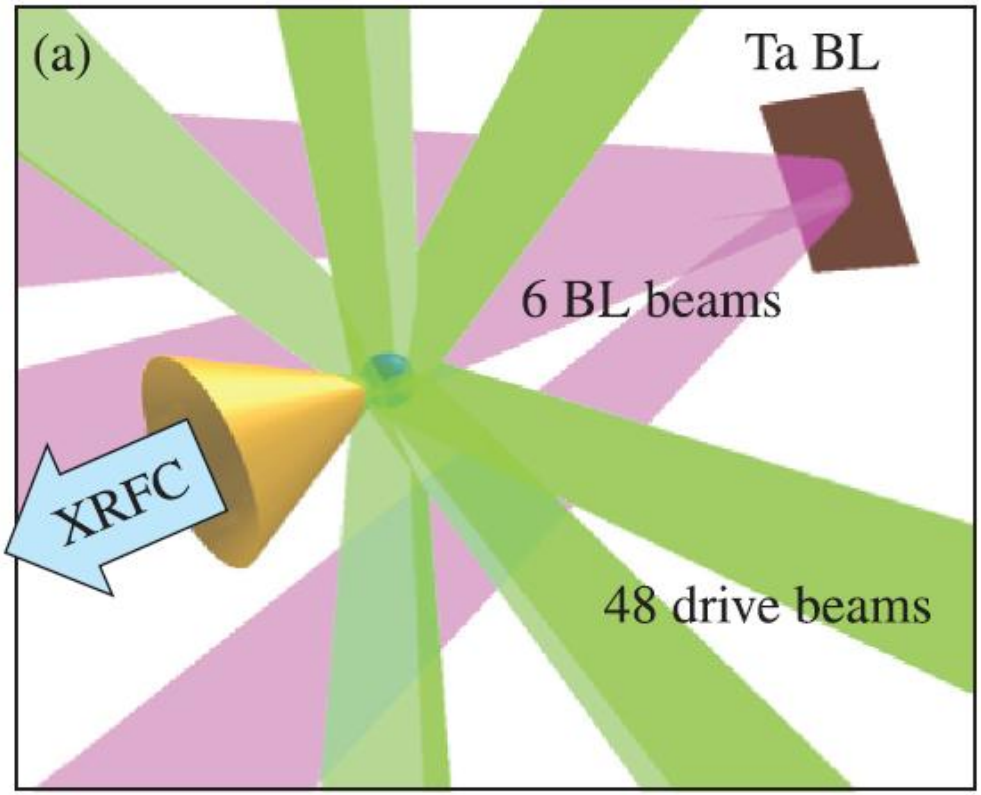

$$I = \int I(\varepsilon)\exp(-\mu(\varepsilon)\rho\delta)d\varepsilon$$

$$I = I_{\mathrm{BL}}\exp(-\bar{\mu}\rho\delta)$$

$$\ln I = \ln I_{BL} - \mu\rho r$$

G. Fiksel *et al.*, Phys. Plasmas **19**, 062704 (2012)

X-ray radiography of an X-pinch by using another X-pinch or two X-pinches as point sources of probing radiation

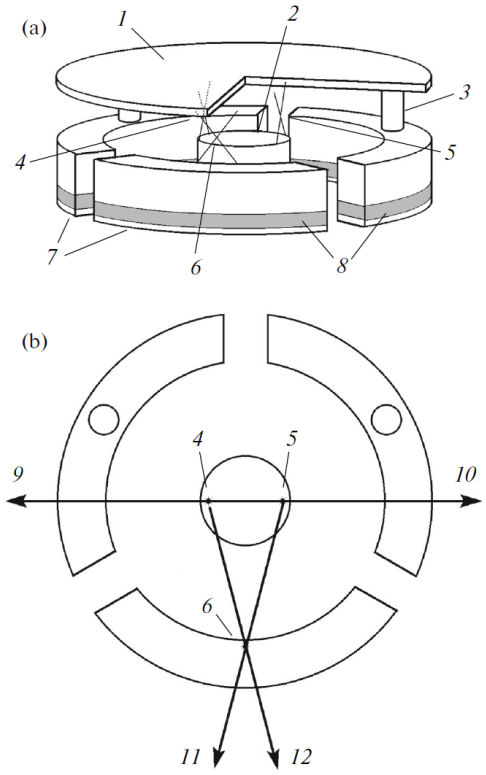

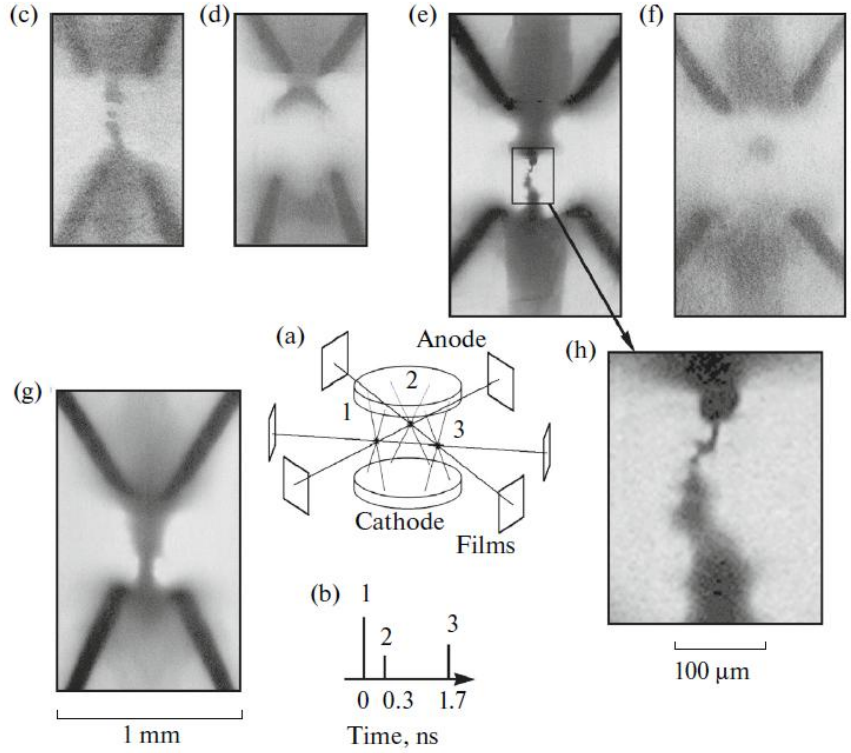

Fig. 44. X-ray radiographs obtained in the system of three parallel 2 × 12.5-μm Mo X-pinches: (a) arrangement of the pinches and films, (b) temporal positions and relative intensities of probing X-ray pulses, (c) image of X-pinch 1 in the radiation of X-pinch 2, (d) image of X-pinch 1 in the radiation of X-pinch 3, (e) image of X-pinch 2 in the radiation of X-pinch 1, (f) image of X-pinch 2 in the radiation of X-pinch 3, (g) image of X-pinch 3 in the radiation of X-pinch 1 emission, and (h) enlarged fragment of the image.

S. A. Pikuz *et al.*, Plasma Phys. Rep. **41**, 291 (2015)

We demonstrated using x-ray pinhole camera to capture the radiation from an imploded x pinch

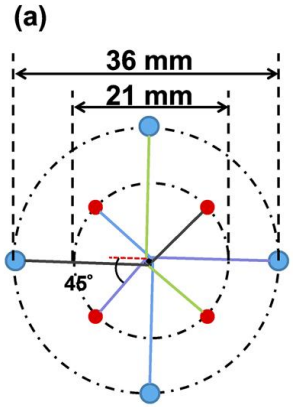

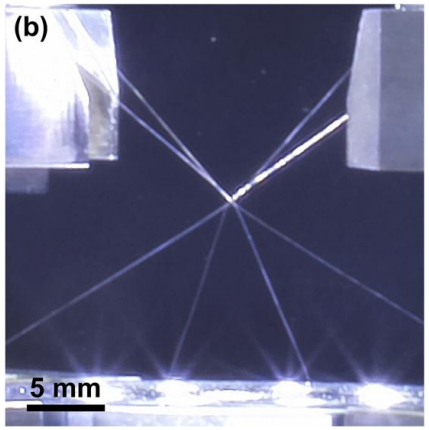

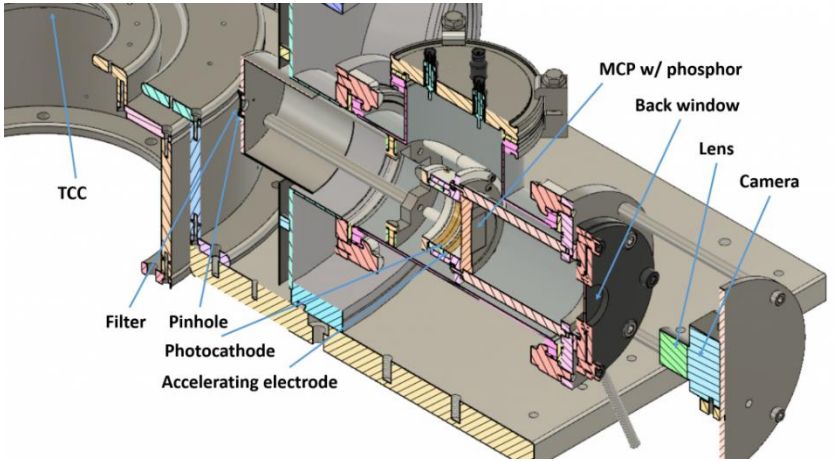

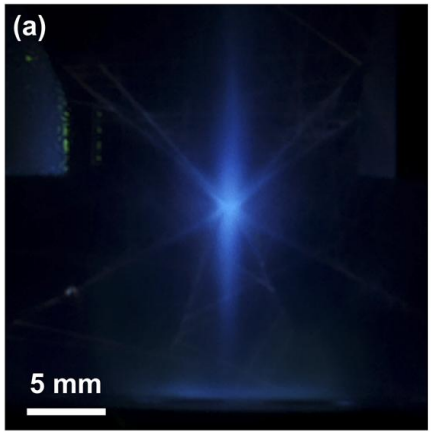

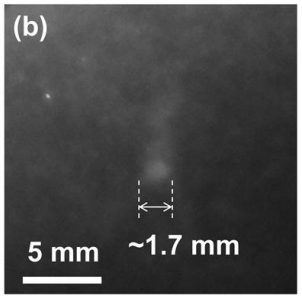

P.-Y. Chang *et al.*, Rev. Sci. Instrum **93**, 043505 (2022)

Shock velocities are measured using time-resolved Velocity Interferometer System for Any Reflector (VISAR)

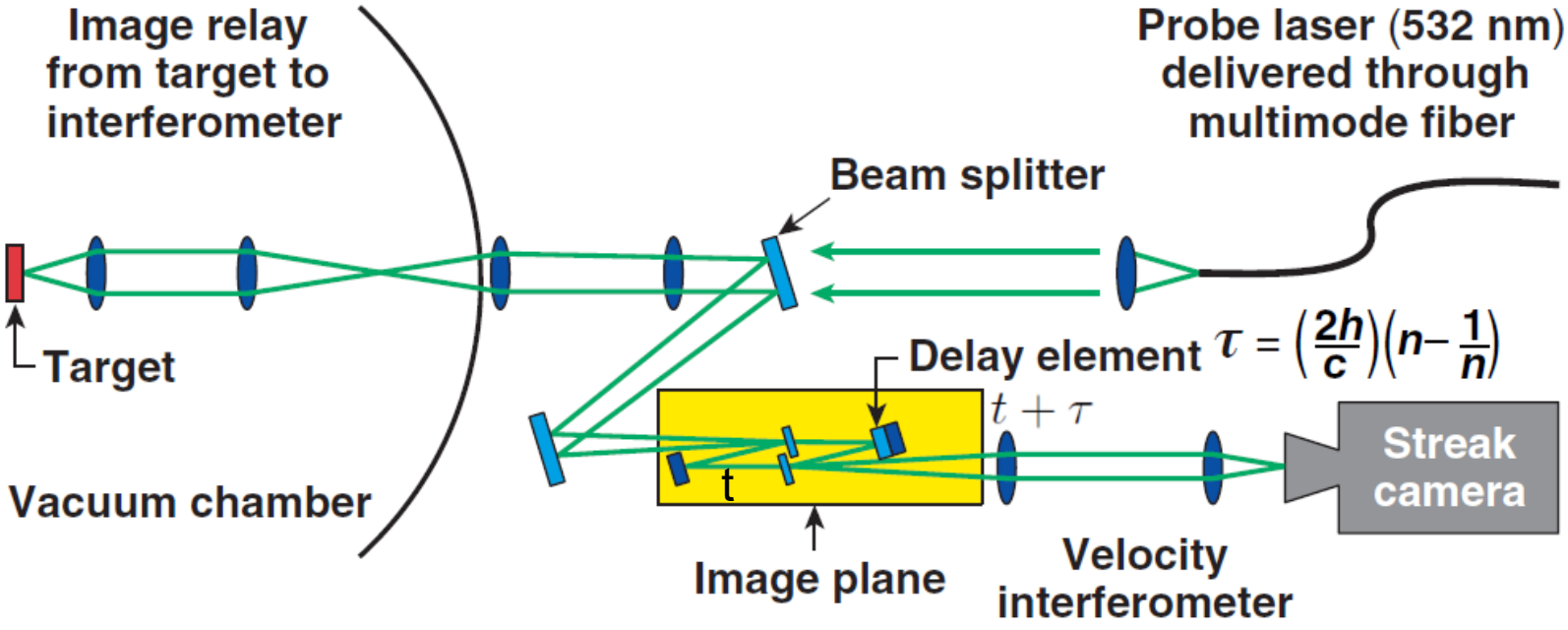

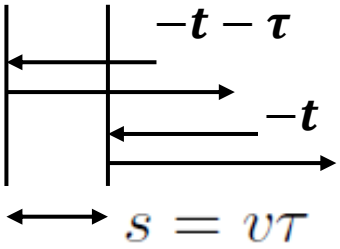

$$\Delta\phi = \frac{v\tau}{\lambda} \propto v$$

http://hedpschool.lle.rochester.edu/1000_proc2013.php

Shock velocities are measured using time-resolved Velocity Interferometer System for Any Reflector (VISAR)

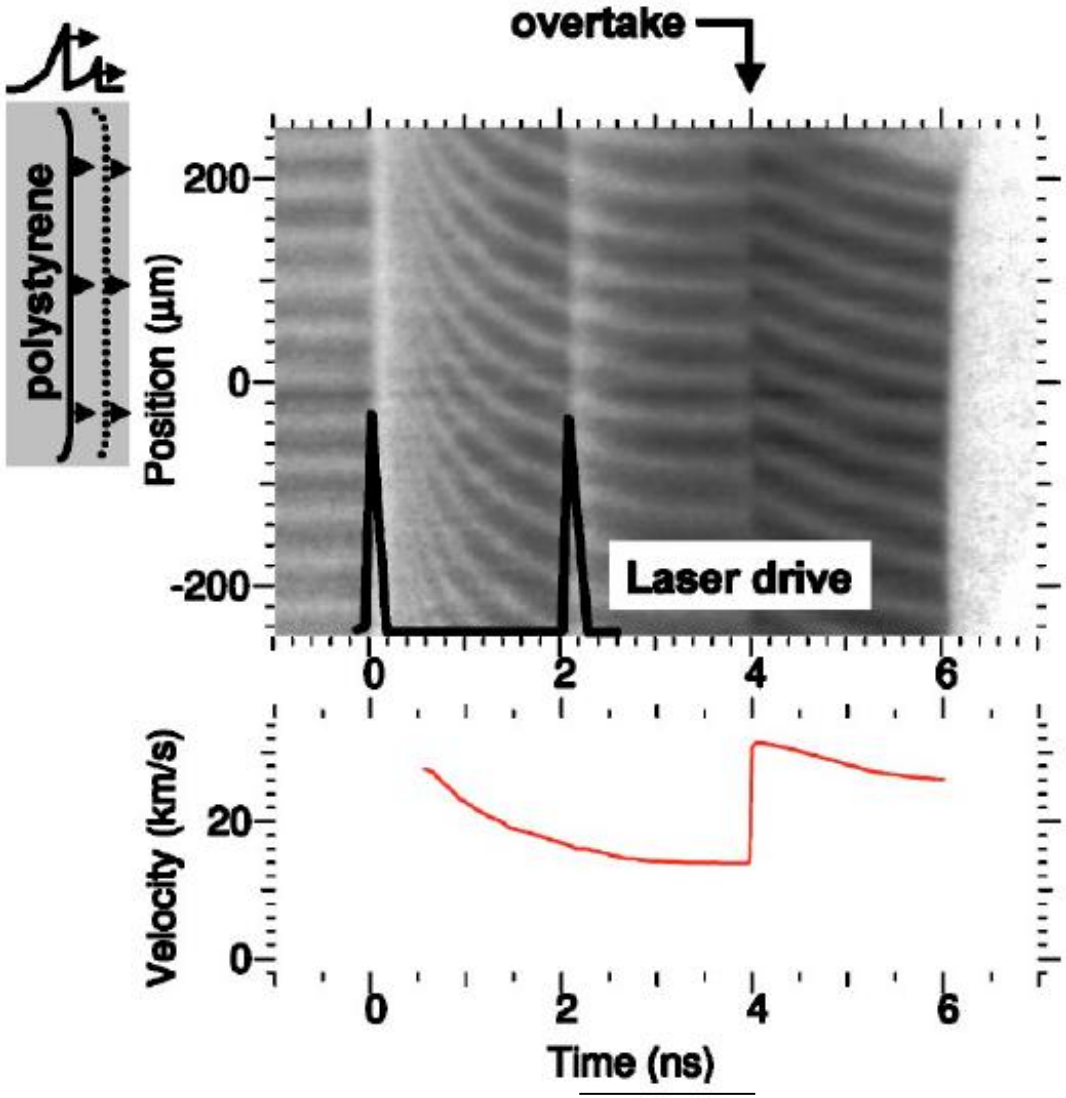

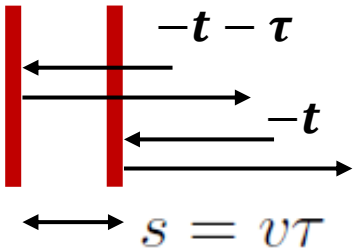

P. M. Celliers *et al.*, Rev. Sci. Insytum. **75**, 4916 (2004)

Neutron average temperature is obtained using Neutron Time of Flight (NToF)

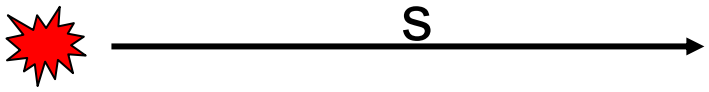

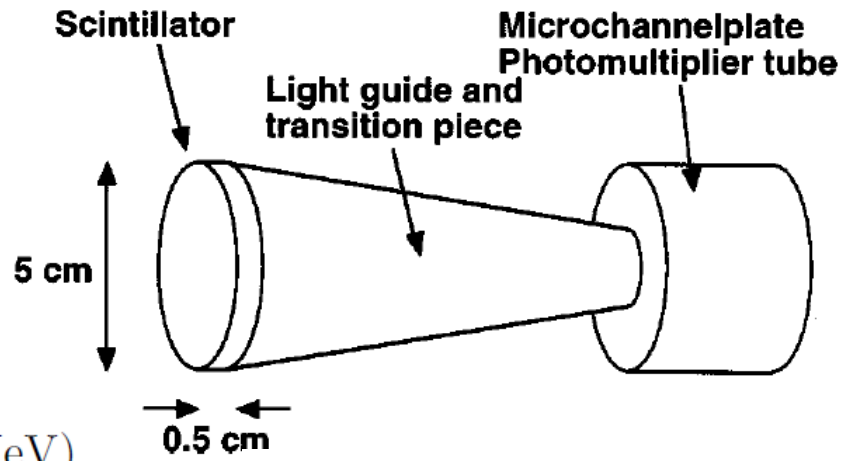

$$D + D \longrightarrow He^3\,(0.82\ \mathrm{MeV}) + n\,(2.45\ \mathrm{MeV})$$

$$D + T \longrightarrow He^4\,(3.5\ \mathrm{MeV}) + n\,(14.1\ \mathrm{MeV})$$

$$s = vt \qquad v = \frac{s}{t}$$

$$f(v) = \sqrt{\left(\frac{m}{2\pi kT}\right)}\exp\left(-\frac{mv^2}{2kT}\right)$$

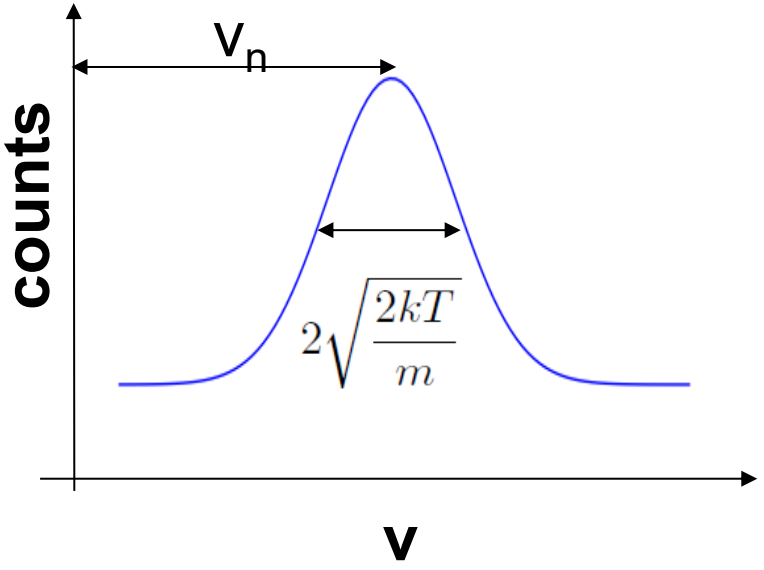

T. J. Murphy *et al.*, Rev. Sci. Instrum. **72**, 773 (2001)

The OMEGA Facility is carrying out ICF experiments using a full suite of target diagnostics

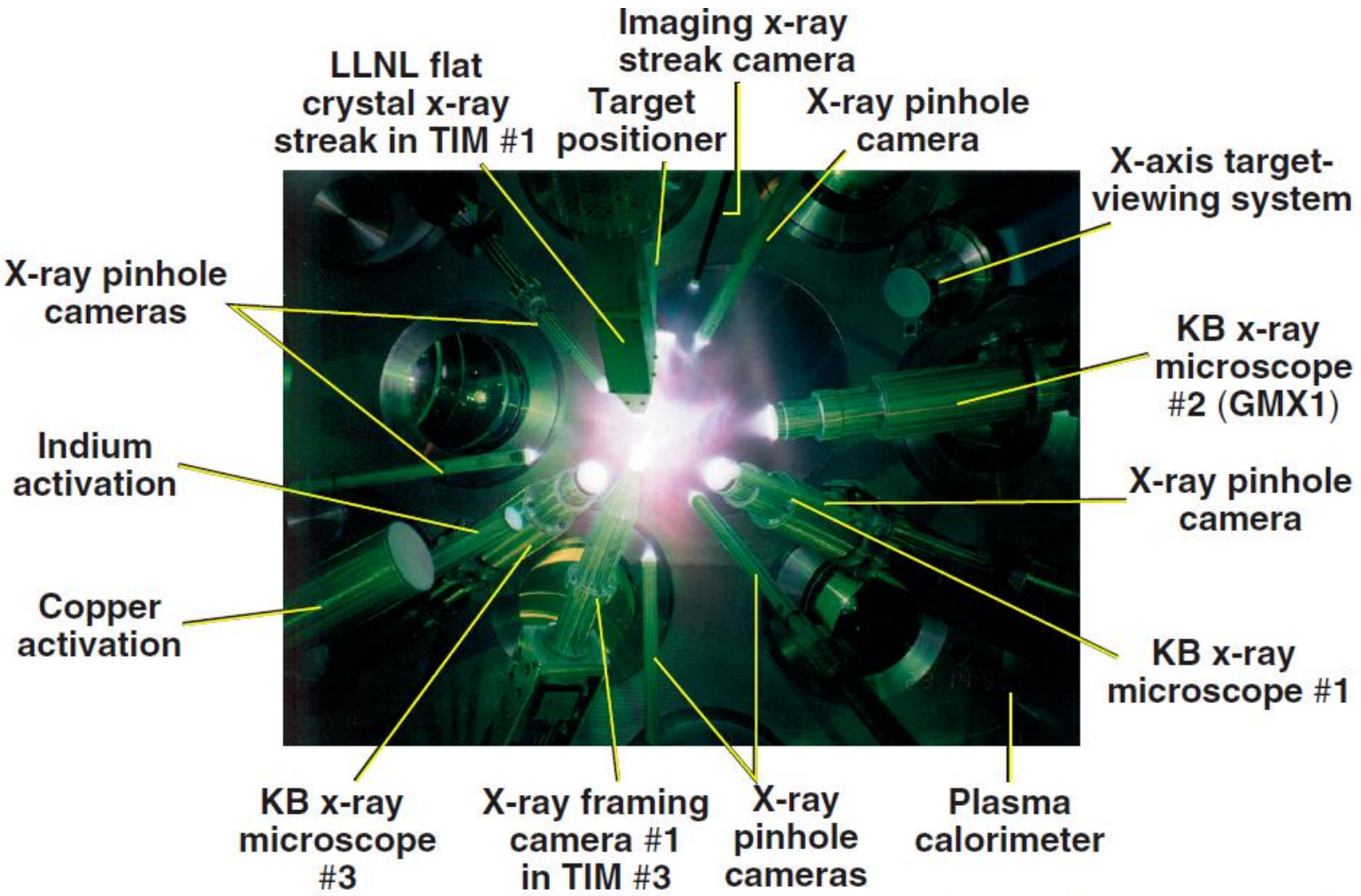

A peak current of ~135 kA with a rise time of ~1.6 us is provided by the pulsed-power system

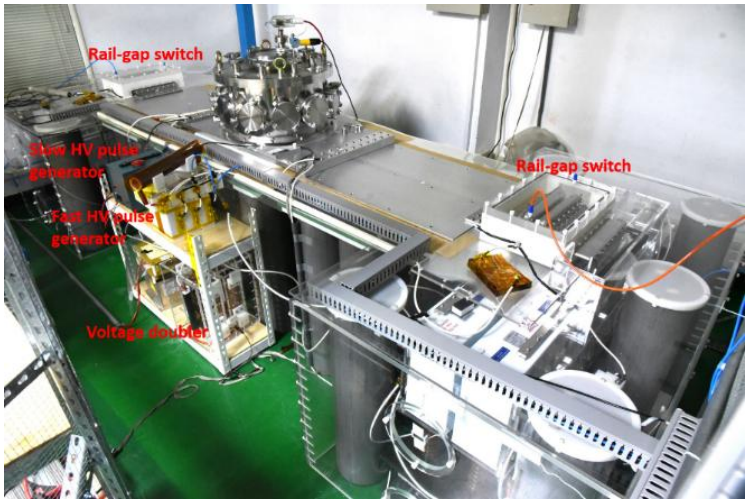

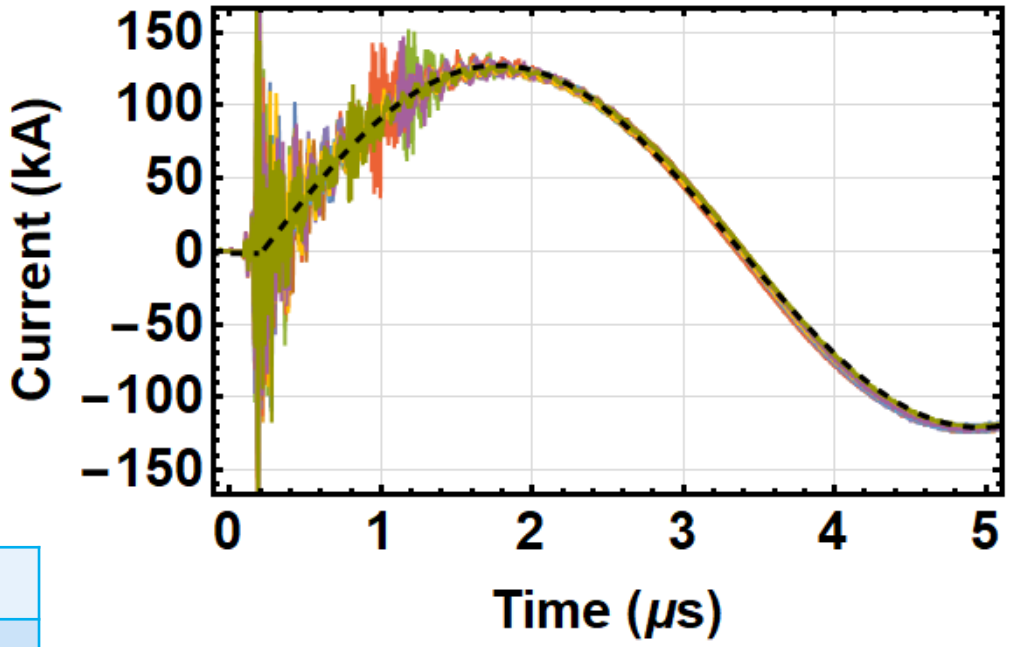

Capacitance (μF)	5
V_{charge} (kV)	20
Energy (kJ)	1
Inductance (nH)	204 ± 4
Rise time (quarter period, ns)	1592 ± 3
I_{peak} (kA)	135 ± 1

A suit of diagnostics in the range of (soft) x-ray are being built

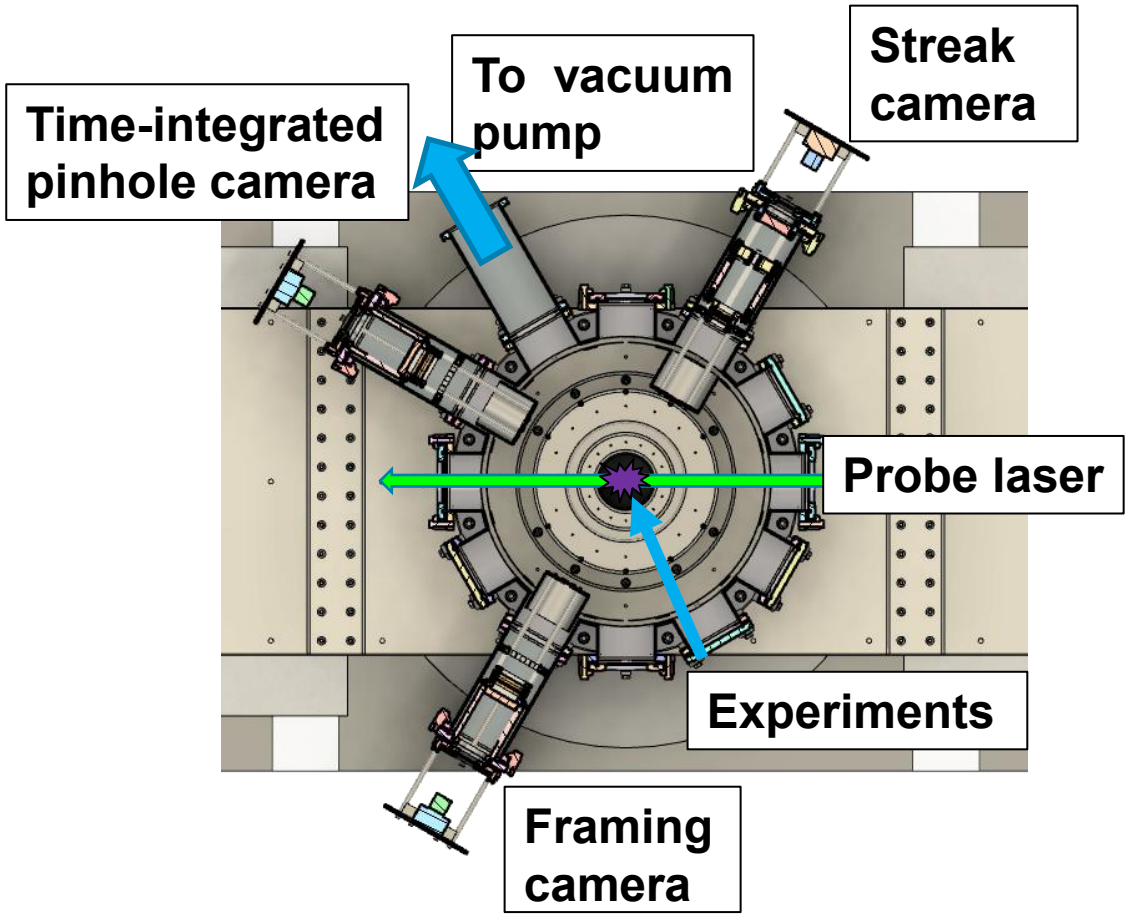

- CsI are used as the photocathode for all x-ray imaging system.
- Au photocathode may be used in the future.

- **Pinhole camera:**
  - Magnification: 1x
  - Exposure time: 1 us
- **Streak camera:**
  - Magnification: 1x
  - Temporal resolution: 15 ps
- **Framing camera:**
  - Magnification: 0.3x
  - Temporal resolution: ~ns using 4 individual MCPs
- **Laser probing:**
  - For interferometer, schlieren, shadowgraphy, Thomson scattering.
  - Temporal resolution: ~300 ps using stimulated brillouin scattering (SBS) pulse compression in water

Time-resolved imaging system with temporal resolution in the order of nanoseconds was implemented

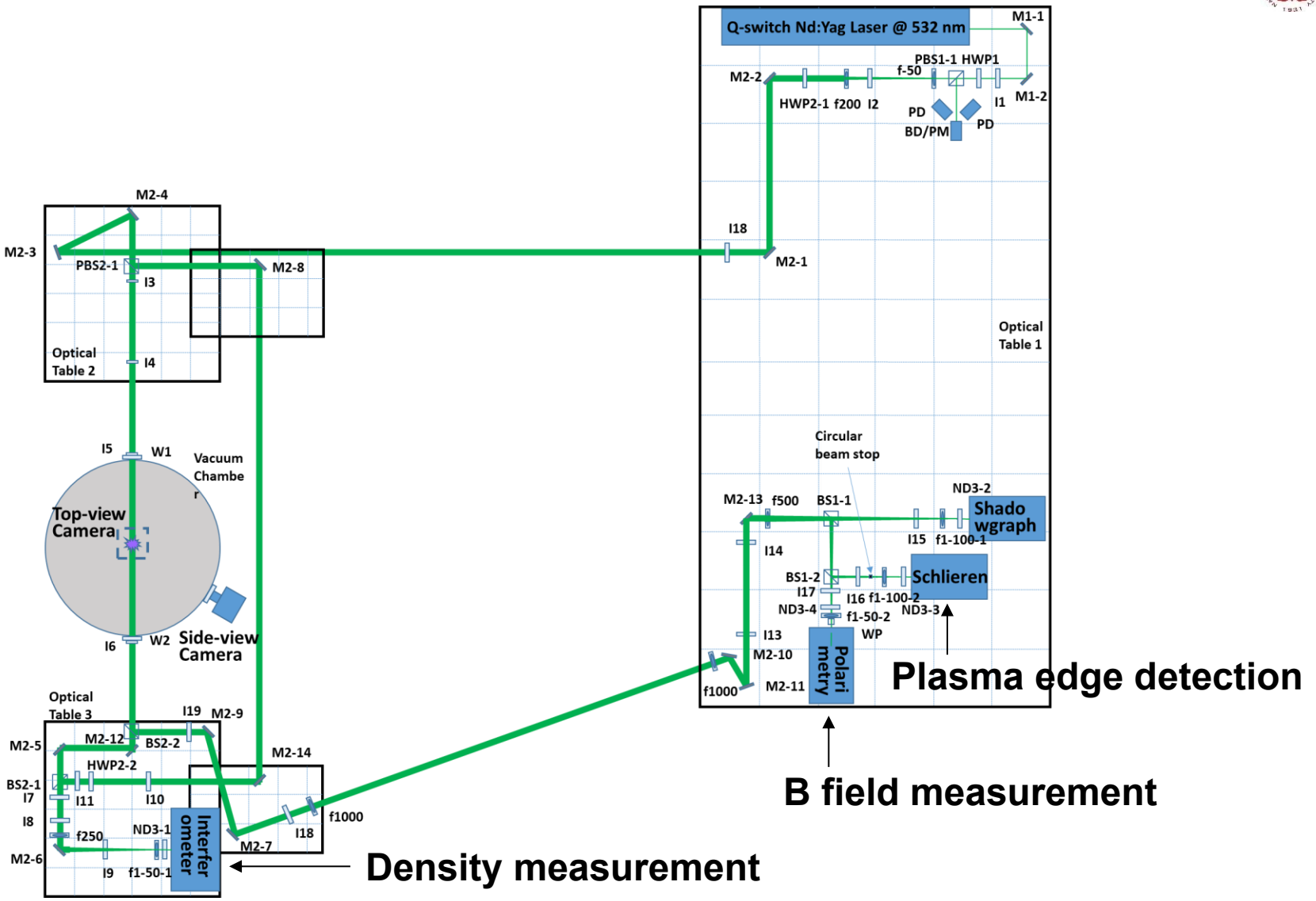

Varies diagnostics were integrated to the system

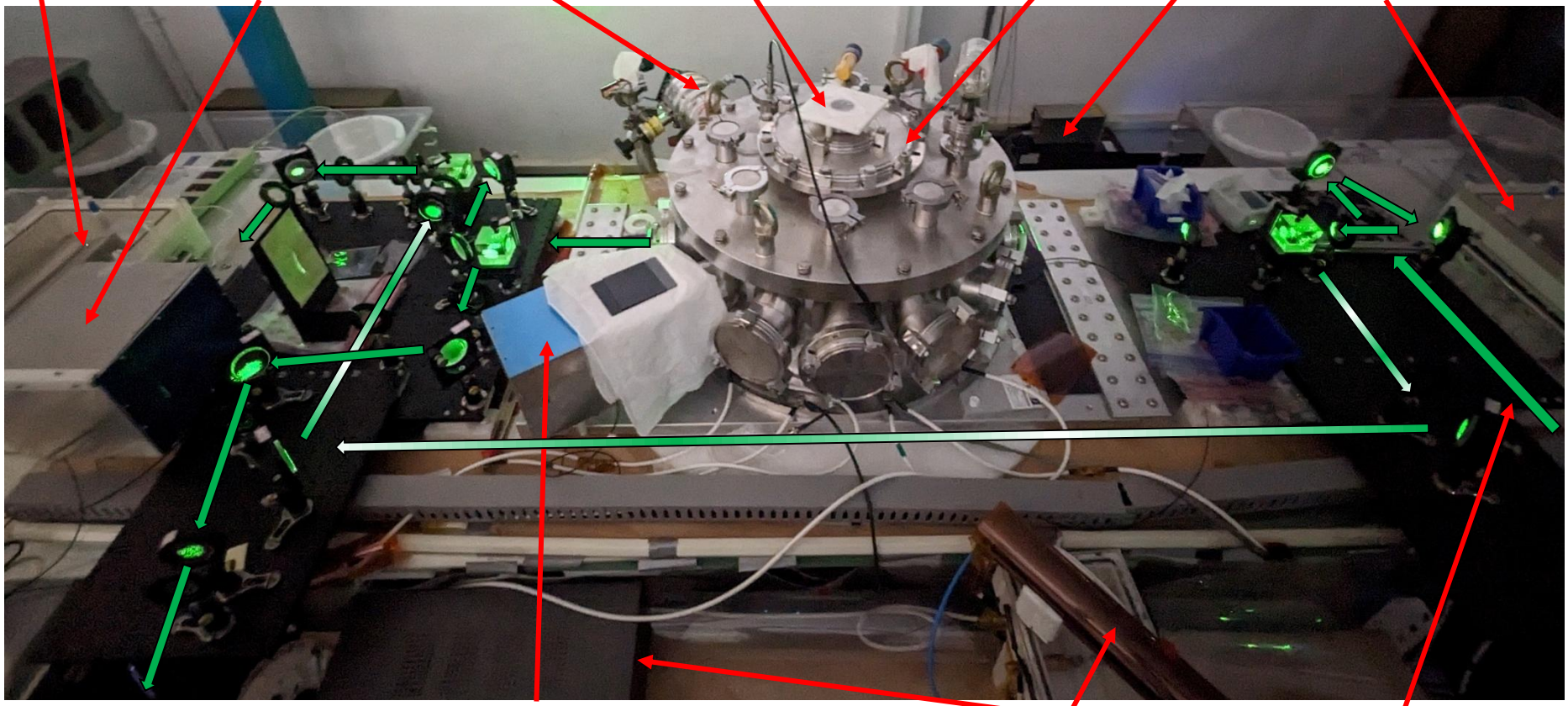

A plasma jet can be generated by a conical-wire array due to the nonuniform z-pinch effect

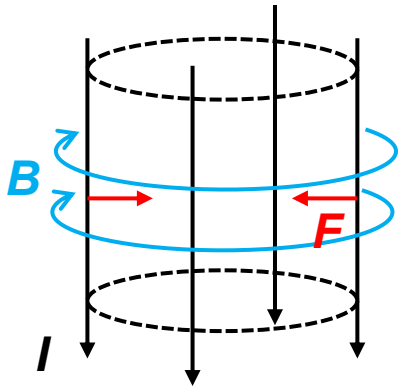

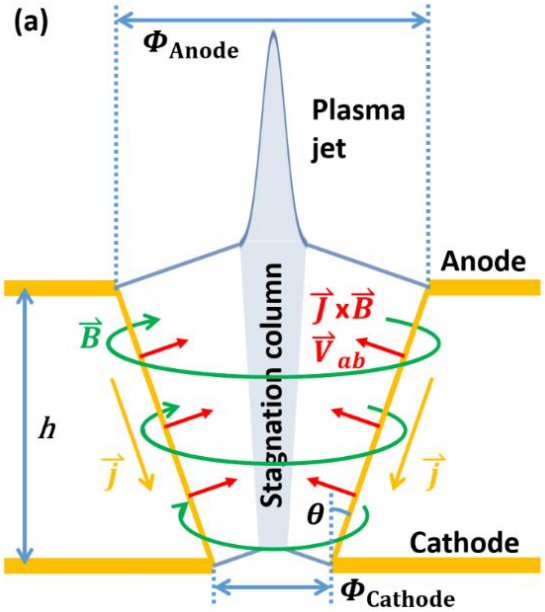

$$V_j = V_{ab}\frac{1+\cos\theta}{\sin\theta}$$

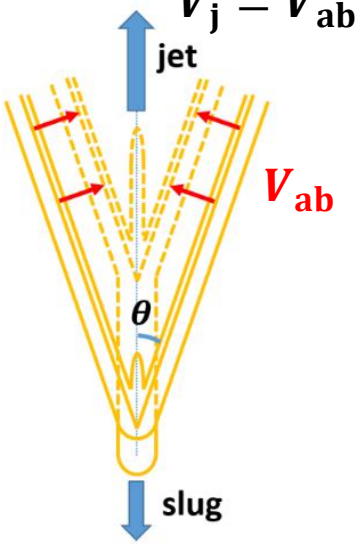

1. Wire ablation : corona plasma is generated by wire ablations.
2. Precursor : corona plasma is pushed by the $\vec{J}\times\vec{B}$ force and accumulated on the axis forming a precursor.
3. Plasma jet is formed by the nonuniform z-pinch effect due to the radius difference between the top and the bottom of the array.

D. J. Ampleforda, et al., Phys. Plasmas 14, 102704 (2007)
G. Birkhoff, et al., J. Applied Physics 19, 563 (1948)

Our conical-wire array consists of 4 tungsten wires with an inclination angle of 30° with respect to the axis

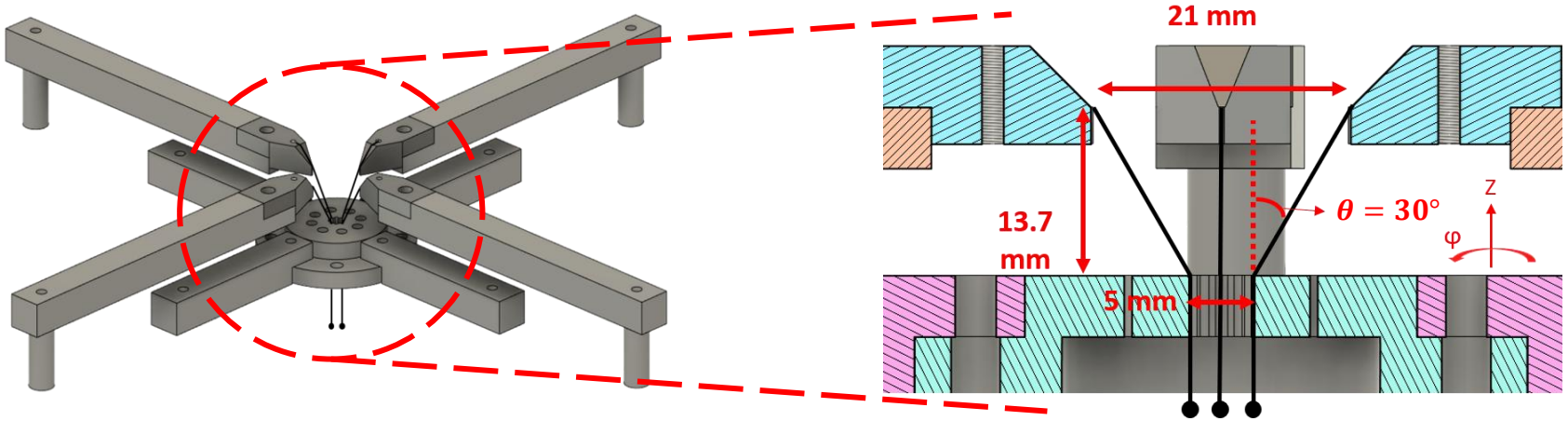

- Conical-wire array

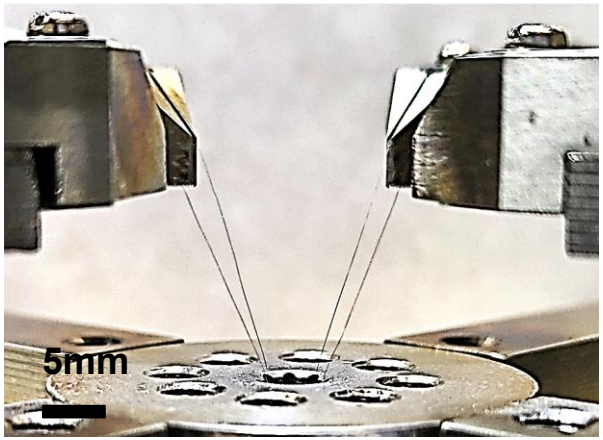

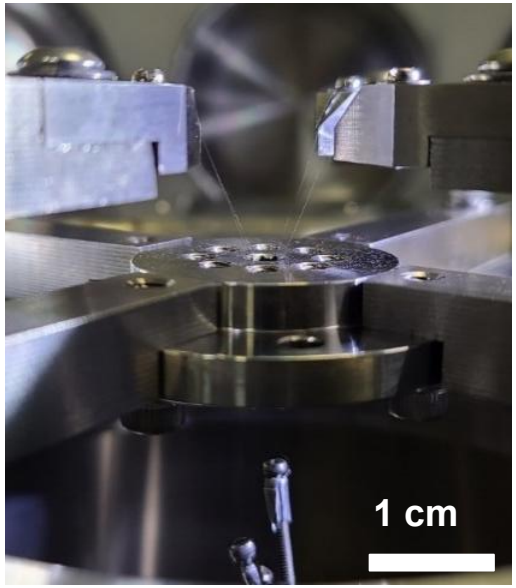

- Material : Tungsten.
- Number of wires : 4.
- Diameter : 20 μm.

Y.-C. Lin, NCKU Master Thesis 2021

Self-emission of the plasma jet in the UV to soft x-ray regions was captured by the pinhole camera

- **Image in UV/soft x ray**

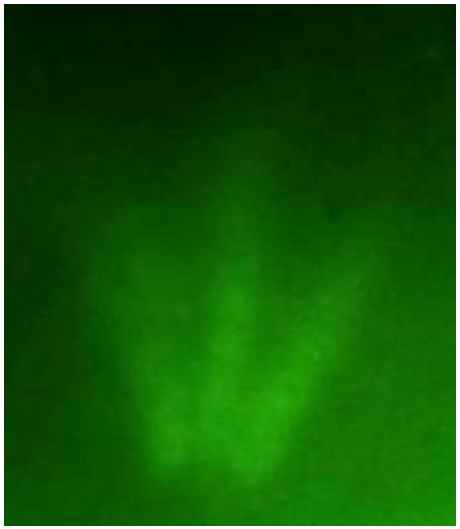

(Brightness is increased by 40 %.)

- **Pinhole diameter: 0.5 mm, i.e., spatial resolution: 1 mm.**

- **Image in visible light**

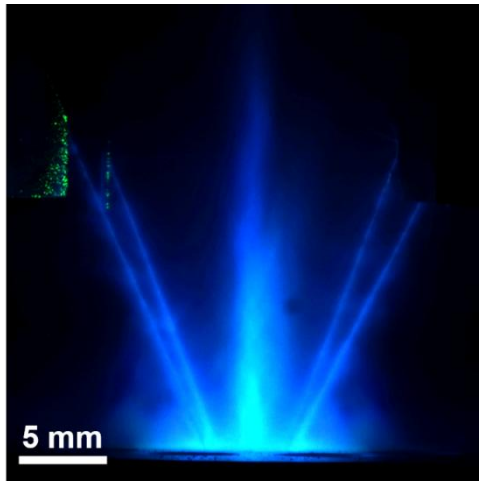

(Enhanced by scaling the intensity range linearly from 0 − 64 to 0 − 255.)

Y.-C. Lin, NCKU Master Thesis 2021

Plasma jet propagation was observed using laser diagnostics

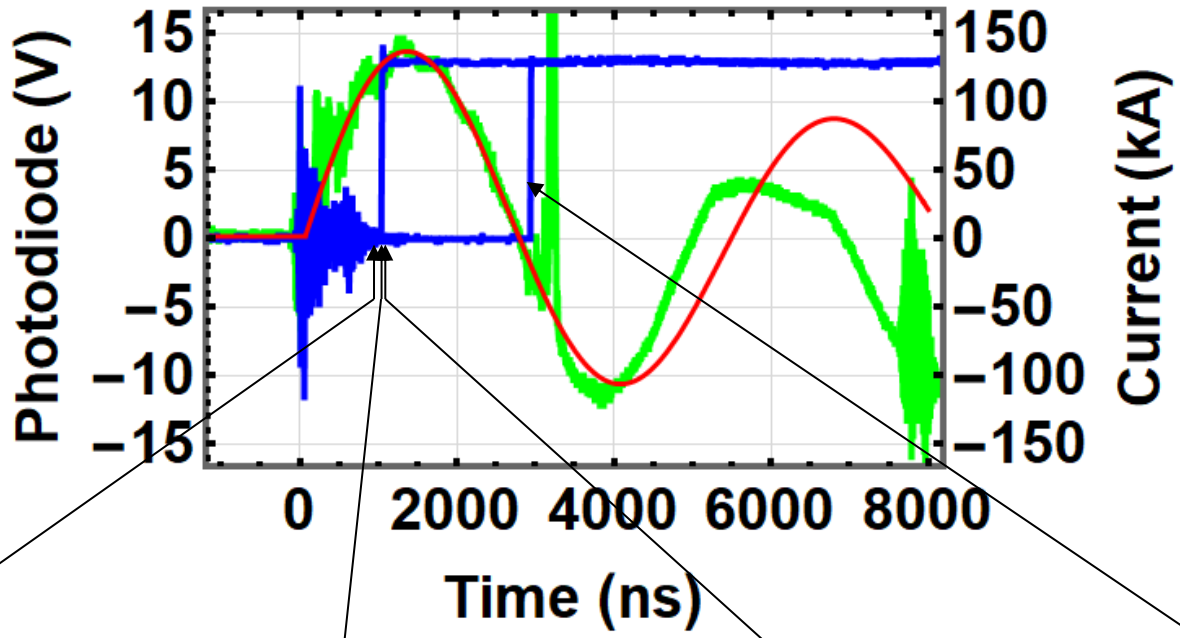

- **Shadowgraph images:**

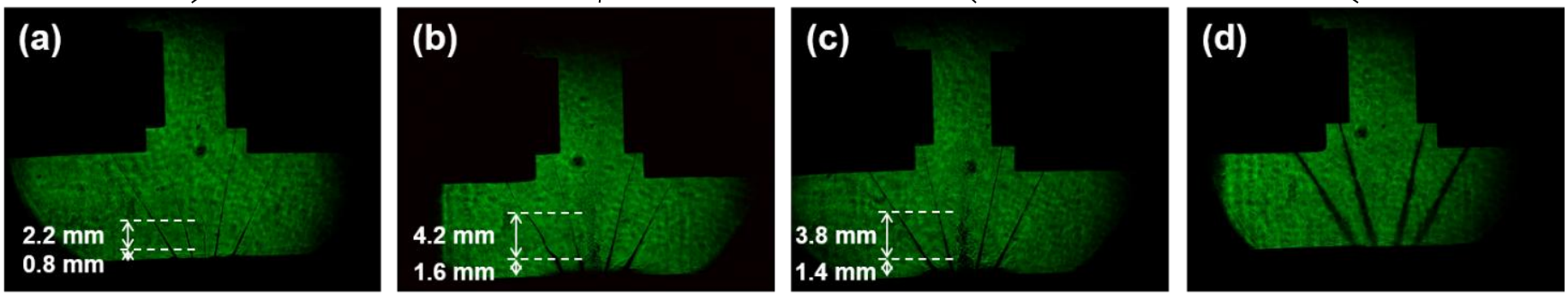

930 ± 20 ns 975 ± 2 ns 985 ± 3 ns 2945 ± 2 ns

Length of the plasma jet at different time was obtained by the Schlieren images at different times

- **Shadowgraph images:**

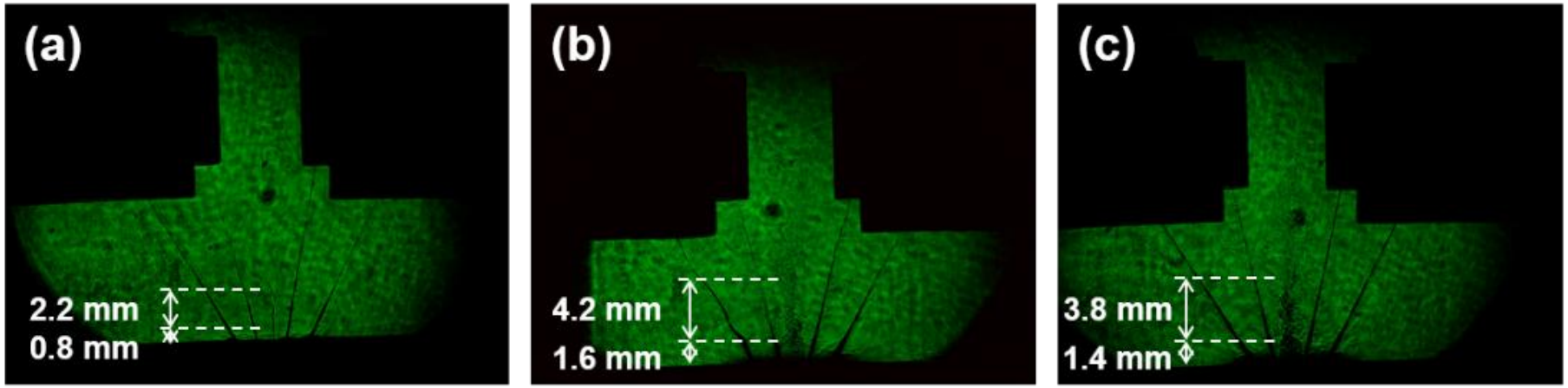

- **Schlieren images:**

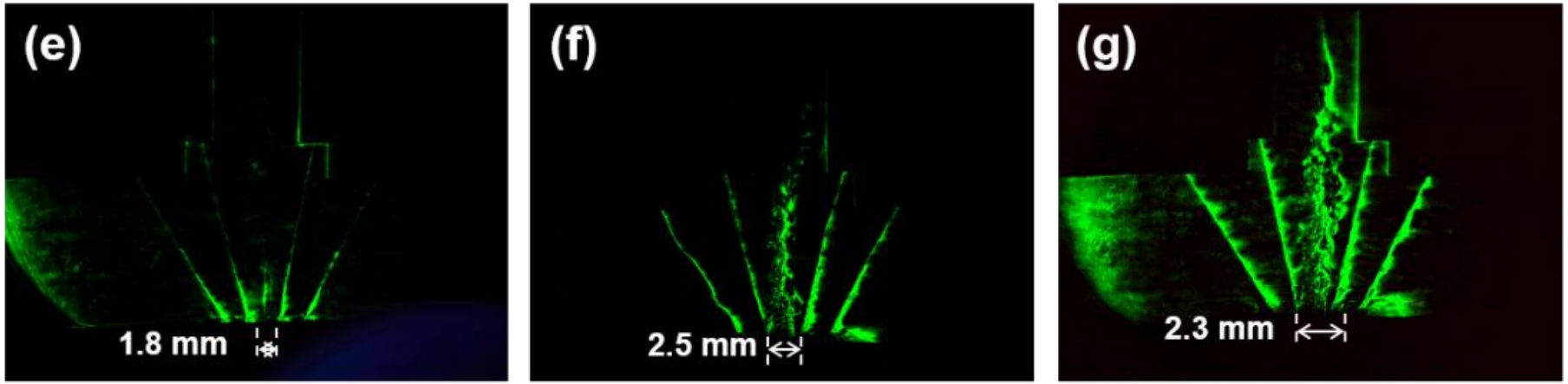

930 ± 20 ns **975 ± 2 ns** **985 ± 3 ns**

The measured plasma jet speed is 170 ± 70 km/s with the corresponding Mach number greater than 5

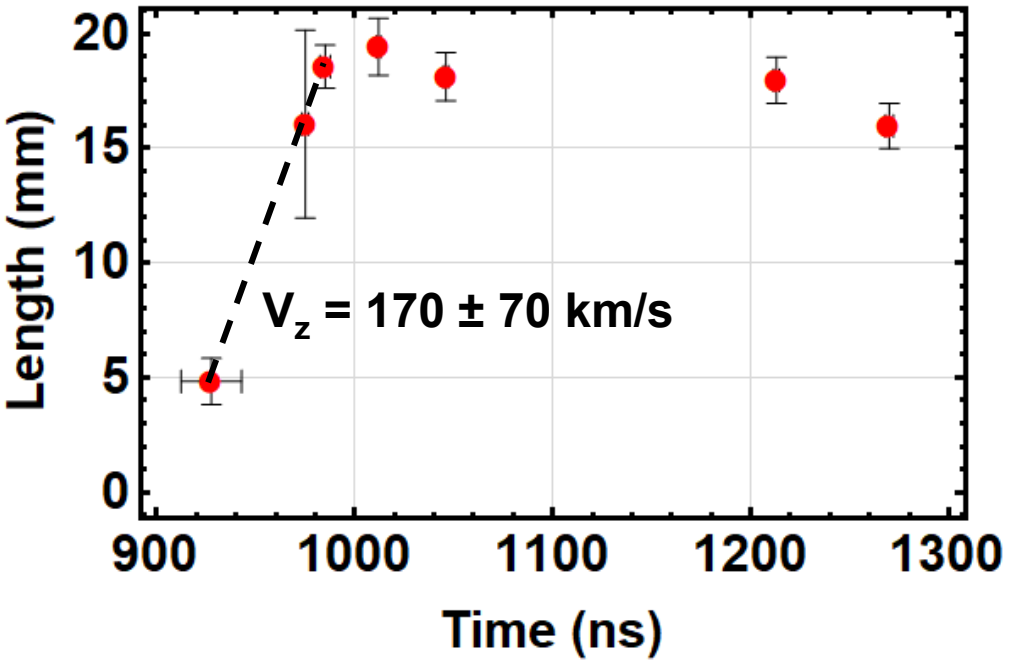

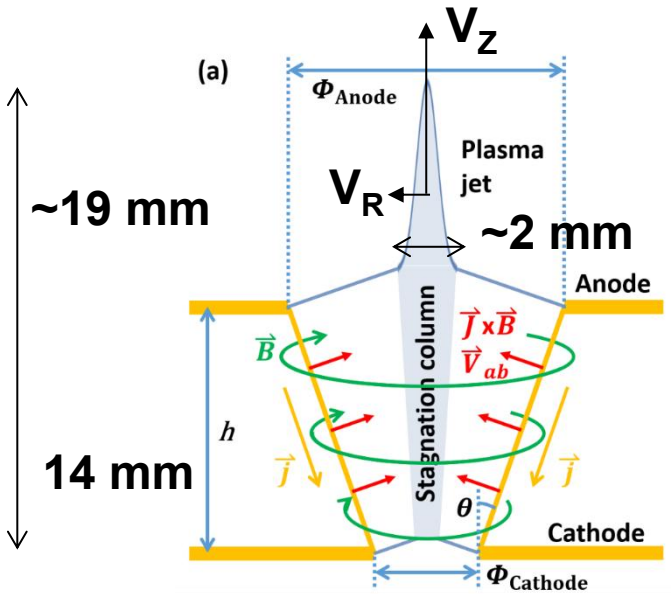

$$M = \frac{V_Z}{V_R} \geq \frac{Z}{r} \approx \frac{(19-14)\ \text{mm}}{\frac{2\ \text{mm}}{2}} = 5$$

$$V_{ab} = V_j \frac{\sin\theta}{1+\cos\theta} = 50\ \pm 20\ \text{km/s}$$

Plasma disk can be formed when two head-on plasma jets collide with each other

- **Astronomers Find a ‘Break’ in One of the Milky Way’s Spiral Arms.**

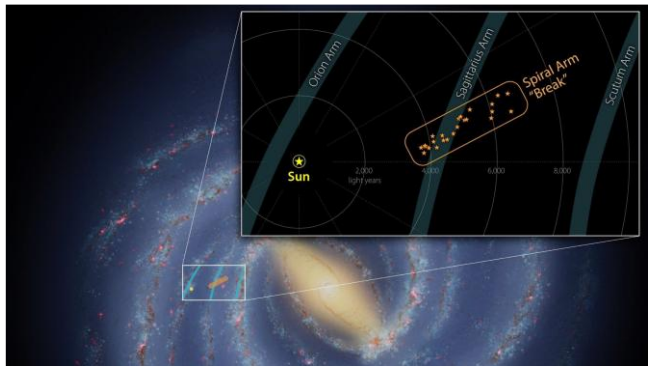

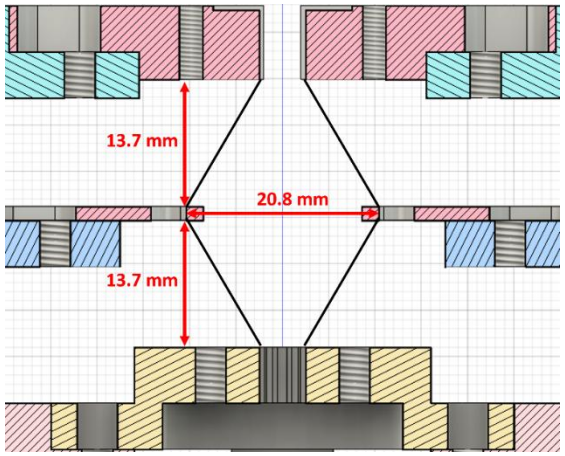

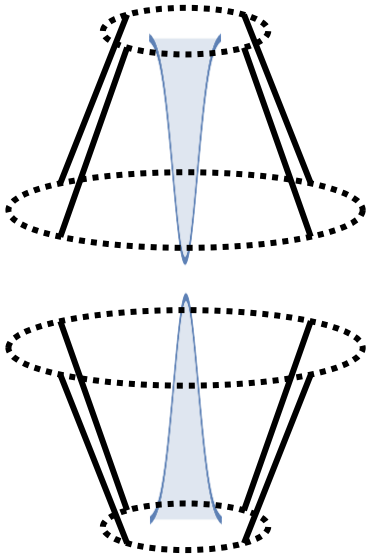

Jet Propulsion Laboratory [NASA/JPL] Astronomers Find a ‘Break’ in One of the Milky Way’s Spiral Arms (Aug 17, 2021)

Plasma disk can be formed when two head-on plasma jets collide with each other

Schlieren

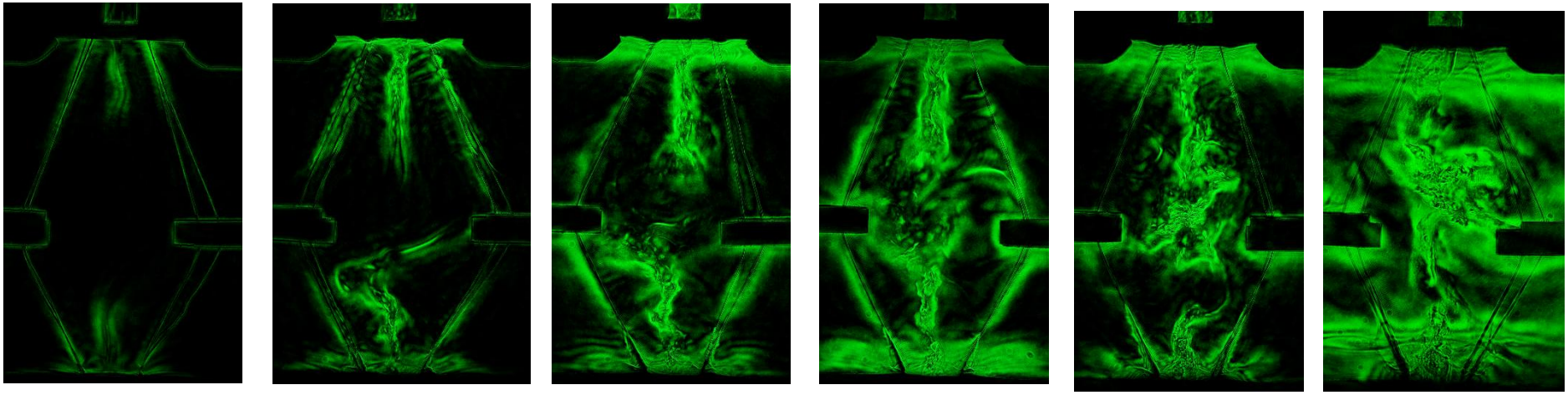

Interferometer

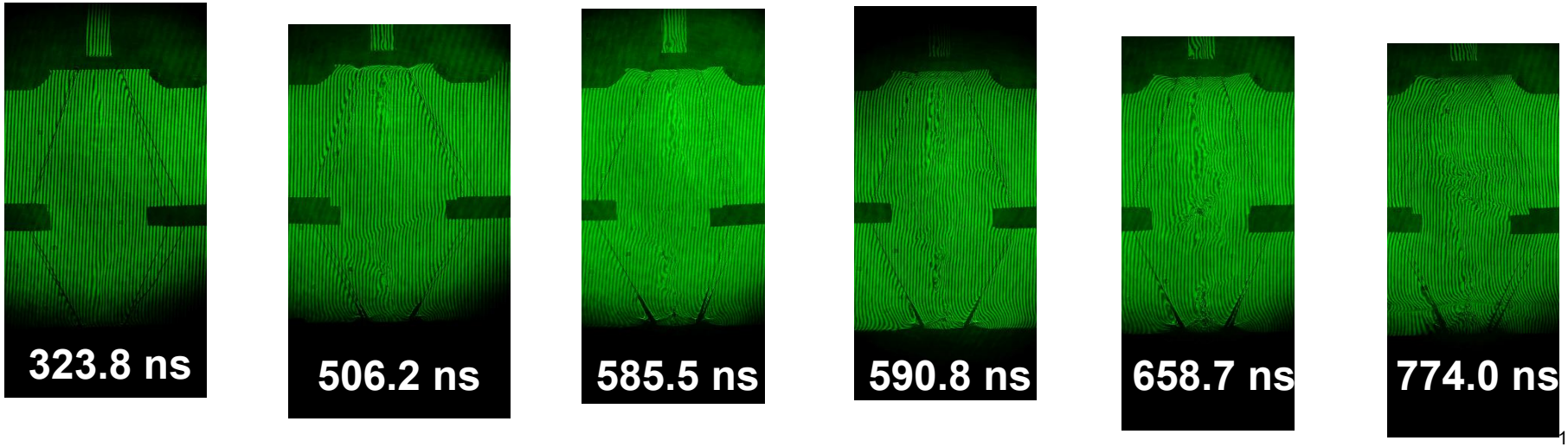

Plasma disk can be formed when two head-on plasma jets collide with each other

Schlieren

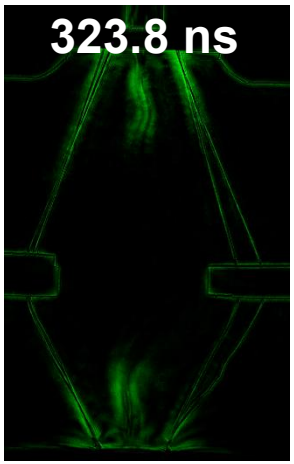

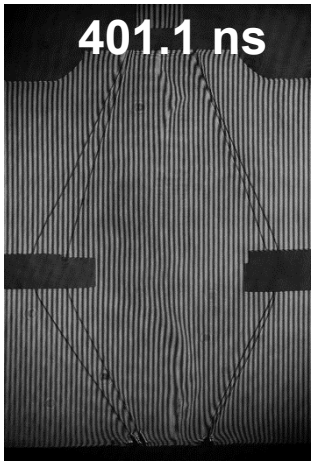

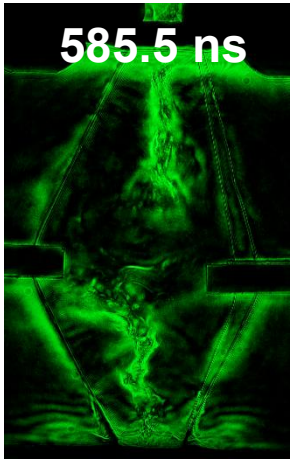

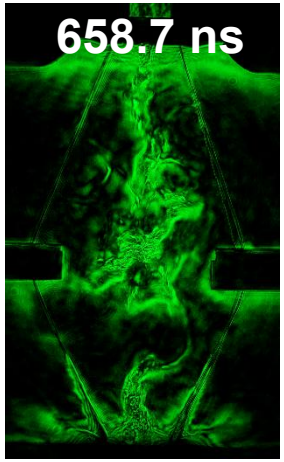

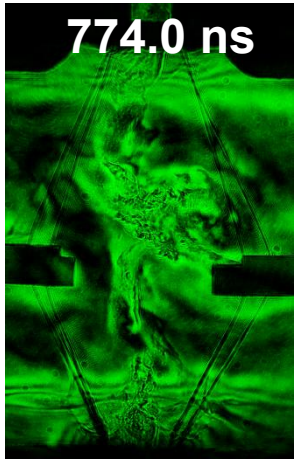

Interferometer

$-2\pi \sim 2\pi \Rightarrow 0 \sim 4.2 \times 10^{17}\ cm^{-2} \Rightarrow 8.4 \times 10^{17}\ cm^{-3}$ for l= 5mm

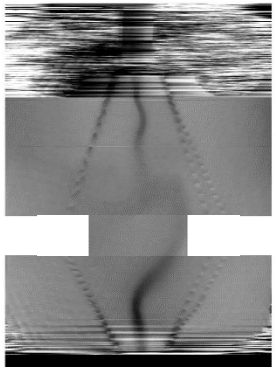

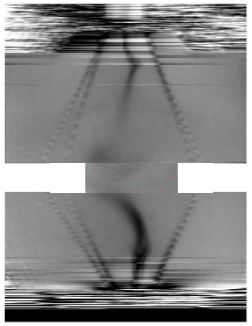

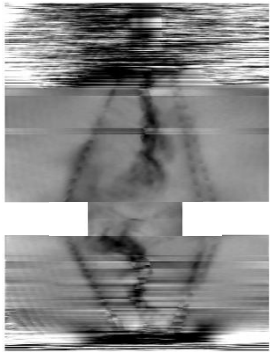

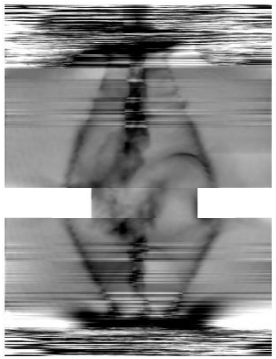

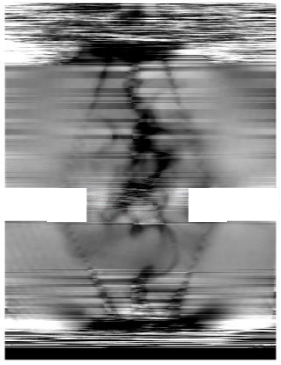

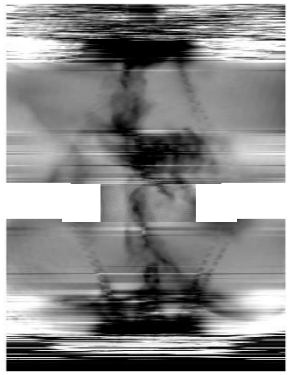

Φ(rad)

Energetic charged particles losses most of its energy right before it stops

Momentum transfer:

$$\Delta p_\perp = \int F_\perp dt = \int F_\perp \frac{dt}{dx} dx = \int F_\perp \frac{dx}{v}$$

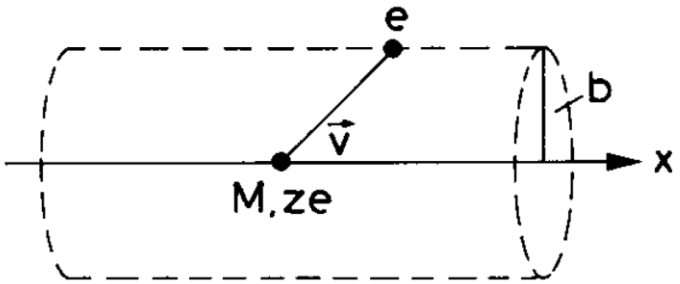

$$= \int_{-\infty}^{\infty} \frac{ze^2}{(x^2+b^2)} \cdot \frac{b}{\sqrt{x^2+b^2}} \cdot \frac{1}{v}\, dx = \frac{ze^2 b}{v} \left[\frac{x}{b^2\sqrt{x^2+b^2}} \right]_{-\infty}^{\infty} = \frac{2ze^2}{bv}$$

$\Delta p_\parallel$: averages to zero

$$\Delta E(b) = \frac{\Delta p^2}{2m_e} \qquad N_e = n \cdot (2\pi b) \cdot db\, dx$$

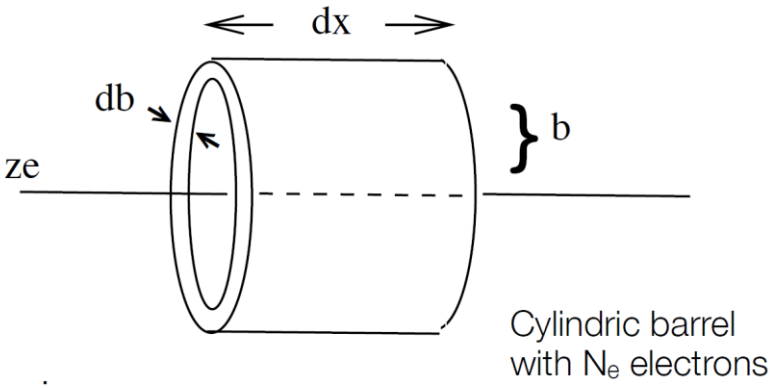

$$-dE(b) = \frac{\Delta p^2}{2m_e} \cdot 2\pi n b\, db\, dx$$

$$-\frac{dE}{dx} = \frac{4\pi\, n\, z^2 e^4}{m_e v^2} \cdot \int_{b_{min}}^{b_{max}} \frac{db}{b} = \frac{4\pi\, n\, z^2 e^4}{m_e v^2} \ln \frac{b_{max}}{b_{min}}$$

Proton therapy takes the advantage of using Bragg peak

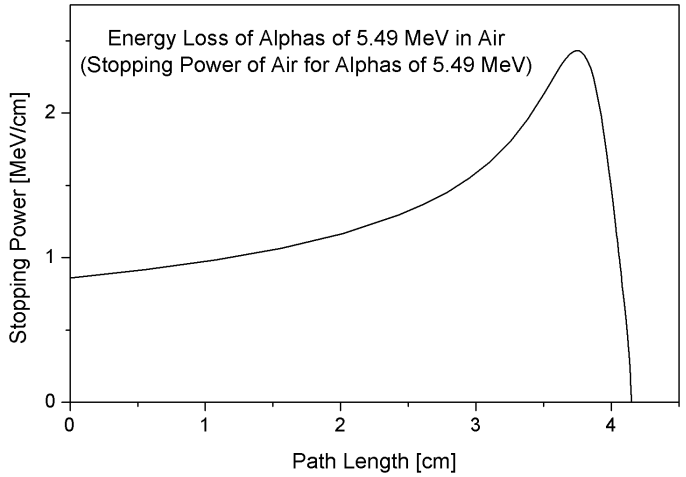

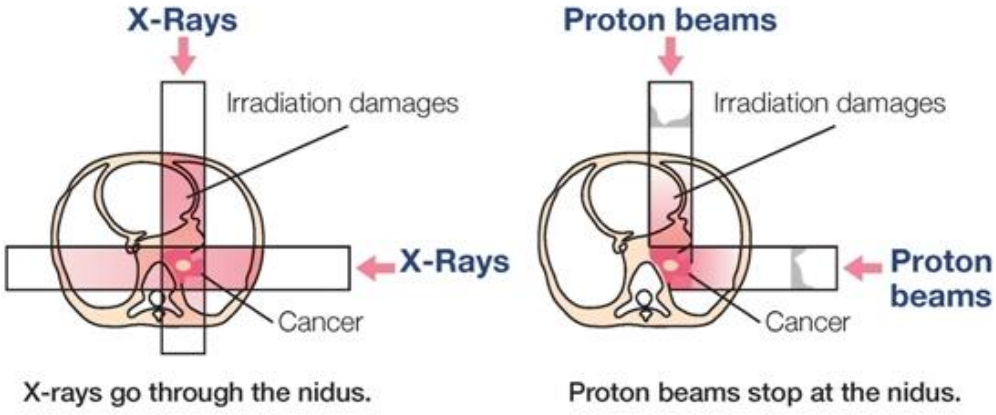

http://www.shi.co.jp/quantum/eng/product/proton/proton.html

There are two suggested website for getting the information of proton stopping power in different materials

http://www.nist.gov/pml/data/star/

NIST Time | NIST Home | About NIST | Contact Us | A-Z Site Index Search

Physical Measurement Laboratory

About PML ▼ Publications Topic/Subject Areas ▼ Products/Services ▼ News/Multimedia Programs/Projects Facilities ▼

NIST Home > PML > Physical Reference Data > Stopping-Power & Range Tables: e-, p+, Helium Ions

NISTIR 4999 | **Version History** | **Disclaimer**

Stopping-Power and Range Tables for Electrons, Protons, and Helium Ions

M.J. Berger, J.S. Coursey, M.A. Zucker and J. Chang
(NIST, Physical Measurement Laboratory)

estar* astar* pstar*

Abstract:

The databases ESTAR, PSTAR, and ASTAR calculate stopping-power and range tables for electrons, protons, or helium ions, according to methods described in ICRU Reports 37 and 49. Stopping-power and range tables can be calculated for electrons in any user-specified material and for protons and helium ions in 74 materials.

Contents:

1. Introduction
2. ESTAR: Stopping Powers and Ranges for Electrons
3. PSTAR and ASTAR: for Protons and Helium Ions (alpha particles)

References

Appendix: Significance of Calculated Quantities

Access the Data:

1. Electrons
2. Protons

請選取語言 SHARE

由「Google 翻譯」技術提供

© Creations/2010 Shutterstock.com

Access the Data

Electrons | Protons | Helium Ions

NIST Standard Reference Database 124
Rate our products and services.
Online: October 1998 - **Last update:** August 2005

Contact

Stephen Seltzer

http://www.srim.org/

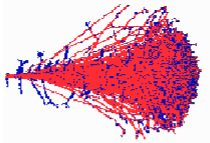

NEW! **SRIM Textbook** NEW!

Software	Science
SRIM / TRIM Introduction	Historical Review
Download SRIM-2013	Details of SRIM-2013
SRIM Install Problems	Experimental Data Plots Stopping of Ions in Matter
SRIM Tutorials	Stopping in Compounds
Download TRIM Manual Part-1, Part-2	Scientific Citations of Experimental Data
Stopping, Range and Damage	High Energy Stopping

The thickness of a filter can be decided from the range data from NIST website

COPPER

To download data in spreadsheet (array) form, choose a delimiter and use the checkboxes in the table heading. After downloading, save the output by using your browser's Save As feature.

Delimiter:
- space
- | (vertical bar)
- tab (some browsers may use spaces instead)
- newline

Download data | Reset

$\frac{dE}{\rho dx}$ ρx

(required) Kinetic Energy (MeV)	Stopping Power (MeV cm²/g)			Range		
	Electronic	Nuclear	Total	CSDA (g/cm²)	Projected (g/cm²)	Detour Factor Projected / CSDA
1.000E-03	3.490E+01	4.408E+00	3.931E+01	4.116E-05	5.620E-06	0.1365
1.500E-03	4.274E+01	4.231E+00	4.697E+01	5.267E-05	8.301E-06	0.1576
2.000E-03	4.935E+01	4.049E+00	5.340E+01	6.263E-05	1.101E-05	0.1759
2.500E-03	5.518E+01	3.876E+00	5.906E+01	7.152E-05	1.374E-05	0.1921
3.000E-03	6.045E+01	3.718E+00	6.416E+01	7.964E-05	1.647E-05	0.2068
4.000E-03	6.980E+01	3.440E+00	7.324E+01	9.419E-05	2.194E-05	0.2329
5.000E-03	7.804E+01	3.207E+00	8.124E+01	1.071E-04	2.739E-05	0.2556
6.000E-03	8.548E+01	3.010E+00	8.849E+01	1.189E-04	3.280E-05	0.2758
7.000E-03	9.233E+01	2.840E+00	9.517E+01	1.298E-04	3.817E-05	0.2940
8.000E-03	9.871E+01	2.692E+00	1.014E+02	1.400E-04	4.347E-05	0.3106
9.000E-03	1.047E+02	2.561E+00	1.073E+02	1.496E-04	4.872E-05	0.3258
1.000E-02	1.104E+02	2.445E+00	1.128E+02	1.587E-04	5.391E-05	0.3398

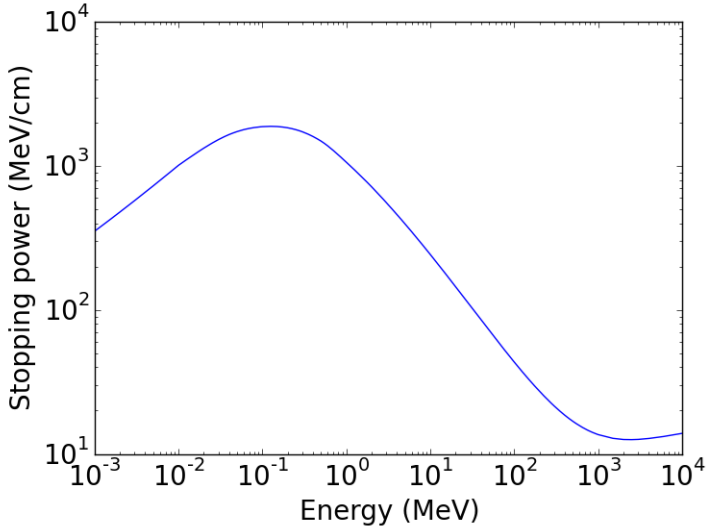

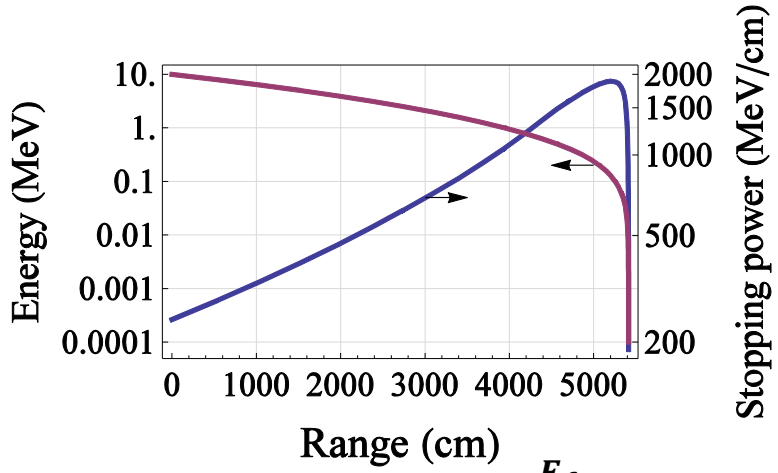

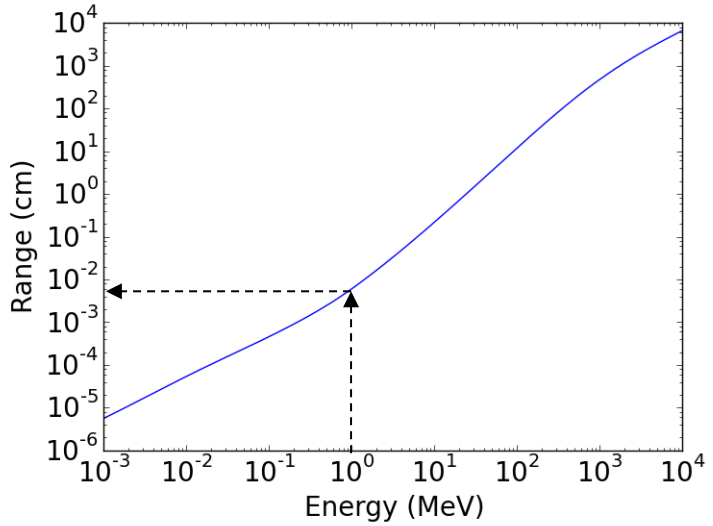

$$\frac{dE}{dx} = f(E) \Rightarrow x = \int_{E_i}^{E_f} \frac{dE}{f(E)}$$

Proton therapy takes the advantage of using Bragg peak

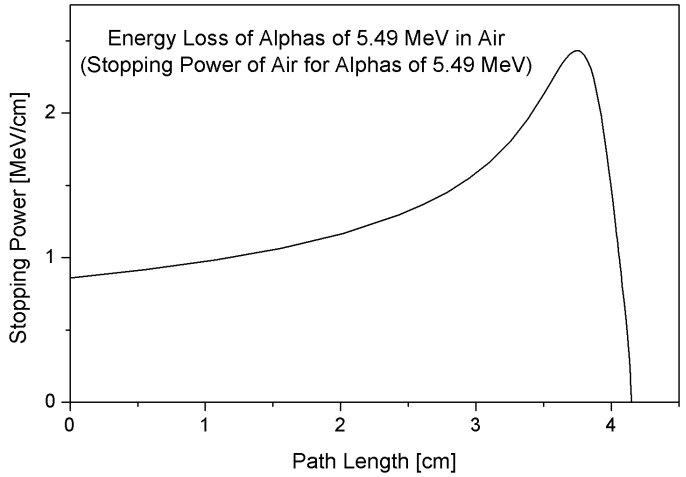

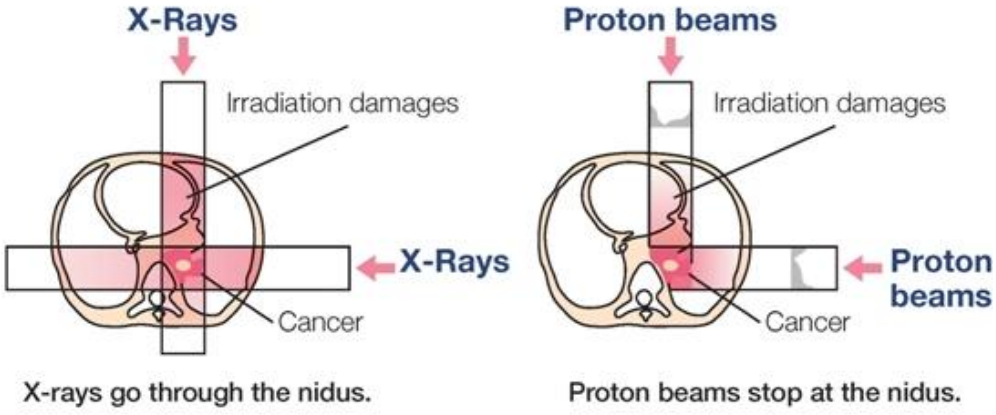

http://www.shi.co.jp/quantum/eng/product/proton/proton.html

A pulse signal is converted to a voltage signal using an integrator

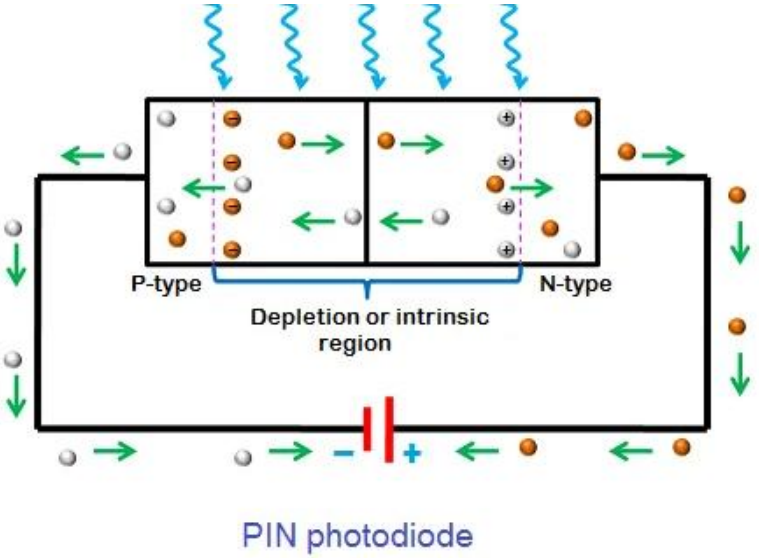

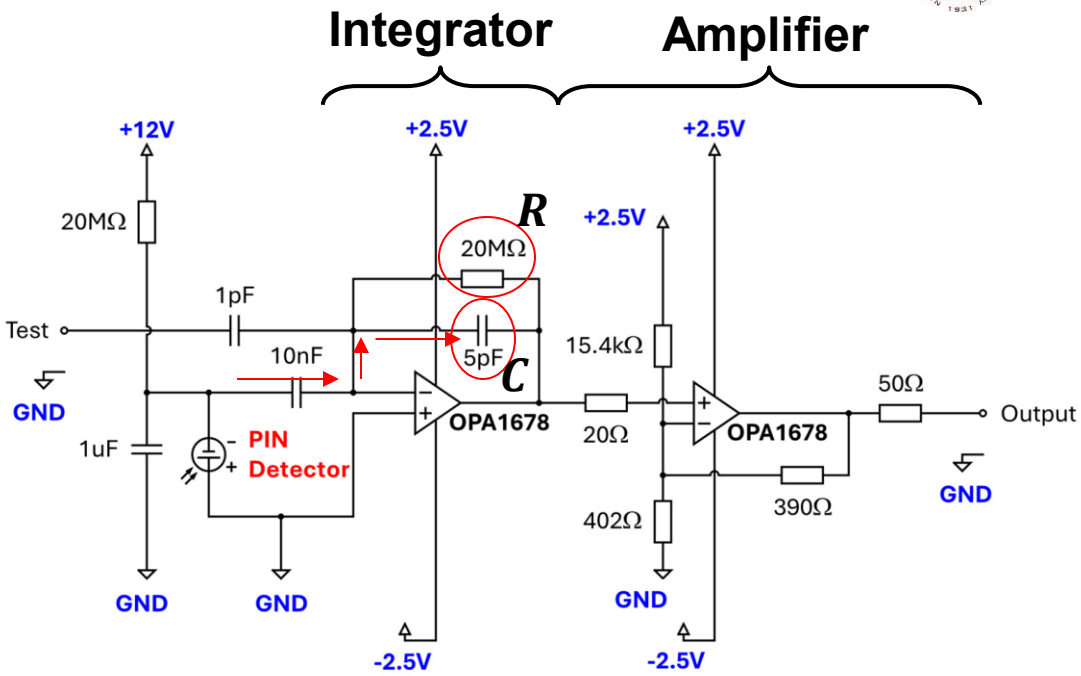

- The 5-pF capacitor is charged by the current from the PIN detector.
- The 5-pF capacitor is discharged by the 20-MΩ resistor.

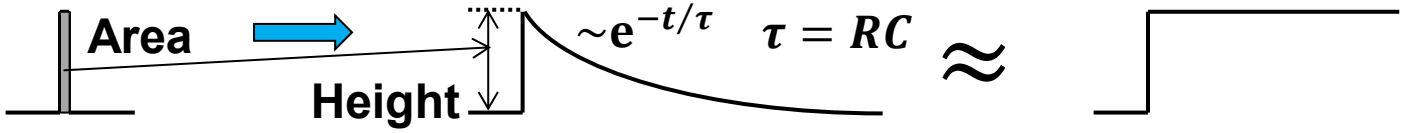

https://www.quarktwin.com/blogs/diode/the-working-principle-and-applications-of-photodiodes/125
Allan Xi Chen, etc., J. Nucl. Eng. 6, 15 (2025)

Pulse Shaping is commonly used in nuclear and particle physics electronics

- **Improve Signal-to-noise ratio S/N**
  - Restrict bandwidth to match measurement time.

  => Increase pulse width.

- **Improve pulse-pair resolution**

  => Decrease pulse width.

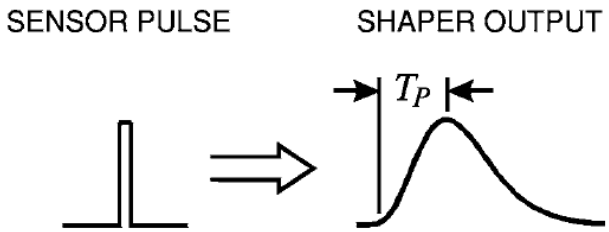

FIGURE 13. A pulse shaper transforms a short sensor pulse into a longer pulse with a rounded cusp and peaking time T_P.

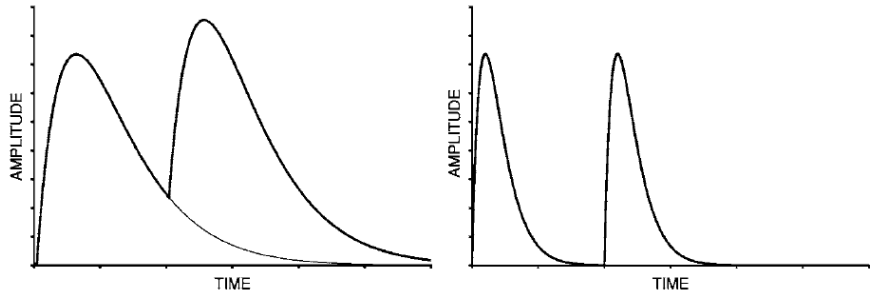

FIGURE 14. Amplitude pileup when two successive pulses overlap (left). Reducing the shaping time allows the first pulse to return to the baseline before the second arrives.

H. Spieler, AIP Conf. Proc. 674, 76 (2003)

Expected data profile

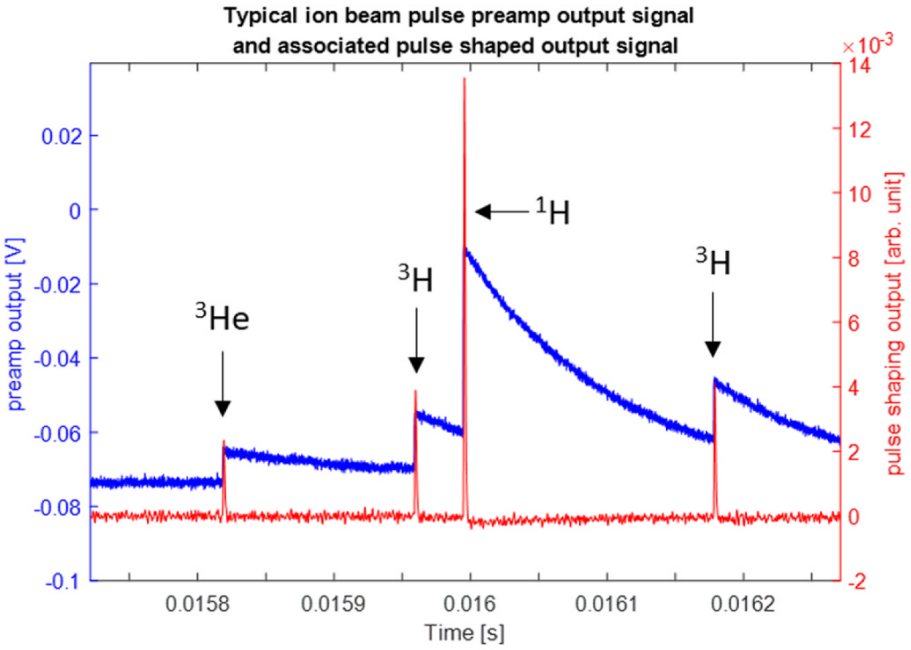

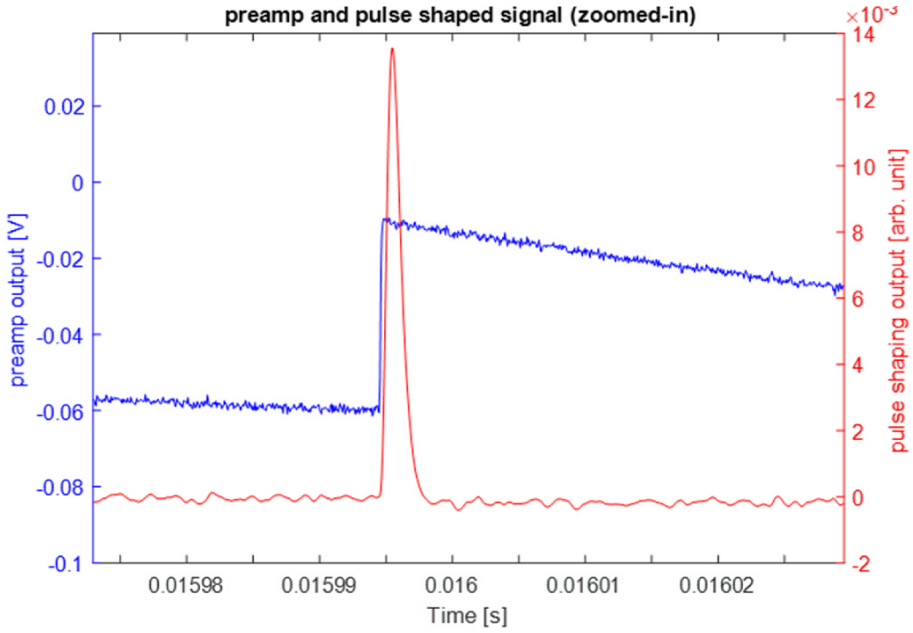

Allan Xi Chen, etc., Physics Open 21, 100234(2024)

CR-RC^n pulse shaping combines a high-pass filter and n low-pass filter

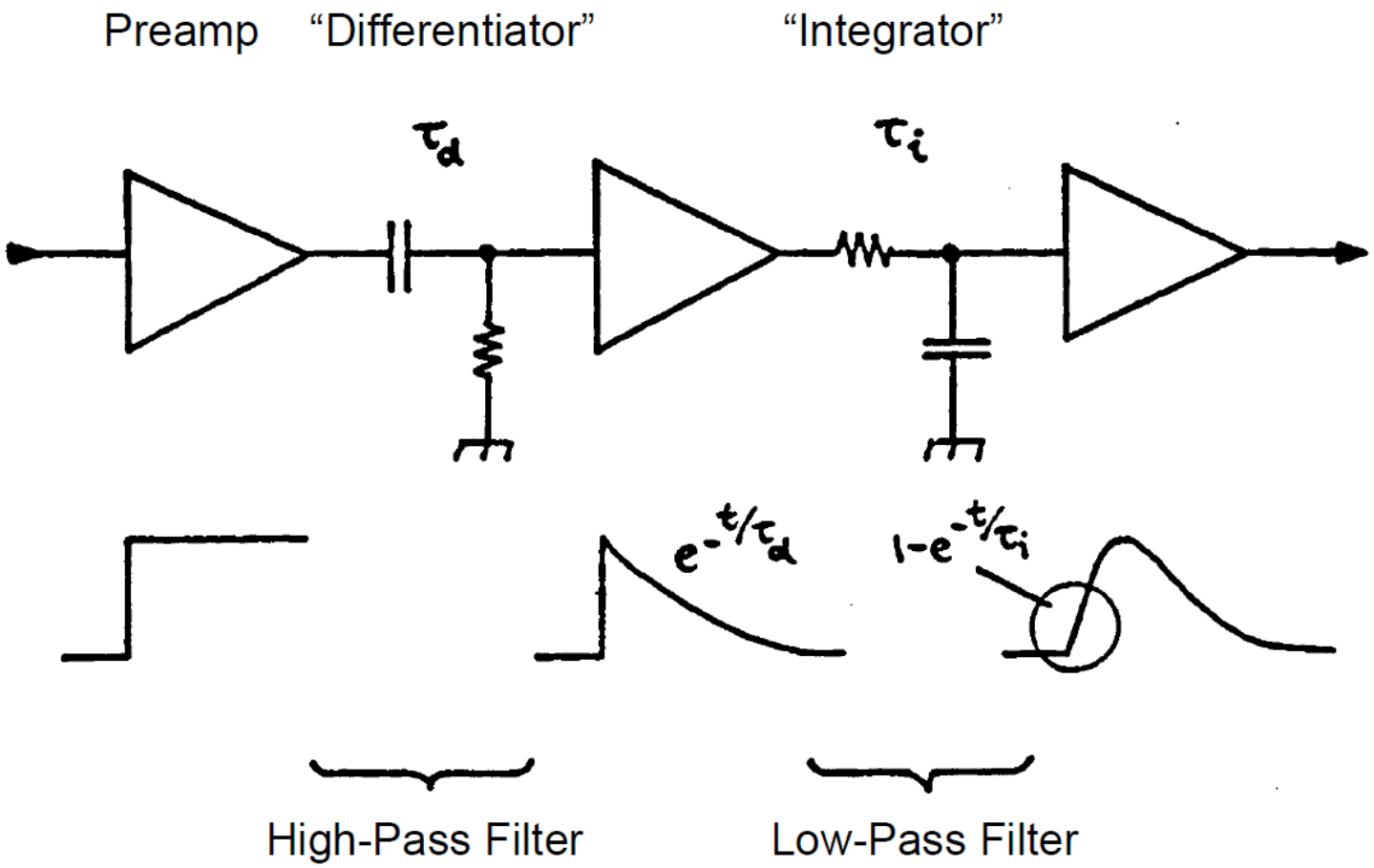

Lecture Notes - VII. Heidelberger Graduate Lectures in Physics by H. Spieler (2001)
https://www-physics.lbl.gov/%7Espieler/Heidelberg_Notes_2001/index.html

Pulses become gaussian-like after multiple integrators

- **Integrating with the same time constant τ**

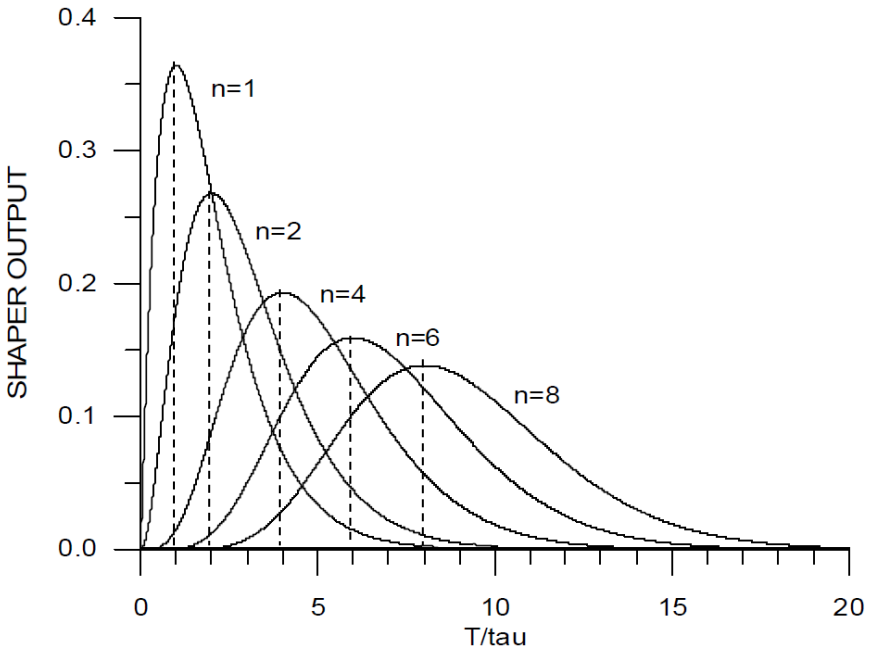

$$T_p = n\tau$$

- **Integrating with the reduced time constant** $\tau_n = \frac{\tau_1}{n}$

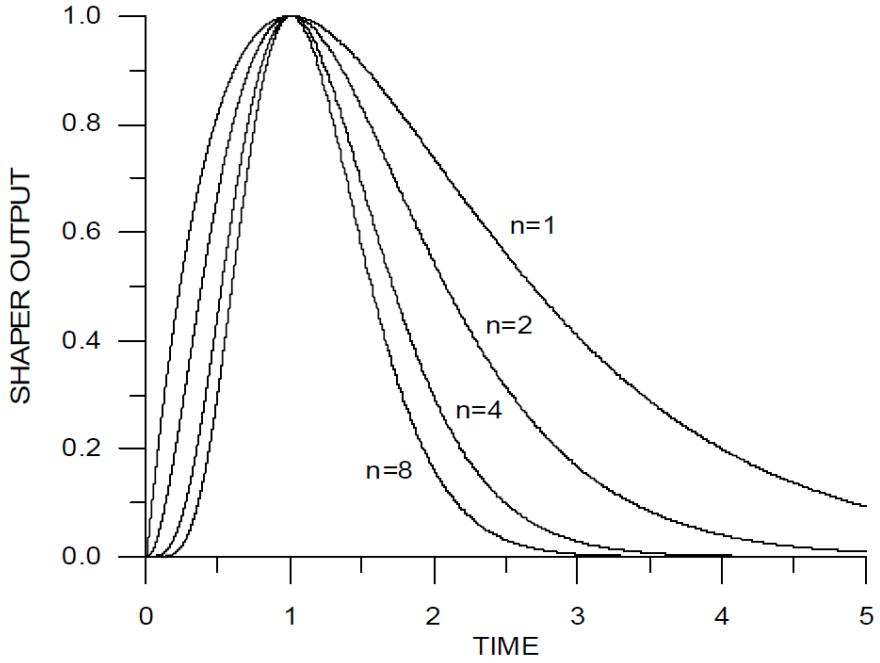

CR is the high pass filter while RC is the low pass filter

- **CR circuit:**

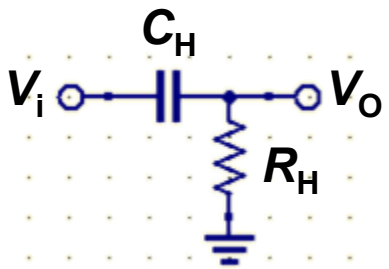

$$\tau_H = R_H C_H$$

$$V_o = V_i \frac{R_H}{\frac{1}{j\omega C_H} + R_H} = V_i \frac{1}{\frac{1}{j\omega R_H C_H} + 1}$$

$$= V_i \frac{1}{\frac{1}{j\omega \tau_H} + 1}$$

For $\omega\tau_H \gg 1$, i.e.,

$$\frac{2\pi f}{f_H} \gg 1 \text{ or } f \gg f_H \quad \text{or} \quad \tau_H \gg t$$

$V_o \approx V_i$ • **High-pass filter!**

- **RC circuit:**

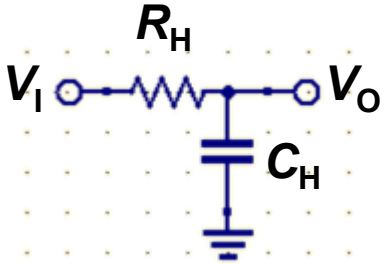

$$\tau_L = R_L C_L$$

$$V_o = V_i \frac{\frac{1}{j\omega C_L}}{\frac{1}{j\omega C_L} + R_L} = V_i \frac{\frac{1}{j\omega R_L C_L}}{\frac{1}{j\omega R_L C_L} + 1}$$

$$= V_i \frac{\frac{1}{j\omega \tau_L}}{\frac{1}{j\omega \tau_L} + 1}$$

For $\omega\tau_L \ll 1$, i.e.,

$$\frac{2\pi f}{f_L} \ll 1 \text{ or } f \ll f_L \quad \text{or} \quad t \ll \tau_L$$

$V_o \approx V_i$ • **Low-pass filter!**

CR is the high pass filter while RC is the low pass filter

- CR circuit:

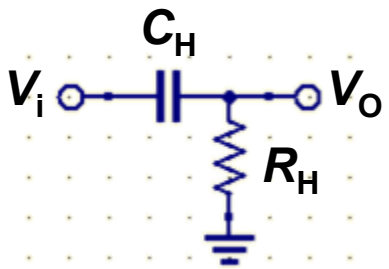

$$\tau_H = R_H C_H$$

$$V_i - V_c - V_o = 0 \qquad V_o = iR_H$$

$$V_c = \frac{1}{C_H}\int i dt = \frac{1}{C_H}\int \frac{V_o}{R_H} dt$$

$$\dot{V}_i = \frac{V_o}{\tau_H} + \dot{V}_o$$

$$V_o(t) = e^{-t/\tau_H}\int_0^t \dot{V}_i(t')e^{t'/\tau_H}dt'$$

- RC circuit:

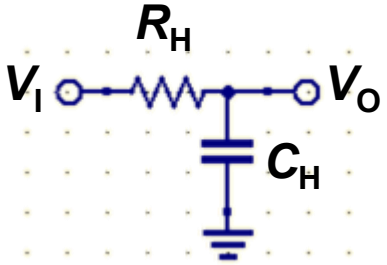

$$\tau_L = R_L C_L$$

$$V_i - V_R - V_o = 0 \qquad i = C_L \dot{V}_o$$

$$V_R = iR_L = R_L C_L \dot{V}_o$$

$$V_i = \tau_L \dot{V}_o + V_o$$

$$V_o(t) = e^{-t/\tau_L}\frac{1}{\tau_L}\int_0^t V_i(t')e^{t'/\tau_L}dt'$$

A step function becomes an exponential decay after the high-pass filter

- **CR circuit:**

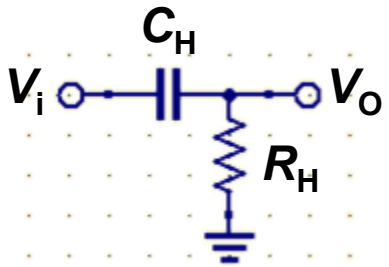

$$\tau_H = R_H C_H$$

$$V_o(t) = e^{-t/\tau_H} \int_0^t \dot{V}_i(t') e^{t'/\tau_H} dt'$$

$$V_i(t) = \begin{cases} 0 & t < 0 \\ V_{i0} & t \geq 0 \end{cases}$$

$$\dot{V}_i(t) = V_{i0}\delta(t)$$

$$V_o(t) = e^{-t/\tau_H} \int_0^t V_{i0}\delta(t') e^{t'/\tau_H} dt'$$

$$= V_{i0} e^{-t/\tau_H} \, e^{t'/\tau_H}\Big|_{t'=0} = V_{i0} e^{-t/\tau_H}$$

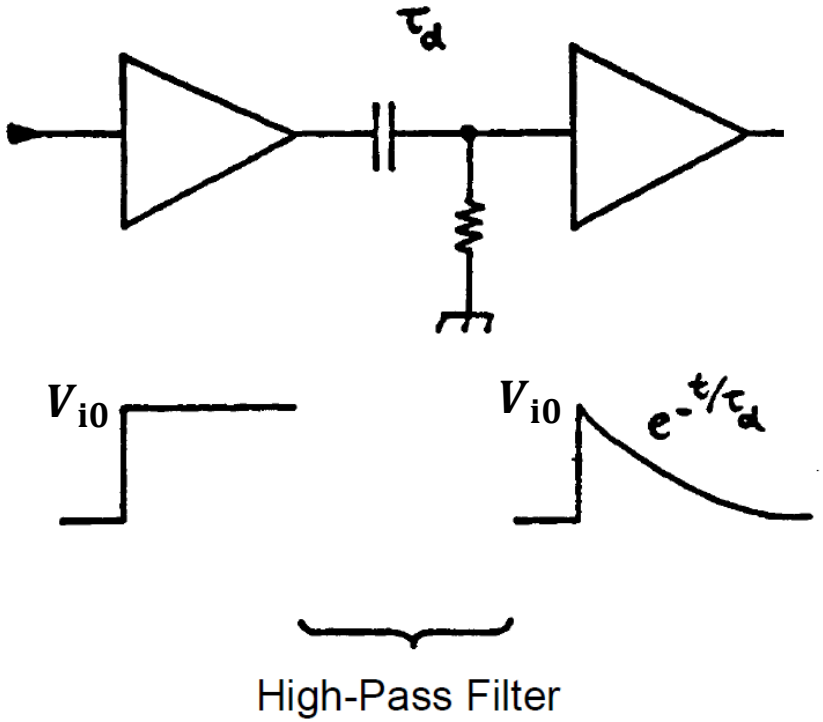

CR is the high pass filter while RC is the low pass filter

- **RC circuit:**

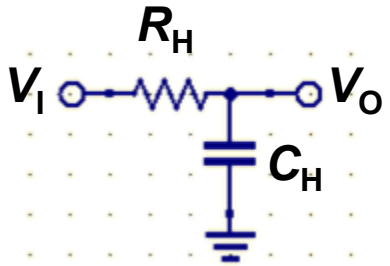

$$\tau_L = R_L C_L$$

$$V_o(t) = e^{-t/\tau_L}\frac{1}{\tau_L}\int_0^t V_i(t')e^{t'/\tau_L}dt'$$

$$V_i(t) = V_{i0}e^{-t/\tau_H}$$

For $t \ll \tau_L$ $\quad e^{-t/\tau_L} \sim e^{t/\tau_L} \sim 1$

$$V_o(t) \sim \frac{1}{\tau_L}\int_0^t V_i(t')dt' = \frac{1}{\tau_L}\int_0^t V_{i0}e^{-t'/\tau_H}dt'$$

$$= \frac{\tau_H}{\tau_L}V_{i0}\left(1 - e^{-t/\tau_H}\right)$$

$$V_o(t) = e^{-t/\tau_L}\frac{1}{\tau_L}\int_0^t V_{i0}e^{-t'/\tau_H}e^{t'/\tau_L}dt'$$

$$= e^{-t/\tau_L}\frac{1}{\tau_L}\int_0^t V_{i0}e^{t'/\tau_{eff}}dt'$$

$$= e^{-t/\tau_L}\frac{\tau_{eff}}{\tau_L}V_{i0}\left(e^{t/\tau_H} - 1\right)$$

$$\frac{1}{\tau_{eff}} = \frac{1}{\tau_L} - \frac{1}{\tau_H} < \frac{1}{\tau_L}$$

CR-RC^n pulse shaping combines a high-pass filter and n low-pass filter

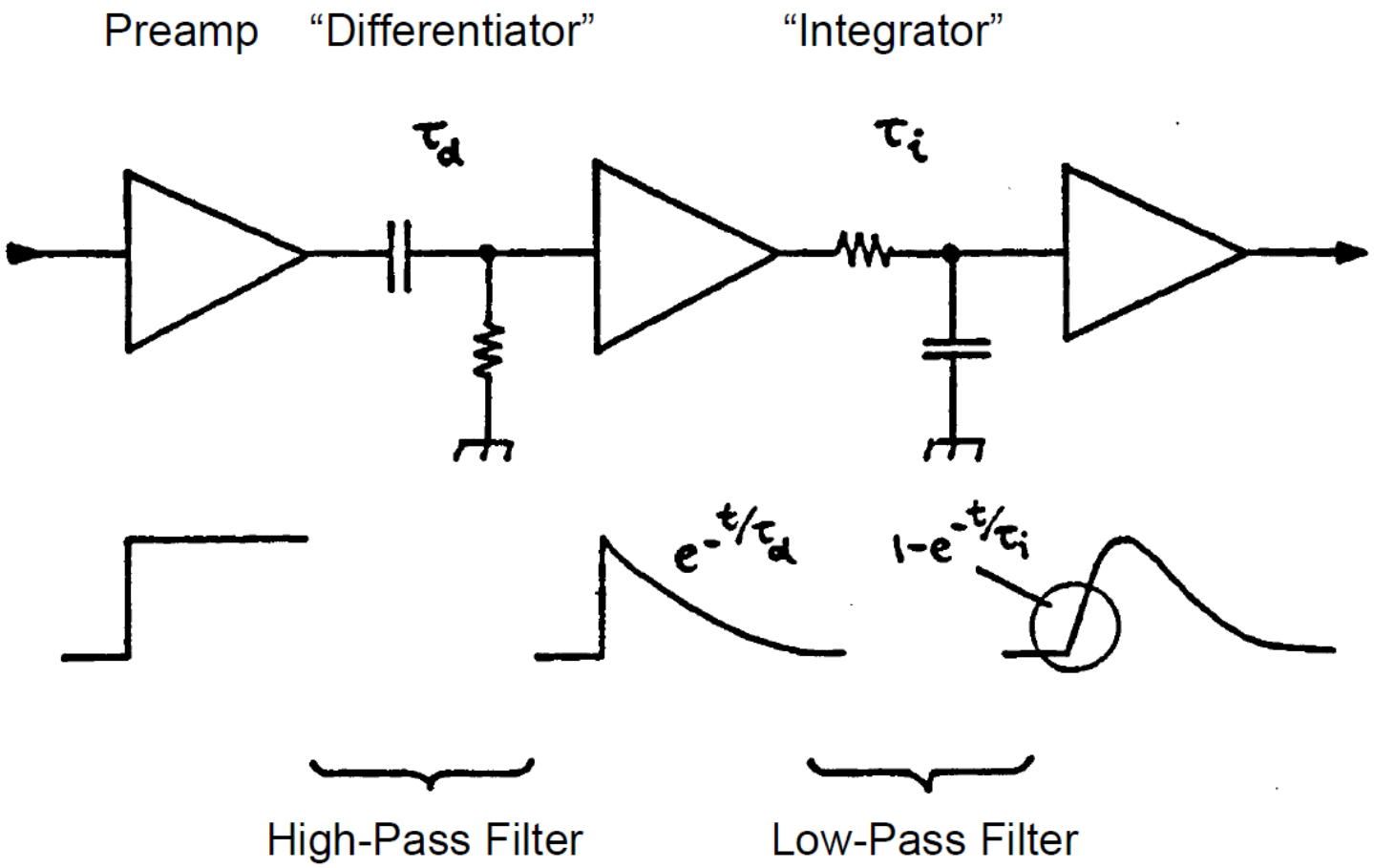

Lecture Notes - VII. Heidelberger Graduate Lectures in Physics by H. Spieler (2001)
https://www-physics.lbl.gov/%7Espieler/Heidelberg_Notes_2001/index.html

Finite difference method is used to numerically applying the CR-RC pulse shaping

- **CR circuit:**

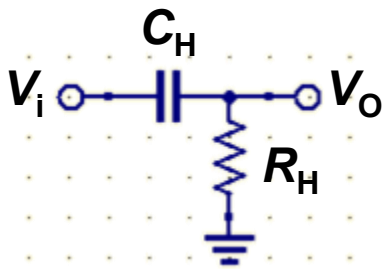

$$\tau_H = R_H C_H$$

$$\dot{V}_i = \frac{V_o}{\tau_H} + \dot{V}_o$$

- **RC circuit:**

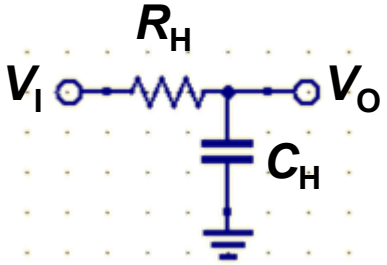

$$\tau_L = R_L C_L$$

$$V_i = \tau_L \dot{V}_o + V_o$$

$$\frac{V_i(t_j) - V_i(t_{j-1})}{\Delta t} \approx \frac{V_o(t_{j-1})}{\tau_H} + \frac{V_o(t_j) - V_o(t_{j-1})}{\Delta t}$$

$$\approx \frac{V_o(t_j)}{\tau_H} + \frac{V_o(t_j) - V_o(t_{j-1})}{\Delta t}$$

$$V_o(t_j) = \alpha_{CR} V_o(t_{j-1}) + \alpha_{CR}\left[V_i(t_j) - V_i(t_{j-1})\right]$$

$$\alpha_{CR} \equiv \frac{\frac{\tau_H}{\Delta t}}{\frac{\tau_H}{\Delta t} + 1} = \frac{\frac{R_H C_H}{\Delta t}}{\frac{R_H C_H}{\Delta t} + 1}$$

$$\frac{dV}{dt} = \lim_{\Delta t \to 0} \frac{V(t_j) - V(t_{j-1})}{\Delta t}$$

$$\approx \frac{V(t_j) - V(t_{j-1})}{\Delta t}$$

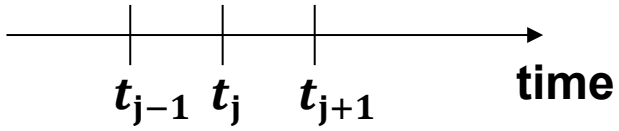

Finite difference method is used to numerically applying the CR-RC pulse shaping

- **CR circuit:**

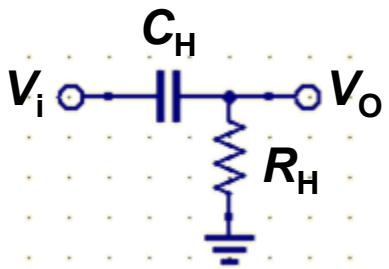

$$\tau_H = R_H C_H$$

$$\dot{V}_i = \frac{V_o}{\tau_H} + \dot{V}_o$$

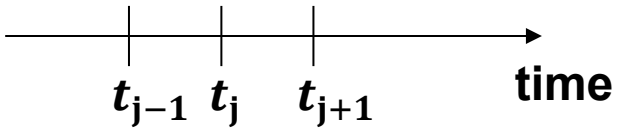

- **RC circuit:**

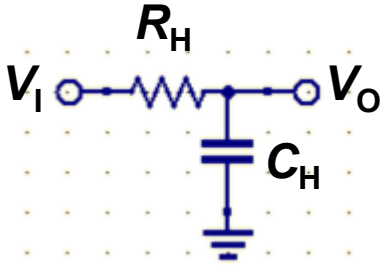

$$\tau_L = R_L C_L$$

$$V_i = \tau_L \dot{V}_o + V_o$$

$$V_i(t_j) \approx \tau_L \frac{V_o(t_j) - V_o(t_{j-1})}{\Delta t} + V_o(t_{j-1})$$

$$\approx \tau_L \frac{V_o(t_j) - V_o(t_{j-1})}{\Delta t} + V_o(t_j)$$

$$V_o(t_j) = (1 - \alpha_{RC}) V_o(t_{j-1}) + \alpha_{RC} V_i(t_j)$$

$$\alpha_{RC} \equiv \frac{1}{\frac{\tau_L}{\Delta t} + 1} = \frac{1}{\frac{R_L C_L}{\Delta t} + 1}$$

Iteration can be used to have more orders of CR-RC^n pulse shaping

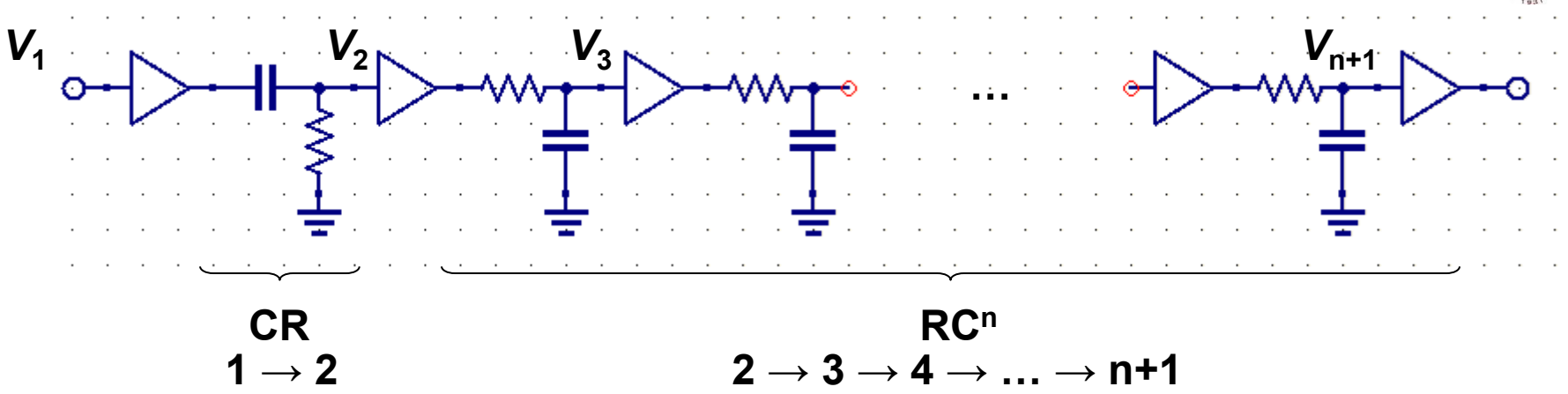

$$V_2(t_j) = \alpha_{CR} V_2(t_{j-1}) + \alpha_{CR}\left[V_1(t_j) - V_1(t_{j-1})\right]$$

$$\alpha_{CR} \equiv \frac{\frac{\tau_H}{\Delta t}}{\frac{\tau_H}{\Delta t} + 1} = \frac{\frac{R_H C_H}{\Delta t}}{\frac{R_H C_H}{\Delta t} + 1}$$

$$V_3(t_j) = (1 - \alpha_{RC,2}) V_3(t_{j-1}) + \alpha_{RC,2} V_2(t_j)$$

$$\vdots$$

$$V_m(t_j) = (1 - \alpha_{RC,m-1}) V_m(t_{j-1}) + \alpha_{RC,m-1} V_{m-1}(t_j)$$

$$\alpha_{RC,m} \equiv \frac{1}{\frac{\tau_{L,m}}{\Delta t} + 1}$$

$$\tau_L = R_L C_L$$

$$\vdots$$

$$V_{n+1}(t_j) = (1 - \alpha_{RC,n}) V_{n+1}(t_{j-1}) + \alpha_{RC,n} V_n(t_j)$$

$$\tau_{L,m} = \frac{\tau_L}{m - 1}$$

$$m \geq 2$$

Let's try using excel first

$$\alpha_{CR} \equiv 0.85$$

$$\alpha_{RC,2} \equiv 0.15 \qquad \Delta t = 64\ \text{ns}$$

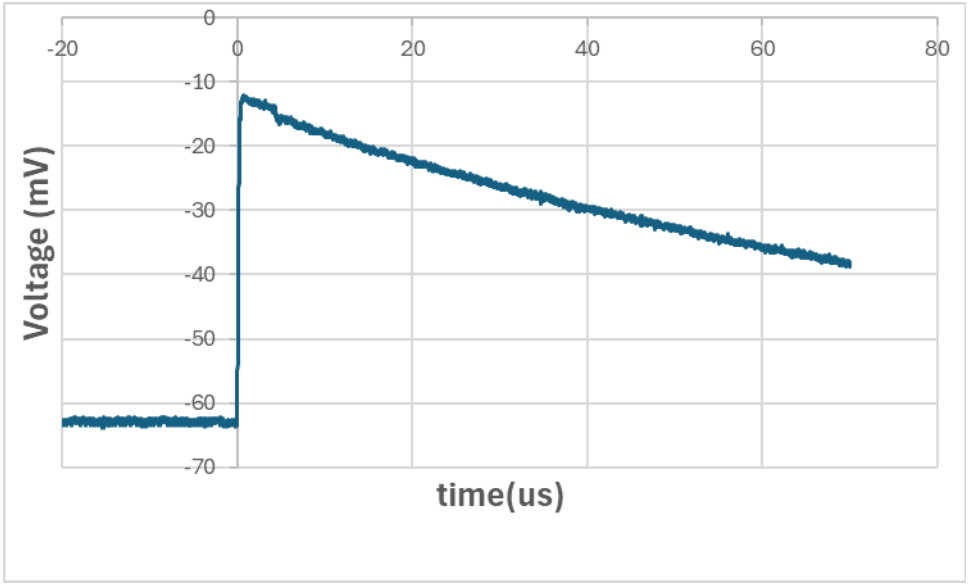

$$\alpha_{CR} \equiv \frac{\frac{\tau_H}{\Delta t}}{\frac{\tau_H}{\Delta t}+1} = 0.85$$

$$\alpha_{RC,m} \equiv \frac{1}{\frac{\tau_{L,m}}{\Delta t}+1} = 0.15$$

$$\tau_{L,m} = \frac{\tau_L}{m-1}$$

$$\tau_H = 362.7\ \text{ns}$$

$$\tau_{L,m} = 362.7/(m-1)\ \text{ns}$$

$$\frac{\tau_L}{\Delta t} = \frac{0.85}{0.15}$$

$$\alpha_{RC,m} \equiv \frac{1}{\frac{0.85}{0.15}\frac{1}{m-1}+1}$$

$$V_2(t_j) = \alpha_{CR}V_2(t_{j-1}) + \alpha_{CR}\left[V_1(t_j) - V_1(t_{j-1})\right]$$

$$V_3(t_j) = (1-\alpha_{RC,2})V_3(t_{j-1}) + \alpha_{RC,2}V_2(t_j)$$

$$V_m(t_j) = (1-\alpha_{RC,m-1})V_m(t_{j-1}) + \alpha_{RC,m-1}V_{m-1}(t_j)$$

$$V_{n+1}(t_j) = (1-\alpha_{RC,n})V_{n+1}(t_{j-1}) + \alpha_{RC,n}V_n(t_j)$$

Let's try using excel first

$\Delta t = 64\ \text{ns}$

$\alpha_{CR} \equiv 0.85$

$\tau_H = 362.7\ \text{ns}$

$\tau_{L,m} = 362.7/(m-1)\ \text{ns}$

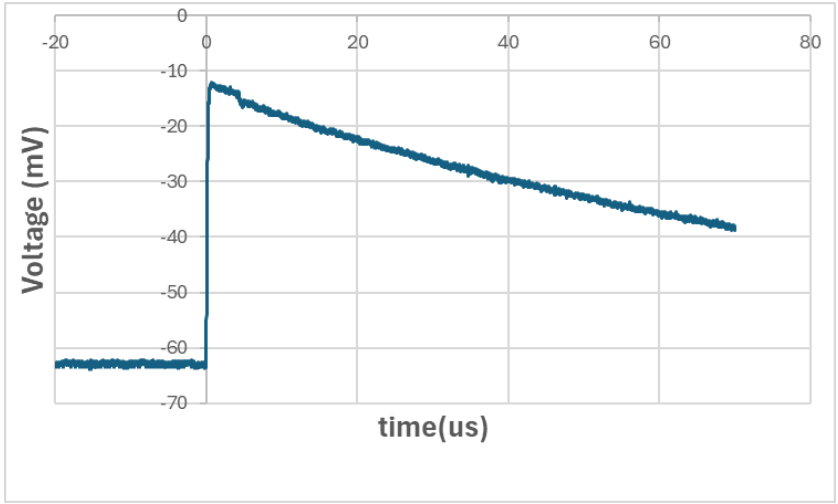

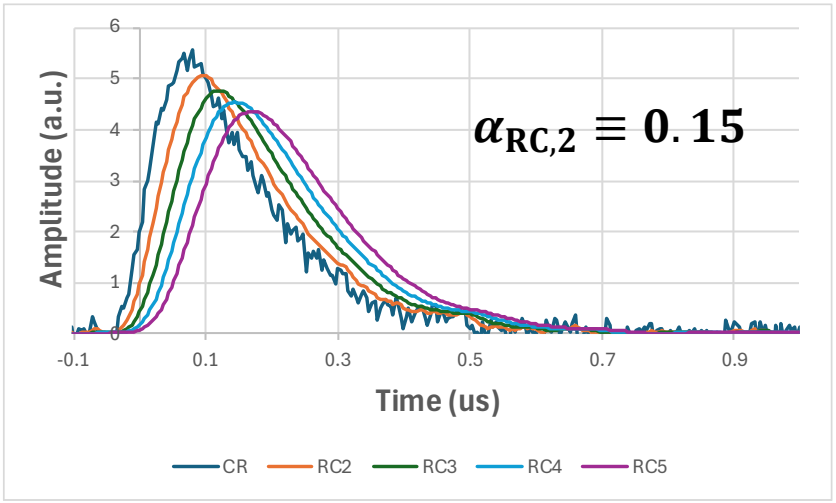

$\alpha_{RC,2} \equiv 0.15$

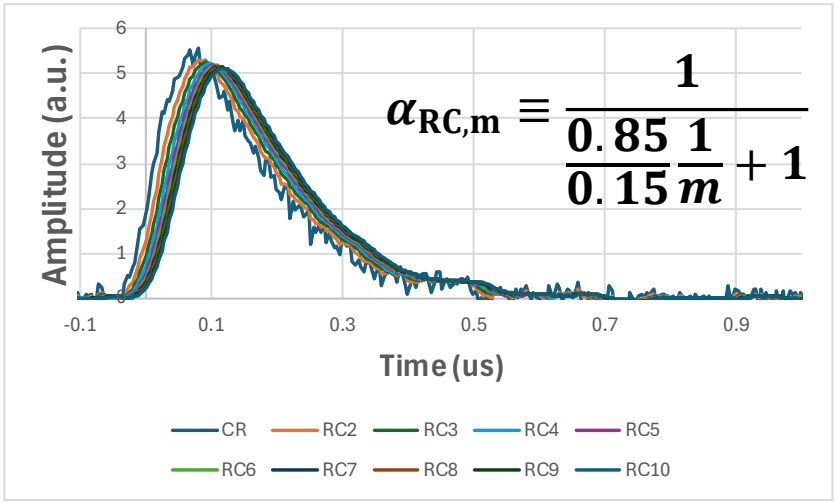

$$\alpha_{RC,m} \equiv \frac{1}{\frac{0.85}{0.15}\frac{1}{m}+1}$$

When the pulse is not sharp enough, no significant gaussian feature is observed

$$\Delta t = 64\ \text{ns}$$

$$\alpha_{\text{CR}} \equiv 0.85$$

$$\tau_{\text{H}} = 362.7\ \text{ns}$$

$$\tau_{\text{L,m}} = 362.7/(m-1)\ \text{ns}$$

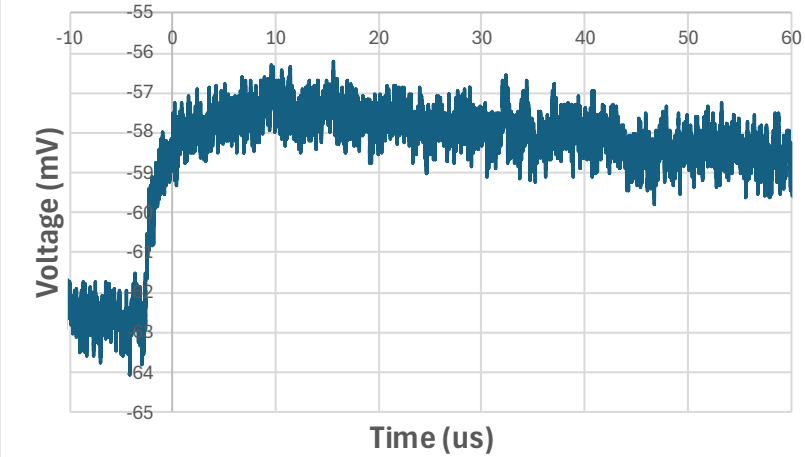

- What's the source?

$$\alpha_{\text{RC,m}} \equiv \frac{1}{\frac{0.85}{0.15}\frac{1}{m-1}+1}$$

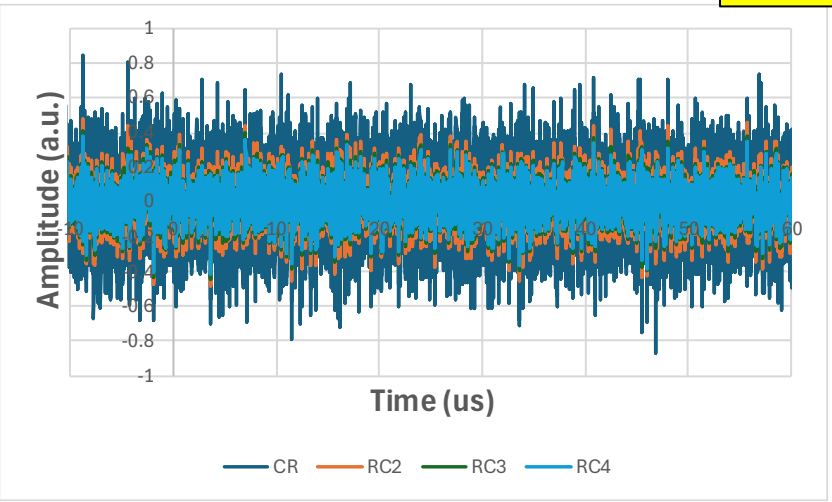

Saha equation gives the relative proportions of atoms of a certain species that are in two different states of ionization in thermal equilibrium

$$\frac{n_{r+1}n_e}{n_r} = \frac{G_{r+1}g_e}{G_r}\frac{(2\pi m_e KT)^{3/2}}{h^3}\exp\left(-\frac{\chi_r}{KT}\right)$$

- n_{r+1}, n_r: Density of atoms in ionization state r+1, r (m^{-3})
- n_e: Density of electrons (m^{-3})
- G_{r+1}, G_r: Partition function of ionization state r+1, r
- g_e=2: Statistical weight of the electron
- m_e: Mass of the electron
- χ_r: Ionization potential of ground level of state r to reach to the ground level of state r+1
- T: Temperature
- h: Planck's constant
- K: Boltzmann constant

Supplement to Ch. 6 of Astrophysics Processes by Hale Bradt
(http://homepages.spa.umn.edu/~kd/Ast4001-2015/NOTES/n052-saha-bradt.pdf)

Some backgrounds of quantum mechanics

- **Planck blackbody function:**

$$u(\nu, T) = \frac{8\pi h\nu^3}{c^3}\frac{1}{e^{h\nu/KT} - 1}\left(W/m^3\,\mathrm{Hz}\right)$$

- **Boltzmann formula:**
  - **g_i, g_j: statistical weight**

$$\frac{n_i}{n_j} = \frac{g_i e^{-\epsilon_i/KT}}{g_j e^{-\epsilon_j/KT}} = \frac{g_i}{g_j} e^{-h\nu_{ij}/KT} \qquad \frac{g_i}{g_j} = \frac{2J_i + 1}{2J_j + 1}$$

    (J: angular momenta quantum number)
  - **Number in the ith state to the total atom:**

$$\frac{n_i}{n} = \frac{n_i}{\Sigma n_j} \equiv \frac{g_i e^{-\epsilon_i/KT}}{G} \qquad G \equiv \Sigma g_j e^{-\epsilon_j/KT}$$

G: partition function of statistical weight for the atom, taking into account all its excited states.

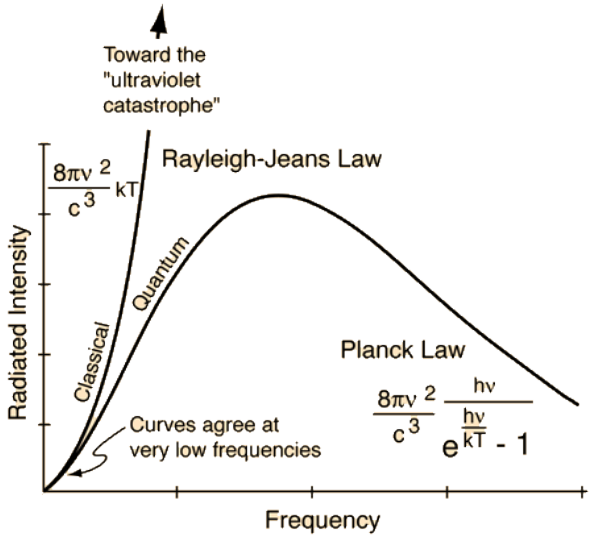

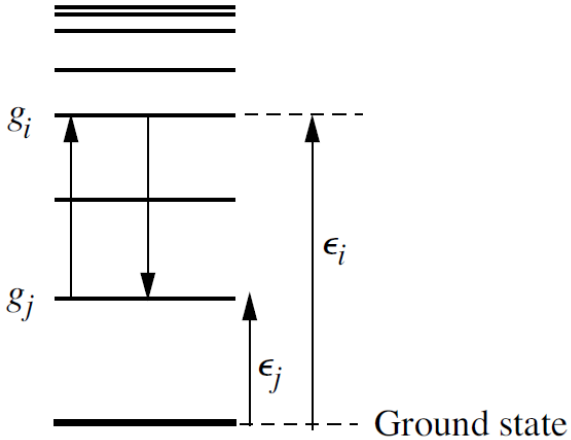

http://hyperphysics.phy-astr.gsu.edu/hbase/mod6.html

Einstein coefficient

- **Probability of electron energy transition:**
  - **Excitation (↑):** $P_{ji} = B_{ji}u(\nu, T)$
  - **De-excitation (↓):** $P_{ij} = A_{ij} + B_{ij}u(\nu, T)$
- **In thermal equilibrium:**

$$n_i(A_{ij} + B_{ij}u) = n_j B_{ji} u$$

$$\frac{g_i}{g_j} e^{-x}(A_{ij} + B_{ij}u) = B_{ji}u \qquad x \equiv \frac{h\nu}{KT}$$

$$u = a(e^x - 1)^{-1} \qquad a \equiv \frac{8\pi h\nu^3}{c^3}$$

$$a\left(e^x B_{ji} - \frac{g_i}{g_j} B_{ij}\right) = (e^x - 1)\frac{g_i}{g_j} A_{ij}$$

- **The Einstein coefficients are independent of T or ν.**

$x \to 0, e^x \to 1$ $\qquad$ $x \to \infty, e^x \to \infty$

$$\frac{B_{ij}}{B_{ji}} = \frac{g_j}{g_i} \qquad aB_{ji} = \frac{g_i}{g_j} A_{ij} \qquad \frac{A_{ij}}{B_{ij}} = \frac{8\pi h\nu^3}{c^3}$$

- **Photoexcitation:**

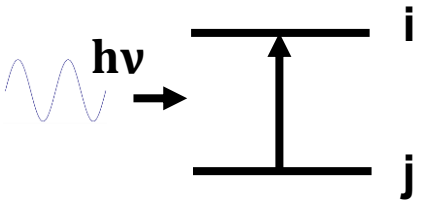

- **Induced radiation:**

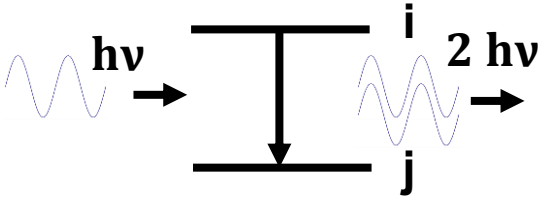

- **Spontaneous radiation:**

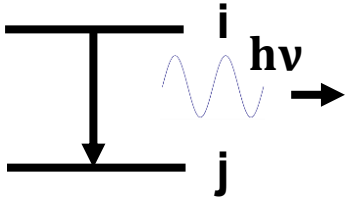

Saha equation is derived using the transition between different ionization states

- **Required photon energy for transition 1 from the ground state of r ionization state to the ground state of r+1 ionization state:**

$$h\nu = \chi_r + \frac{p^2}{2m}$$

Energy of the free electron

- **Required photon energy for transition 2 from the energy level k of r ionization state to the energy level j of r+1 ionization state:**

$$h\nu = \chi_r + \epsilon_{r+1,j} - \epsilon_{r,k} + \frac{p^2}{2m}$$

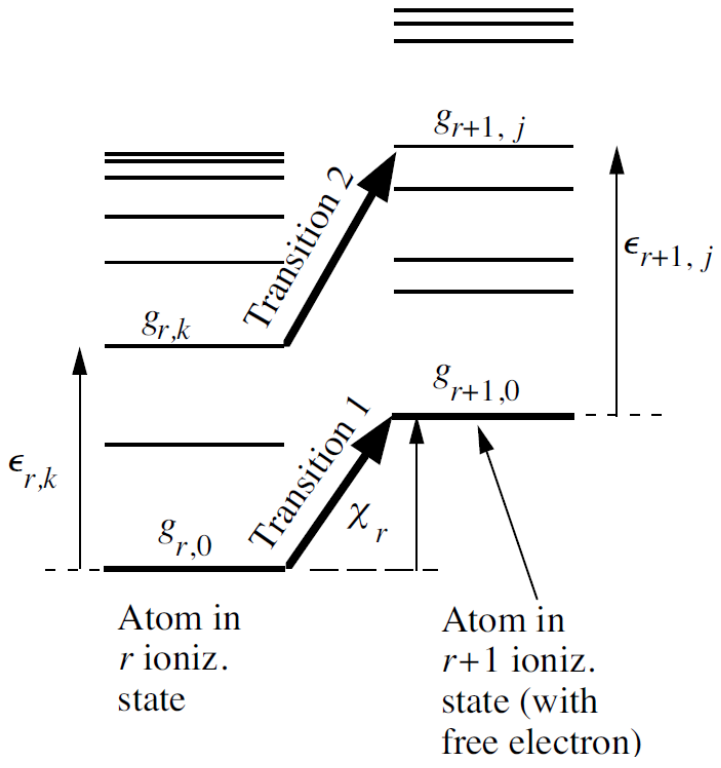

Saha equation is derived using the transition between different ionization states

- **Photoionization:**

$$R_{\text{pi}} = n_{r,k} u(\nu) B_{r,k \to r+1,j}$$

- **Induced radiation:**

$$R_{\text{ir}} = n_{r+1,j} n_{e,p}(p) u(\nu) B_{r+1,j \to r,k}$$

- **Spontaneous emission:**

$$R_{\text{sr}} = n_{r+1,j} n_{e,p}(p) A_{r+1,j \to r,k}$$

- **In thermal equilibrium:**

$$n_{r+1,j} n_{e,p} A_{r+1,j \to r,k} + n_{r+1,j} n_{e,p} u B_{r+1,j \to r,k} = n_{r,k} u B_{r,k \to r+1,j}$$

- **Einstein coefficients:**

$$\frac{B_{r,k \to r+1,j}}{B_{r+1,j \to r,k}} = \frac{g_{r+1,j}}{g_{r,k}} \frac{g_e 4\pi p^2}{h^3}$$

$$\frac{A_{r+1,j \to r,k}}{B_{r+1,j \to r,k}} = \frac{8\pi h \nu^3}{c^3}$$

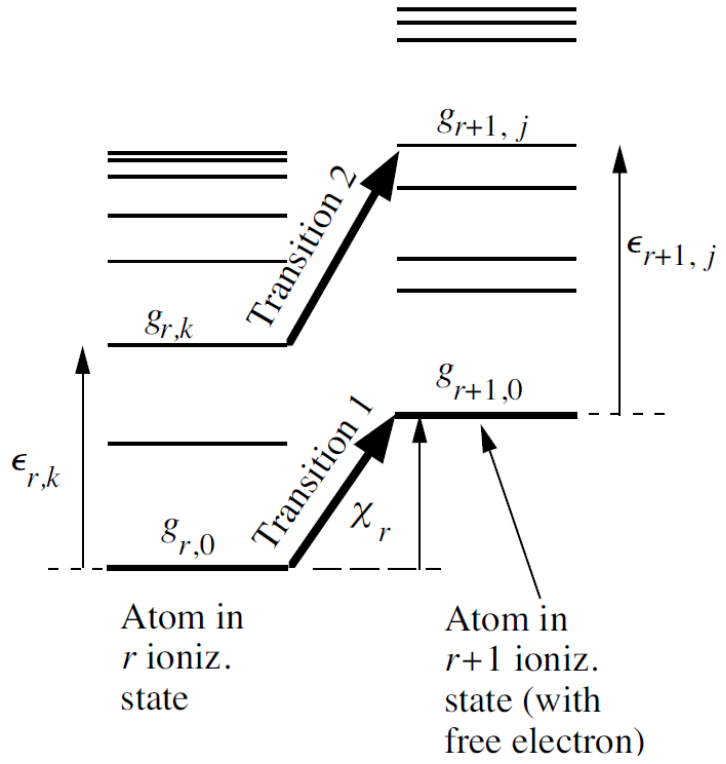

Saha equation - continued

$$n_{r+1,j}n_{e,p}A_{r+1,j\to r,k} + n_{r+1,j}n_{e,p}uB_{r+1,j\to r,k} = n_{r,k}uB_{r,k\to r+1,j}$$

$$n_{r+1,j}n_{e,p}\frac{A_{r+1,j\to r,k}}{B_{r+1,j\to r,k}} + n_{r+1,j}n_{e,p}u = n_{r,k}u\frac{B_{r,k\to r+1,j}}{B_{r+1,j\to r,k}}$$

$$\frac{n_{r+1,j}n_{e,p}}{n_{r,k}} = \left(\frac{A_{r+1,j\to r,k}}{uB_{r+1,j\to r,k}} + 1\right)^{-1}\frac{B_{r,k\to r+1,j}}{B_{r+1,j\to r,k}}$$

$$\frac{B_{r,k\to r+1,j}}{B_{r+1,j\to r,k}} = \frac{g_{r+1,j}}{g_{r,k}}\frac{g_e 4\pi p^2}{h^3}$$

$$n_{e,p}(p) = \frac{n_e 4\pi p^2}{(2\pi mKT)^{3/2}}\exp\left(-\frac{p^2}{2mKT}\right)$$

$$\frac{A_{r+1,j\to r,k}}{B_{r+1,j\to r,k}} = \frac{8\pi h\nu^3}{c^3}$$

$$\frac{n_{r+1,j}n_e}{n_{r,k}} = \frac{(2\pi mKT)^{3/2}}{4\pi p^2}\exp\left(\frac{p^2}{2mKT}\right)\left[\frac{c^3}{8\pi h\nu^3}\left(e^{h\nu/KT}-1\right)\frac{8\pi h\nu^3}{c^3}+1\right]^{-1}\frac{g_{r+1,j}}{g_{r,k}}\frac{g_e 4\pi p^2}{h^3}$$

$$\frac{n_{r+1,j}n_e}{n_{r,k}} = \frac{(2\pi mKT)^{3/2}}{h^3}\frac{g_{r+1,j}g_e}{g_{r,k}}\exp\left[\frac{1}{KT}\left(\frac{p^2}{2m}-h\nu\right)\right]$$

Saha equation - continued

$$\frac{n_{r+1,j}n_e}{n_{r,k}} = \frac{(2\pi mKT)^{3/2}}{h^3}\frac{g_{r+1,j}g_e}{g_{r,k}}\exp\left[\frac{1}{KT}\left(\frac{p^2}{2m} - h\nu\right)\right]$$

$$\frac{n_{r+1,j}n_e}{n_{r,k}} = \frac{(2\pi mKT)^{3/2}}{h^3}\frac{g_{r+1,j}g_e}{g_{r,k}}\exp\left[\frac{1}{KT}\left(\frac{p^2}{2m} - \chi_r - \epsilon_{r+1,j} + \epsilon_{r,k} - \frac{p^2}{2m}\right)\right]$$

$$\frac{n_{r+1,j}n_e}{n_{r,k}} = \frac{(2\pi mKT)^{3/2}}{h^3}\frac{g_{r+1,j}\exp\left(\frac{\epsilon_{r+1,j}}{KT}\right)g_e}{g_{r,k}\exp\left(\frac{\epsilon_{r,k}}{KT}\right)}\exp\left(-\frac{\chi_r}{KT}\right)$$

$$\frac{n_{r,k}}{n_r} = \frac{g_{r,k}e^{-\epsilon_{r,k}/KT}}{G_r} \qquad G_r = \Sigma g_{r,k}e^{-\epsilon_{r,k}/KT}$$

$$\frac{n_{r+1,j}}{n_{r+1}} = \frac{g_{r+1,j}e^{-\epsilon_{r+1,j}/KT}}{G_{r+1}} \qquad G_{r+1} = \Sigma g_{r+1,j}e^{-\epsilon_{r+1,j}/KT}$$

$$\boxed{\frac{n_{r+1}n_e}{n_r} = \frac{G_{r+1}g_e}{G_r}\frac{(2\pi m_e KT)^{3/2}}{h^3}\exp\left(-\frac{\chi_r}{KT}\right)}$$

Saha equation – example: hydrogen plasma of the sun

- **Photosphere of the sun – hydrogen atoms in an optically thick gas in thermal equilibrium at temperature T=6400 K.**
  - **Neutral hydrogen (r state / ground state)**

$$G_r = \Sigma g_{r,k} = g_{r,0} + g_{r,1}\exp\left(-\frac{\epsilon_{r,1}}{KT}\right) + \cdots = 2 + 8\exp\left(-\frac{10.2eV}{0.56eV}\right) + \cdots$$

$$= 2 + 9.8 \times 10^{-8} + \cdots \approx 2$$

  - **Ionized state (r+1 state)**

$$G_{r+1} = \Sigma g_{r+1,j} = g_{r+1,0} + g_{r+1,1}\exp\left(-\frac{\epsilon_{r+1,1}}{KT}\right) + \cdots \approx 1$$

  - **Other information:** $g_e = 2$ $\chi_r = 13.6eV;\ kT = 0.56eV$ $n_{r+1} = n_e$

$$\frac{{n_{r+1}}^2}{n_r} = 2.41 \times 10^{21}\frac{1 \times 2}{2}(6400)^{3/2}\exp\left(-\frac{13.6}{0.56}\right) = 3.5 \times 10^{16} m^{-3}$$

It is mostly neutral in the photosphere of the sun

- **Assuming 50 % ionization:**

$$n_{r+1} = n_r = 3.5 \times 10^{16} m^{-3} \qquad n = n_{r+1} + n_r = 7 \times 10^{16} m^{-3}$$

- **In the photosphere of the sun:**

$$\rho \sim 3 \times 10^{-4}\ \mathrm{kg}/m^3 \rightarrow n = 2 \times 10^{23} m^{-3} \gg 7 \times 10^{16} m^{-3}$$

- **At higher densities n at the same temperature, there should be more collisions leading to higher recombination rate and thus the plasma is less than 50 % ionization.**

  $\Rightarrow$ **Less than 50 % ionization**

- **Use the total number density to estimate the ionization percentage:**

$$n_{r+1} + n_r = 2 \times 10^{23}$$

$$\frac{n_{r+1}}{n_r} = 4 \times 10^{-4} @ 6400K$$

A semiconductor device is fabricated by many repetitive production process

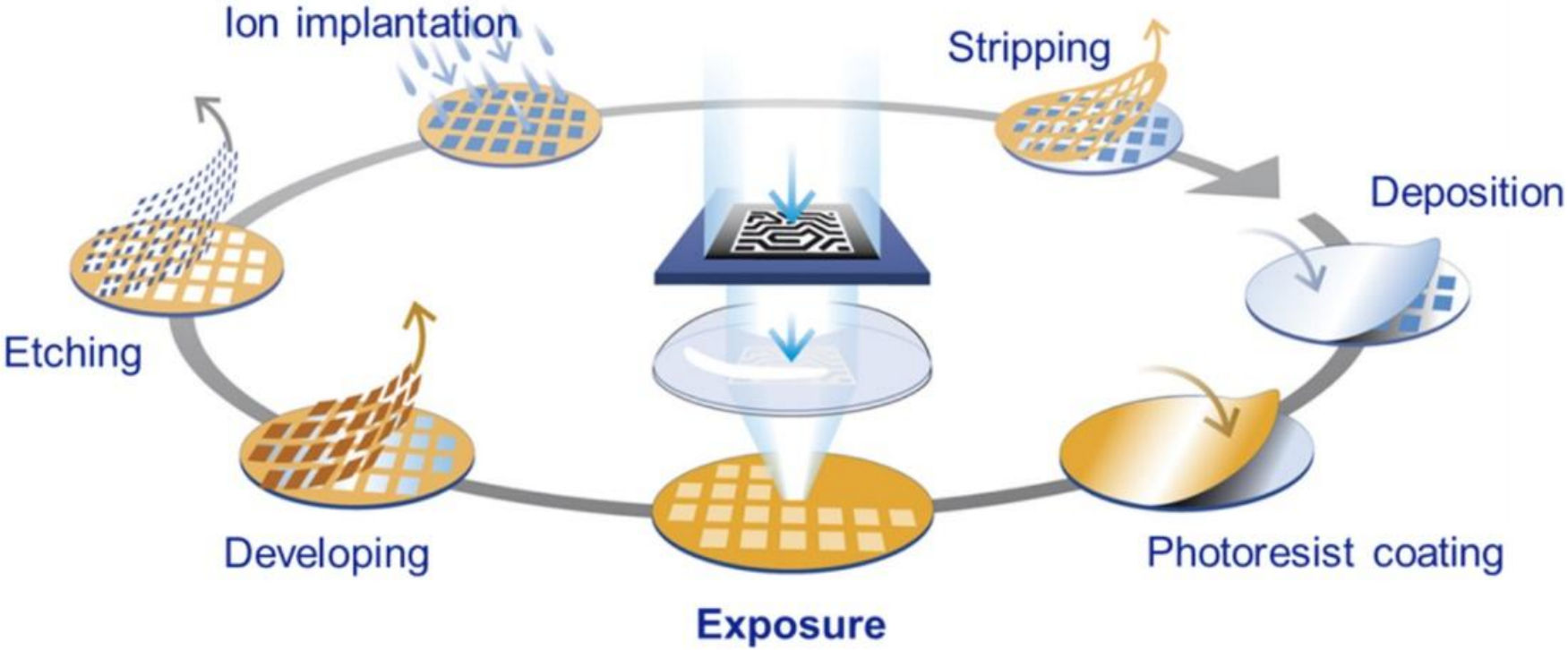

Surf. Topogr.: Metrol. Prop. **4** (2016) 023001

Reference for material processing

- Principles of plasma discharges and materials processing, 2nd edition, by Michael A. Lieberman and Allan J. Lichtenberg
- http://www.eecs.berkeley.edu/~lieber/
- Materials science of thin films, 2nd edition, by Milton Ohring
- Plasma etching, by Dennis M. Manos and Daniel L. Flamm
- Industrial plasma engineering, volume 1, by J. Reece Roth

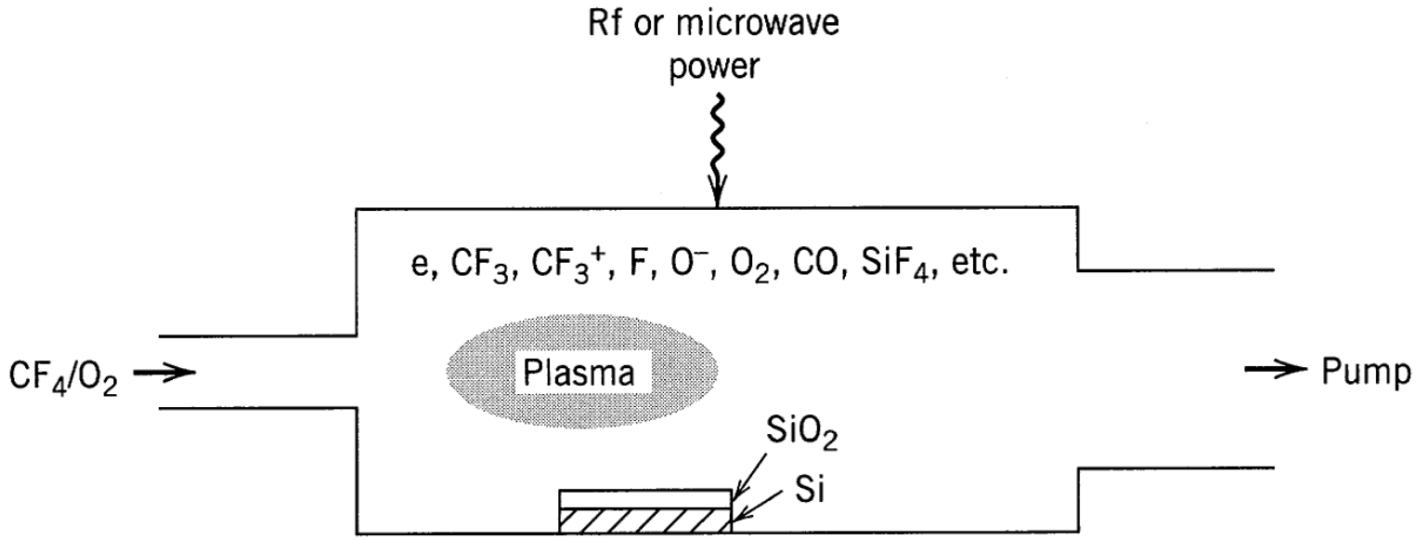

Evolution of etching discharges

1st generation
(1 source, multi-wafer, low density)

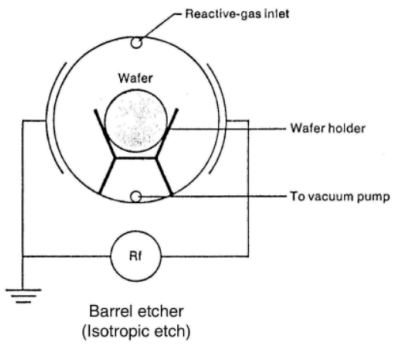

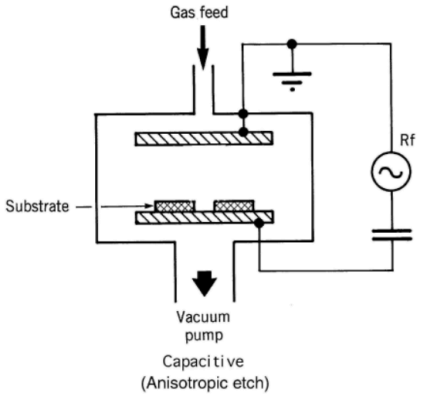

2nd generation
(2 sources, single-wafer, high density)

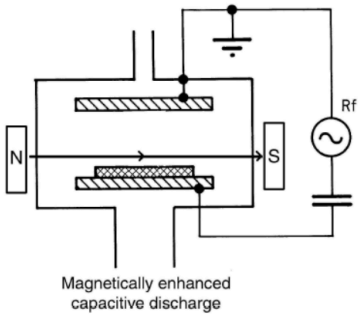

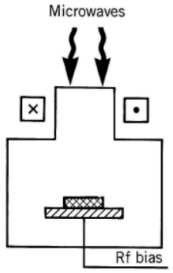

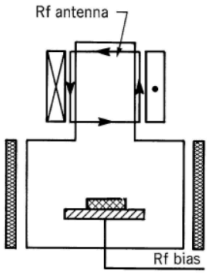

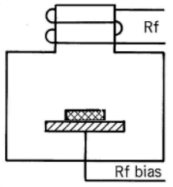

3rd generation
(multi-sources, single-wafer, moderate density)

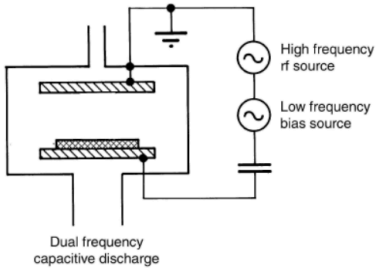

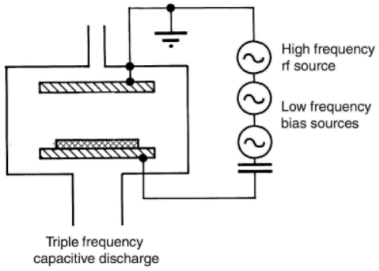

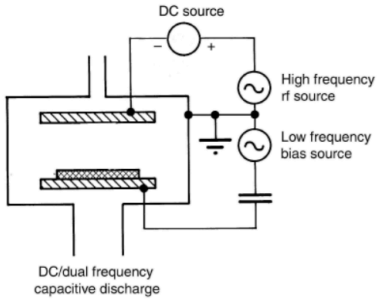

There are two types of etching: isotropic vs anistropic

- Isotropic etching

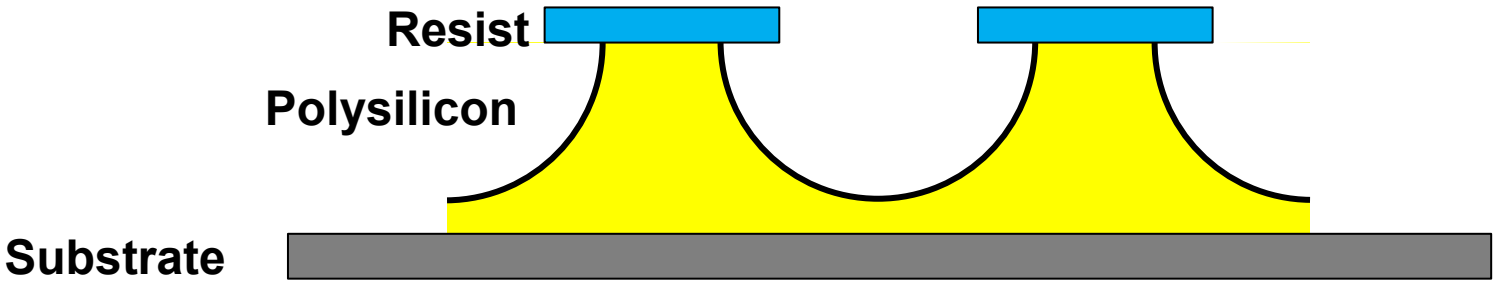

- Anisotropic etching

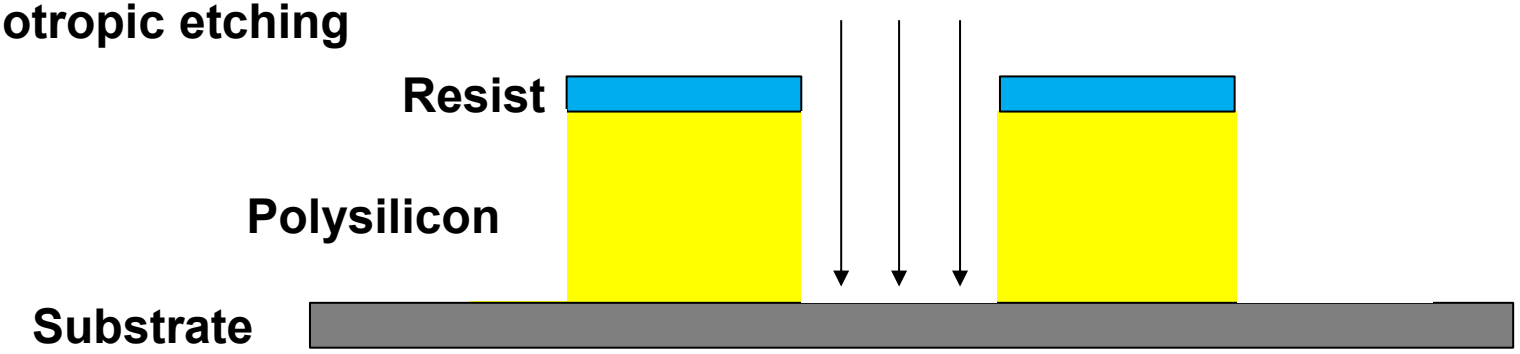

Plasma etch requirements – etch rate

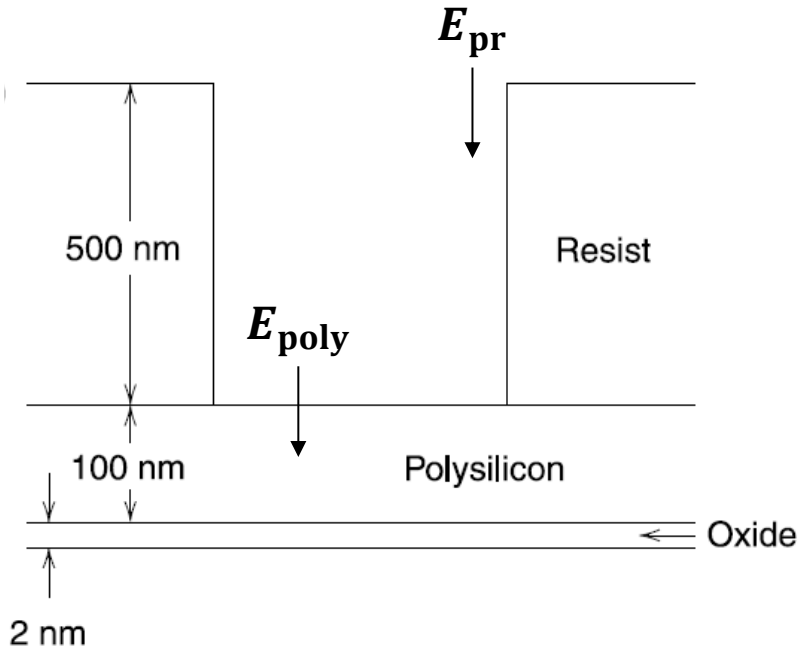

- **Etch time needs to be within a few minutes:**

$$E_{pr} \geq 250\,\mathrm{nm/min}$$

$$E_{poly} \geq 50\,\mathrm{nm/min}$$

Principles of plasma discharges and materials processing, 2nd edition, by Michael A. Lieberman and Allan J. Lichtenberg

Plasma etch requirements - selectivity

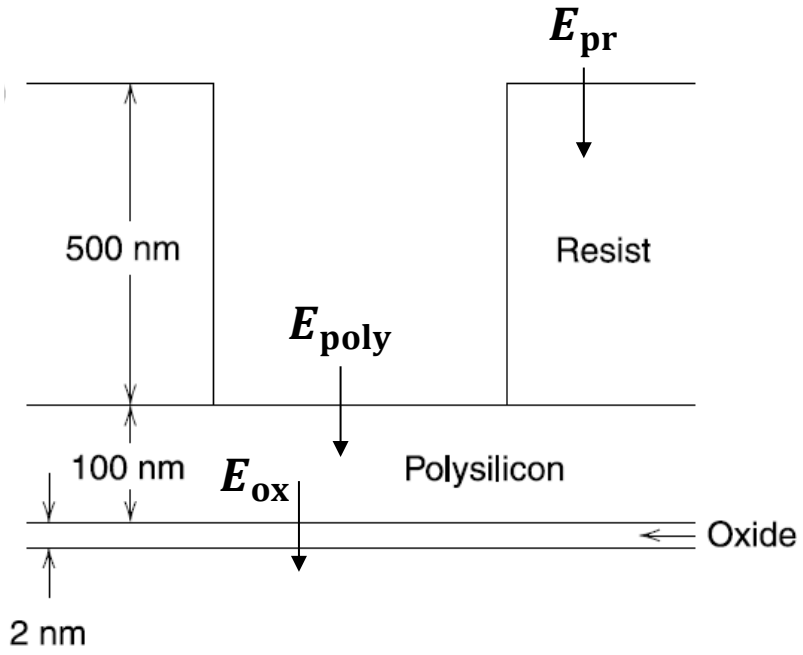

- **Selectivity between polysilicon and resist:**

$$s = \frac{E_{poly} \triangle t}{E_{pr} \triangle t} >> \frac{100nm}{500nm} = 0.2$$

- **Assuming 20% non-uniformity on the wafer:**

$$s = \frac{E_{poly} \triangle t}{E_{ox} \triangle t} >> \frac{20\% \times 100nm}{2nm} = 10$$

Principles of plasma discharges and materials processing, 2nd edition, by Michael A. Lieberman and Allan J. Lichtenberg

Plasma etch requirements – Anisotropy

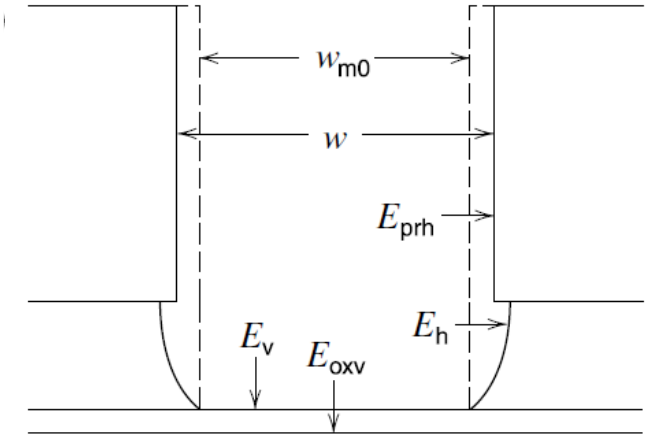

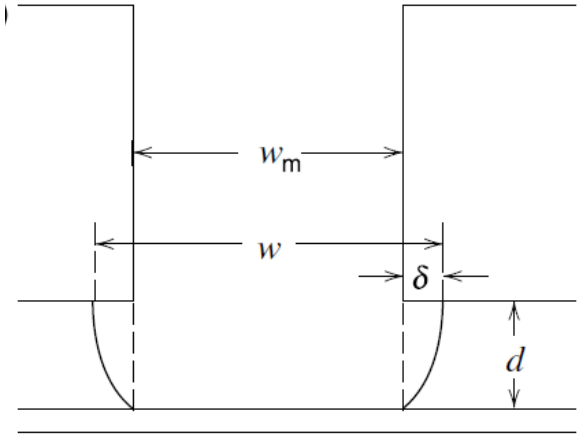

- **Anisotropy**

$$a_h = \frac{E_v}{E_h} = \frac{d}{\delta}$$

$$w = w_m + 2\delta$$

$$a_h \geq \frac{2d}{w - w_m}$$

- **The smallest feature size where w_m=0:**

$$w \approx \frac{2d}{a_h}$$

Principles of plasma discharges and materials processing, 2nd edition, by Michael A. Lieberman and Allan J. Lichtenberg

Plasma etch requirements – Anisotropy including etching on photoresist

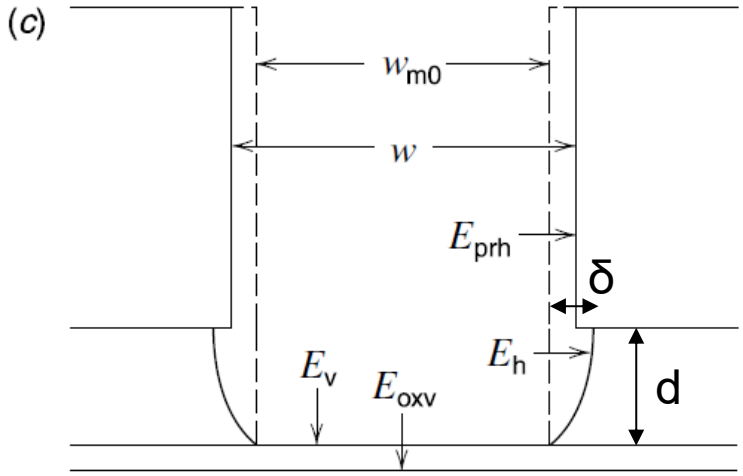

$$\delta \approx (E_h + E_{prh})\, t$$

$$t = \frac{d}{E_v}$$

$$\delta \approx d\frac{E_h + E_{prh}}{E_v}$$

$$\frac{E_h + E_{prh}}{E_v} \approx \frac{\delta}{d}$$

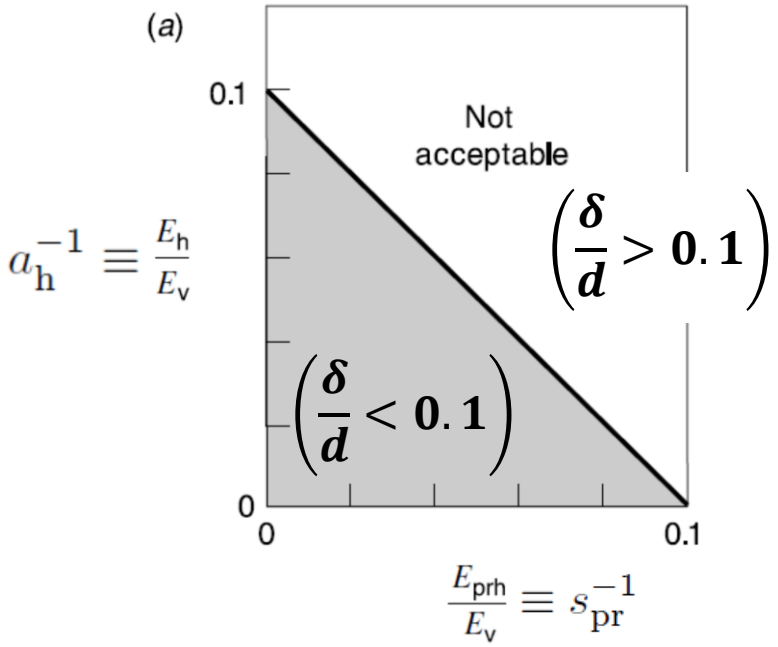

$$a_h^{-1} \equiv \frac{E_h}{E_v}$$

$$\frac{E_h}{E_V} + \frac{E_{prh}}{E_V} = a_h^{-1} + s_{pr}^{-1} \approx \frac{\delta}{d} \equiv 0.1$$

- The contribution of the horizontal etching is from both E_h and E_{prh}.

Principles of plasma discharges and materials processing, 2nd edition, by Michael A. Lieberman and Allan J. Lichtenberg

Plasma etch requirements – Uniformity on selectivity and anisotropy

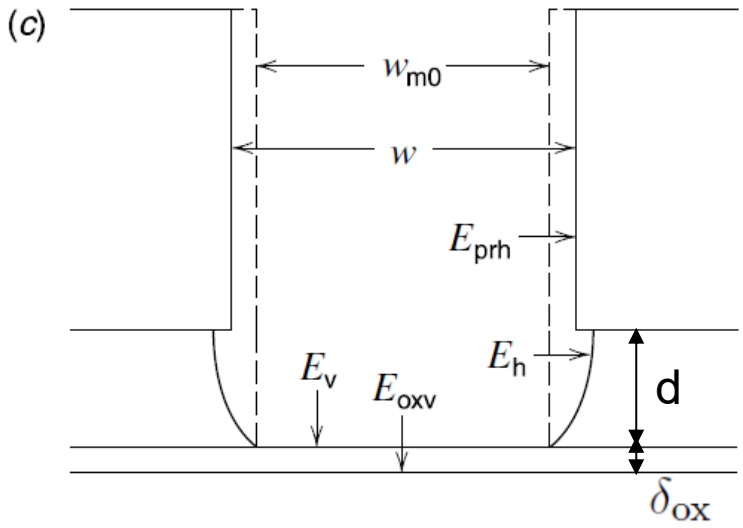

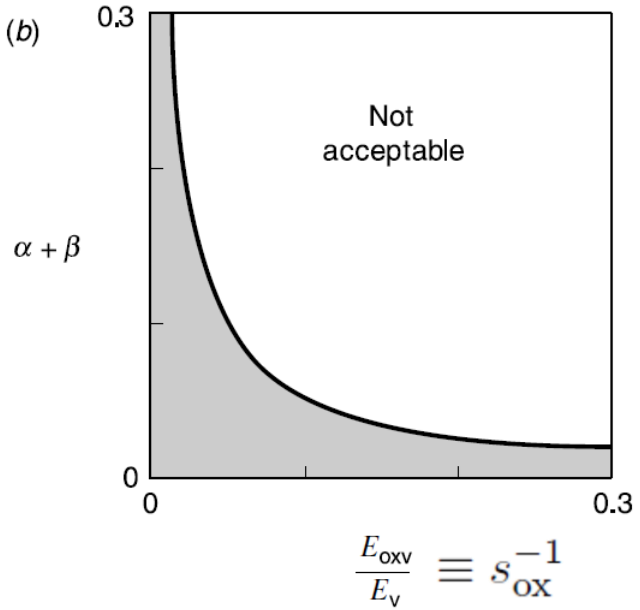

$$d \to d(1 \pm \alpha) \qquad E_v \to E_v(1 \pm \beta)$$

where α, β are variations.

$$t_{max} = \frac{d(1+\alpha)}{E_v(1-\beta)} \approx \frac{d}{E_v}(1+\alpha+\beta)$$

$$t_{min} = \frac{d(1-\alpha)}{E_v(1+\beta)} \approx \frac{d}{E_v}(1-\alpha-\beta)$$

$$\delta_{ox} = (t_{max} - t_{min})E_{oxv}$$

$$= \frac{d}{E_v} 2(\alpha+\beta)E_{oxv}$$

$$2(\alpha+\beta)\frac{E_{oxv}}{E_v} = \frac{\delta_{ox}}{d}$$

Principles of plasma discharges and materials processing, 2nd edition, by Michael A. Lieberman and Allan J. Lichtenberg

There are four major plasma etching mechanisms

- **Sputtering**

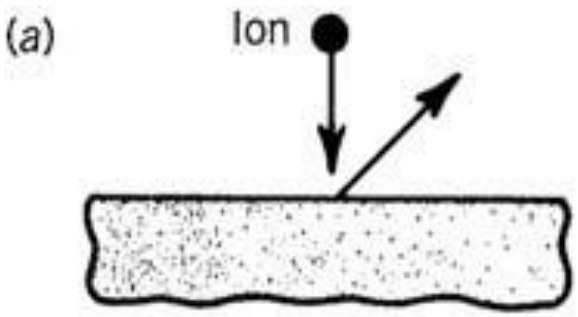

- **Pure chemical etching**

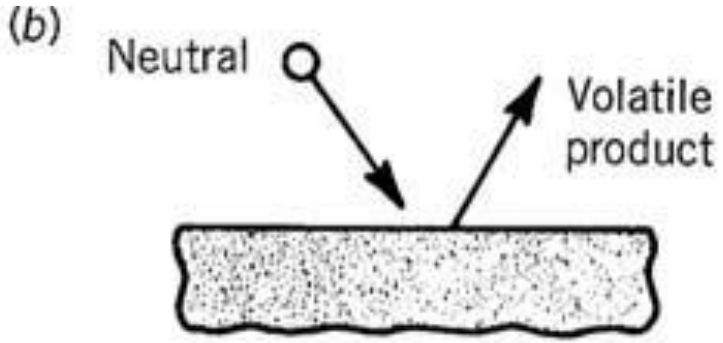

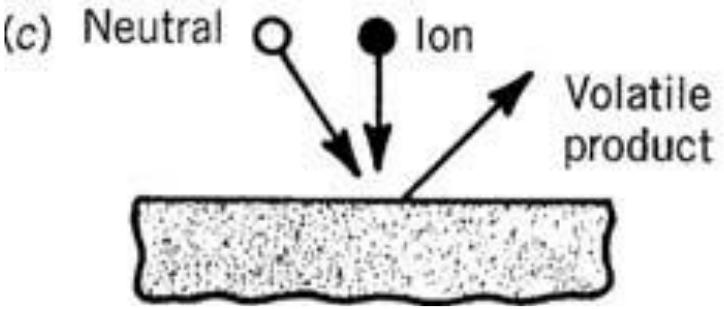

- **Ion energy-driven etching**

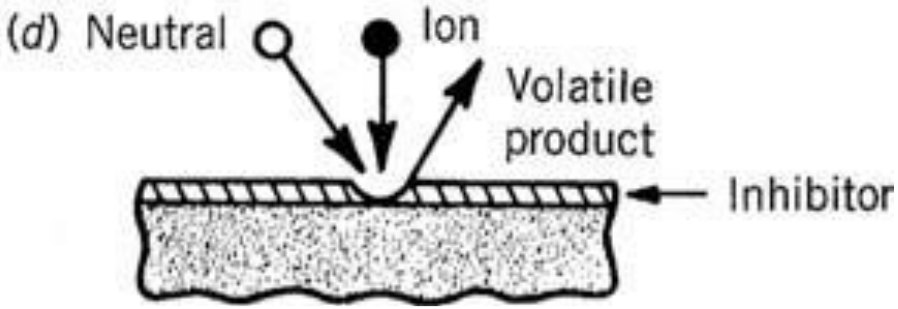

- **Ion-enhanced inhibitor etching**

Principles of plasma discharges and materials processing, 2nd edition, by Michael A. Lieberman and Allan J. Lichtenberg

Sputtering etching

Sputtering is an unselective but anisotropic process

- **Unselective process.**
- **Anisotropic process, strongly sensitive to the angle of incidence of the ion.**
- **Sputtering rates of different materials are roughly the same.**
- **Sputtering rates are generally low because the yield is typically of order one atom per incident ion.**
- **Sputtering is the only one of the four etch processes that can remove nonvolatile products from a surface.**
- **The process is generally under low pressure since the mean free path of the sputtered atoms must be large enough to prevent redeposition on the substrate or target.**

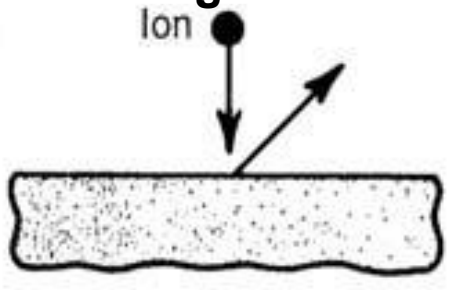

Principles of plasma discharges and materials processing, 2nd edition, by Michael A. Lieberman and Allan J. Lichtenberg

Topographical patterns might not be faithfully transferred during sputter etching

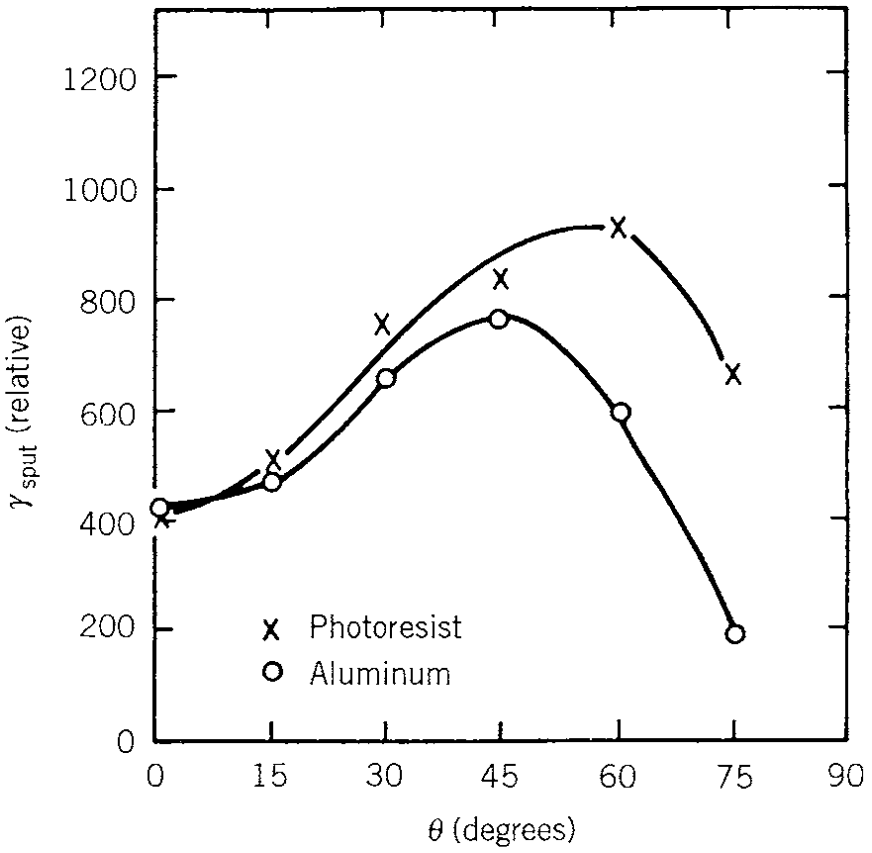

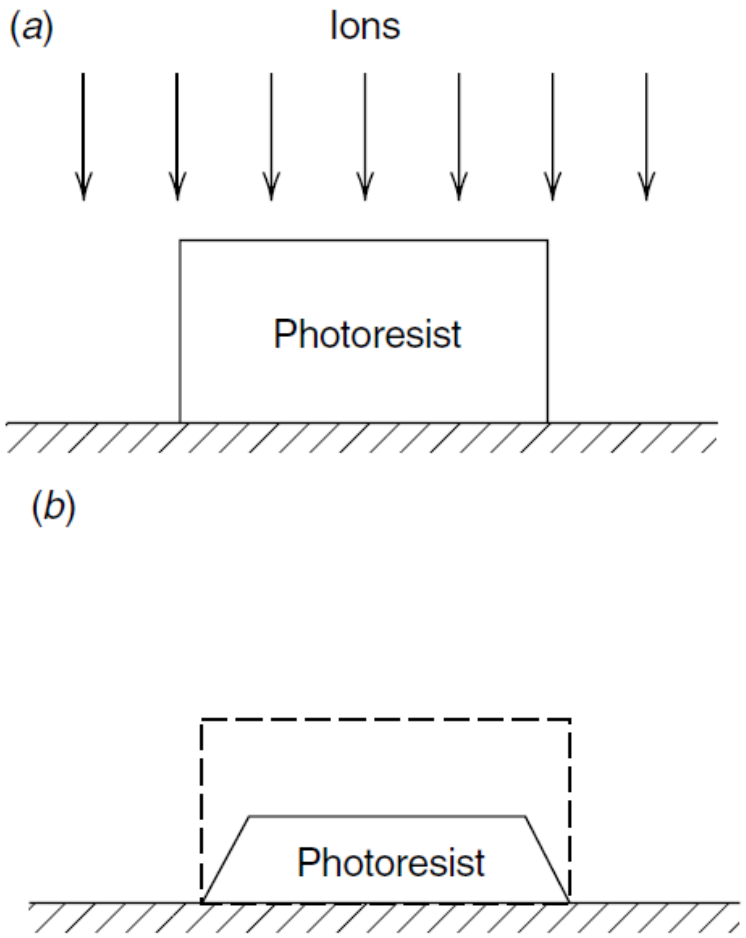

Principles of plasma discharges and materials processing, 2nd edition, by Michael A. Lieberman and Allan J. Lichtenberg

Pure chemical etching

Atoms or molecules chemically react with the surface to form gas-phase products

- **Highly chemically selective, e.g.,**

$$Si(s) + 4F \longrightarrow SiF_4(g)$$

$$\text{photoresist} + O(g) \longrightarrow CO_2(g) + H_2O(g)$$

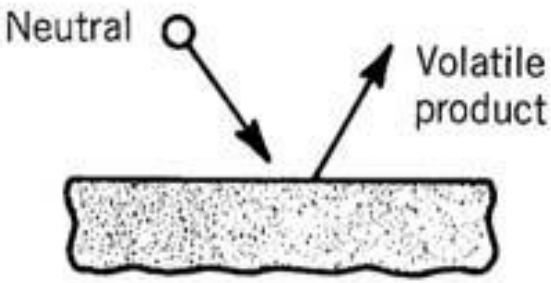

- **Almost invariably isotropic.**
- **Etch products must be volatile.**
- **The etch rate can be quite large.**
- **Etch rate are generally not limited by the rate of arrival of etchant atoms, but by one of a complex set of reactions at the surface leading to formation of etch products.**

Principles of plasma discharges and materials processing, 2nd edition, by Michael A. Lieberman and Allan J. Lichtenberg

Ion-enhanced energy-driven etching

The discharge supplies both etchants and energetic ions to the surface

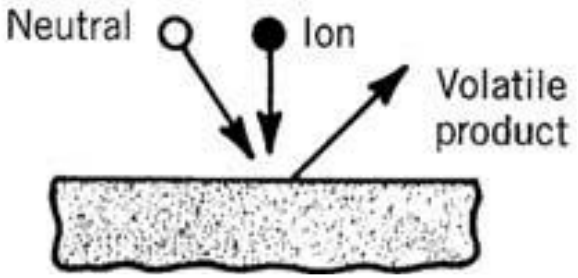

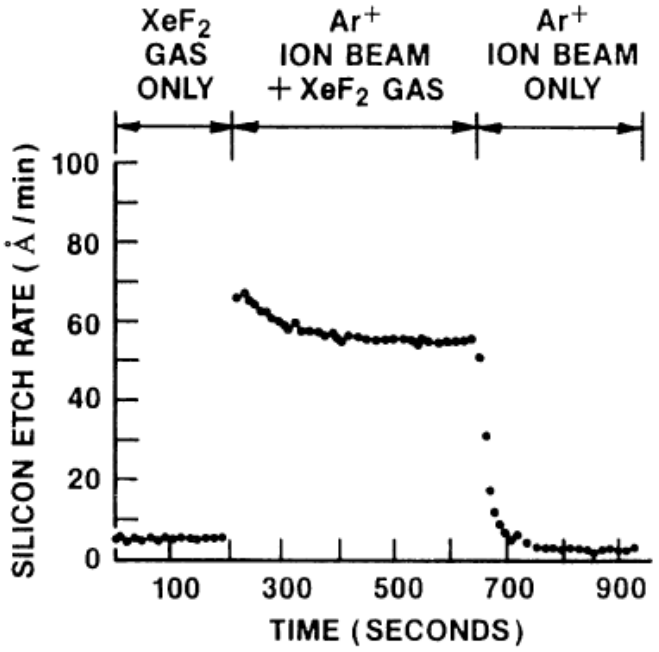

- Low chemical etch rate of silicon substrate in XeF2 etchant gas.
- Tenfold increase in etch rate with XeF_2 + 500 V argon ions, simulating ion-enhanced plasma etching.
- Very low "etch rate" due to the physical sputtering of silicon by ion bombardment alone.

Ion-enhanced energy-driven etching has the characteristic of both sputtering and pure chemical etching

- Chemical in nature but with a reaction rate determined by the energetic ion bombardment.
- Product must be volatile.
- Highly anisotropic.

Ion-enhanced inhibitor etching

An inhibitor species is used

- Inhibitor precursor molecules that absorb or deposit on the substrate form a protective layer or polymer film.
- Etchant is chosen to produce a high chemical etch rate of the substrate in the absence of either ion bombardment or the inhibitor.
- Ion bombardment flux prevents the inhibitor layer from forming or clears it as it forms.
- Where the ion flux does not fall, the inhibitor protects the surface (side wall) from the etchant.
- May not be as selective as pure chemical etching.
- A volatile etch product must be formed.
- Contamination of the substrate and final removal of the protective inhibitor film are other issues.

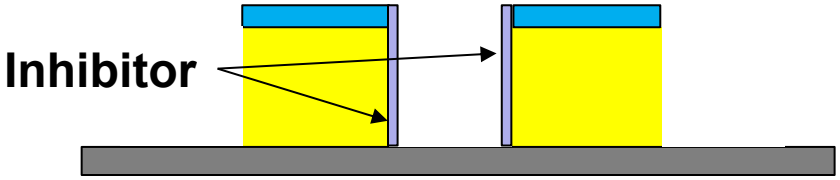

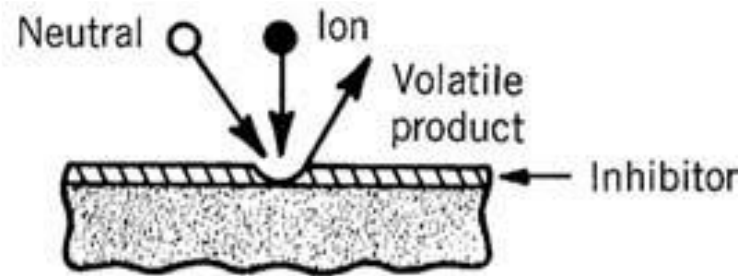

Comparison of different processes

	Sputtering etching	Pure chemical etching	Ion energy-driven etching	Ion-enhanced Inhibitor etching
Selectivity	X	O	O	O
Anisotropic	O	X	O	O
Volatile product	X	O	O	O

TABLE 15.1. Etch Chemistries Based on Product Volatility

Material	Etchant Atoms
Si, Ge	F, Cl, Br
SiO_2	F, F + C
Si_3N_4, silicides	F
Al	Cl, Br
Cu	Cl ($T > 210°C$)
C, organics	O
W, Ta, Ti, Mo, Nb	F, Cl
Au	Cl
Cr	Cl, Cl + O
GaAs	Cl, Br
InP	Cl, C + H

Deposition and implementation

- **Plasma-assisted deposition, implantation, and surface modification are important material processes for producing films on surfaces and modifying their properties**
- **Example processes:**
  - **Plasma-enhanced chemical vapor deposition (PECVD)**
  - **Sputter deposition / physical vapor deposition (PVD)**
  - **Plasma-immersion ion implantation (PIII)**

PECVD

Chemical Vapor Deposition (CVD)

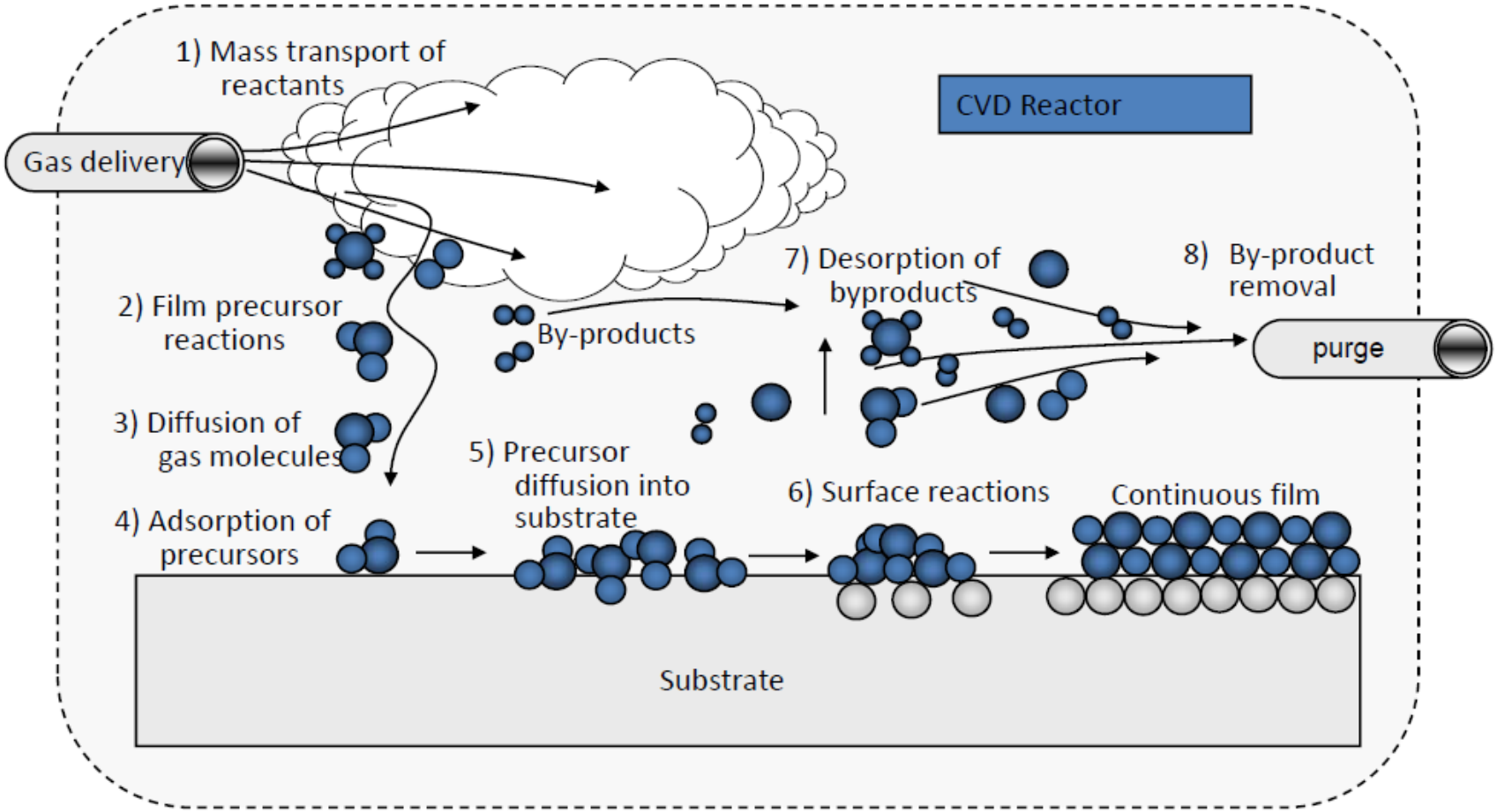

Plasma-enhanced chemical vapor deposition (PECVD)

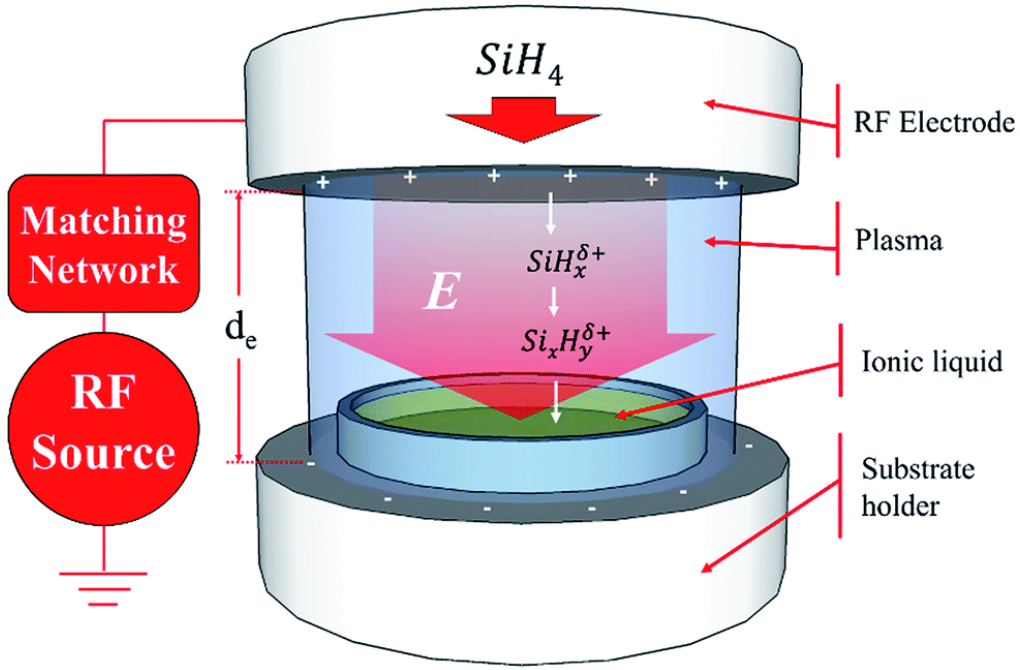

$$SiH_4 \xrightarrow{plasma} SiH_x^{\delta+} \xrightarrow{Intercollision} Si_xH_y^{\delta+}(SiNPs) \xrightarrow{ILs} Stablized\ SiNPs$$

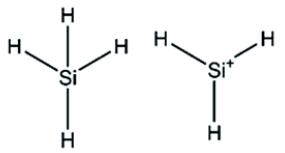

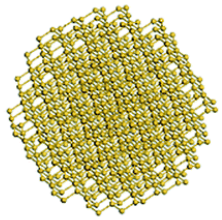

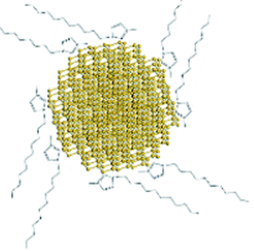

Films can be deposited in low temperatures using plasma deposition

- Device structures are sensitive to temperature, high-temperature deposition processes cannot be used in many cases.
- High-temperature films can be deposited at low temperatures.
- Unique films not found in nature can be deposited, e.g., diamond.

Working temperature is determined by the desired film properties

- CVD – consists of a thermally activated set of gas-phase and surface reactions that produce a solid product at a surface.
- PECVD – gas-phase and the surface reactions are controlled or modified by the plasma properties.
- Te~2-5 eV in PECVD is much greater than the substrate temperature, the temperature in PECVD is much less that CVD.
- Deposition rates are usually not very sensitive to the substrate temperature T.
- Film properties such as composition, stress, and morphology, are functions of T.
- Low-temperature PECVD films are amorphous, not crystalline, which can more easily be achieved with chemical vapor deposition (CVD).

Example of using PECVD – amorphous silicon

- **Amorphous silicon thin films are used in solar cells**

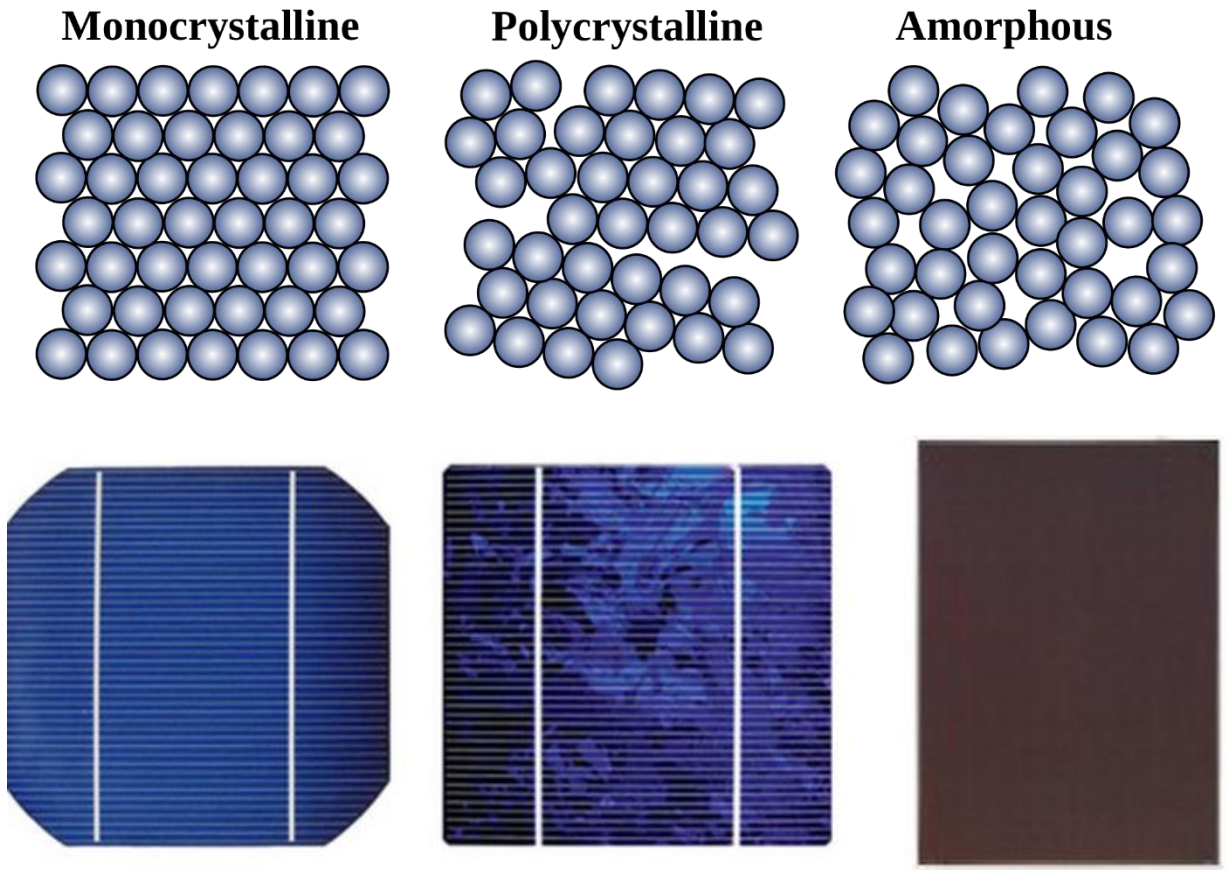

Example of using PECVD – amorphous silicon

- H is required so that SiH_4 is used
  - For the material to be semiconducting.
  - Terminate the dangling bonds.
  - The dangling bonds are created by ion bombardment (SiH_3^+) which also removes hydrogen from the surface.
  - SiH_3 and SiH_2 radicals are important precursors for film growth while SiH_4 also participates in surface reactions.

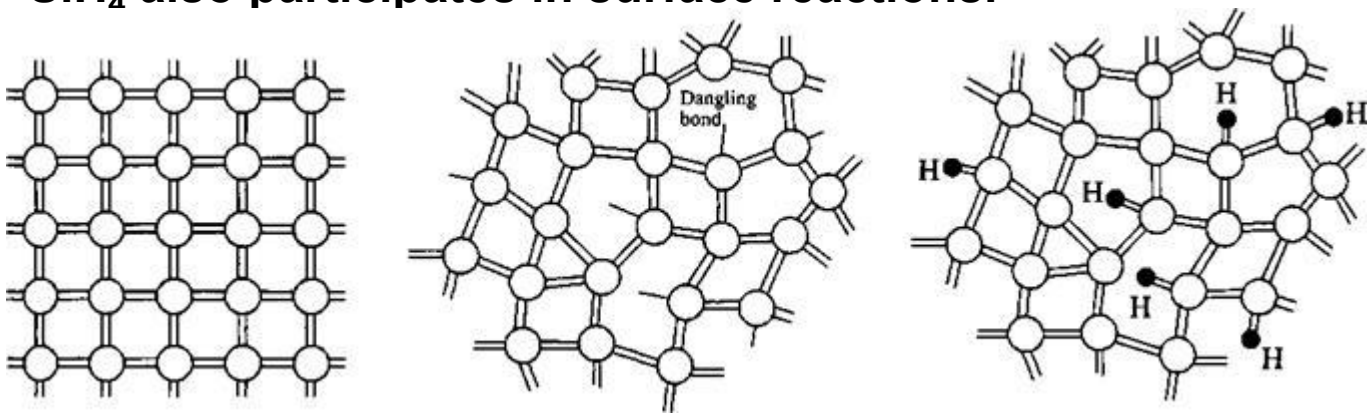

PVD

Physical vapor deposition can be achieved by heating the deposited material

- **Thermal evaporator**

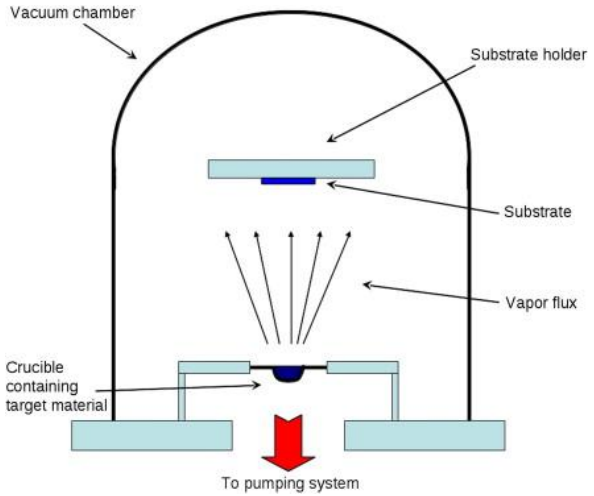

- **Electron-beam evaporator**

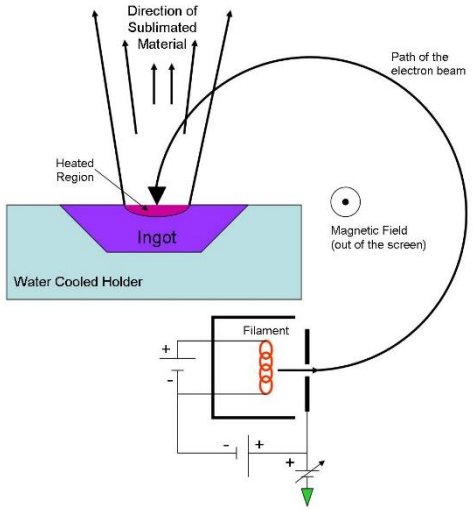

- **Pulsed-laser deposition**

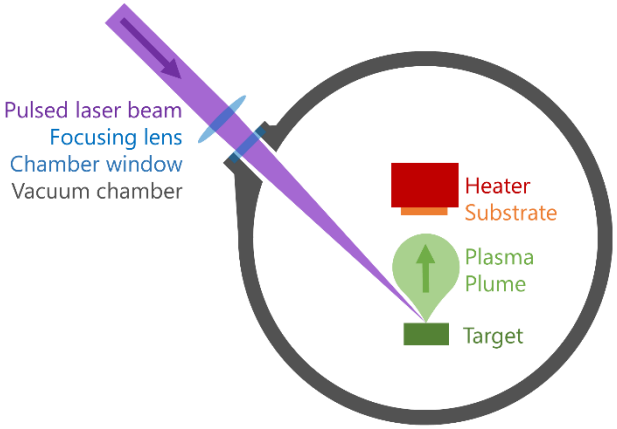

https://en.wikipedia.org/wiki/Pulsed_laser_deposition
Engineered biomimicry by A. Lakhtakia and R. J. Martin-Palma
https://en.wikipedia.org/wiki/Electron-beam_physical_vapor_deposition

Sputtering deposition

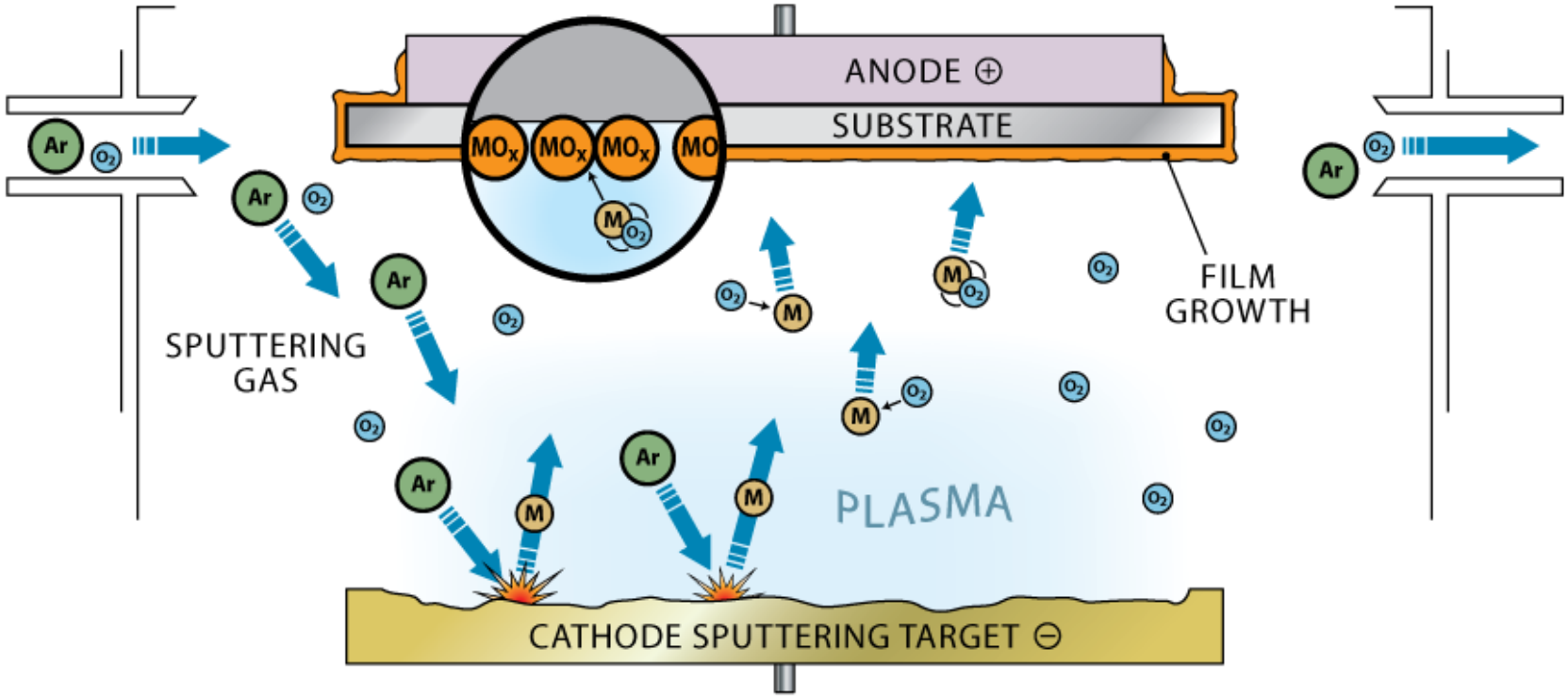

http://Inf-wiki.eecs.umich.edu/wiki/Sputter_deposition

PIII

Plasma-immersion ion implantation (PIII)

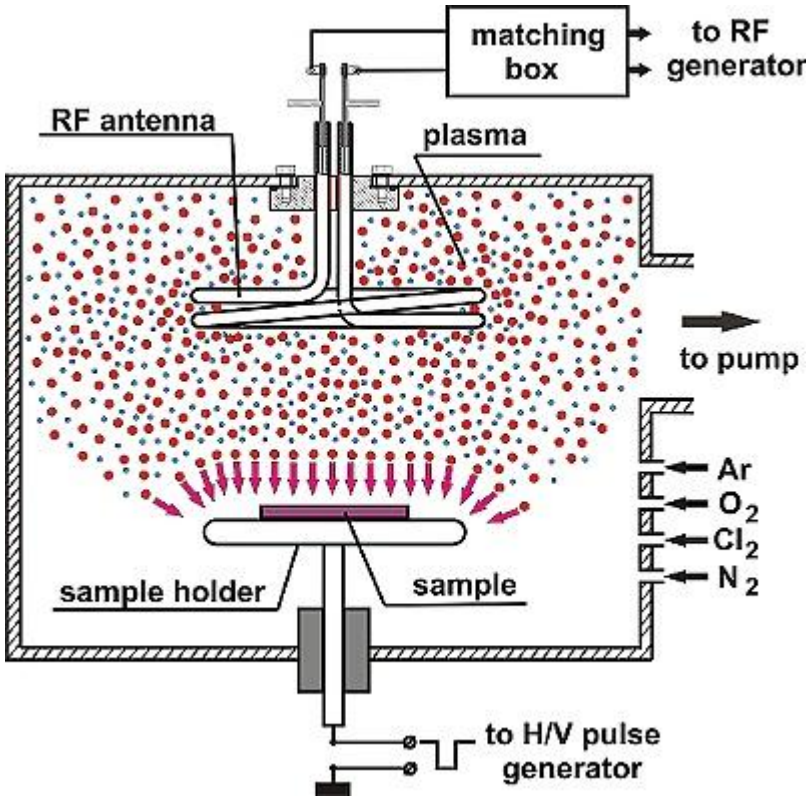

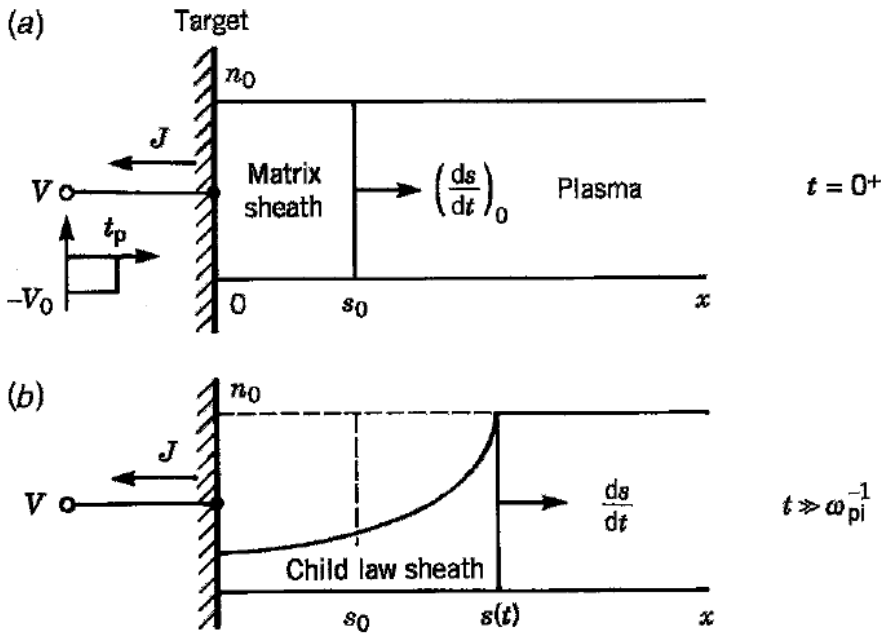

- **Silicon doping – ions such as B, P, As are implanted**
- **Surface hardening of metals – N, C are implanted**

https://www.hzdr.de/db/Cms?pOid=10890&pNid=306

Magnetron sputtering provides higher deposition rates than conventional sputtering

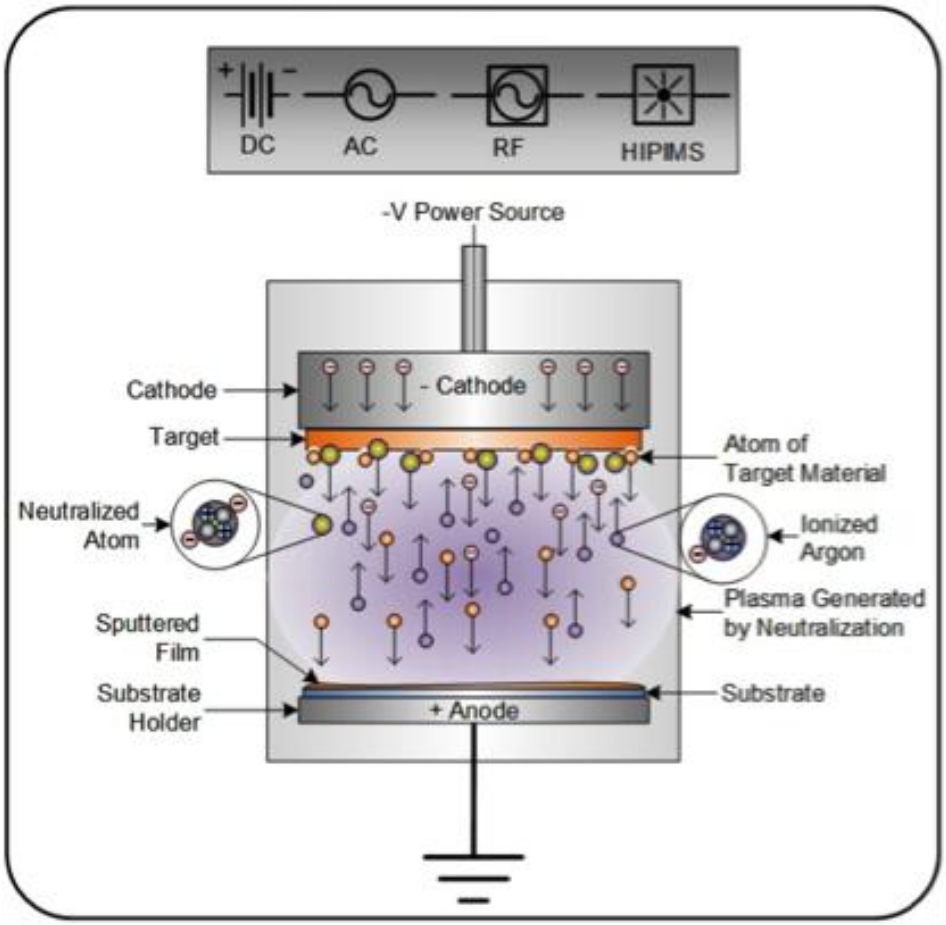

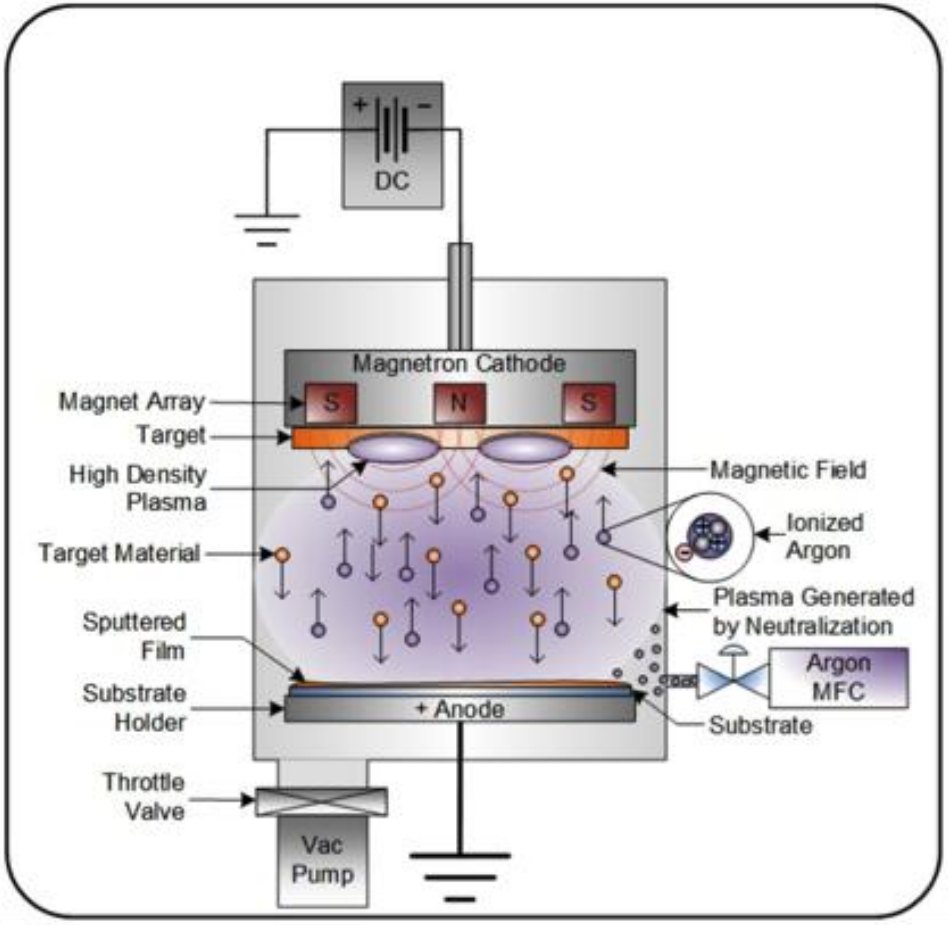

http://www.semicore.com/what-is-sputtering

Demonstration experiments – magnetron sputtering

- System

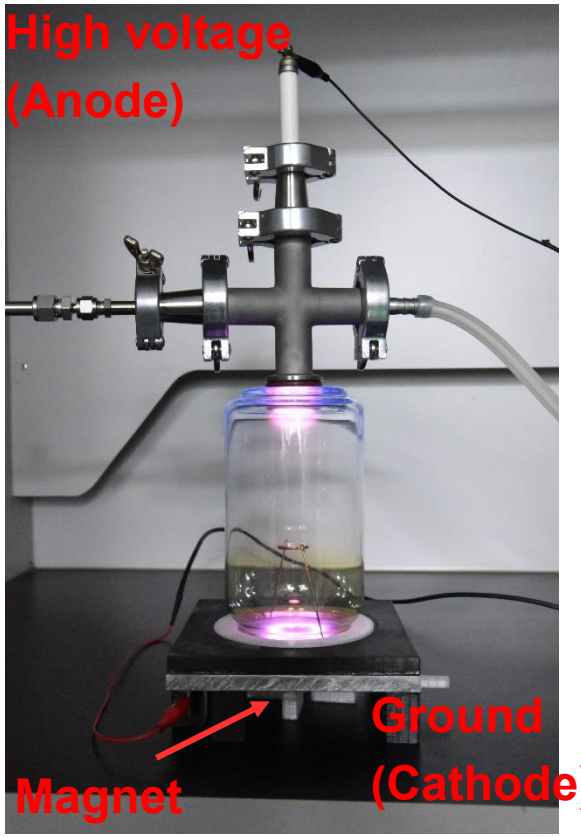

- Without magnet

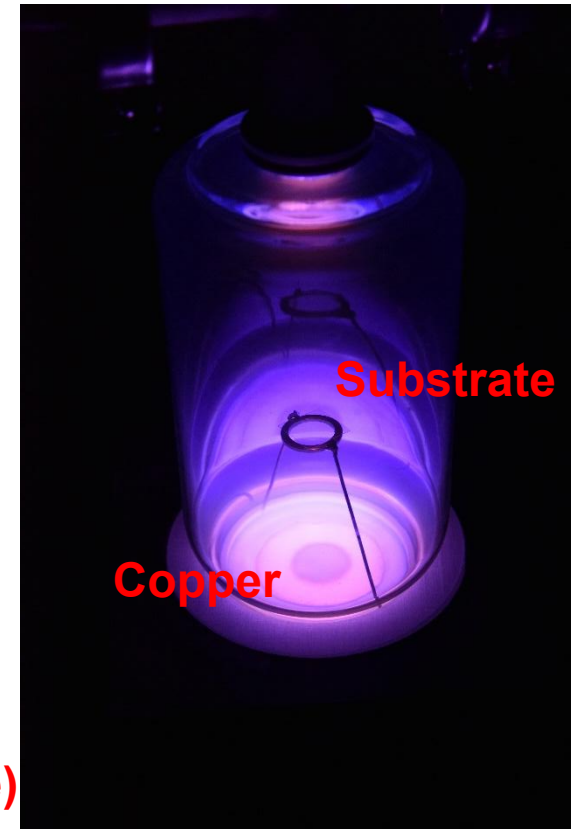

- With magnet

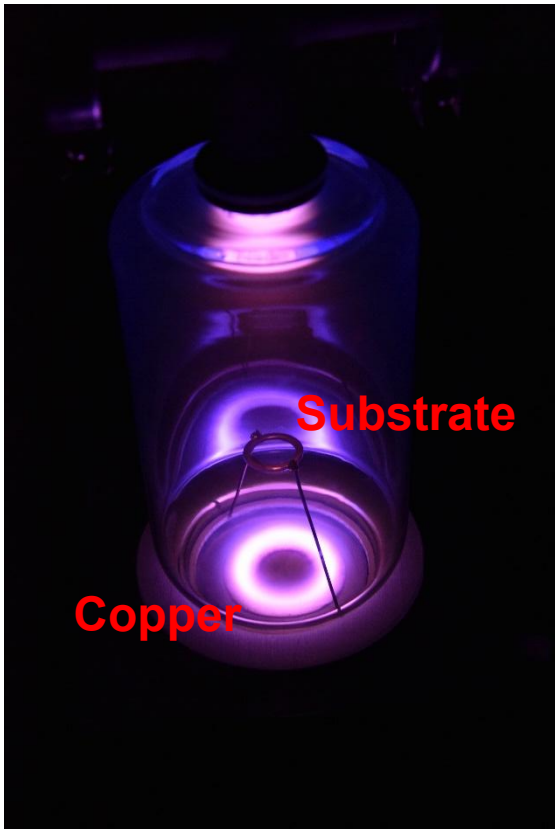

self-aligned quadruple patterning

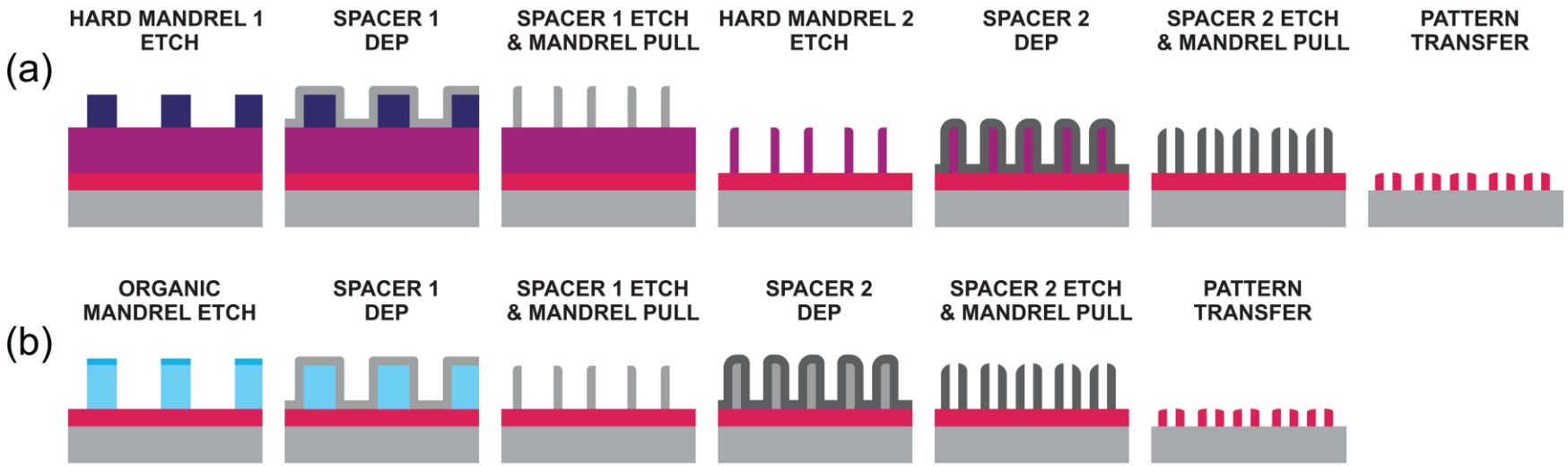

H. C. M. Knoops *et al.*, J. Vac. Sci. Technol. **A 37**, 030902 (2019)

Plasma can be used for cleaning surface

- **Cleaning mechanisms:**
  - **Chemical reactions by free radicals**
  - **Physical sputtering by high energy ions**

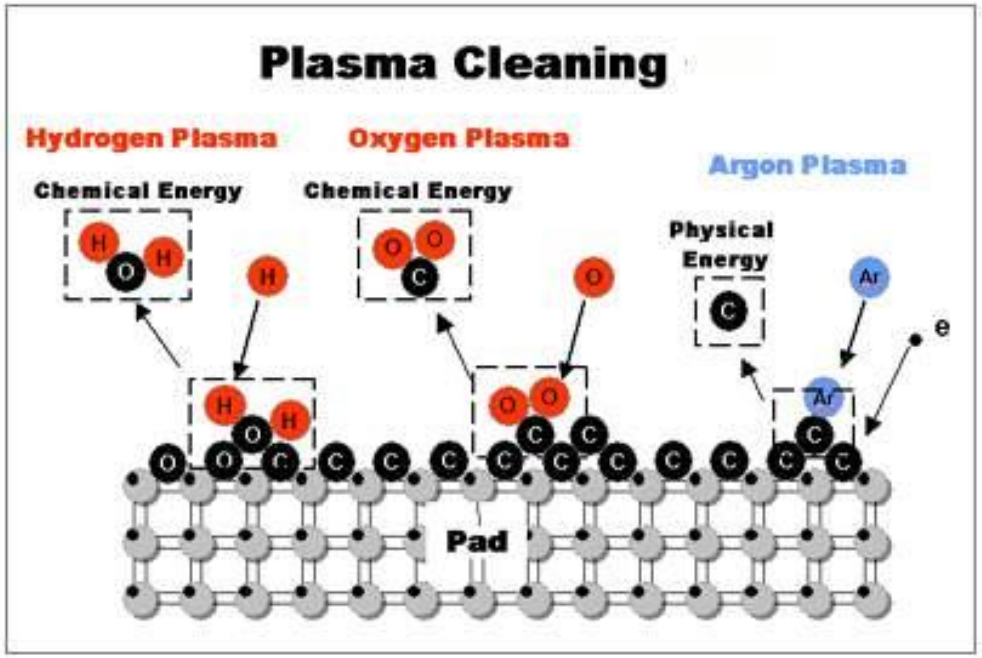

旭鼎奈米科技股份有限公司
https://www.ecplaza.net/products/plasma-cleaning_111807

Free radicals are generated and used in chemical reactions

$$e^- + H_2 \rightarrow 2H\bullet \qquad e^- + O_2 \rightarrow 2O\bullet \qquad \mathrm{O}\bullet + O_2 \rightarrow O_3$$

- **Highly reactive free radicals generated in plasma may react with the hydrocarbon contaminants of surface oxide.**
- **Both H•** and O• can react with grease or oil on surface to form volatile hydrocarbons.

$$\mathrm{H}\bullet_{(g)} + C_nH_{2n+2(s)} \rightarrow \mathrm{CH_{4(s)}}$$

$$\mathrm{O}\bullet_{(g)} + C_nH_{2n+2(s)} \rightarrow \mathrm{CO_{(s)}} + \mathrm{CH}_xO_{y(g)} + H_2O_{(g)}$$

- O• is more reactive than H•. But O• may also react with surface metal to form oxide, deteriorating the material properties. Nevertheless, H• can make metal oxide back to metal.

$$\mathrm{O}\bullet + \mathrm{Me} \rightarrow \mathrm{MeO}$$

$$\mathrm{H}\bullet + \mathrm{MeO} \rightarrow \mathrm{Me} + H_2O$$

The effect of chemical reactions is increased as the pressure increases

- **Advantages:**
  - **Stable gas products are formed.**
  - **No redeposition problem.**
  - **High etching selectivity.**

- **Disadvantages:**
  - **Higher concentration of H_2 or O_2 is required to ensure an appropriate etching rate.**
  - **H_2 safety or O_2 strong oxidation ability needs to be monitored.**

High energy ions are used in physical sputtering cleaning

- Ions generated in plasma can be accelerated toward the substrate to physically bombard away the atoms of contaminants.
- The physical sputtering rate increases as the following quantities increase:
  - Plasma density;
  - Accelerating voltage;
  - Mass of bombardment atoms.
- The physical sputtering is also enhanced by lowering the pressure.
- High cathode bias is used.
- Ar^+ has strong sputtering effect.

The physical sputtering rate increases with higher cathode bias and Ar concentration and lower pressure

- **Advantages:**
  - **Highly efficient cleaning effect can be achieved.**
  - **Gas consumption rate can be very low.**

- **Disadvantages:**
  - **Etching problems – non-selective etching by physical sputtering.**
  - **Redeposition problems: the products sputtered out may be highly unstable and tend to deposit again downstream.**

Plasma cleaning examples

Low-pressure plasma system: Generation with a low-frequency or high-frequency generator

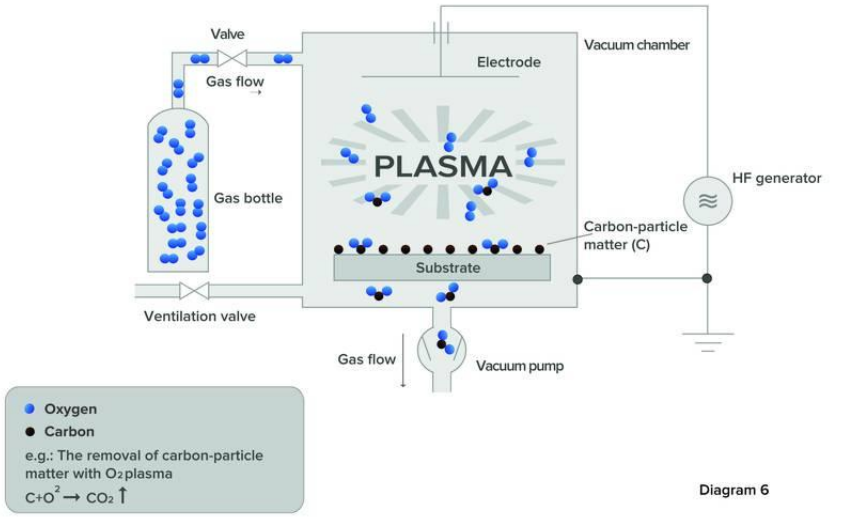

Diagram 6

Low-pressure plasma system: Cleaning with a microwave generator

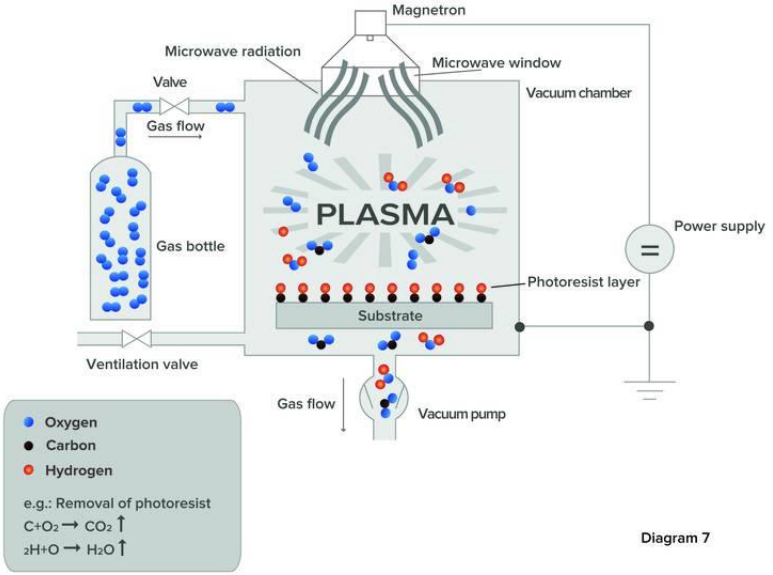

Diagram 7

https://www.plasma.com/en/plasmatechnik/low-pressure-plasma/cleaning/

Plasma cleaning needs to work in the regime of abnormal glow discharge

- Top view

- Side view

A semiconductor device is fabricated by many repetitive production process

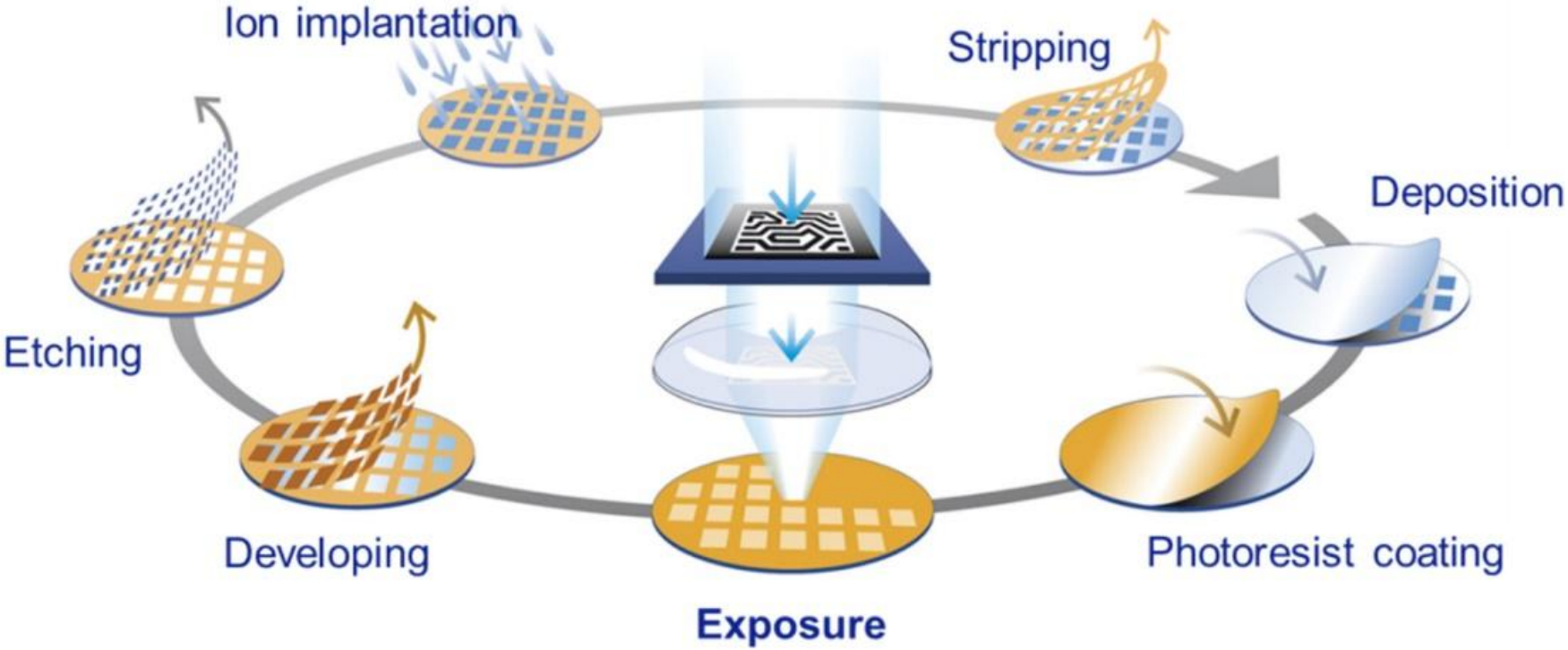

Surf. Topogr.: Metrol. Prop. **4** (2016) 023001

Ultraviolet lithography (EUVL) is one of the key technologies in semiconductor manufacturing nowadays

- **The process technology of Taiwan Semiconductor Manufacturing Company Limited (TSMC):**

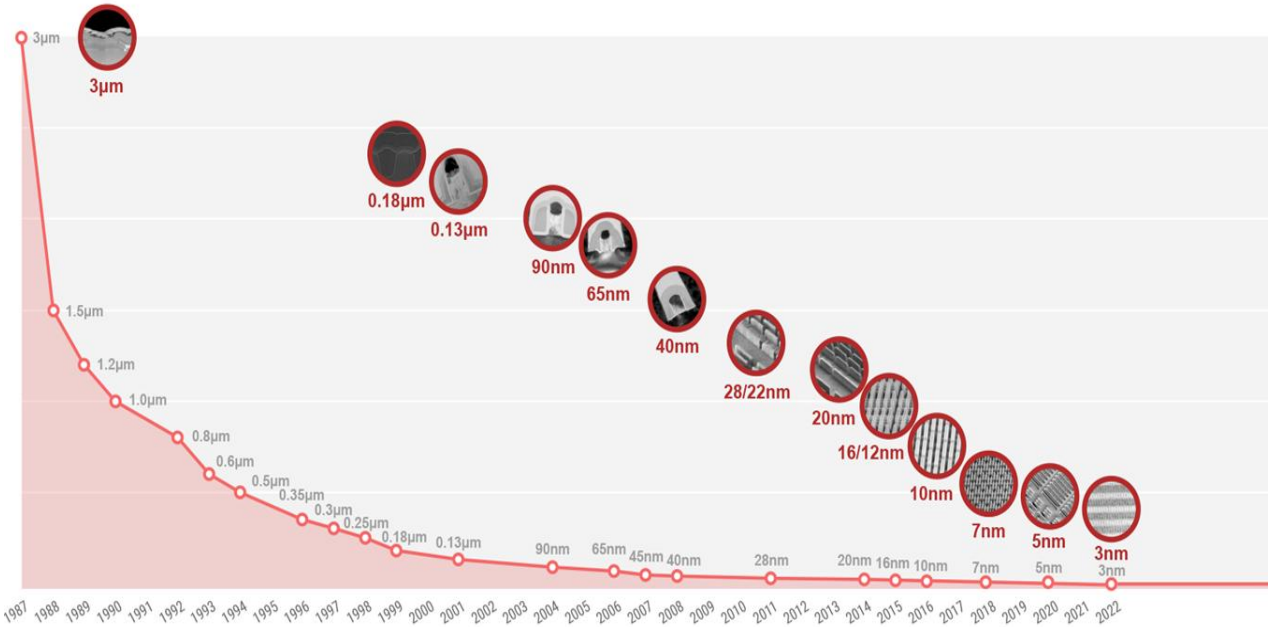

- **Optical diffraction needs to be taken into account.**
- **Shorter wavelength is preferred.**

- **Light source with a center wavelength of 13.5 nm is used.**

https://www.tsmc.com/chinese/dedicatedFoundry/technology/logic.htm

EUV lithography becomes important for semiconductor industry

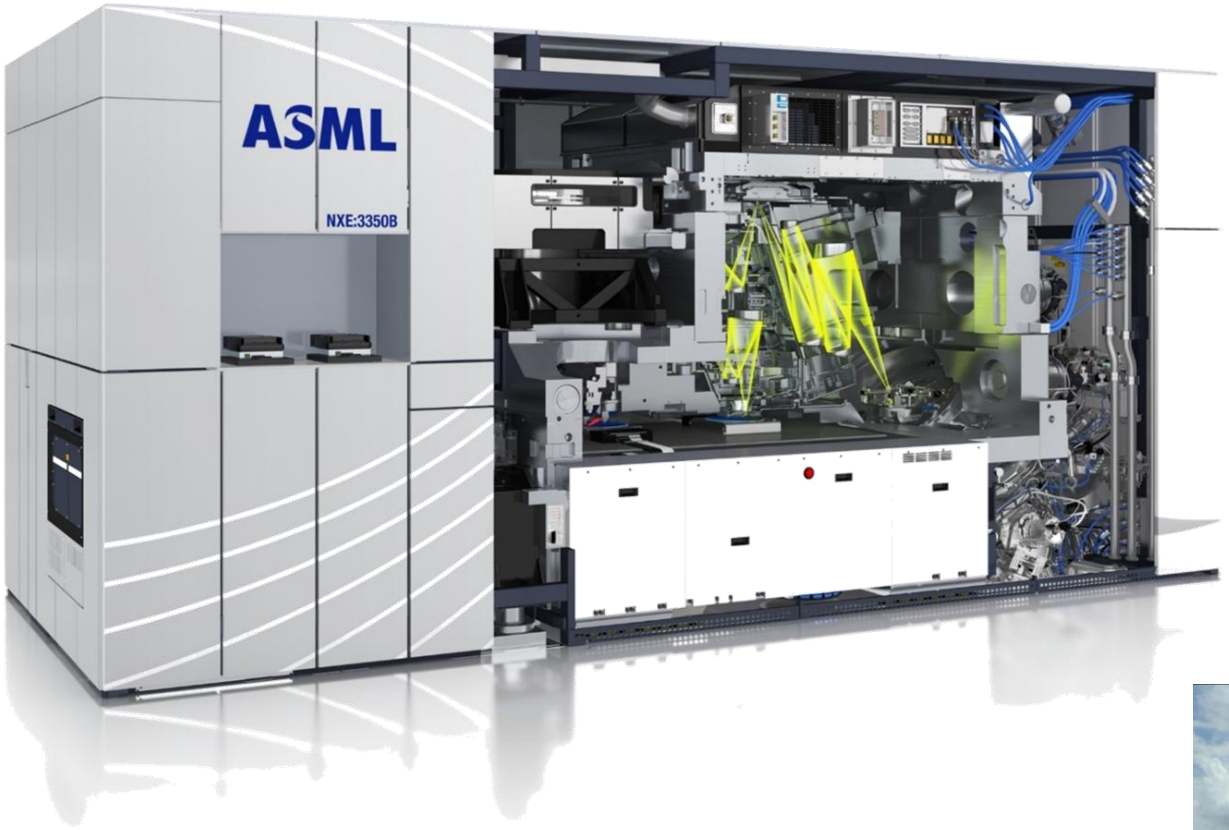

- **0.15 billion USD for each EUV light source.**

https://www.youtube.com/watch?v=NHSR6AHNiDs

http://finance.technews.tw/2019/01/25/euv-asml-2018/

EUV light can only be reflected using multilayer mirrors

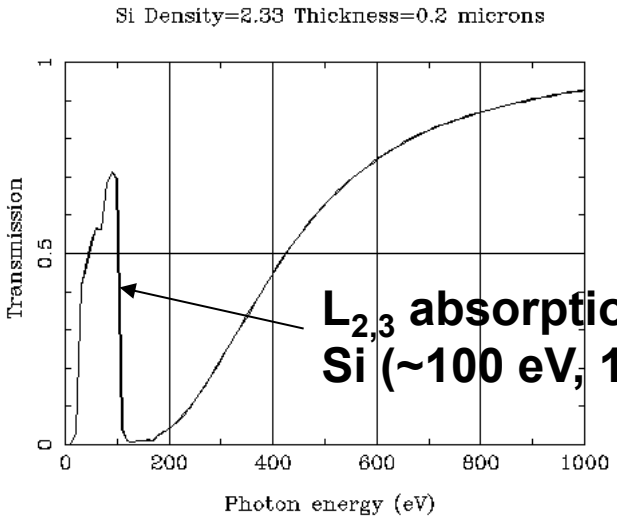

$L_{2,3}$ absorption edge of Si (~100 eV, 12.4 nm)

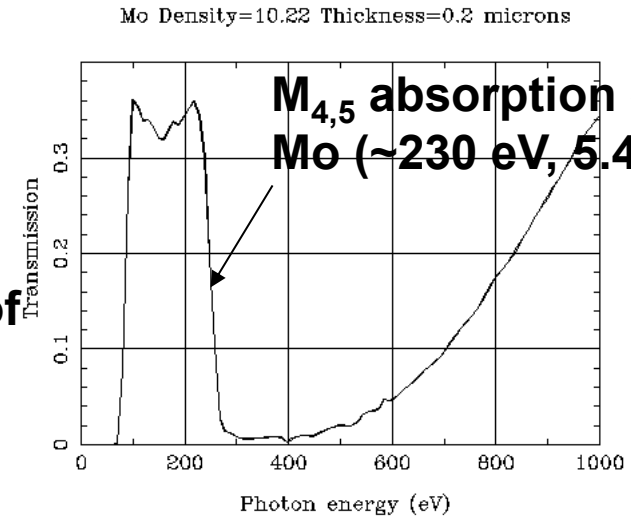

$M_{4,5}$ absorption edge of Mo (~230 eV, 5.4 nm)

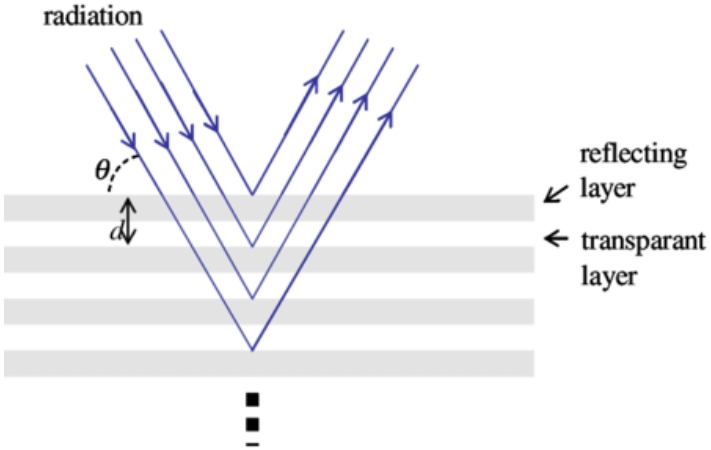

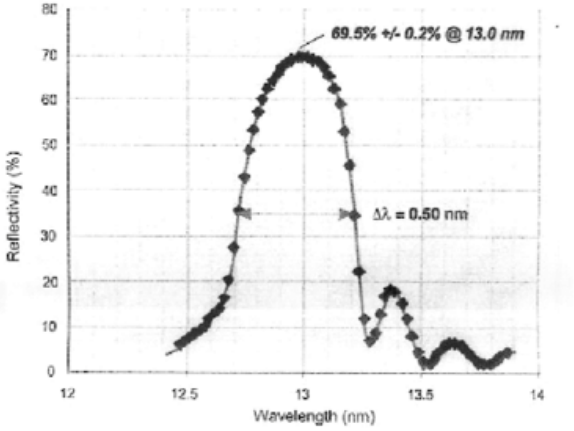

https://henke.lbl.gov/optical_constants/

Mo/Si multilayer coating technology for EUVL, coating uniformity and time stability; E. Louis et al.; SPIE 4146-06, Soft X-ray and EUV Imaging Systems, San Diego, 2000.

13.5-nm EUV light is picked for EUV lithography

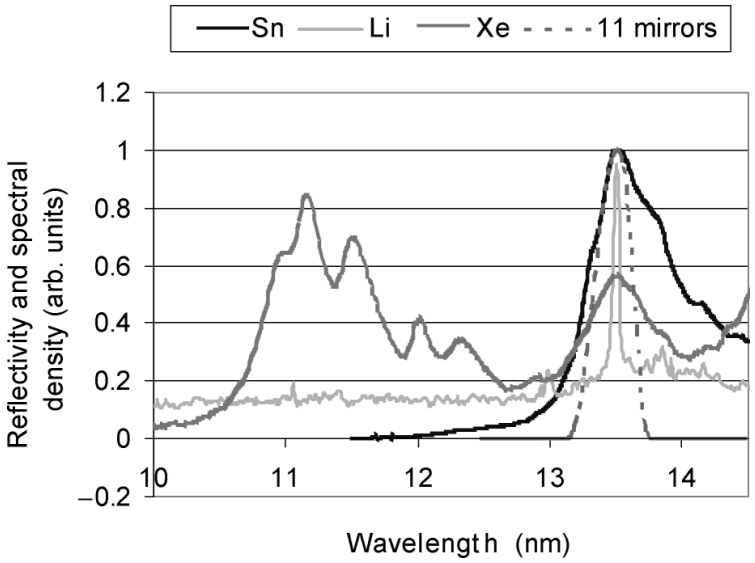

- $\lambda = 13.5\ \text{nm} \pm 1\%$ **is required.**
- **At T=35-40 eV (~450,000 K), in-band emission occurs.**
- **Xenon:**
  - $4p^6 4d^8 \rightarrow 4p^6 4d^7 5p$ **from single ion stage** Xe^{10+}
  - **UTA @ 11 nm**
- **Tin:**
  - $4p^6 4d^N \rightarrow 4p^5 4d^{N+1} + 4p^6 4d^{N-1} 4f$ $(1 \leq N \leq 6)$ in ions ranging from Sn^{8+} to Sn^{12+}
  - **UTA @ 13.5 nm**

- UTA: unresolved transition array

V. Bakshi, EUV sources for lithography
R. S. Abhari, etc., J. Micro/Nanolithography, MEMS, and MOEMS, 11, 021114 (2012)

EUV light is generated from laser-produced plasma (LPP)

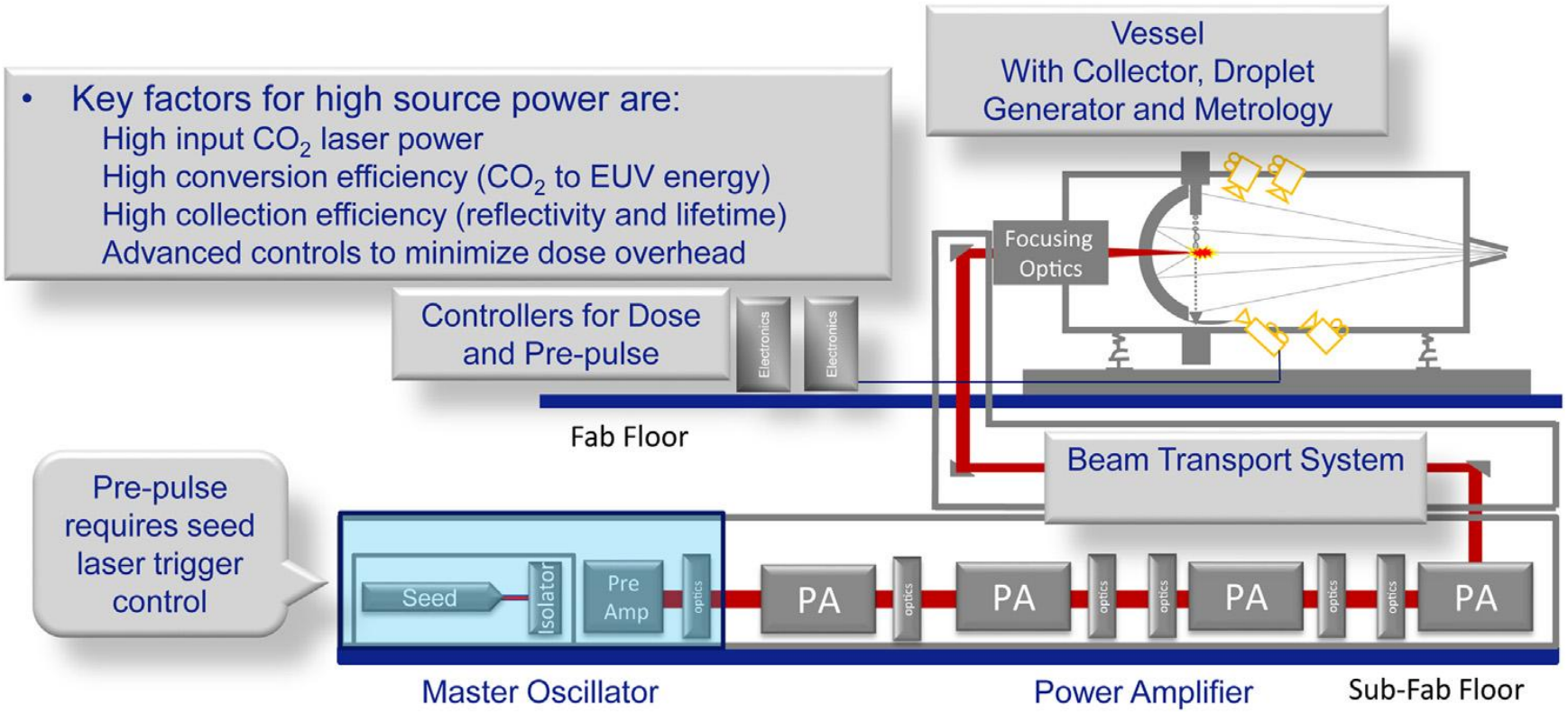

D.-K. Yang, etc., *Chip*, **1**, 100019 (2022)

Two laser pulses are used to heat the plasma

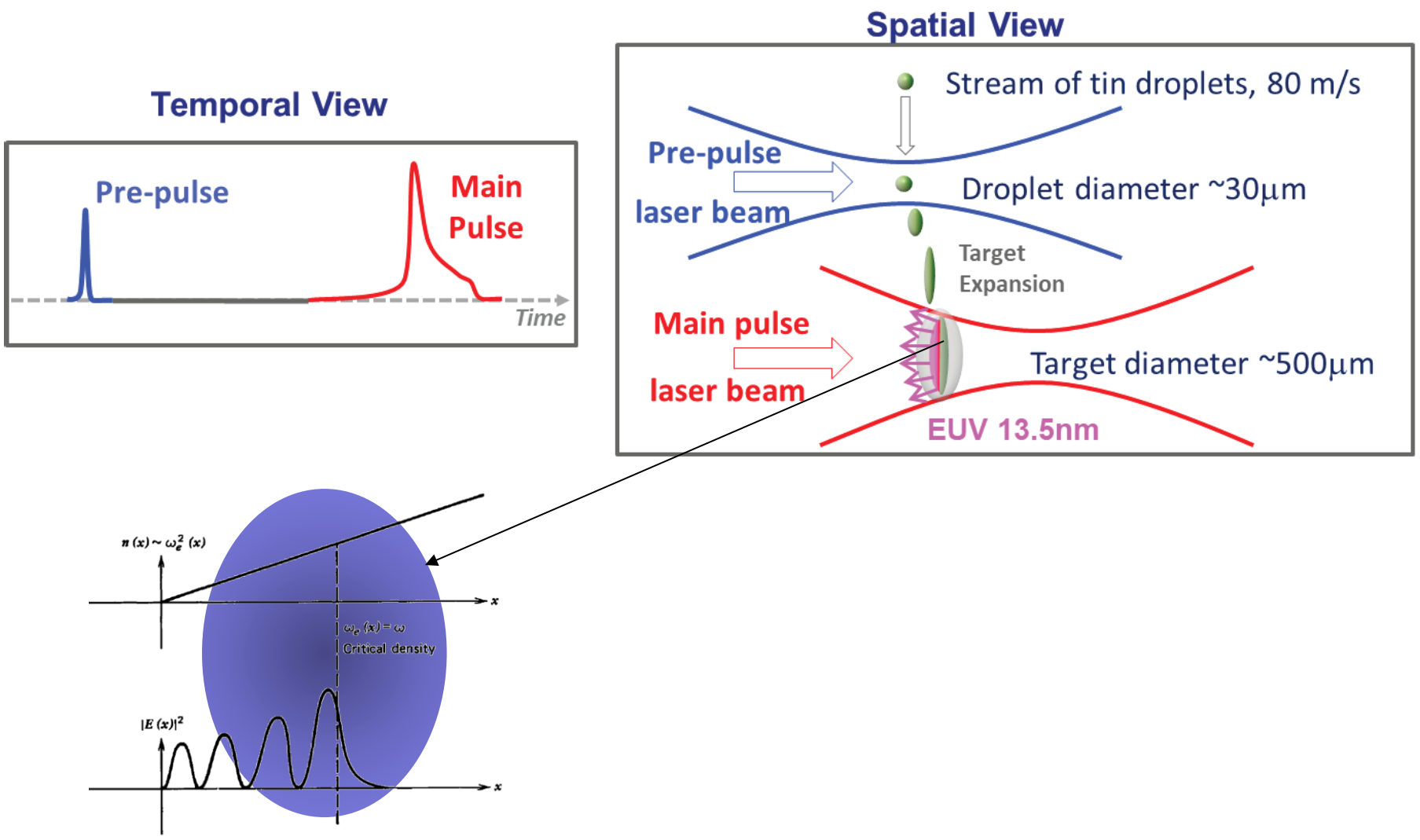

I. Fomenkov, etc., *Synch. Rad. News*, **32**, 3 (2019)

Hydrogen buffer gas with a pressure of ~100 Pa is used to protect the collector mirror

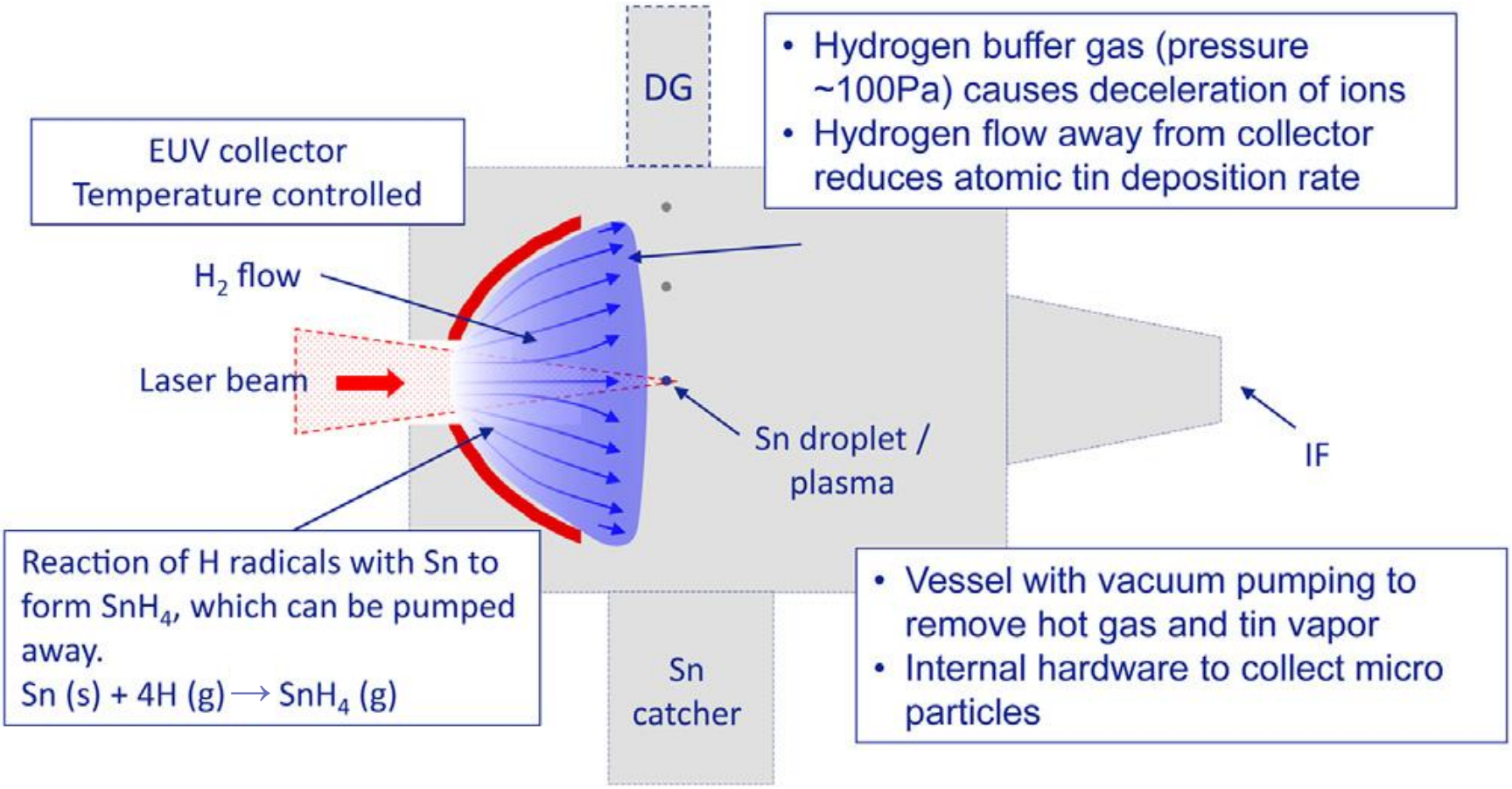

D.-K. Yang, etc., *Chip*, **1**, 100019 (2022)

Laser-produced plasma (LPP) is used in the EUV lithography

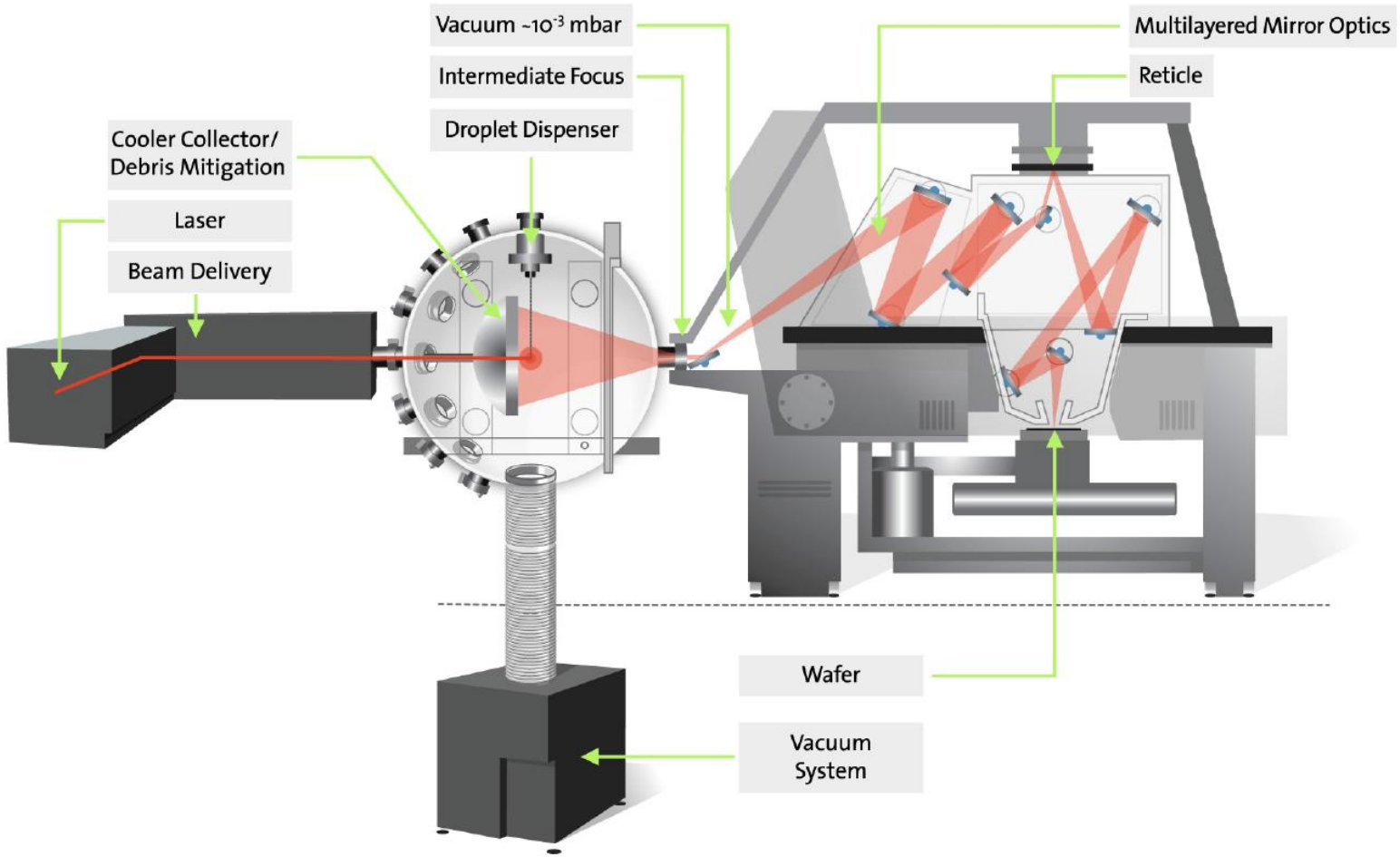

R. S. Abhari, etc., J. Micro/Nanolithography, MEMS, and MOEMS, 11, 021114 (2012)

High harmonic generation from high-power laser

- For I < 10^{18} w/cm^2

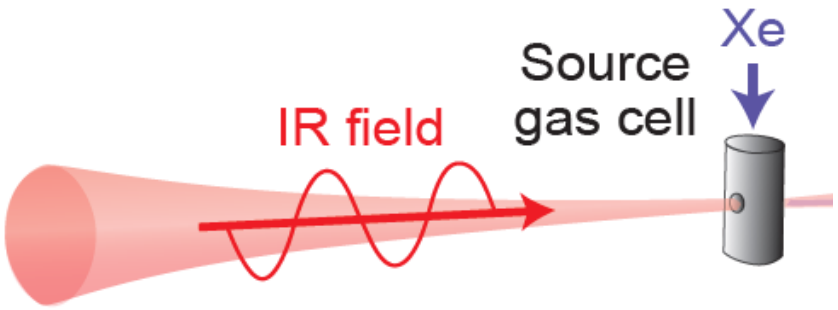

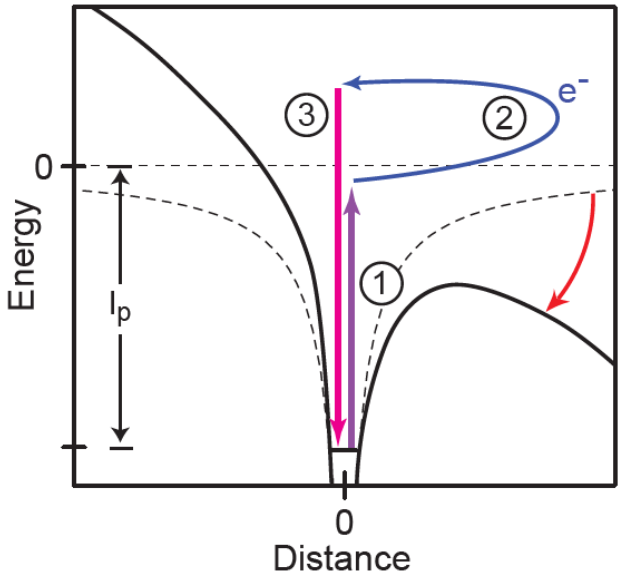

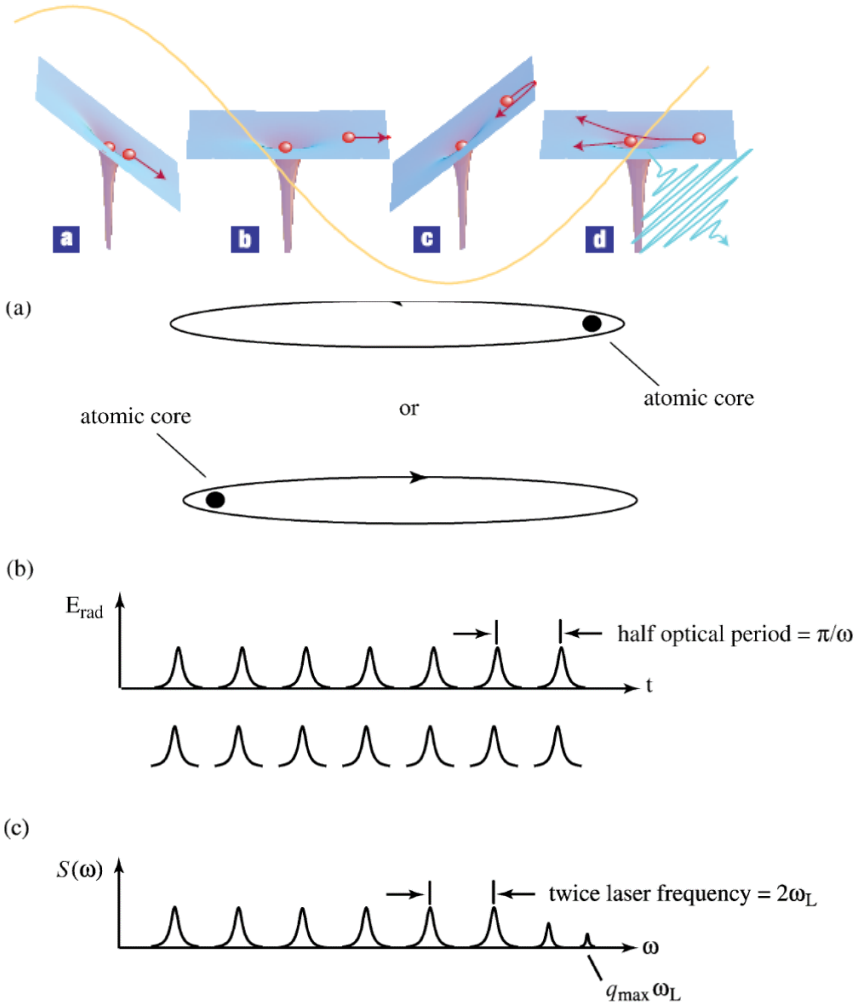

- M. Krüger, etc., Appl. Sci. 9, 378 (2019)
- Nonlinear Optics 3rd edition , by Robert W. Boyd
- P. B. Corkum and F. Krausz, Nature Phys., 3, 381 (2007)

EUV light can be generated using discharged-produced plasma

- **Adiabatic compression:**

$$TV^{\gamma-1} = \text{const} \quad T_f = T_o \left(\frac{r_o}{r_f}\right)^{4/3}$$

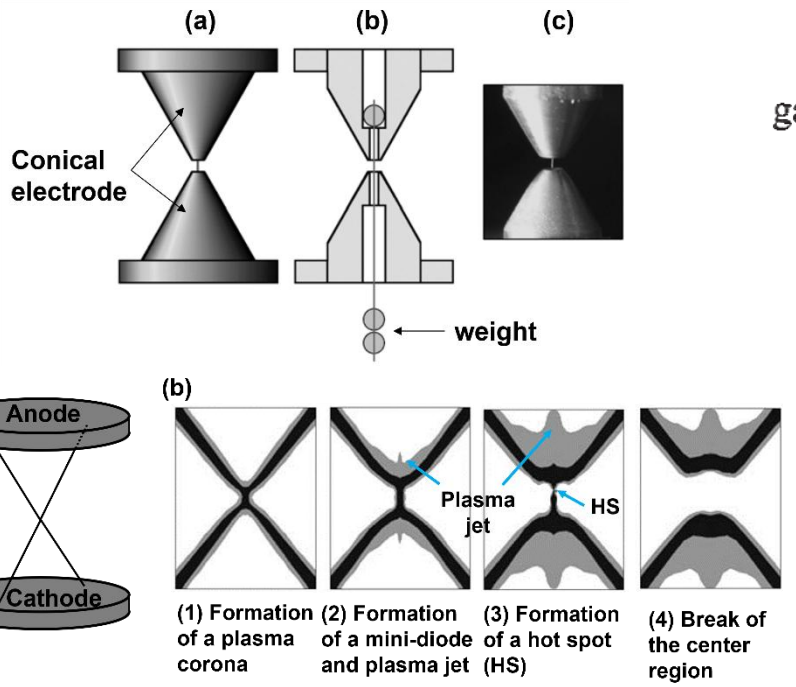

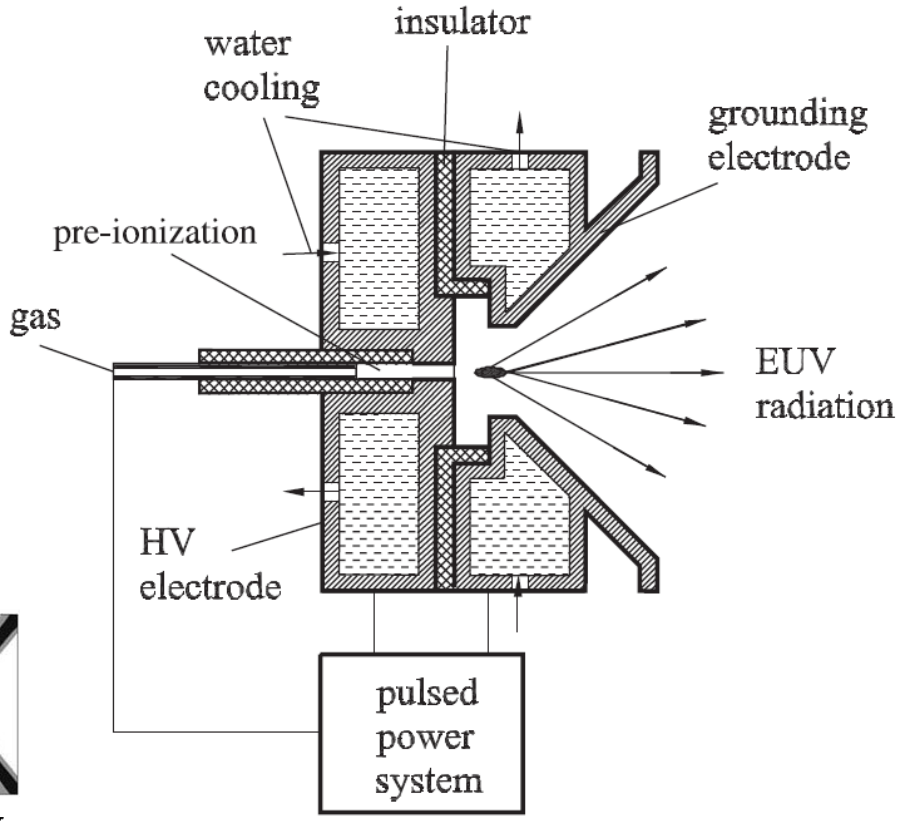

- Plasma Physics Reports, 38(5):359–381 (2012).
- Plasma Physics Reports, 34(8):619–638, (2008).
- JPDAP_37_p3254_2004_EUV sources using Xe and Sn discharge plasmas

Light source and display systems

Plasma display panel (PDP)

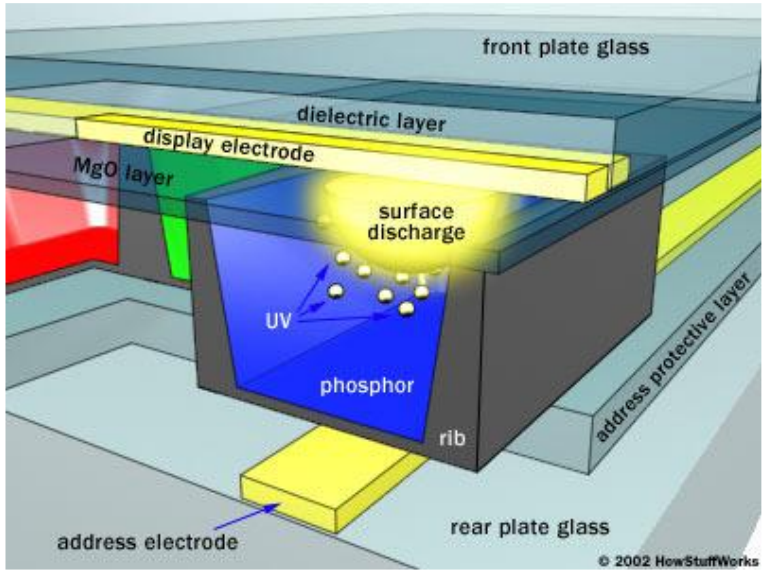

Liquid crystal display (LCD)

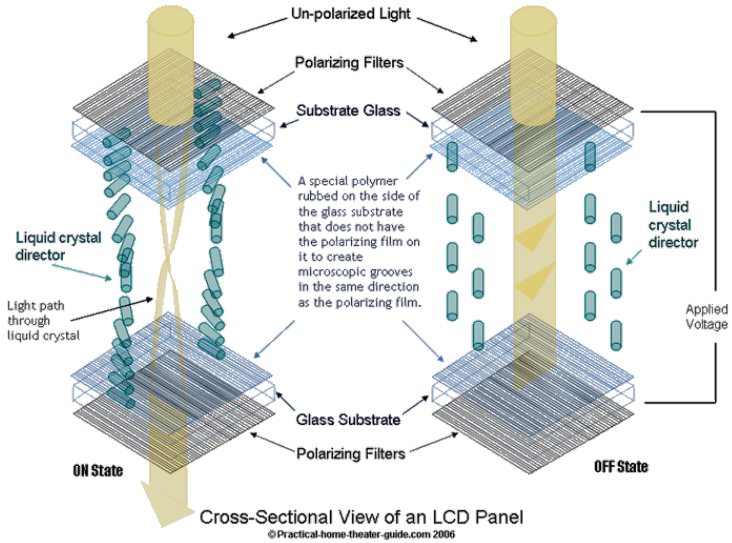

Outlines

- Cathode Ray Tube
- Color space (CIE 1931 color spaces)
- History of plasma display panel (PDP)
- Design of PDP
- Liquid crystal display (LCD)
- LCD vs PDP

CRT

Cathode Ray Tube uses electron beams to light the fluorescent screen

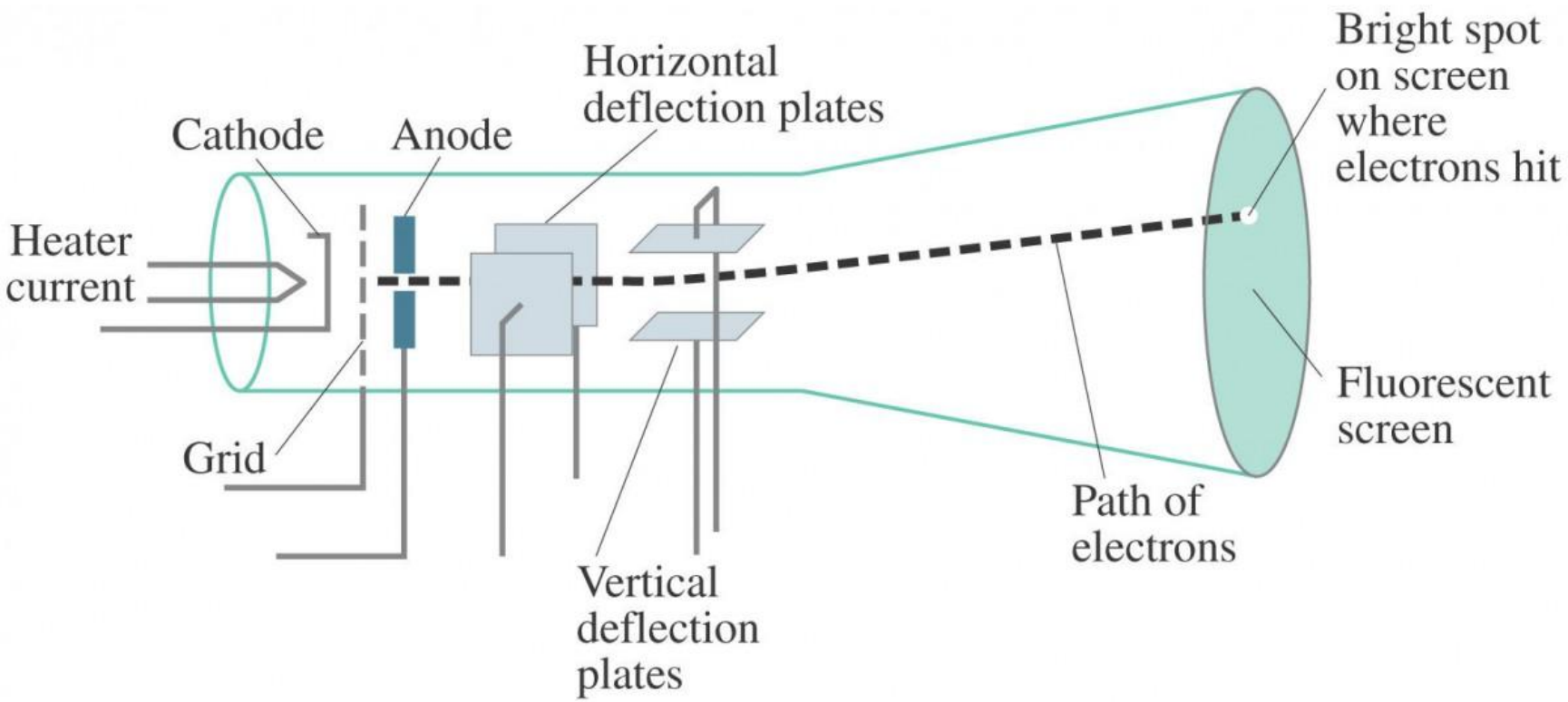

http://www.sciencefacts.net/cathode-ray-tube-crt.html

The image is shown by scanning through the whole screen with the single electron beam

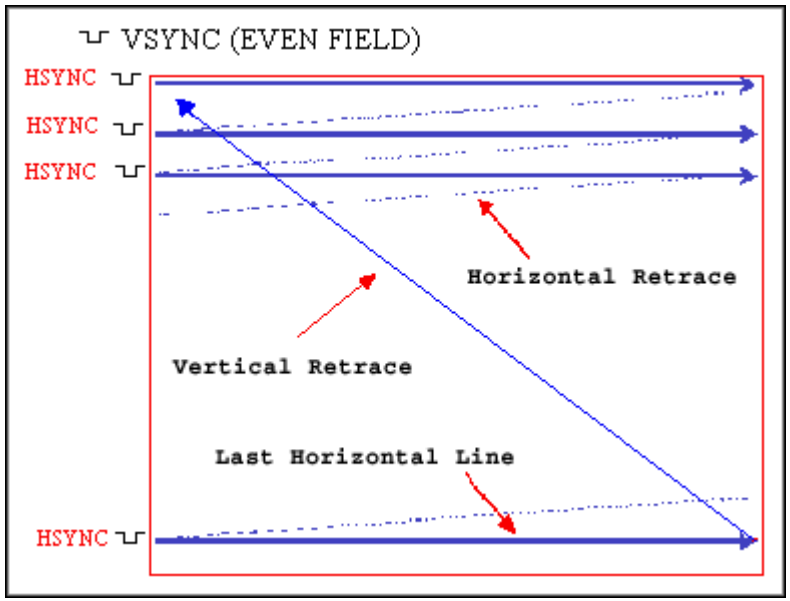

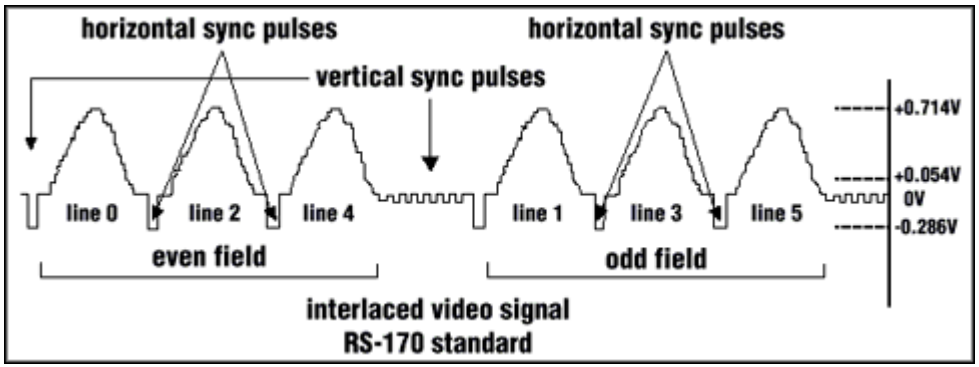

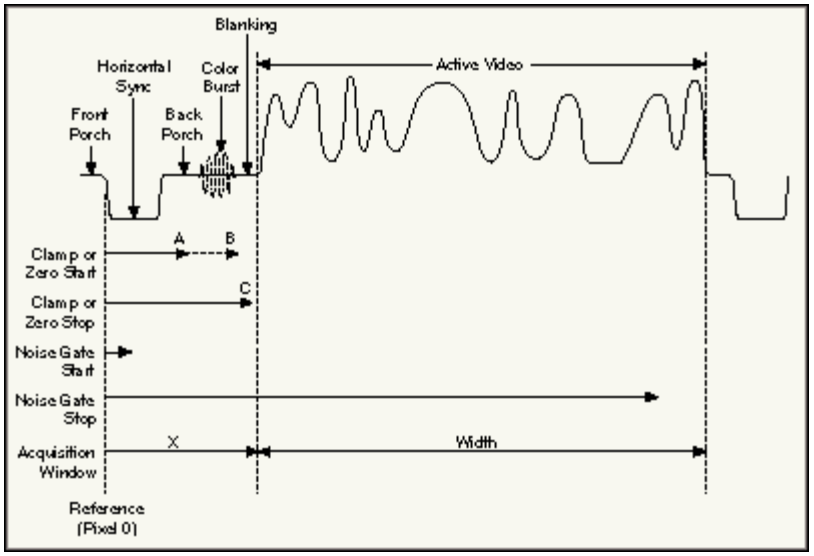

http://www.ni.com/white-paper/3020/en/#toc2

Color image is formed by using three electron beams scanning through three different color channels

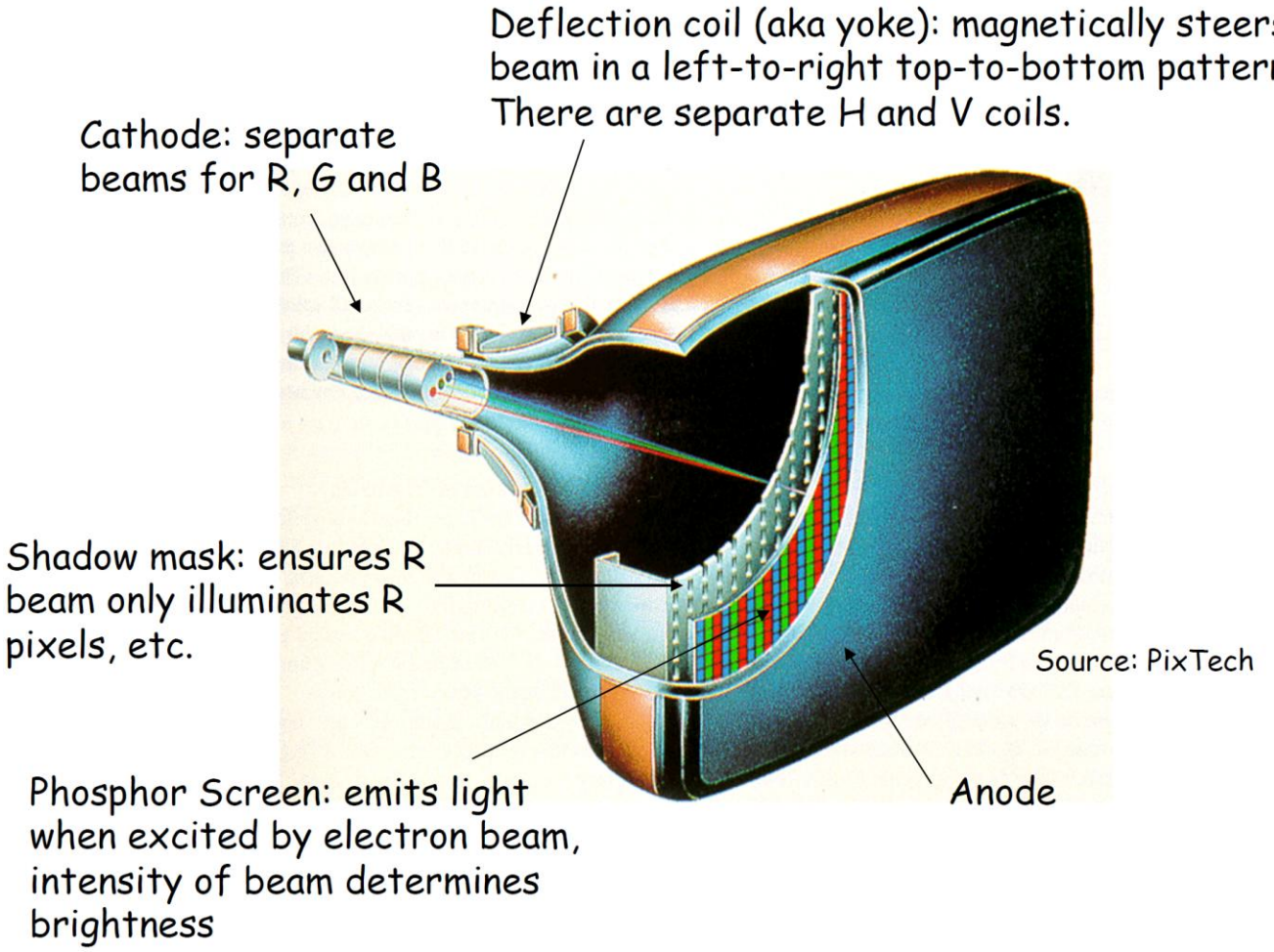

http://web.mit.edu/6.111/www/f2008/handouts/L12.pdf

Color space

Color can be created using three primary colors

Additive primaries

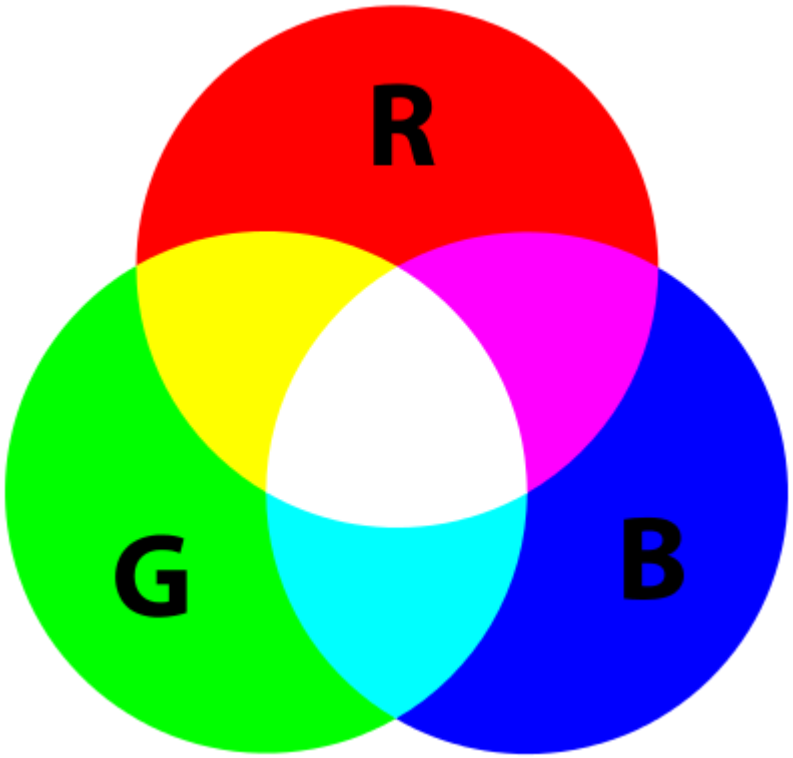

Subtractive primaries

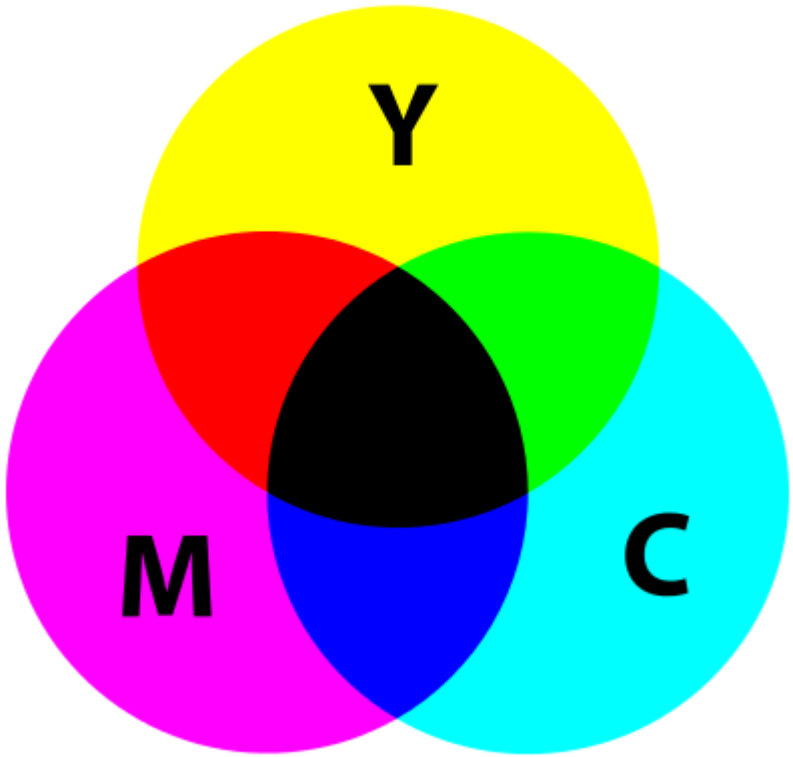

https://en.wikipedia.org/wiki/Primary_color

Human retina has three kinds of “cones” that have different spectral response

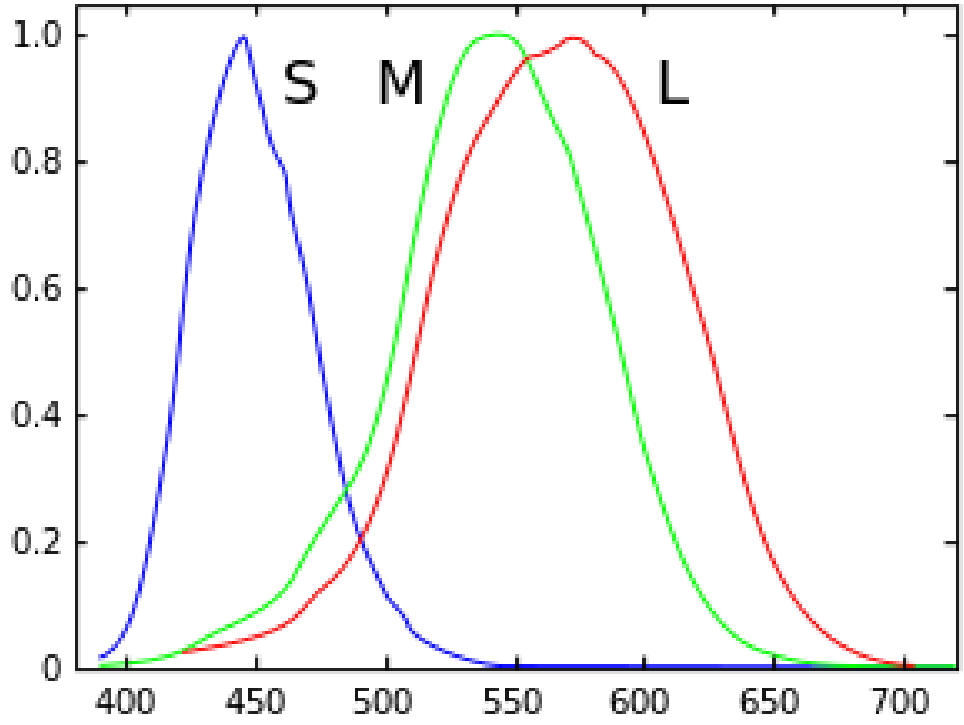

Spectral response of retina “cones” are tested using light sources with single wavelength

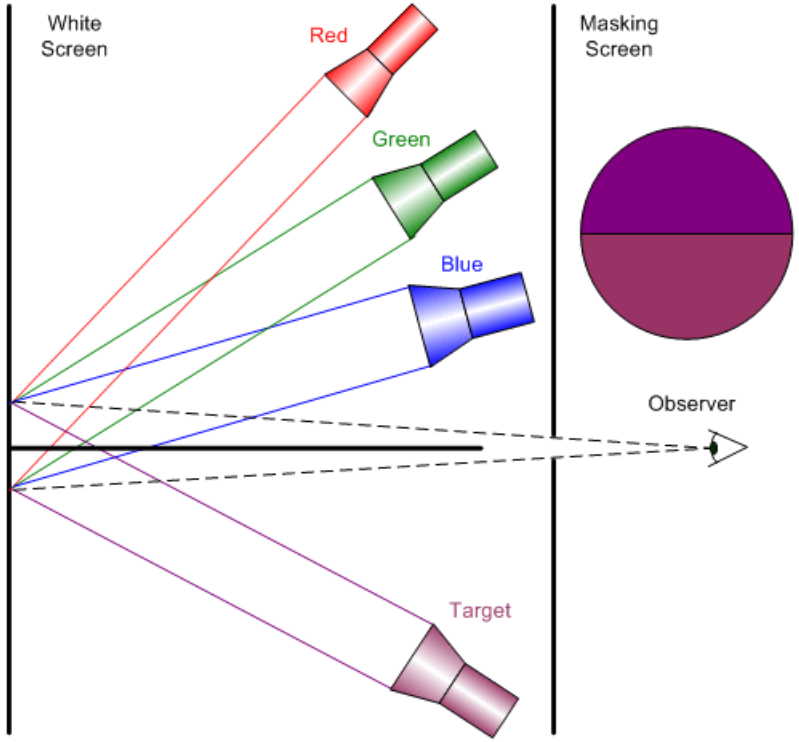

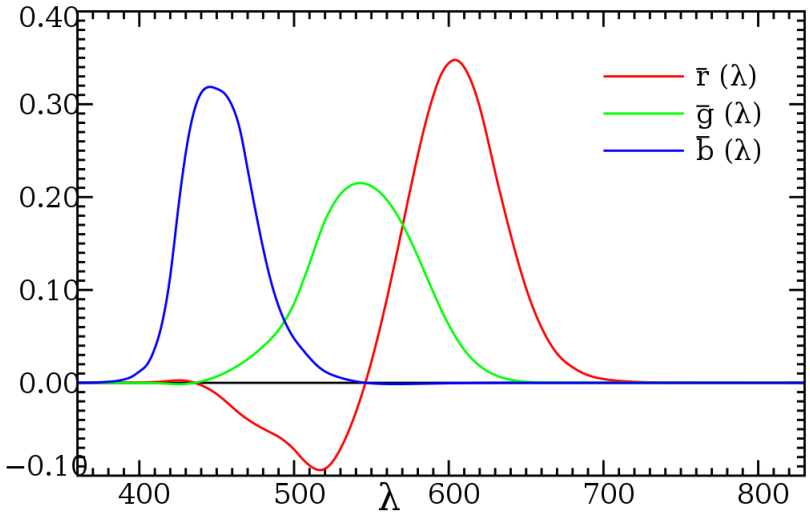

http://betterphotographytutorials.com/2011/08/01/light-and-colors-%E2%80%93-part-3/
https://en.wikipedia.org/wiki/CIE_1931_color_space

The CIE 1931 color space chromaticity diagram is the standard color space

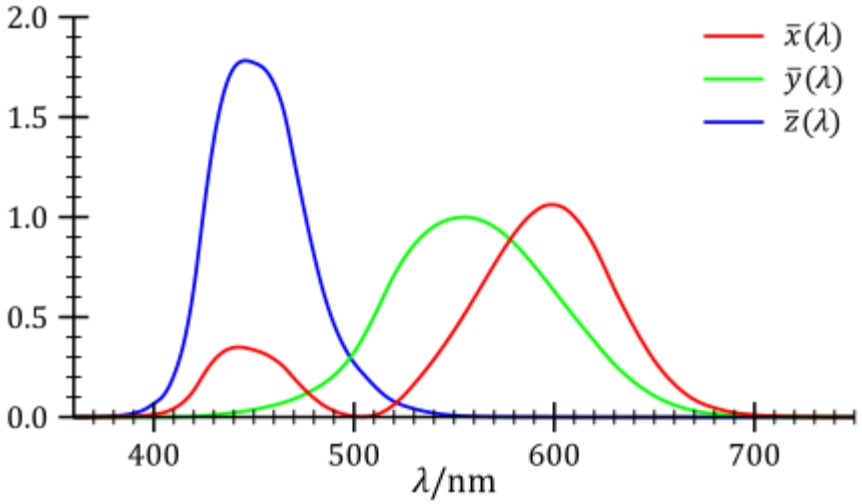

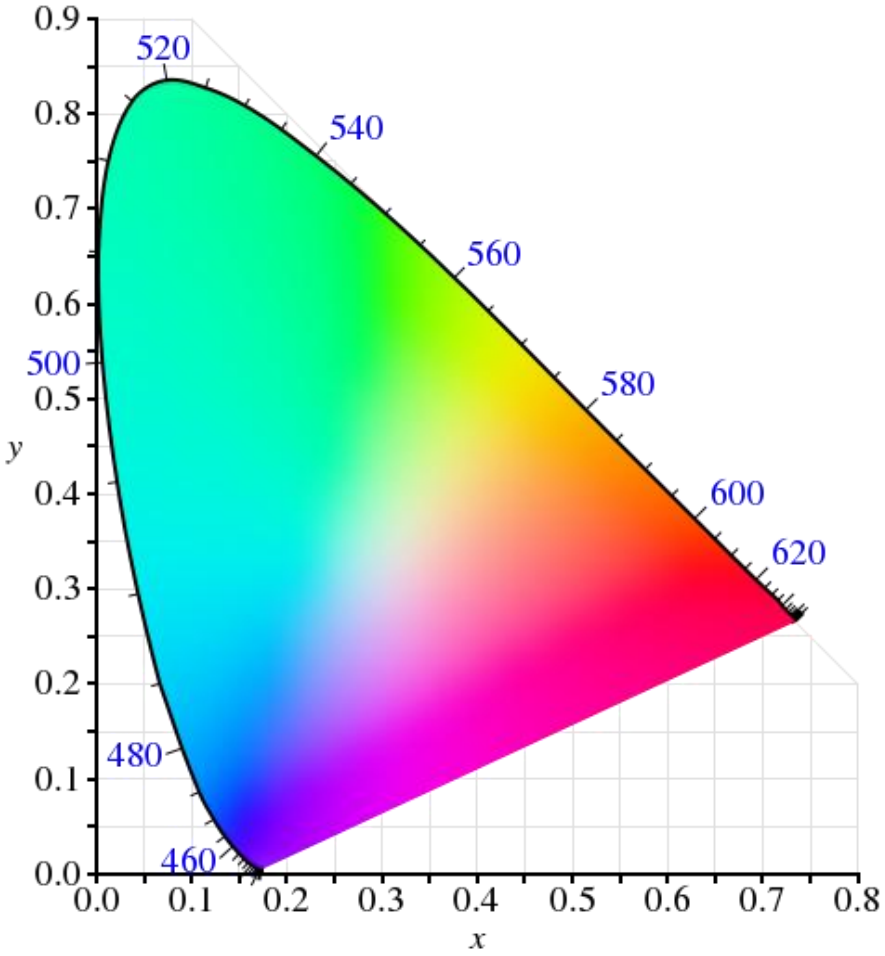

https://en.wikipedia.org/wiki/CIE_1931_color_space

History of PDP

Plasma display panel was invented at the University of Illinois in 1967

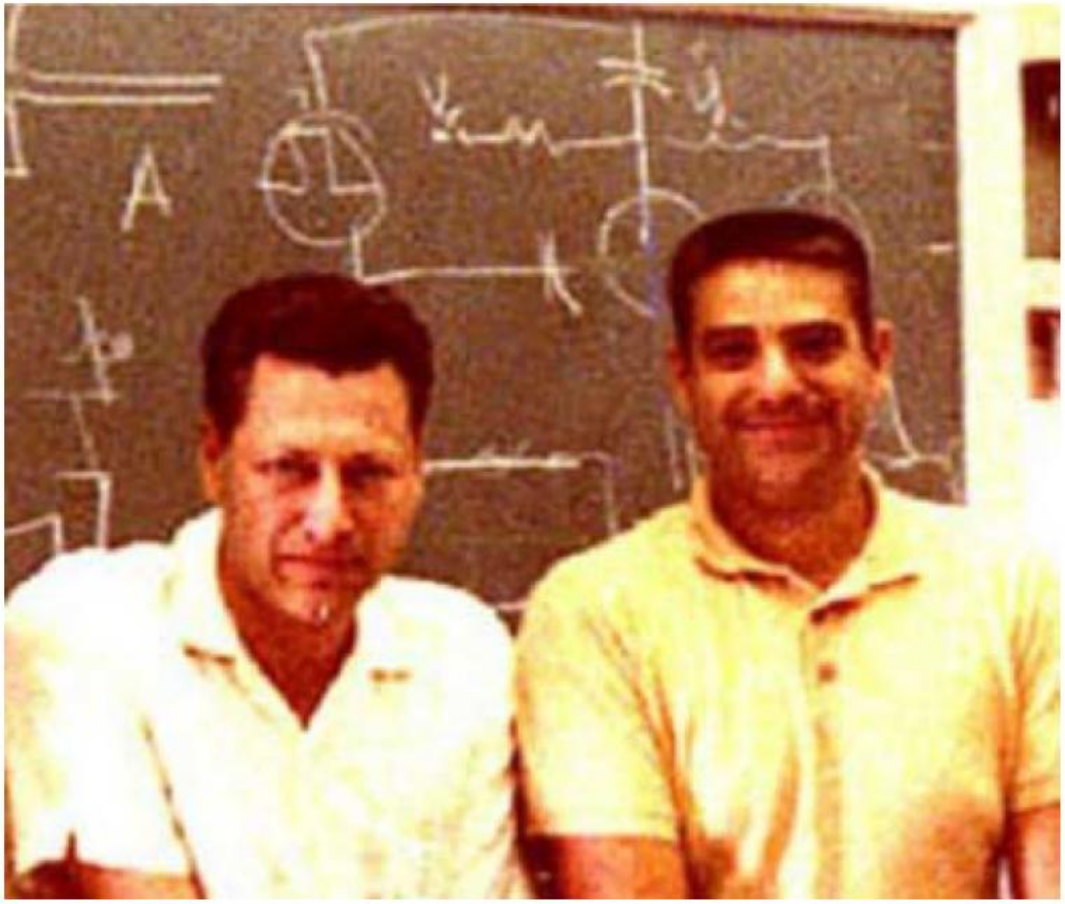

Prof. H. Gene Slottow **Prof. Donald L. Bitzer**

L. F. Weber, IEEE Trans. Plas. Scien., *34*, 268, 2006

PDP was invented due to a need for Programmed Logic for Automatic Teaching Operations (PLATO) in 1960s

1981 Plato V

https://topwallpapers.pw/computer/keyboards-computers-history-teletype-typewriters-desktop-hd-wallpaper-1035981/
https://en.wikipedia.org/wiki/Punched_tape
https://en.wikipedia.org/wiki/PLATO_(computer_system)

The positive column in a glow discharge is used to excite phosphors in color PDP

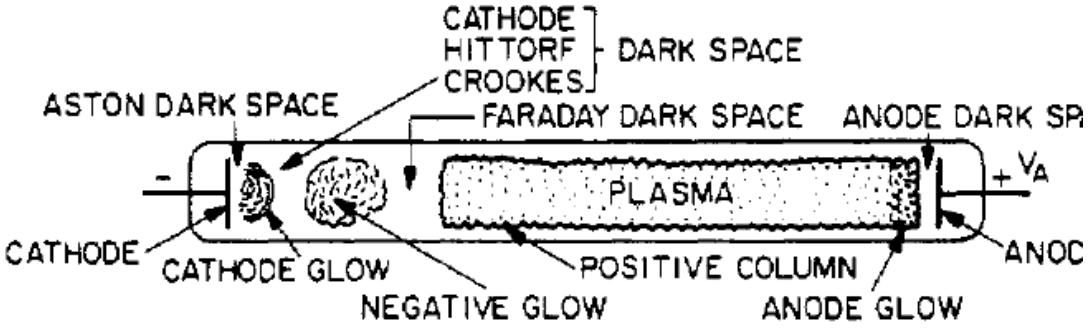

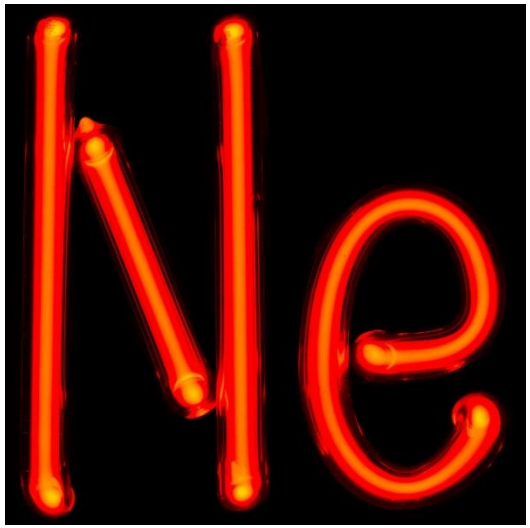

- **Majority of monochrome PDPs use the negative glow as the light source**
- **The positive column is used to excite phosphors in fluorescent lamps and in color PDPs**

Industrial plasma engineering, volume 1, by J. Reece Roth
https://en.wikipedia.org/wiki/Neon_lighting

Early plasma panel (PD) attached to the glass vacuum system used for the first plasma displays at UI

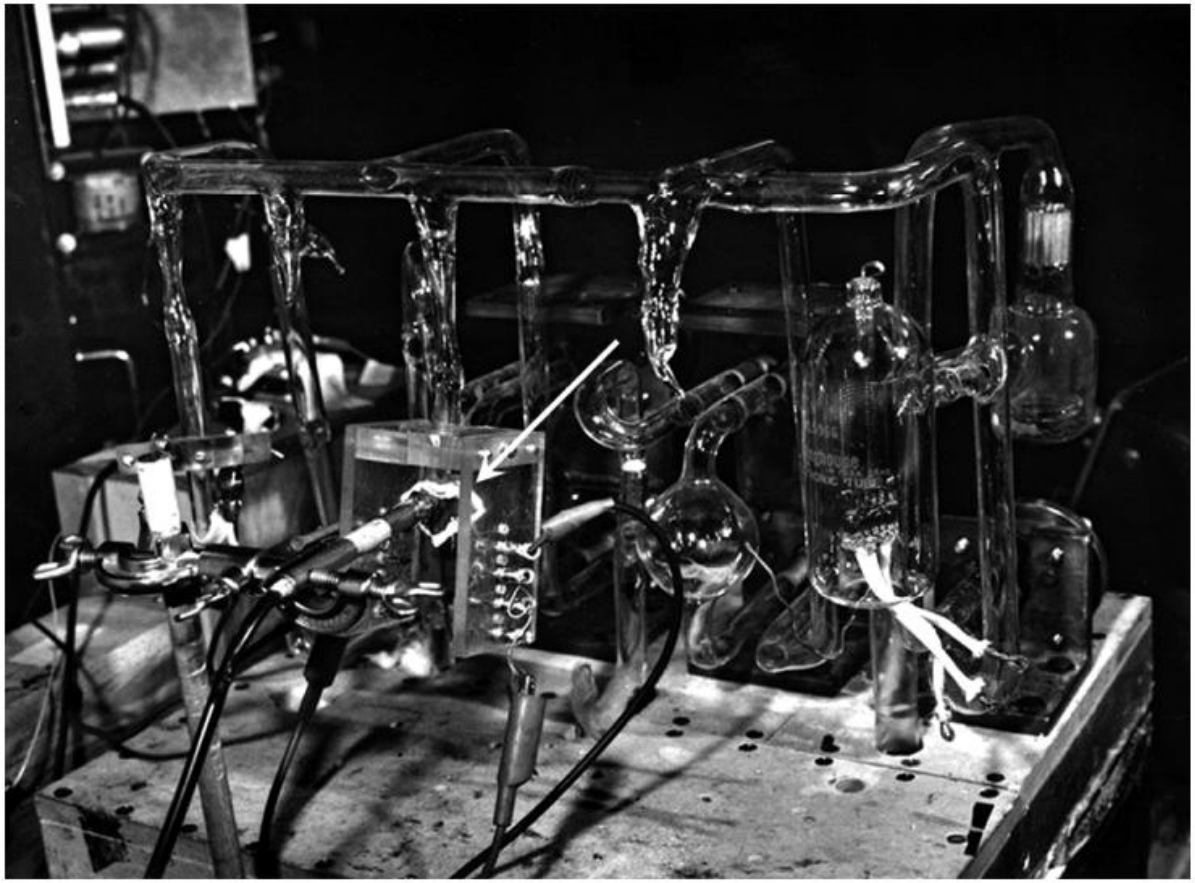

- **It had the same alternating sustain voltage, neon, gas, and dielectric glass insulated electrodes that are used for plasma TVs today.**

L. F. Weber, IEEE Trans. Plas. Scien., *34*, 268, 2006

Early plasma panel (PD) attached to the glass vacuum system used for the first plasma displays at UI

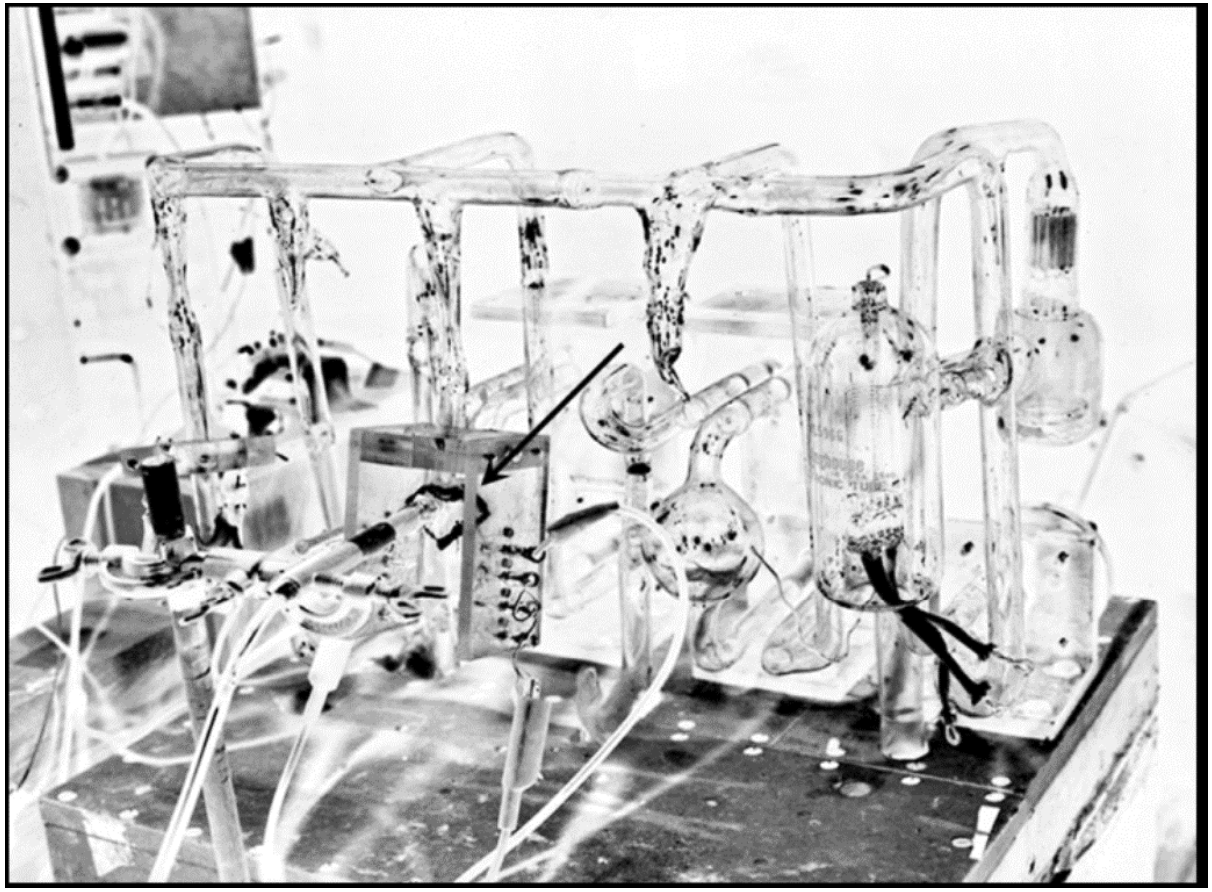

- **It had the same alternating sustain voltage, neon, gas, and dielectric glass insulated electrodes that are used for plasma TVs today.**

L. F. Weber, IEEE Trans. Plas. Scien., *34*, 268, 2006

Early 4x4 pixel panel has achieved matrix addressability for the first time

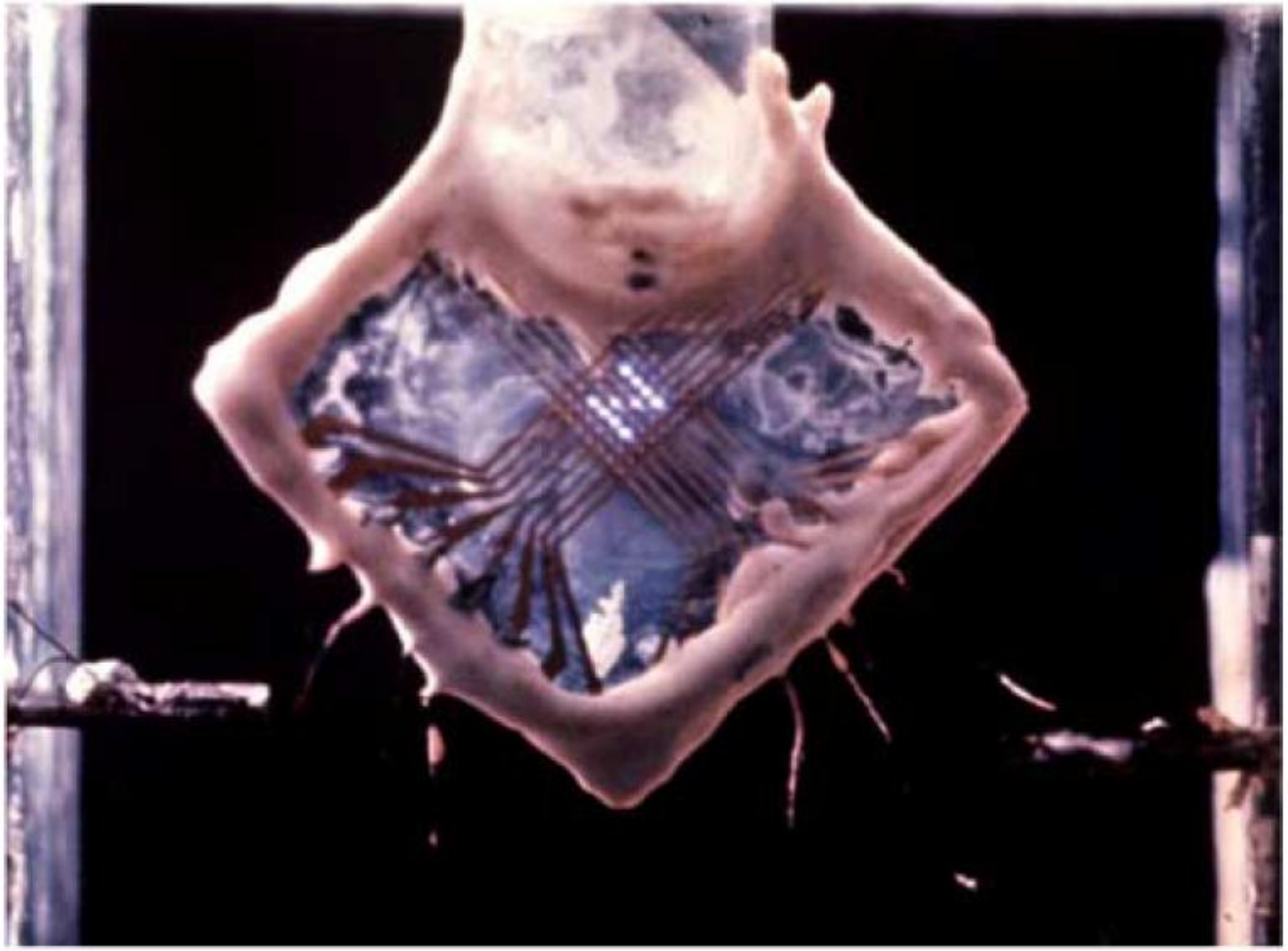

L. F. Weber, IEEE Trans. Plas. Scien., *34*, 268, 2006

Early 4x4 pixel panel has achieved matrix addressability for the first time

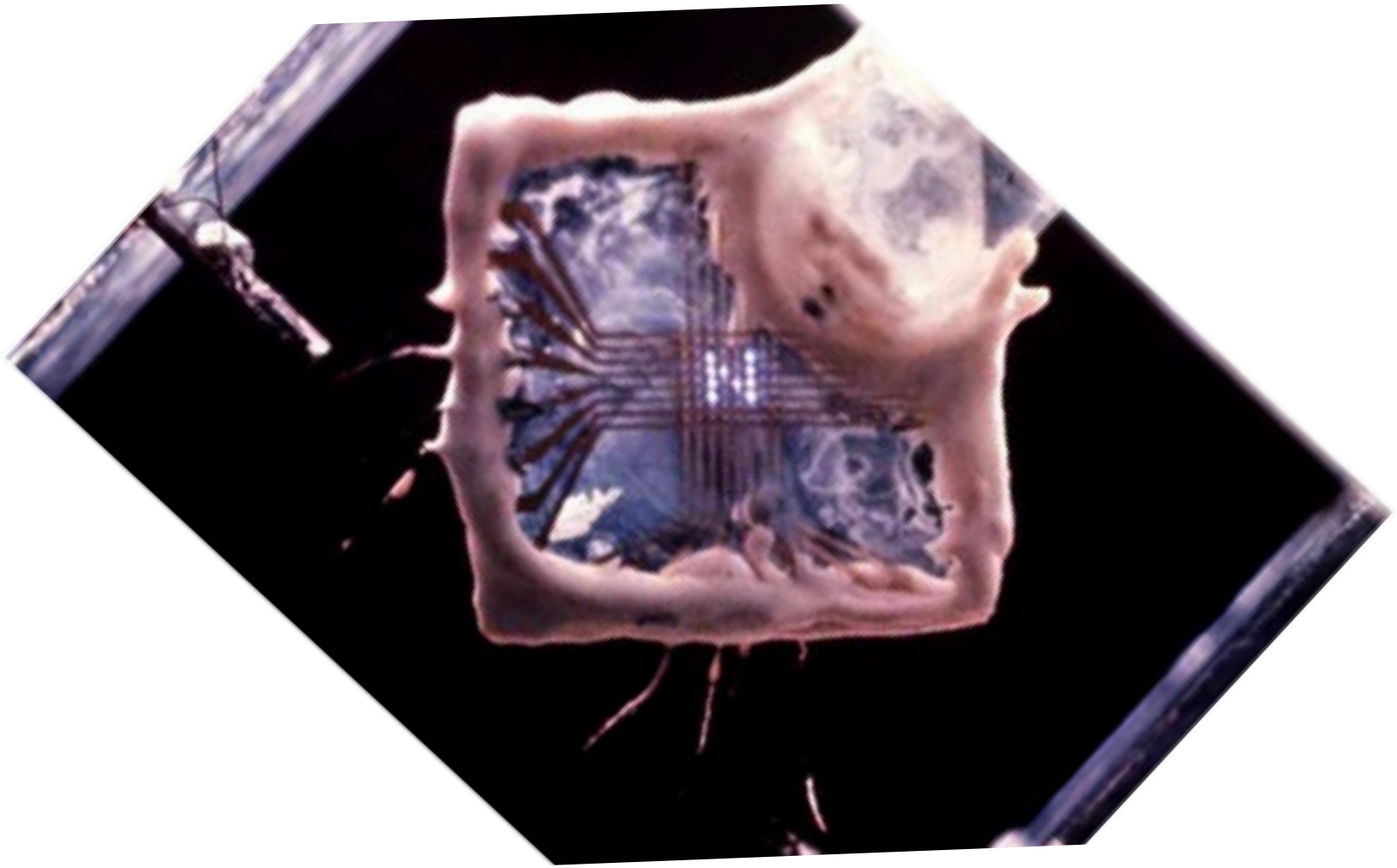

L. F. Weber, IEEE Trans. Plas. Scien., *34*, 268, 2006

A 16x16 pixel PD, developed in 1967, needed to be addressed manually

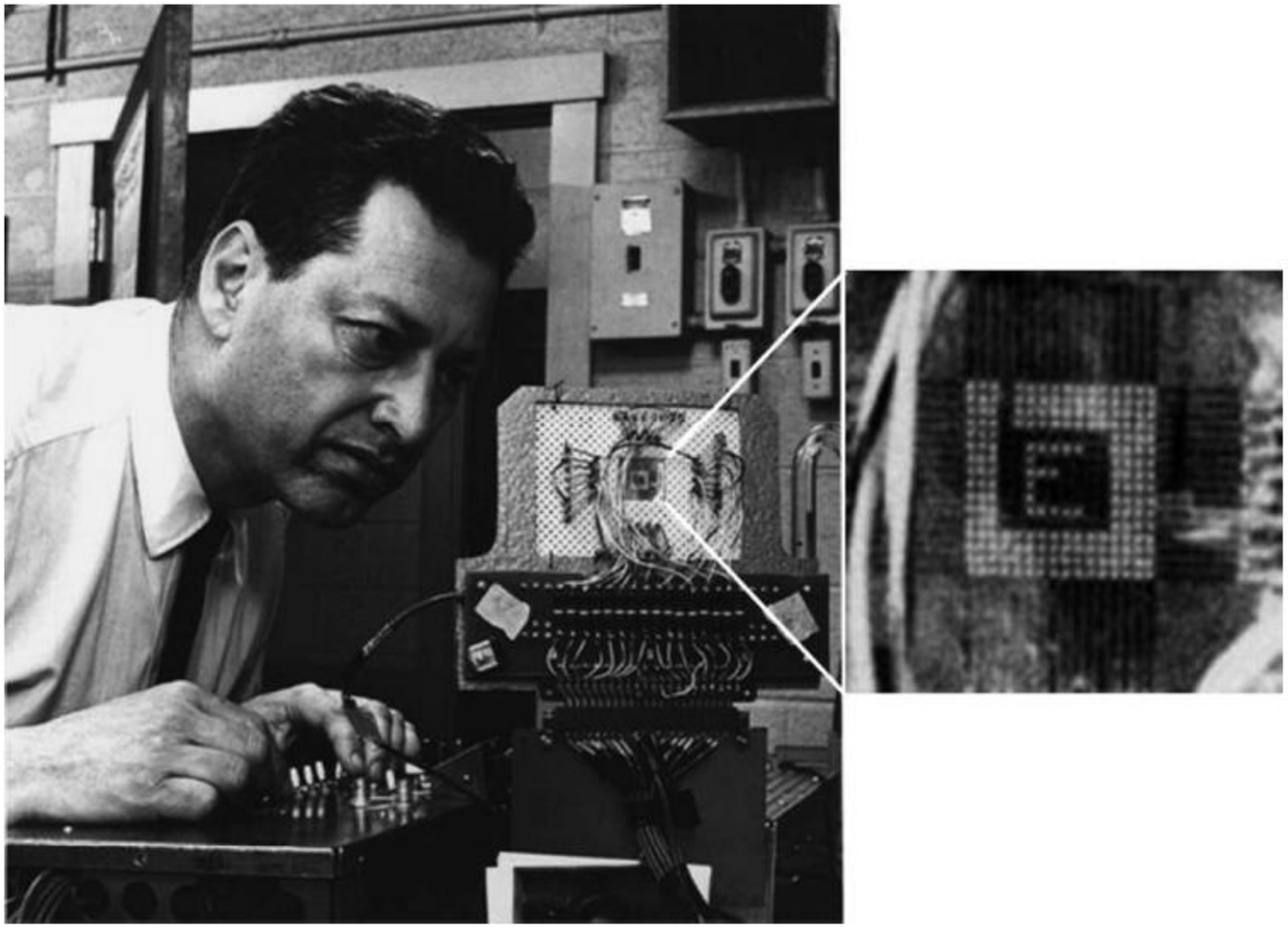

L. F. Weber, IEEE Trans. Plas. Scien., *34*, 268, 2006

First color PD was three cell prototype with red and green color phosphors excited by a xenon gas discharge

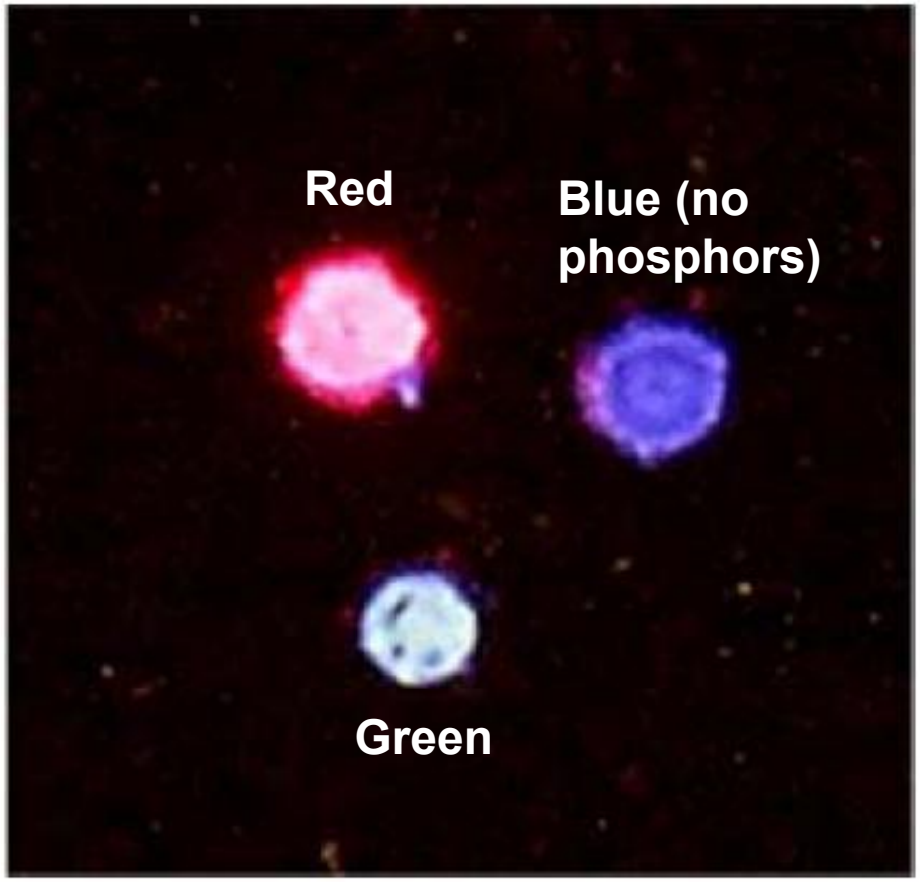

L. F. Weber, IEEE Trans. Plas. Scien., *34*, 268, 2006

Open-cell structure developed in 1968

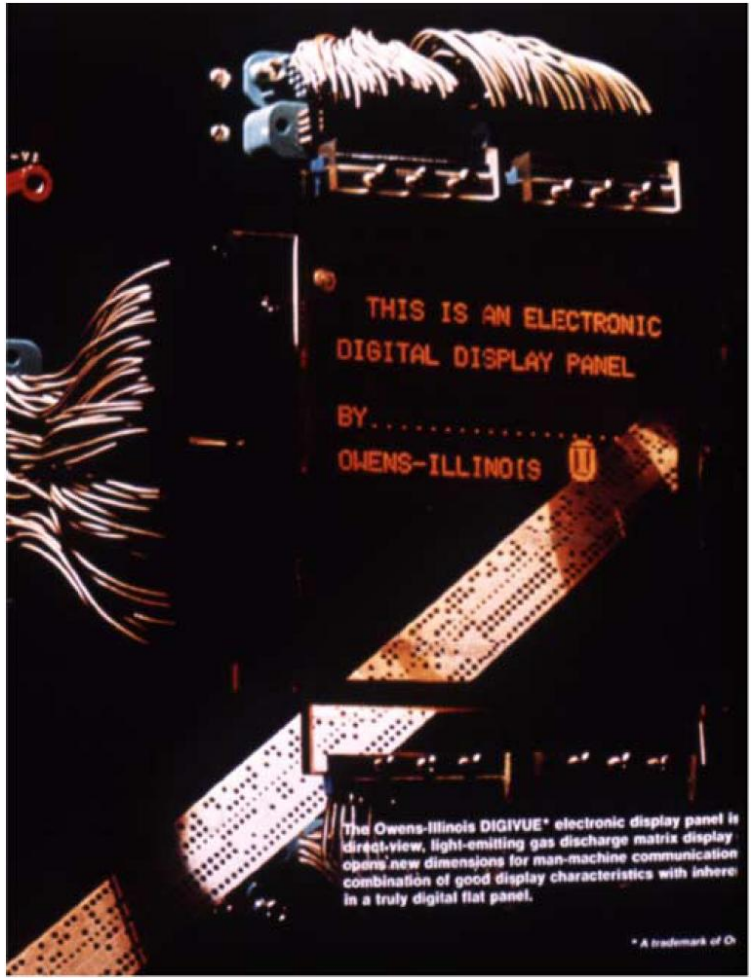

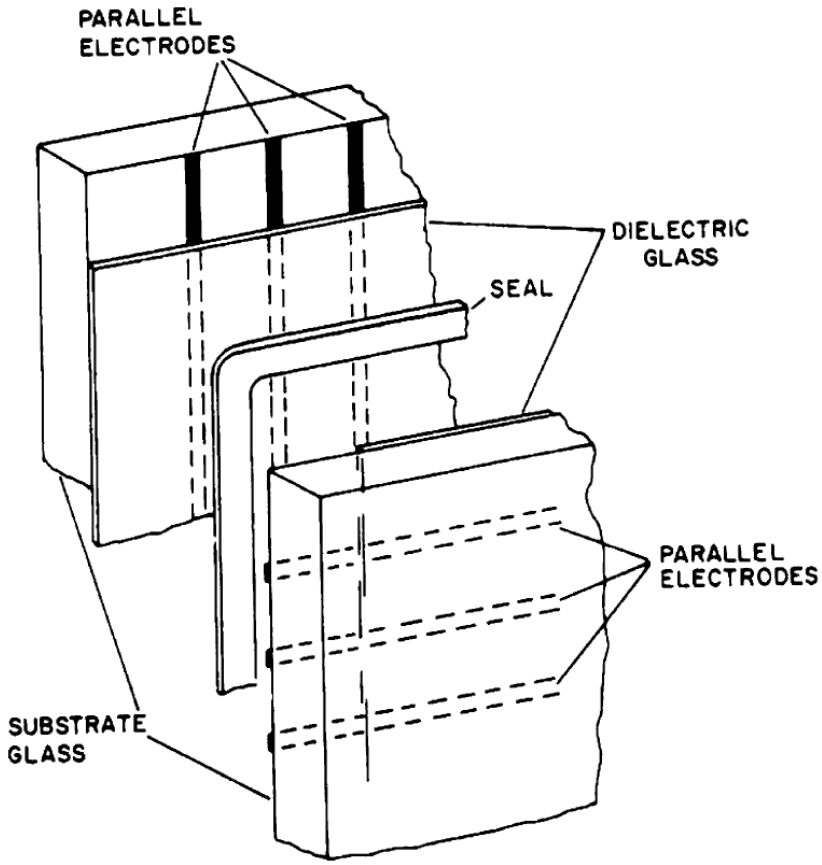

- **It could be baked under vacuum at 350 ^{o}C to drive out contaminants.**

L. F. Weber, IEEE Trans. Plas. Scien., *34*, 268, 2006

More progress

1968, University of Illinois
16x16 pixels

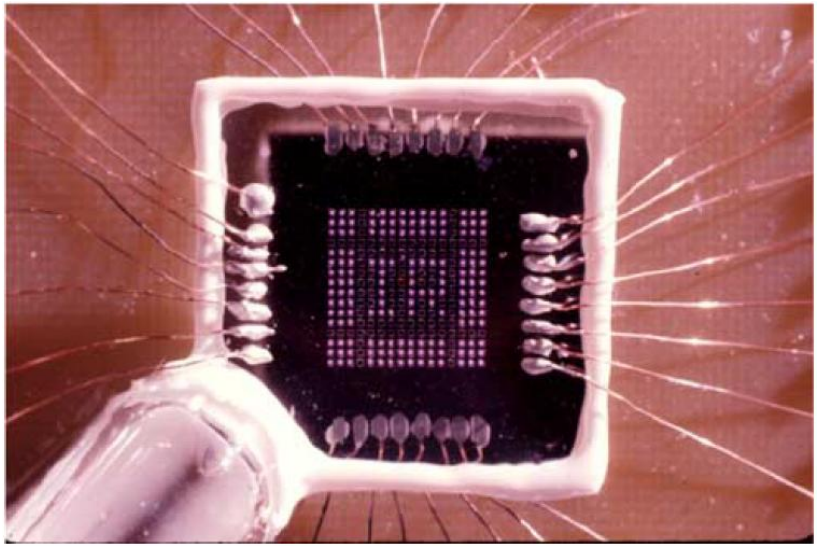

1971, Owens-Illinois
512x512 pixels

L. F. Weber, IEEE Trans. Plas. Scien., *34*, 268, 2006

Color PDPs had short display lifetime due to the degradation of color phosphors caused by ion sputtering

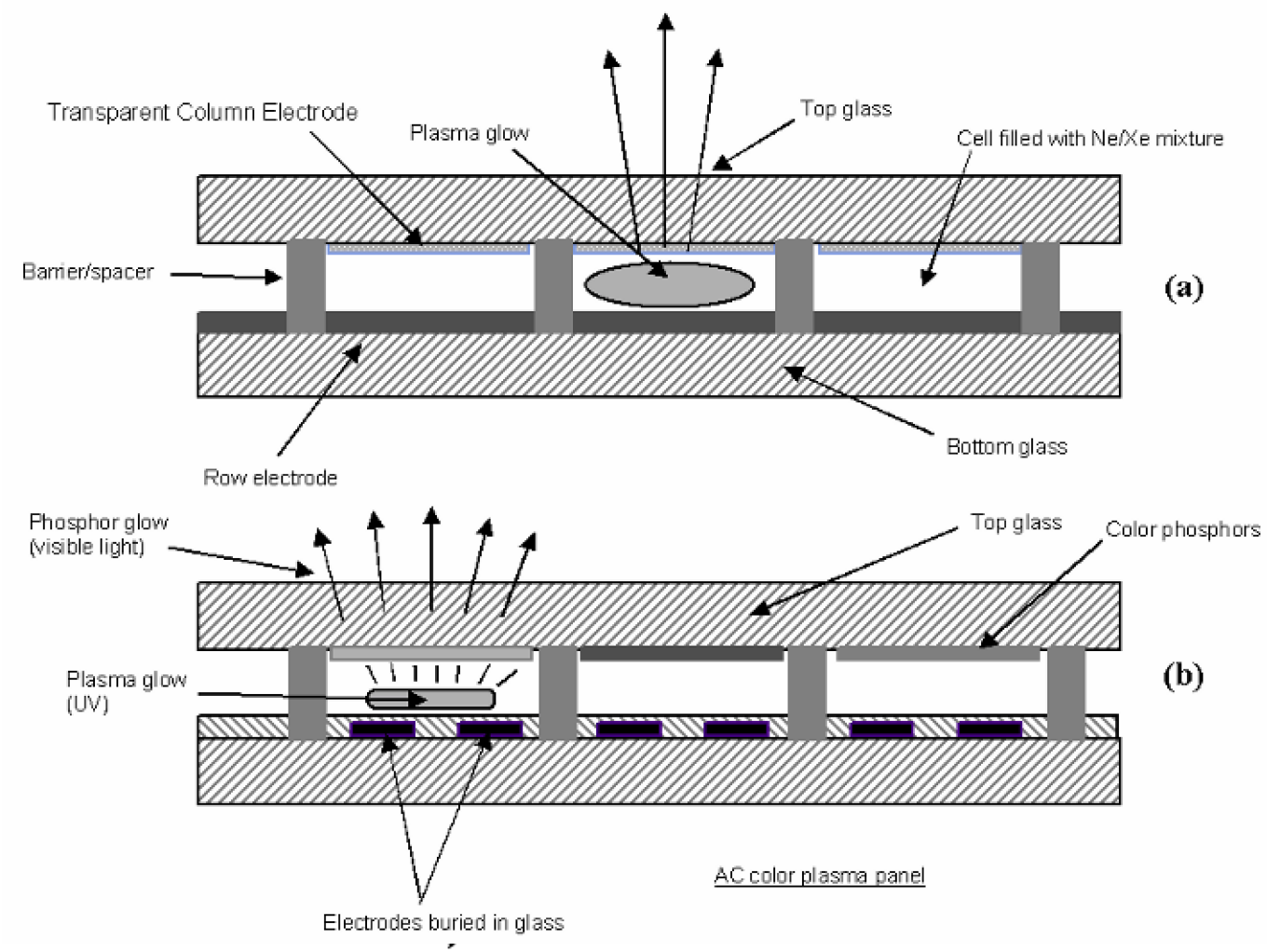

http://what-when-how.com/display-interfaces/display-technologies-and-applications-display-interfaces-part-3/

Design of PDP

A lower breakdown voltages can be obtained with very small amounts of added gas

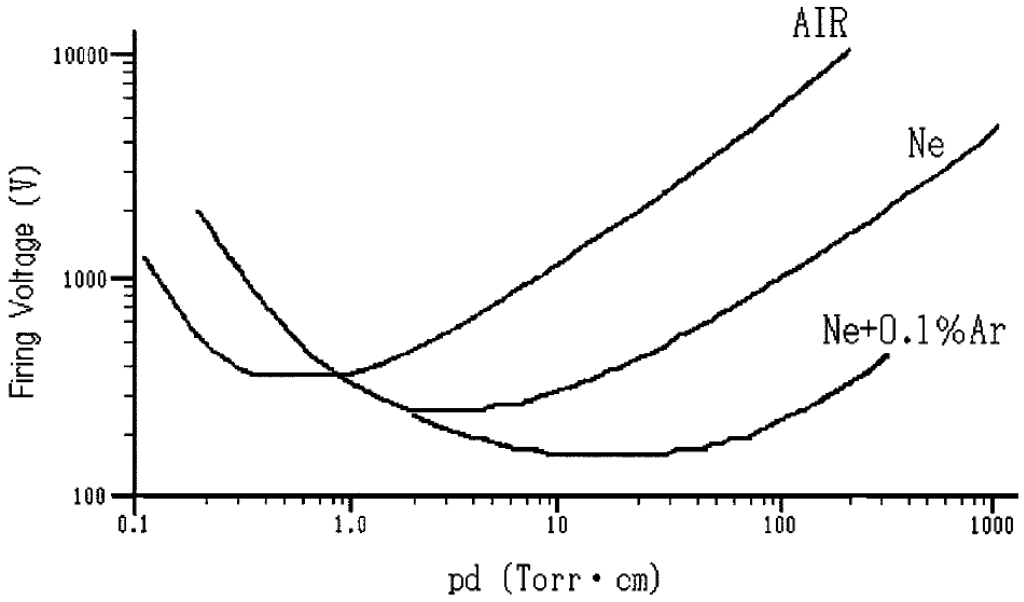

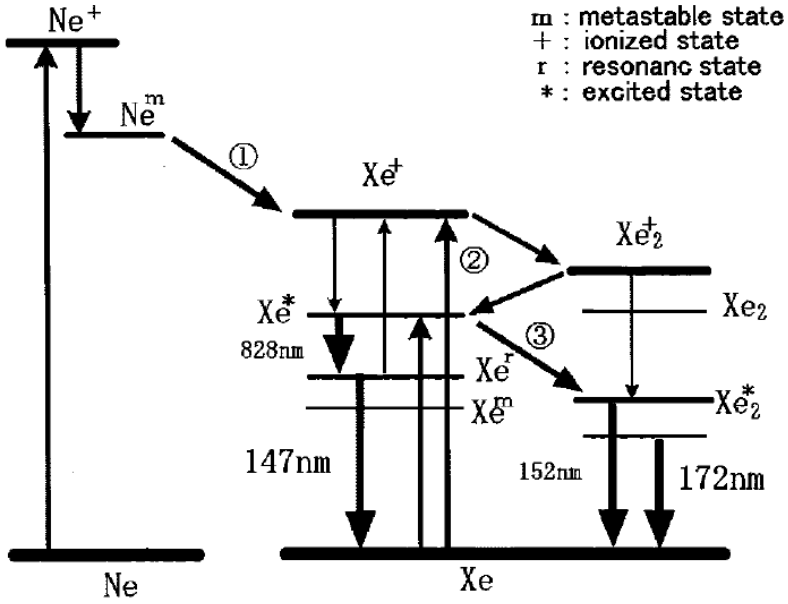

AT&T three-electrode patent

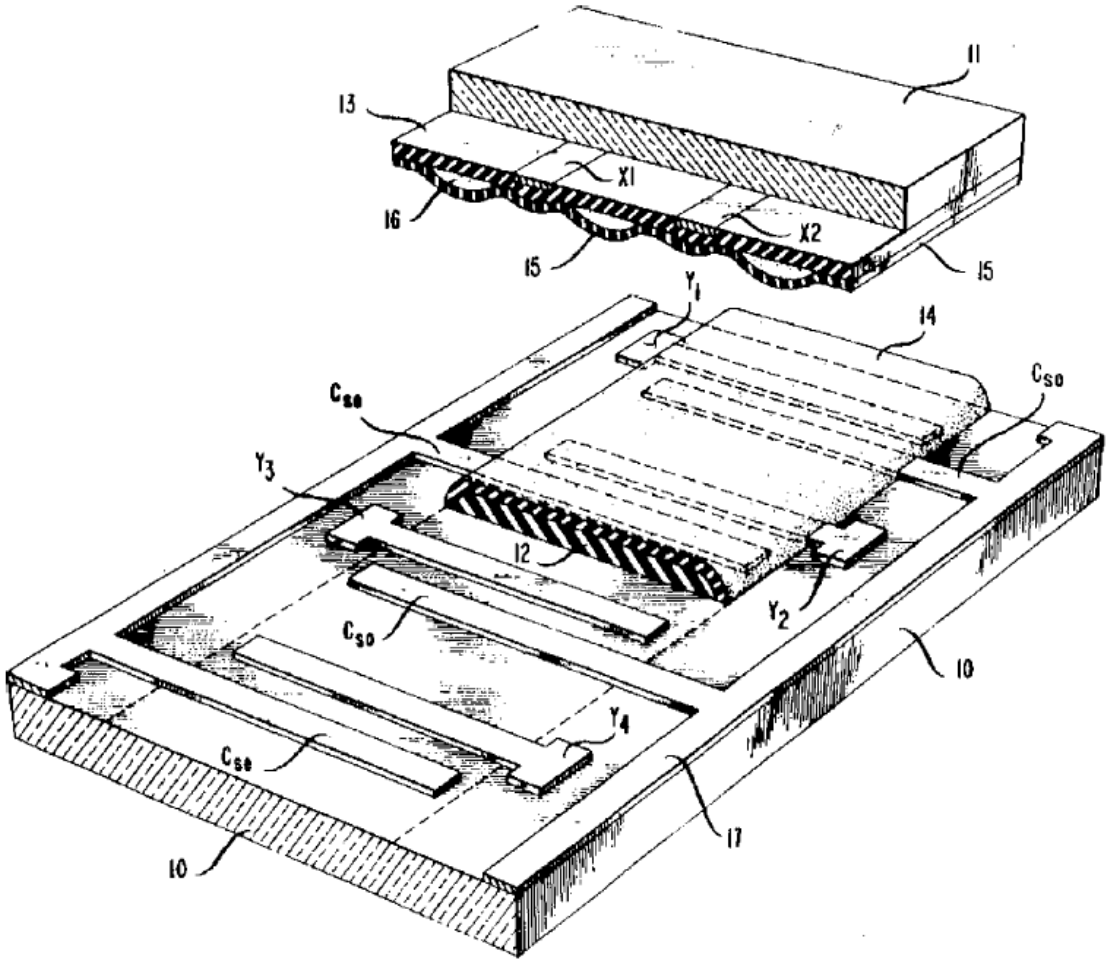

L. F. Weber, IEEE Trans. Plas. Scien., *34*, 268, 2006

Reflective phosphor geometry is used in most of today's plasma TVs

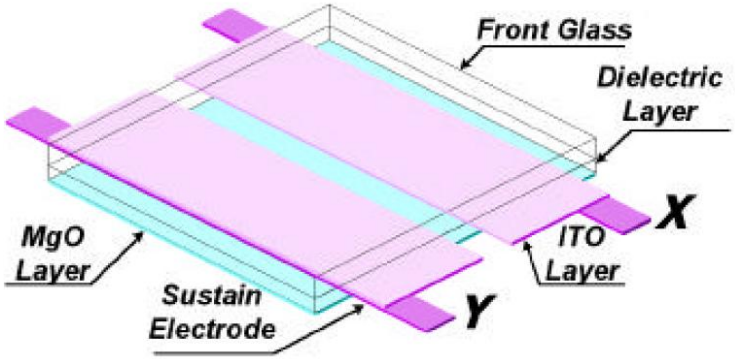

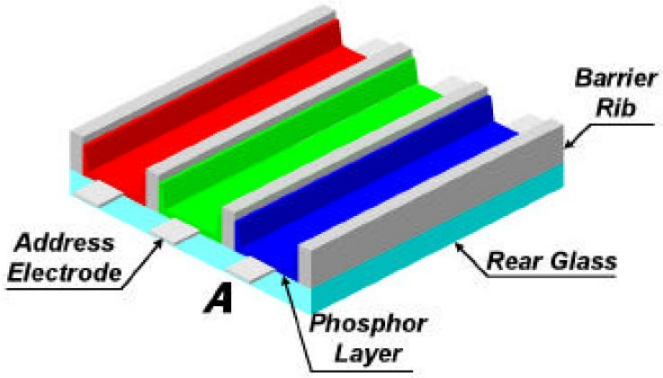

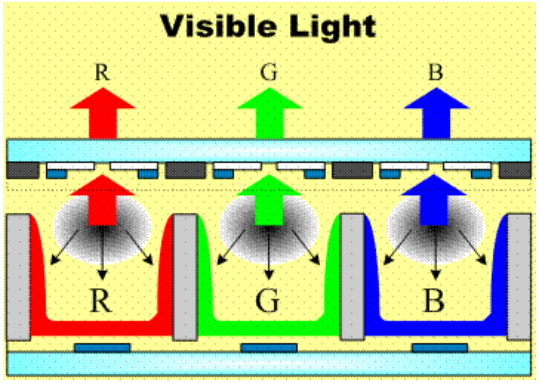

Spectrum of the different phosphors

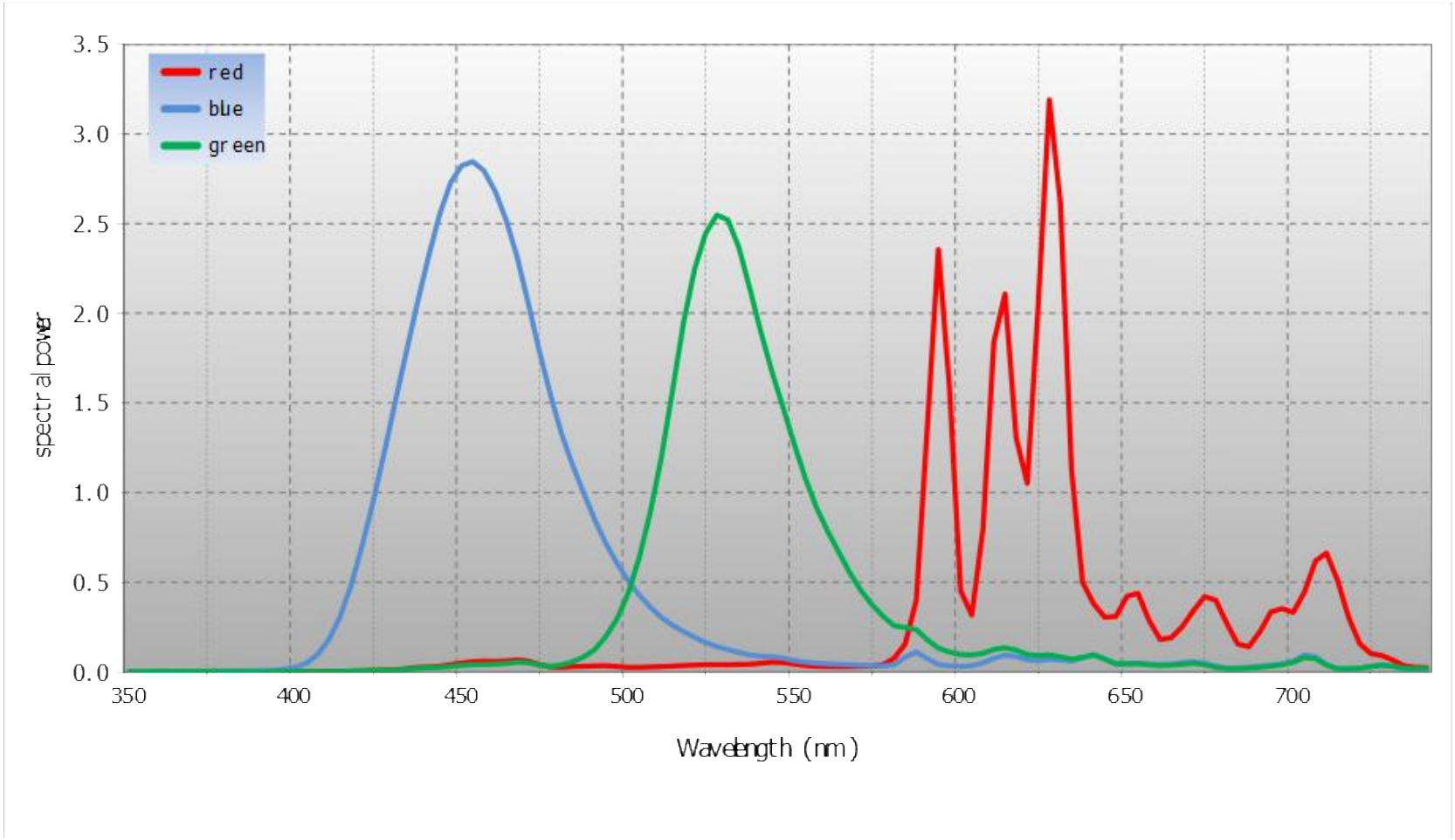

The foundation of AC discharge

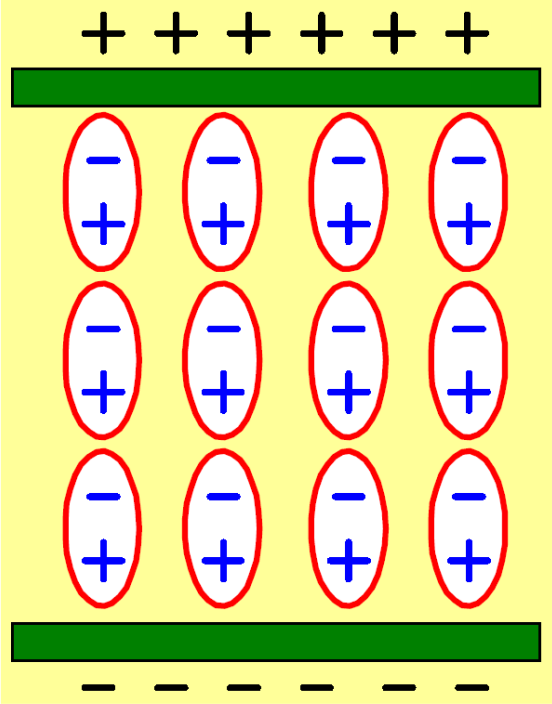

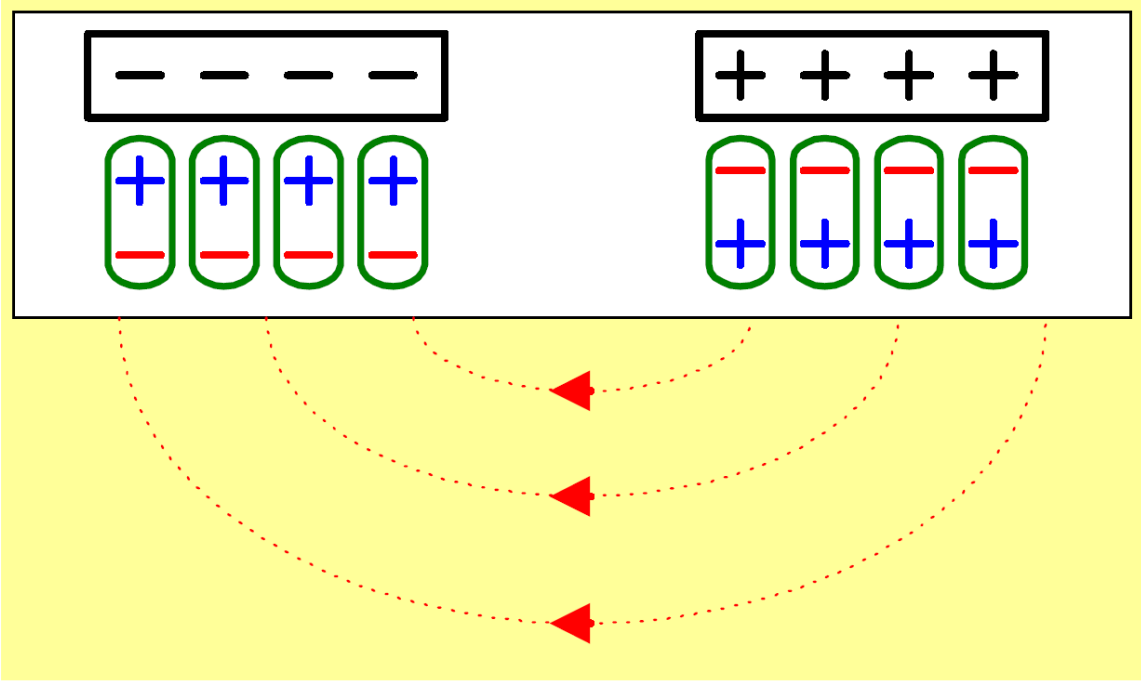

The plasma can be sustained using ac discharged

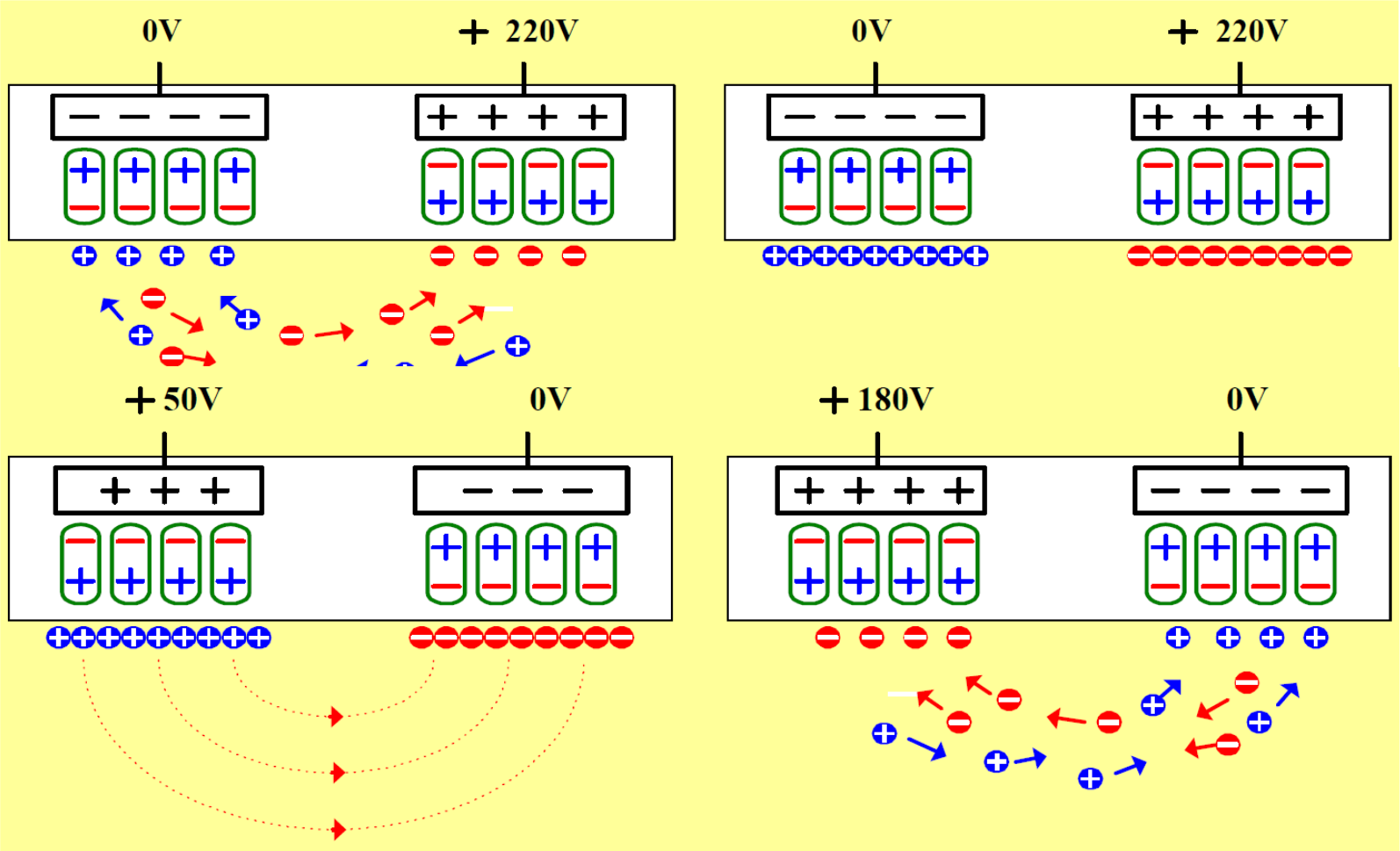

- **Wall discharge reduced the required discharge voltage**

Wall discharge reduced the required discharge voltage

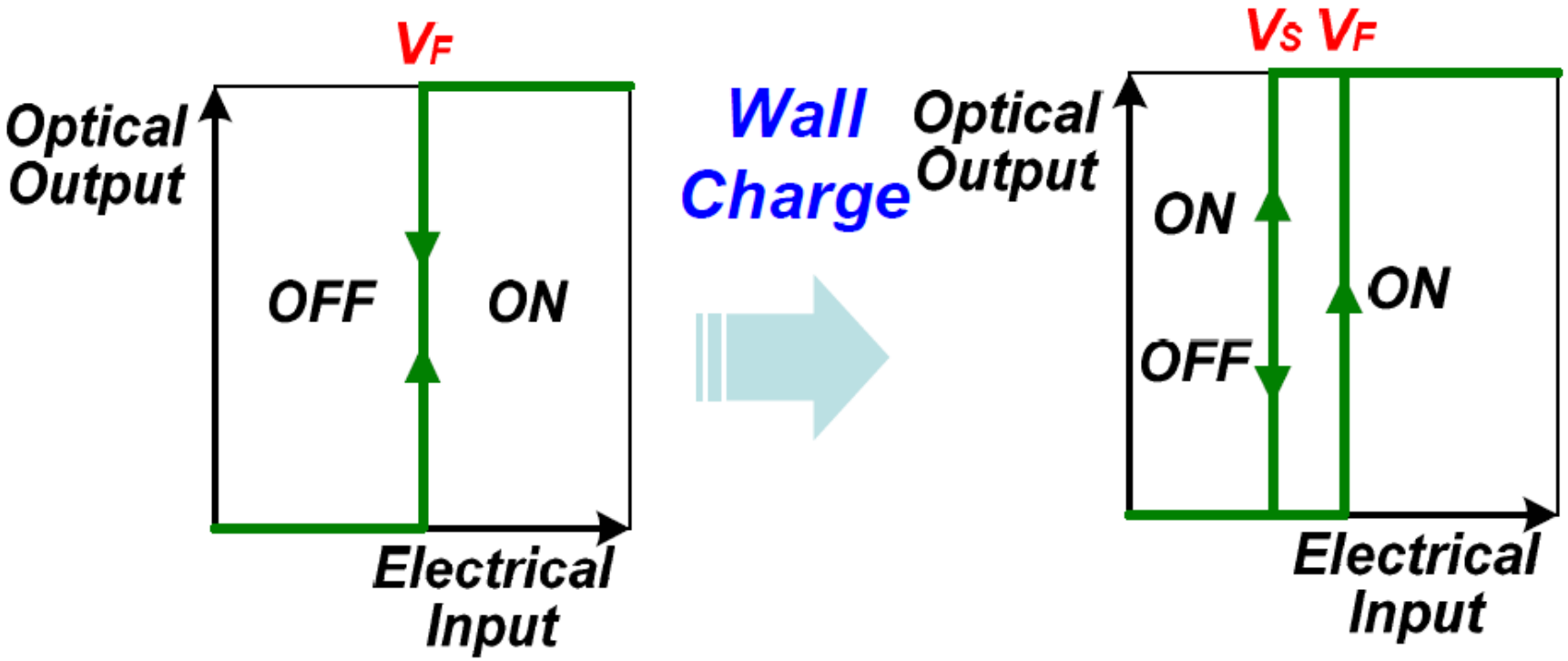

ON/OFF State Selection

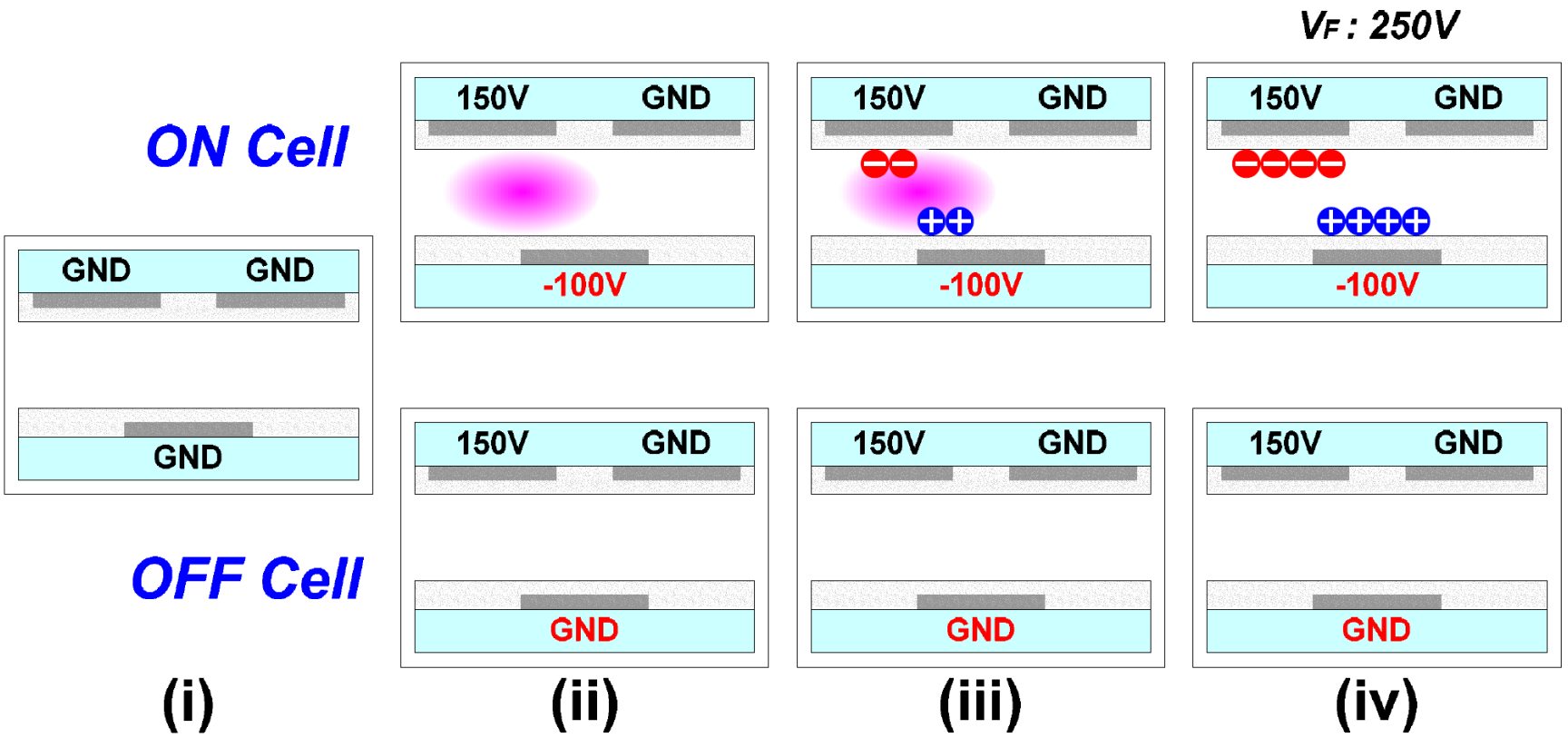

Sustain discharge

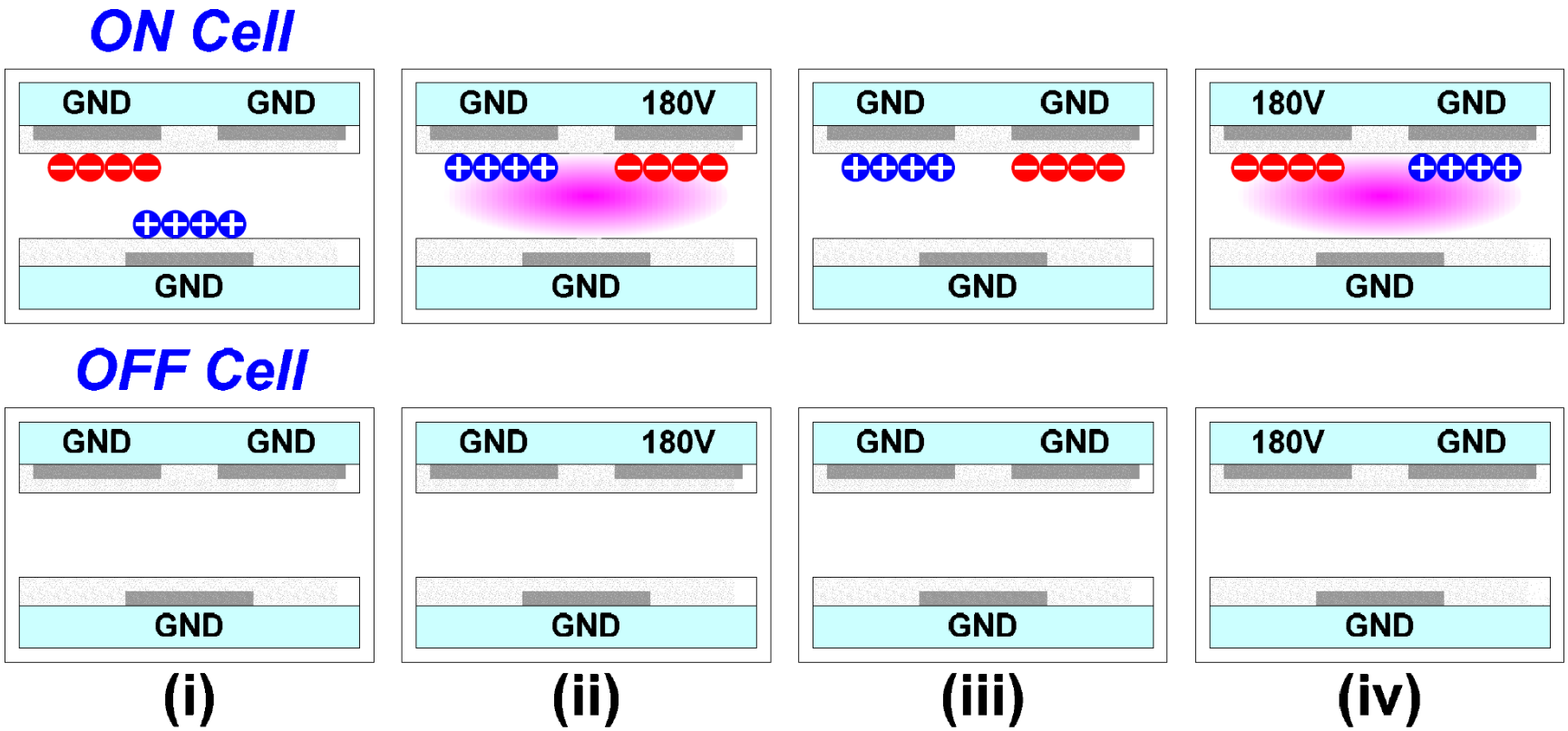

Address and sustain electrodes are connected to different drivers

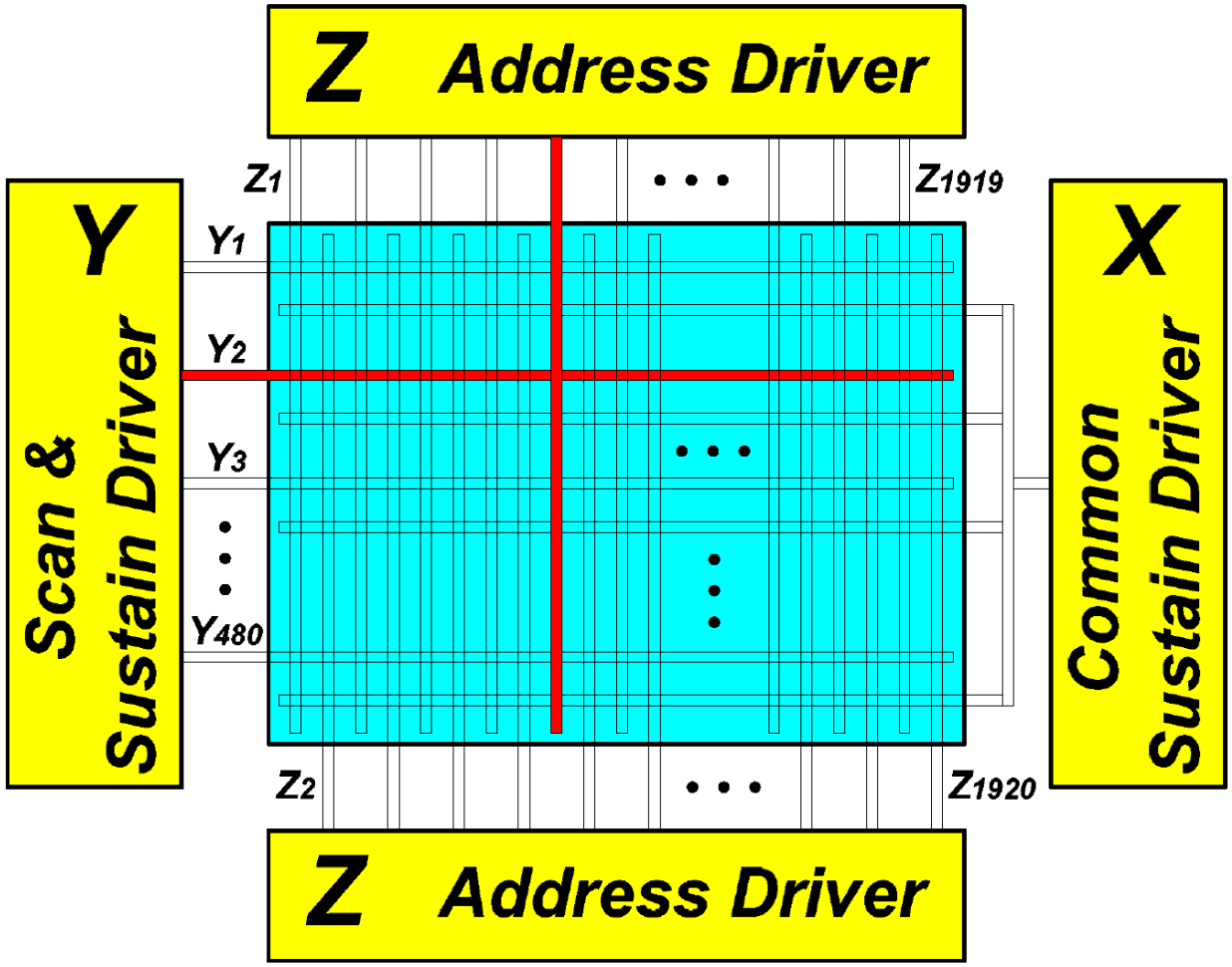

PDP pixel can only be either ON or OFF

- Cathode Ray Tube :

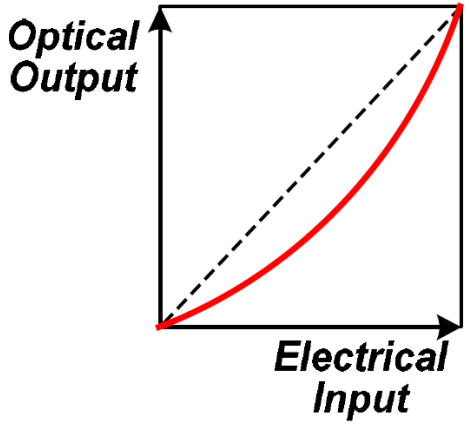

- Plasma Display Panel :

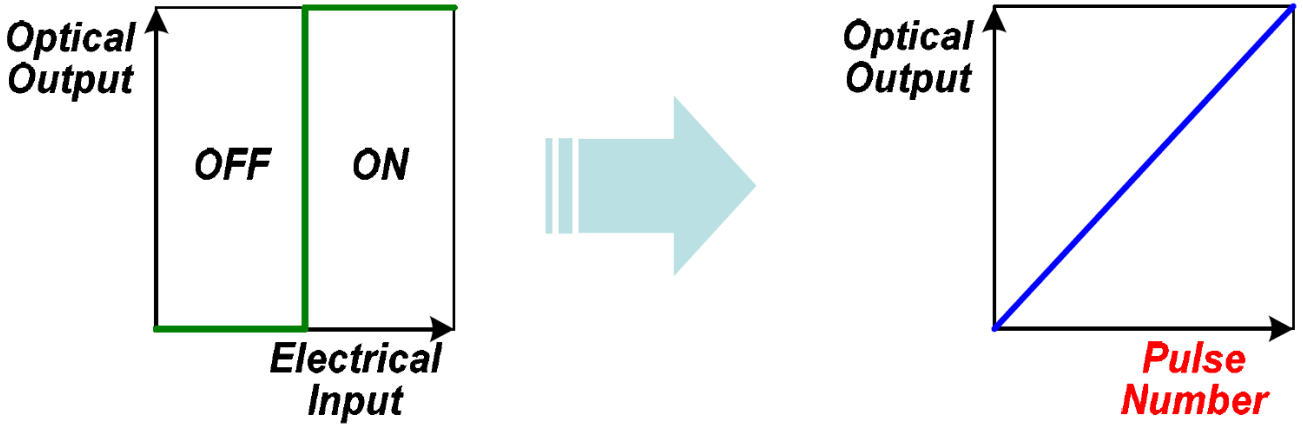

PDP luminance is controlled by using number of light pulses

- CRT : Control the Luminance using Electron Beam Intensity

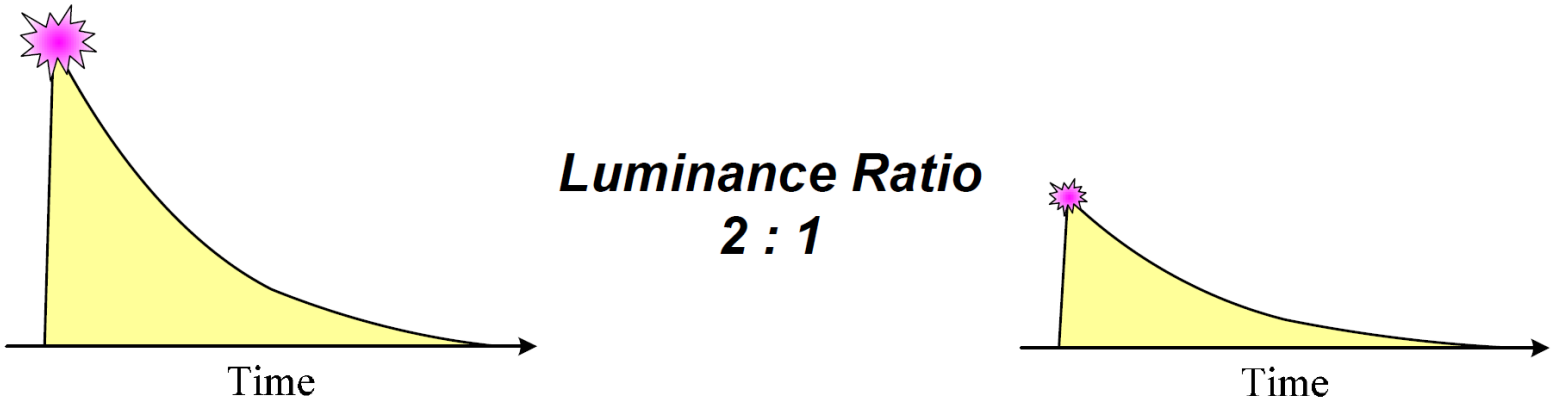

- PDP : Control the Luminance using Number of Light Pulses

A single field is divided into 8 subfield

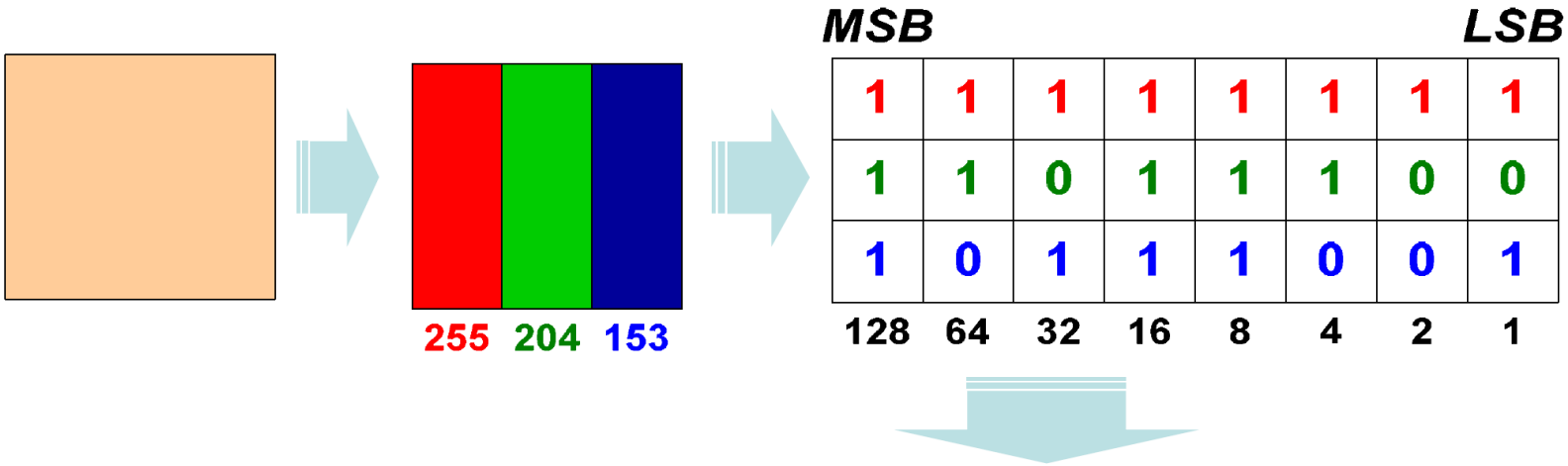

Composition of each subfield

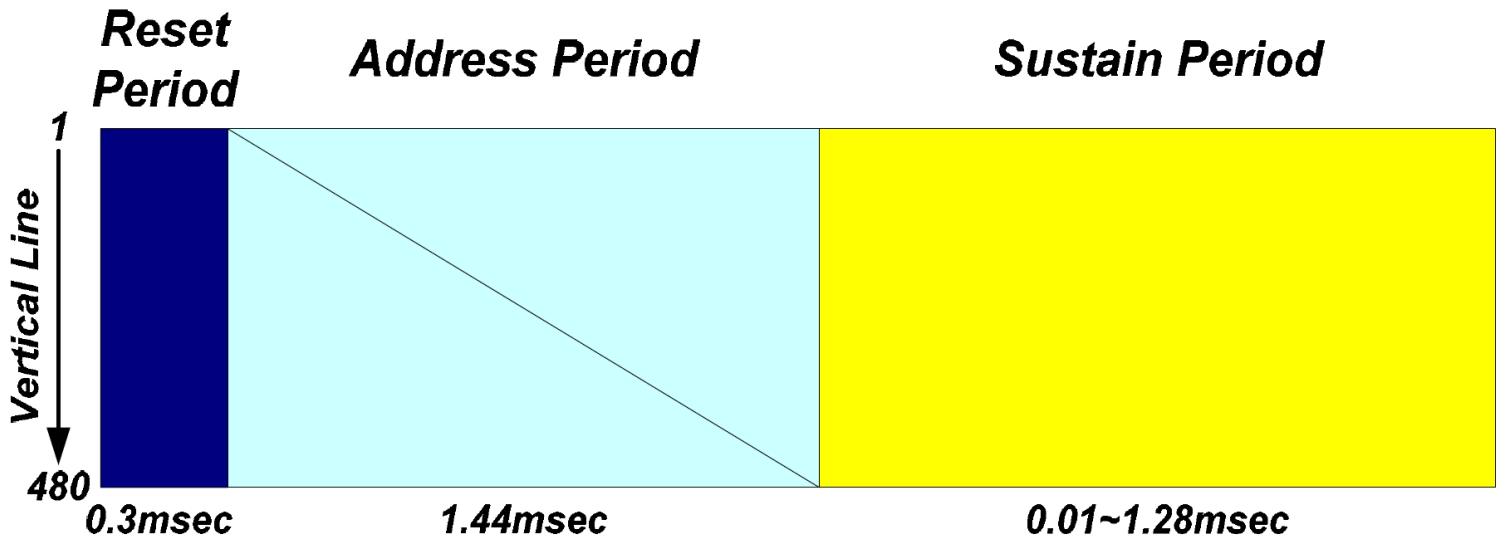

Spec : VGA (640*480)
8 Subfield
0.03msec Address Pulse
100KHz Sustain Freq.

8 subfield in one TV-Field (ADS)

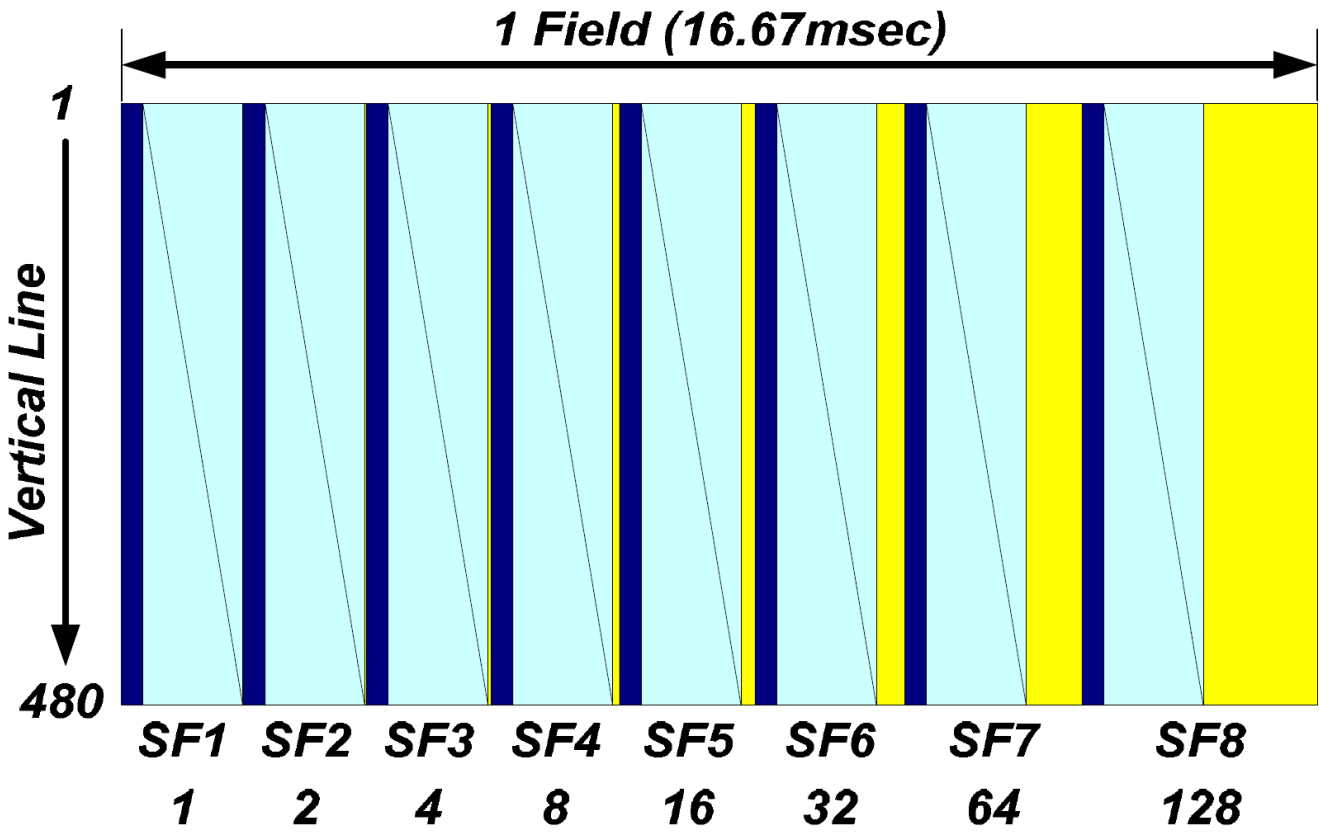

PDP uses line-by-line scanning

- Cathode Ray Tube : Cell-by-Cell Scanning

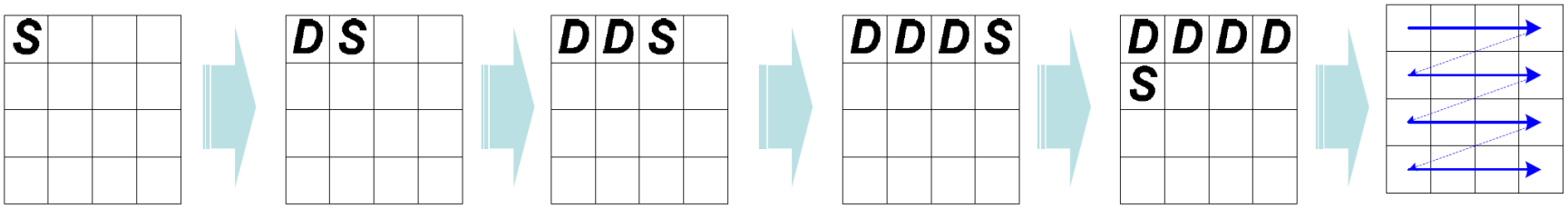

- PDP : Line-by-Line Scanning

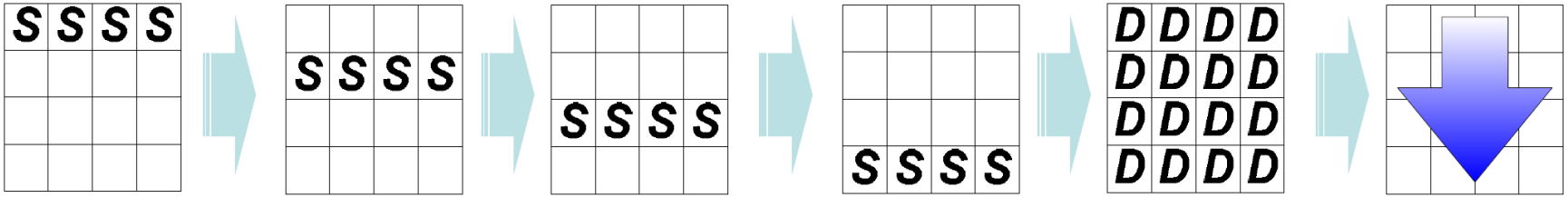

Slides from Prof. Heung-Sik Tae, School of Electronic and Electrical Engineering, Kyungpook National University

Video signal processing

- Analog Video Signal ⇨ Digital Pulse Signal

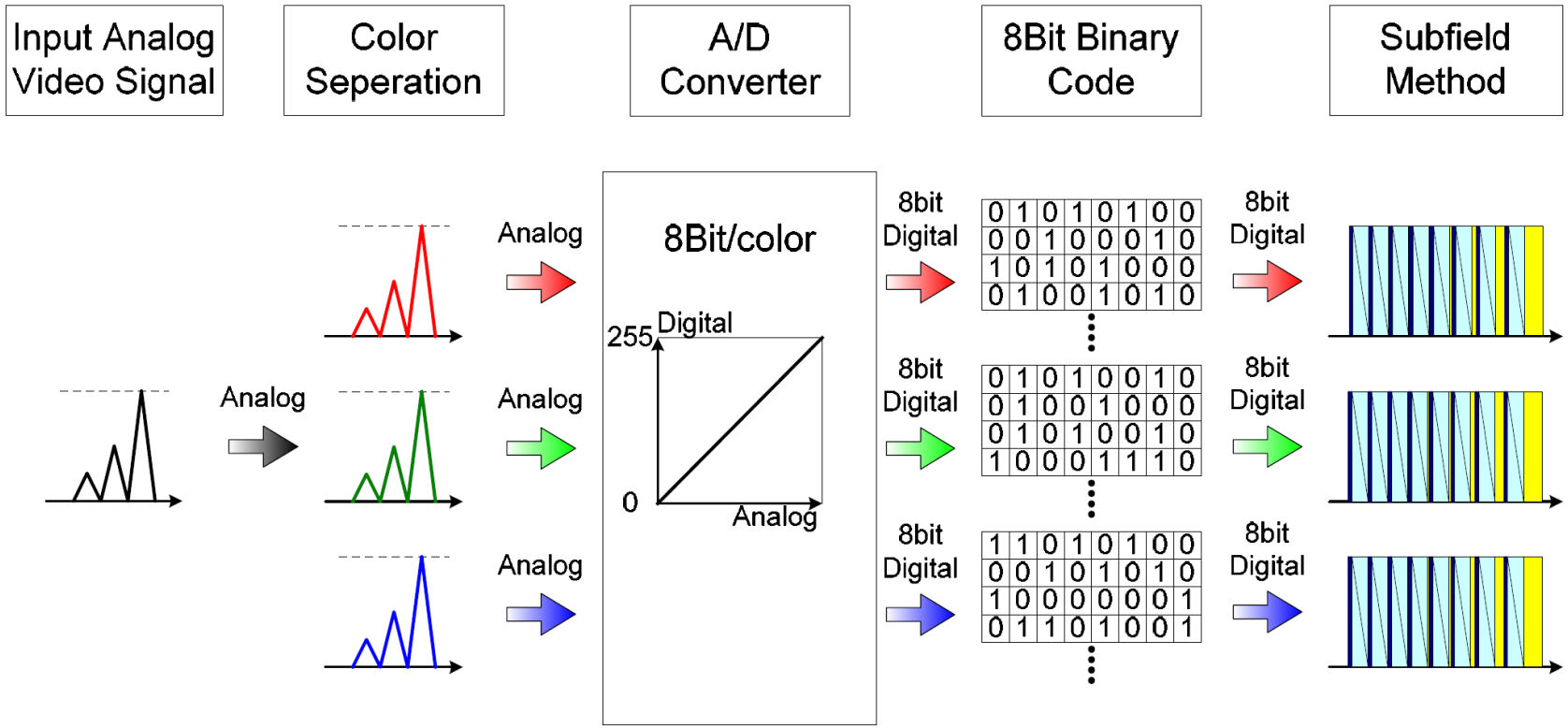

Addressing period

Slides from Prof. Heung-Sik Tae, School of Electronic and Electrical Engineering, Kyungpook National University

Displaying period

Original Image

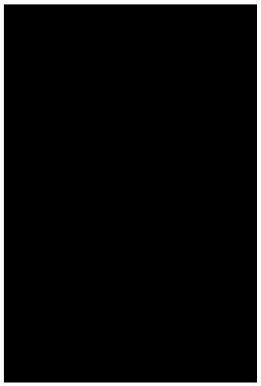

SF1

SF2

SF3

SF4

SF5

SF6

SF7

SF8

Liquid crystal are a special state of matter between liquid and crystal

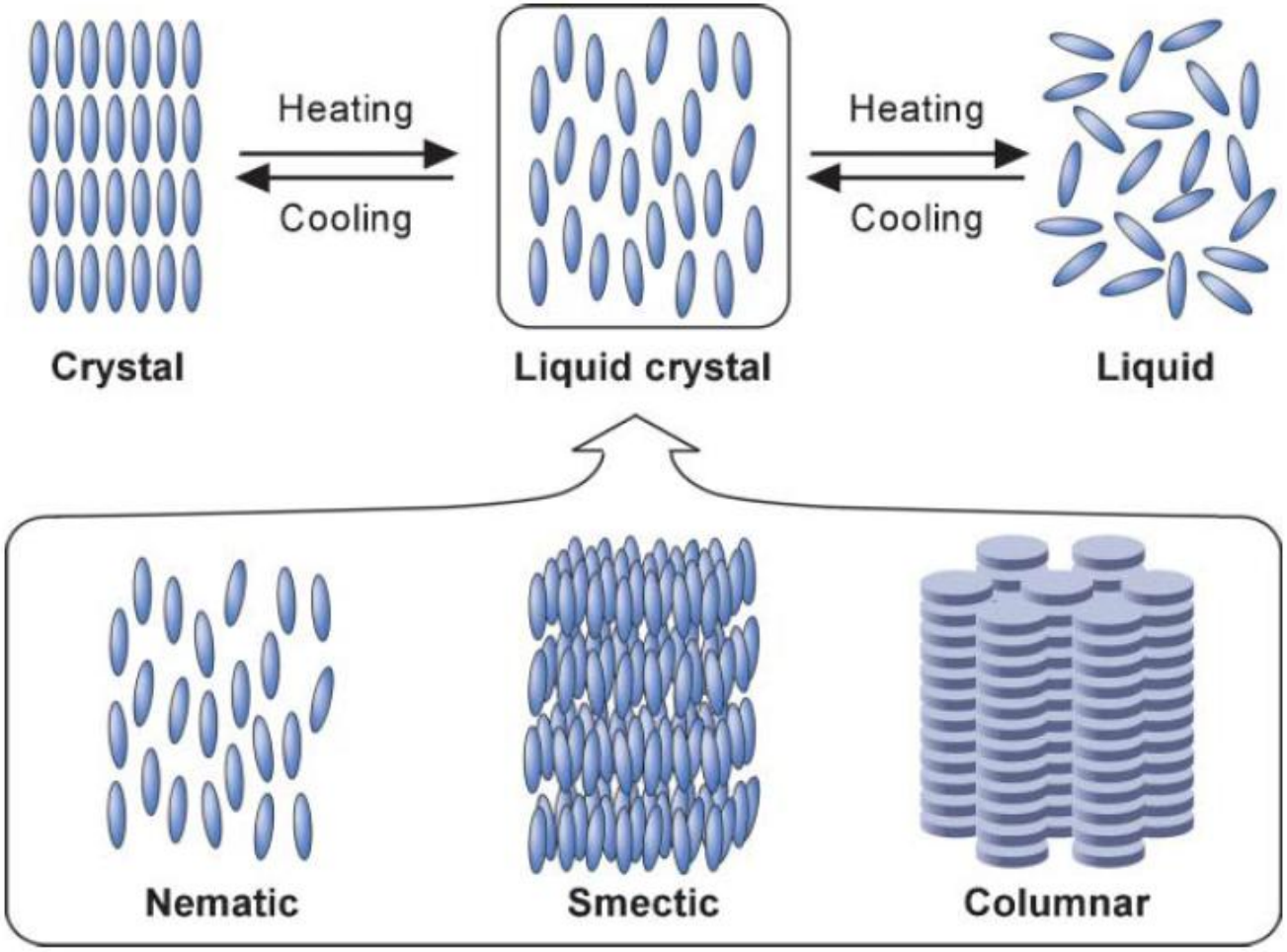

T. Kato, *et. al.*, Chem. Soc. Rev., *36*, 1845, 2007

Linear polarization of a light can be rotated by miss aligned liquid crystal

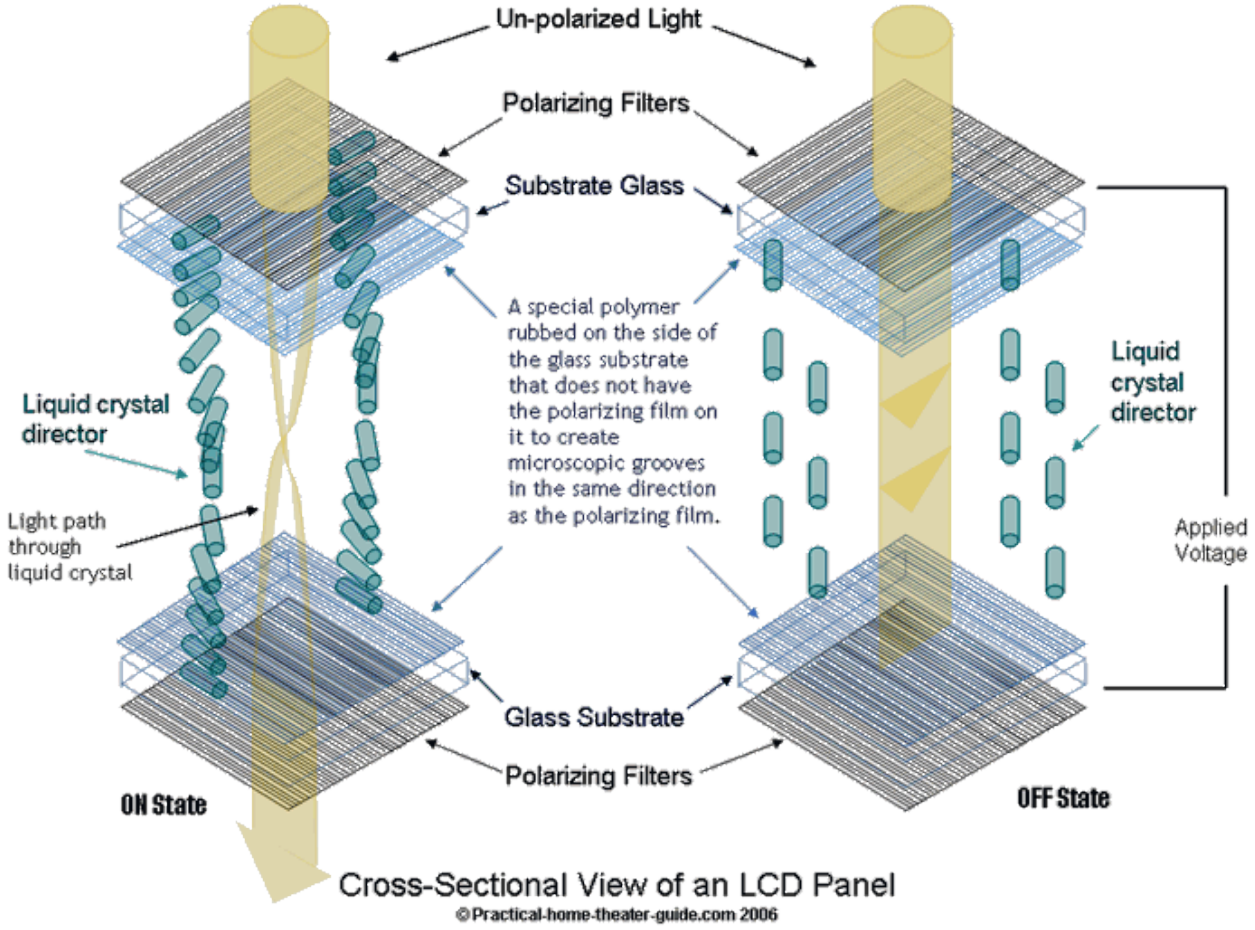

http://www.practical-home-theater-guide.com/lcd-display.html

Structure of Liquid crystal display (LCD)

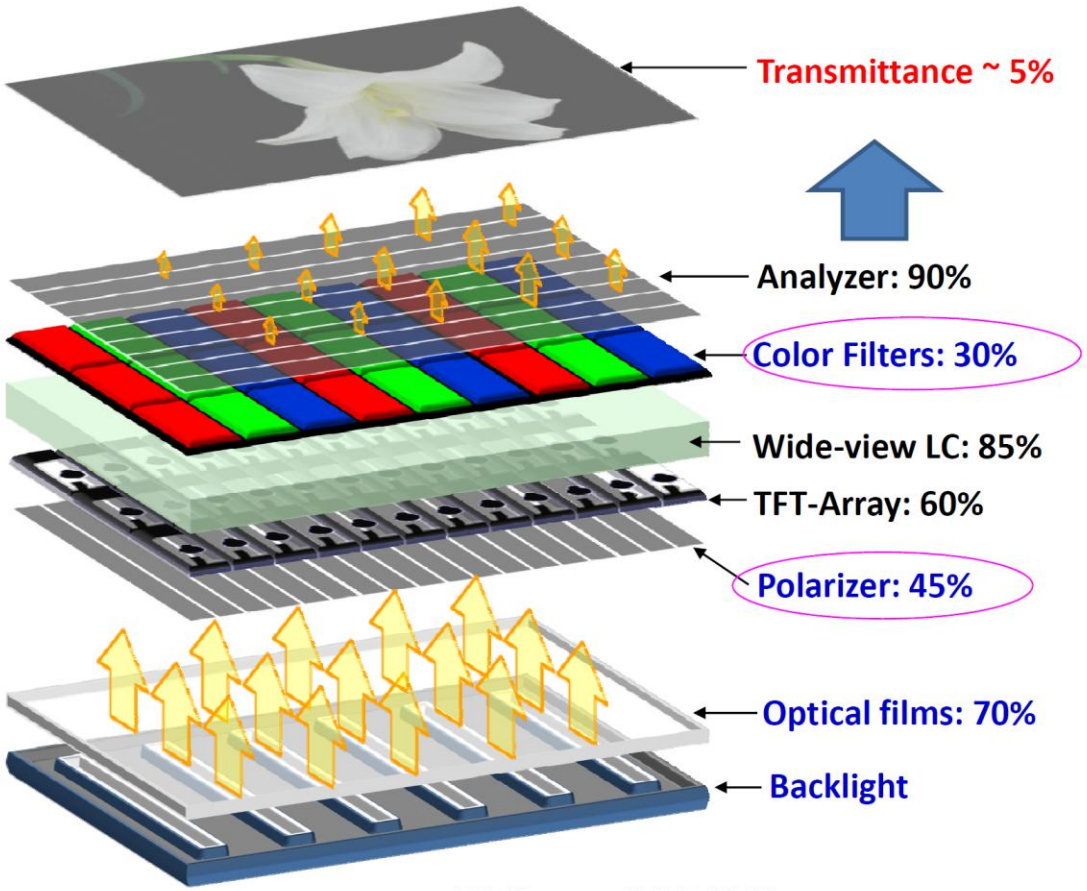

YB Huang, IDRC 2008

Notes from ST Wu, UCF

http://www6.cityu.edu.hk/cityu25/events/engineering/pdf/proftang.pdf

Optimistic projection of PDP market

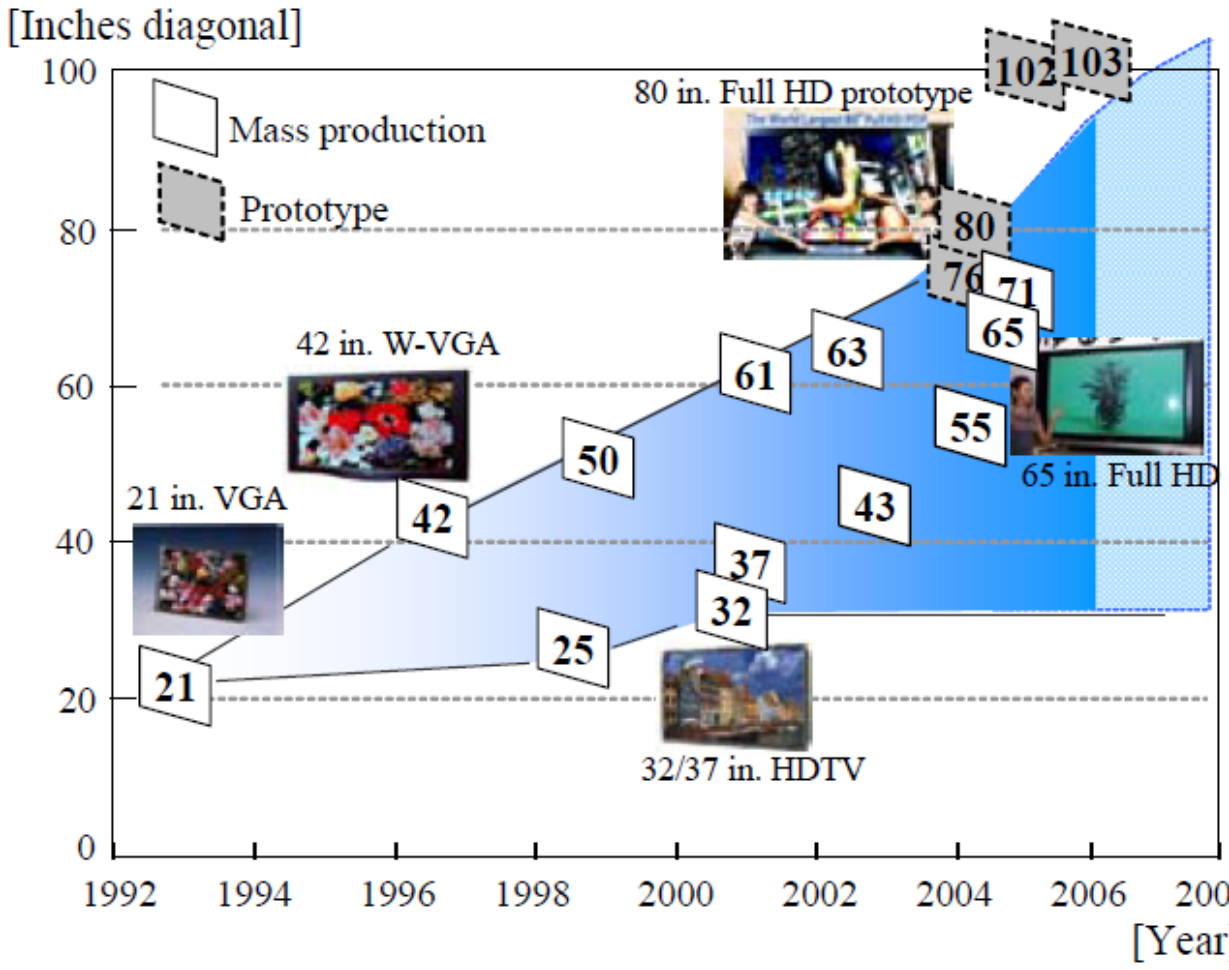

Reality

TV Shipment Growth by Technology

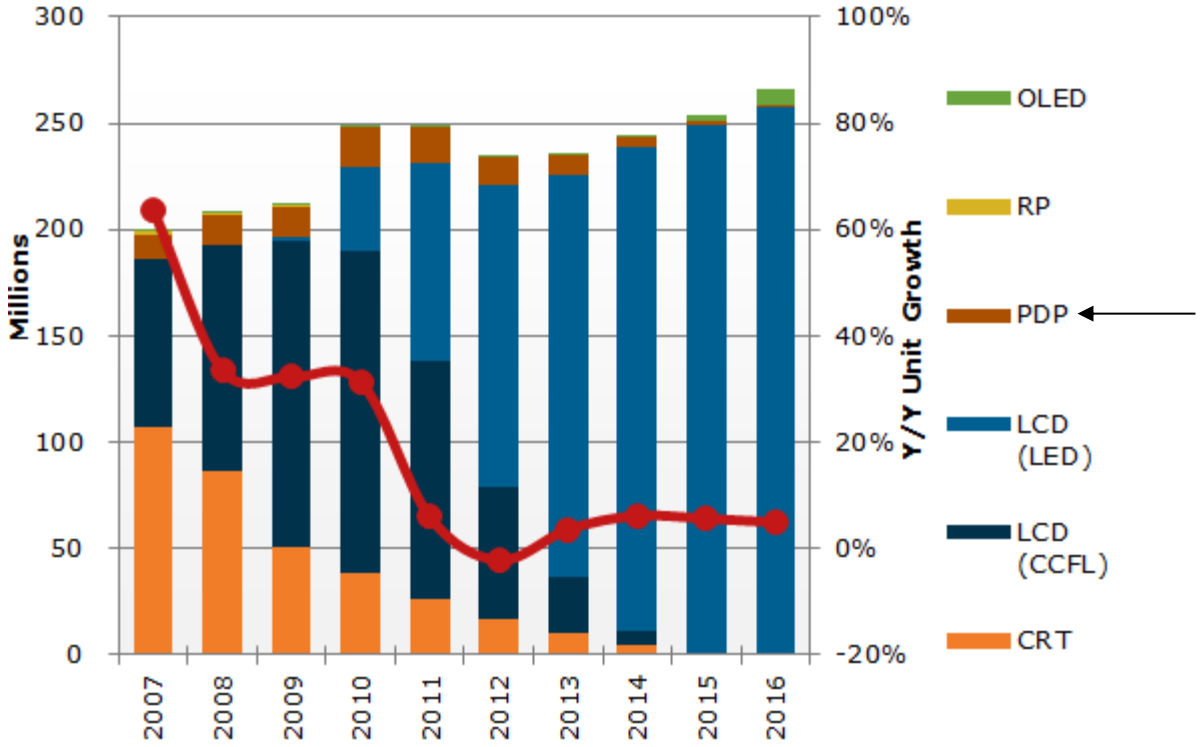

http://www.digitaltvnews.net/?p=22108

Too many reasons that PDP died!

- Bright showroom conditions put plasmas at a distinct disadvantage versus LED-lit LCDs
- Aesthetics may have played a role in hastening plasma's demise
- UHD/4K caught on quickly
- Screen-size limitations also played a part in plasmas plight
- You can't bend a plasma
- Plasmas were harder to deal with than LCDs
- While OLED is still in the early stages of development, there's no question it offers greater potential than plasma
- Energy efficiency may have played a part in putting plasma out to pasture
- Plasma was the original flat-panel technology, People just thought of it as old technology.
- Projectors improved in quality and prices dropped

http://www.avsforum.com/forum/40-oled-technology-flat-panels-general/2080650-10-reasons-plasma-died.html

Let’s stand up and do exercise!!

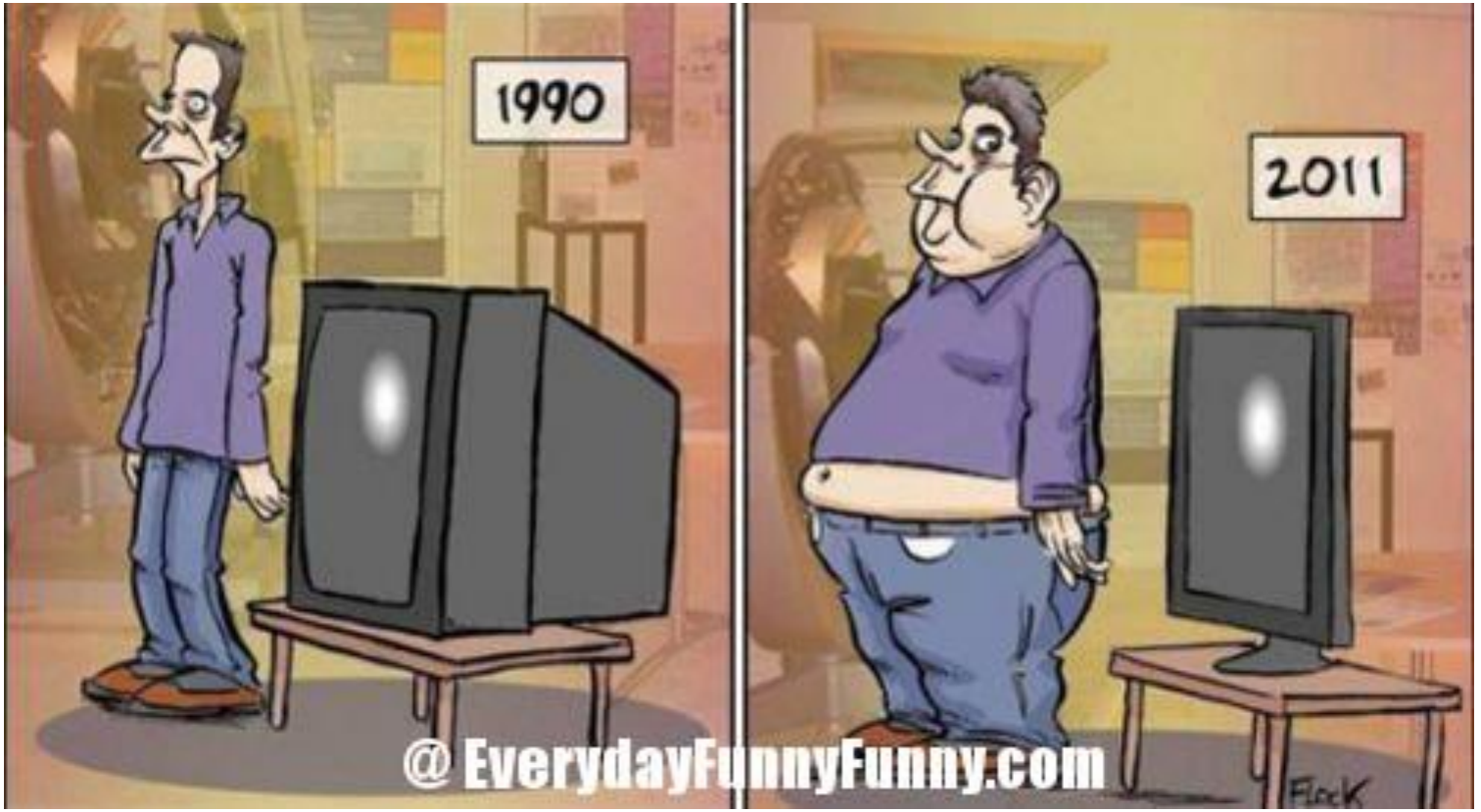

The hydrogen bomb

The “iron group” of isotopes are the most tightly bound

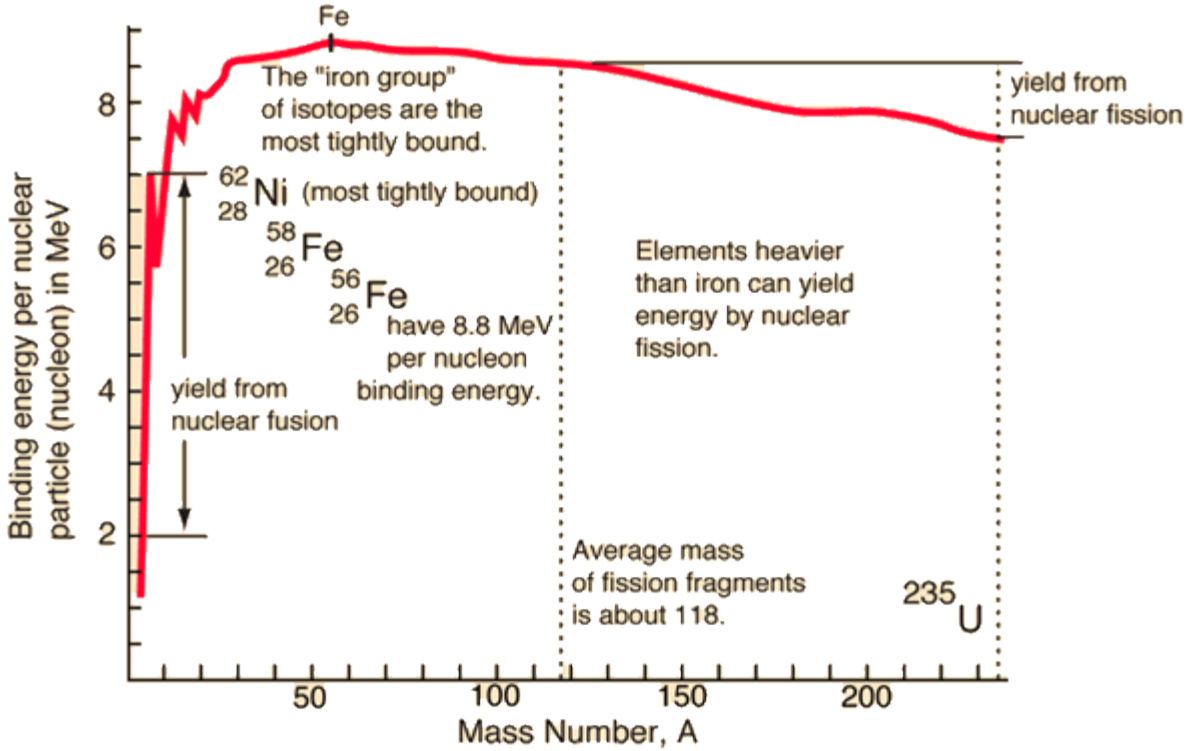

http://hyperphysics.phy-astr.gsu.edu/hbase/nucene/nucbin.html

Chain reaction can happen in U^{235} fission reaction

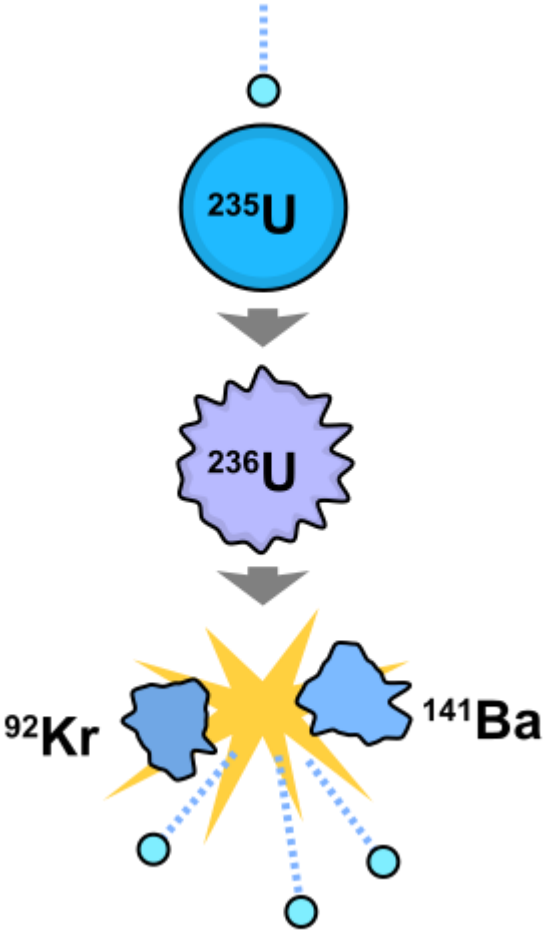

- ~ 200 million electron volts (MeV)/fission, ~million times more than chemical reactions
- Energy for bombs, or for civilian power can generate huge amounts of energy (and toxicity) in a small space with a modest amount of material
- Source of safety, security issues for nuclear power

https://en.wikipedia.org/wiki/Uranium-235
Talk given by Matthew Bunn, IGA-232: Controlling the World's Most Dangerous Weapons, Harvard Kennedy School, 2013

The neutrons are leaking out and stopping the chain reaction in a sub-critical mass

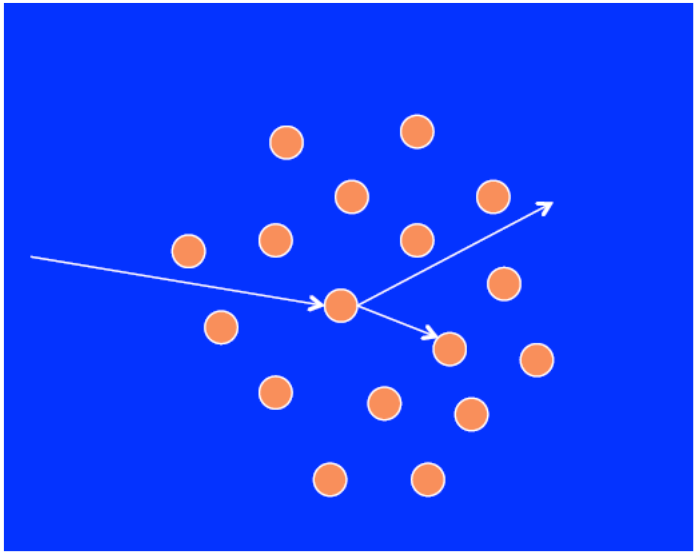

Solution 1: add more material

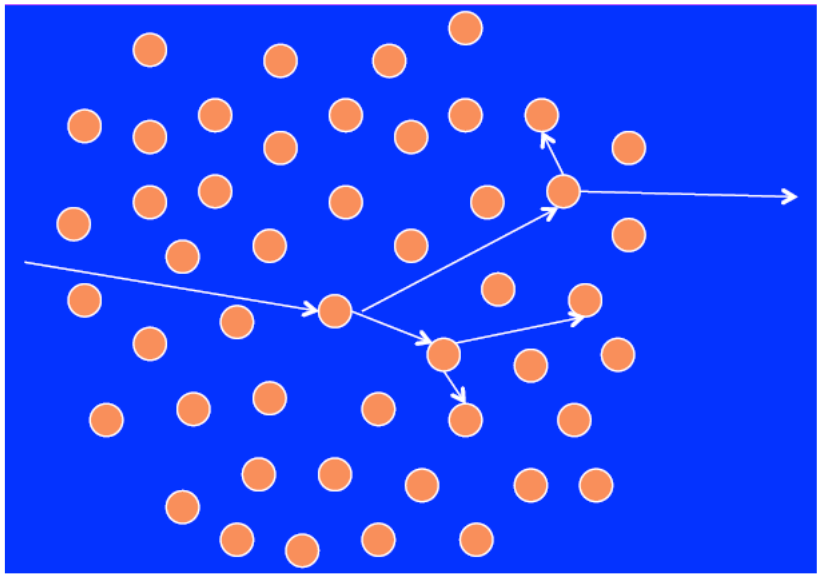

Solution2: reflect the neutron back in

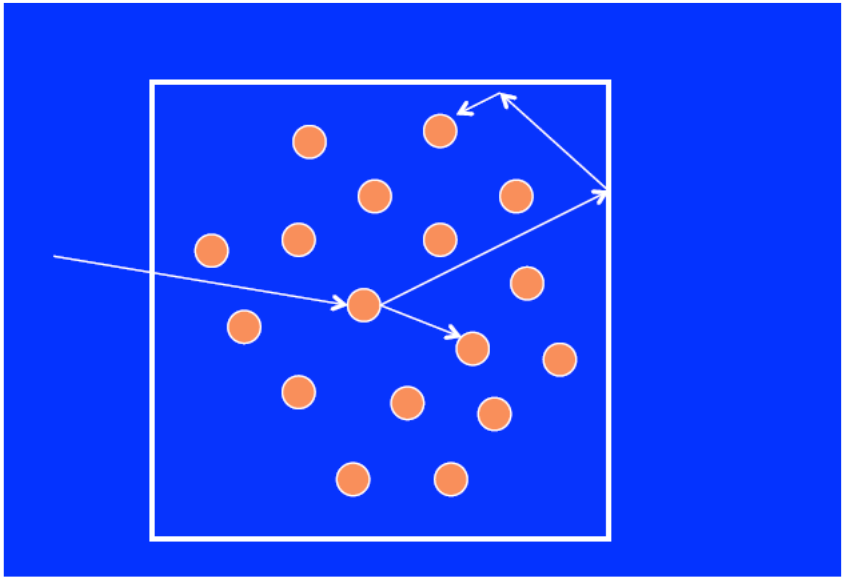

Solution 3: increase the density

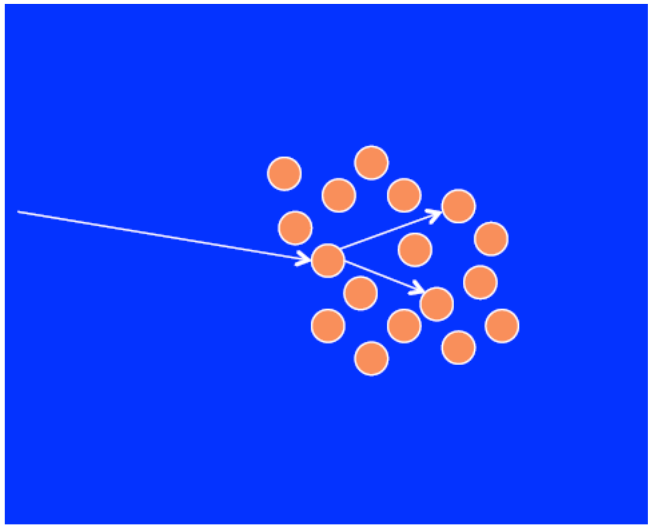

How to get the material together before it blows apart?

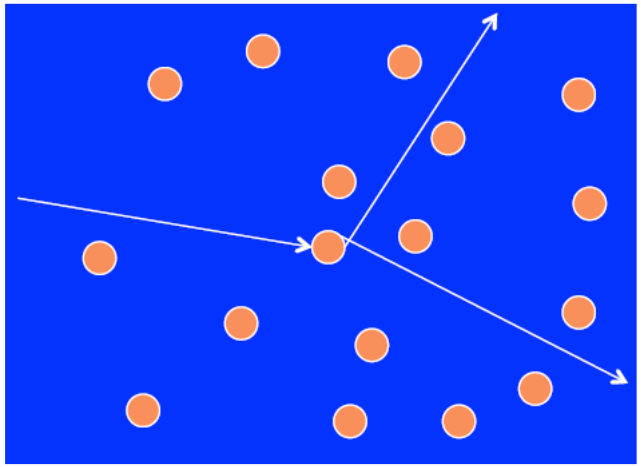

- **There are always neutrons around**
- **Once chain reaction starts, material will heat up, expand, stop reaction**
- **How to get enough material together fast enough?**

Gun-type bomb

- **Simple, reliable – can be built without testing**
- **Highly inefficient – require lots of nuclear material (50-60 kg of 90% enriched HEU)**
- **Can only get high yield with HEU, not plutonium**
- **Hiroshima bomb: cannon that fired HEU projectile into HEU target**

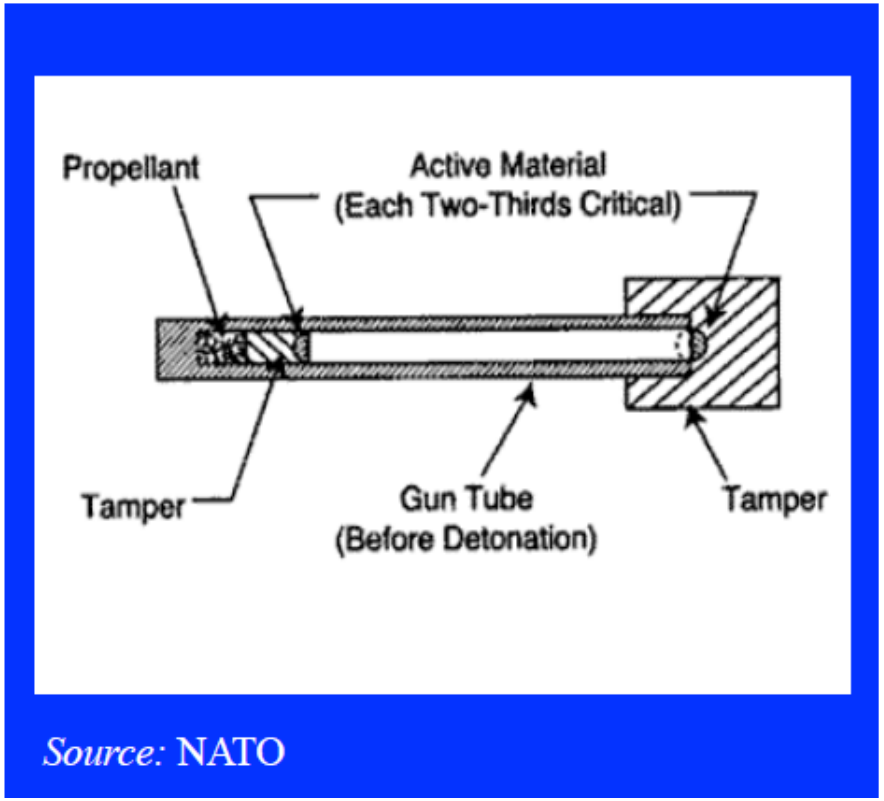

Implosion design

- **A schematic diagram of an implosion bomb**

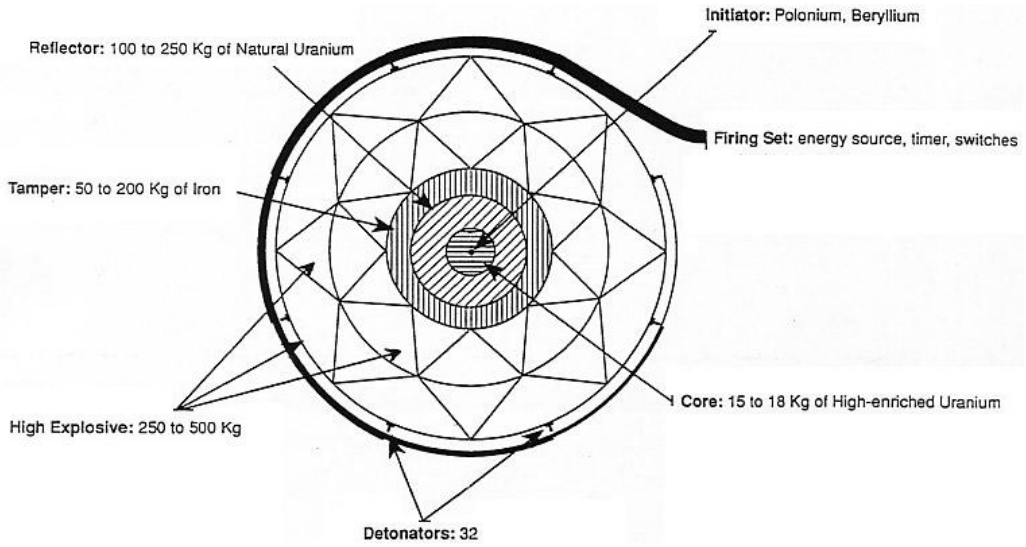

- **Small-scale slow-motion cross-section of a shaped charge implosion design**

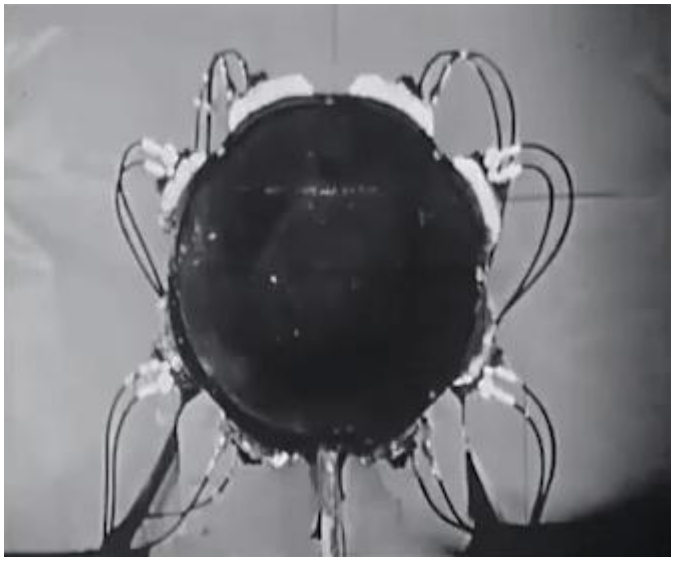

https://www.wisconsinproject.org/nuclear-weapons/
https://en.wikipedia.org/wiki/Trinity_%28nuclear_test%29

The 1st nuclear bomb: Trinity (Bradbury Science Museum)

- **Model of the Trinity Gadget**

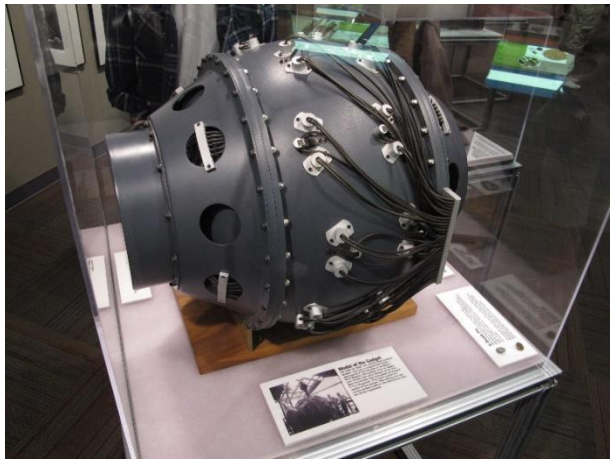

- **Project Y Atomic Bomb Detonator System**

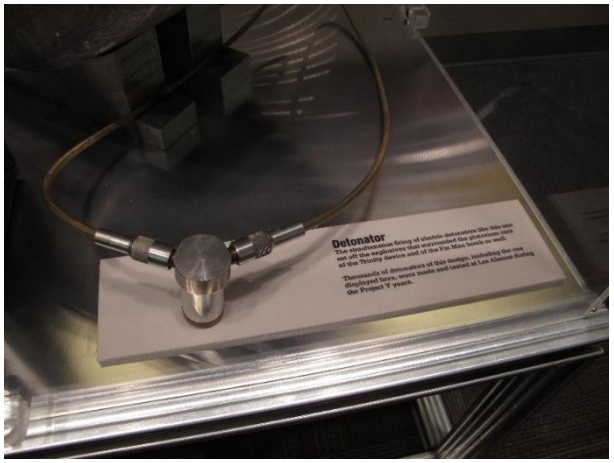

- **Project Y Atomic Bomb Detonator System**

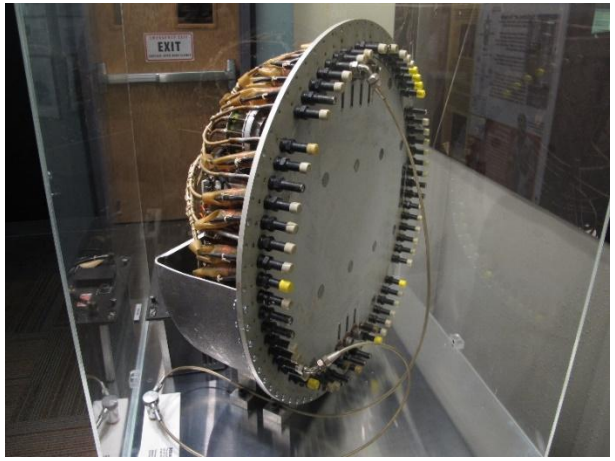

- **Project Y Atomic Bomb Detonator System Spark Gap Switch**

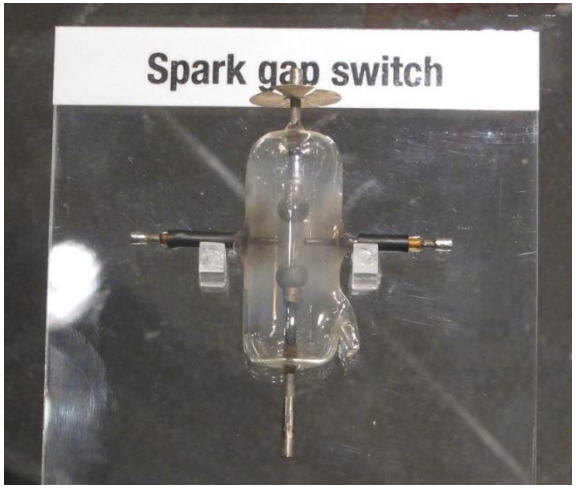

https://www.flickr.com/photos/rocbolt/with/8061684482

The 1st nuclear bomb: Trinity

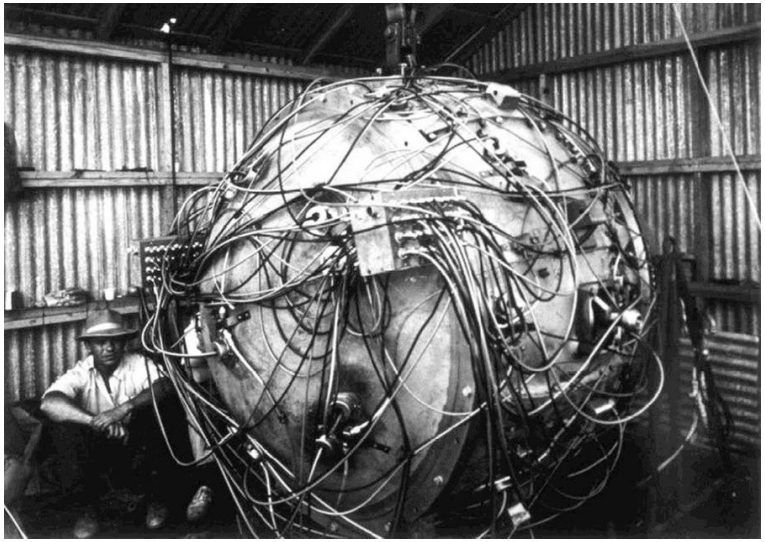

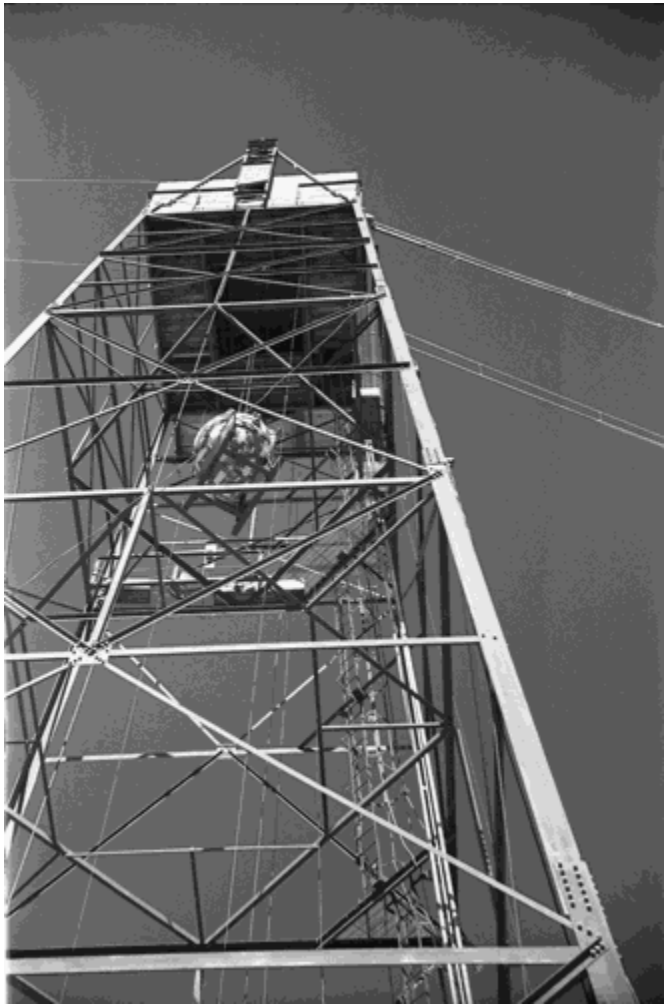

https://www.theatlantic.com/photo/2015/07/70-years-since-trinity-when-we-tested-nuclear-bombs/398735/
https://saddlebagnotes.com/arts-and-leisure/tucson-seismographs-detected-first-nuclear-test-at-trinity-n-m/article_b01c5b20-f6fb-11eb-a221-6327df2feaeb.html

Trinity explosion on July 16, 1945

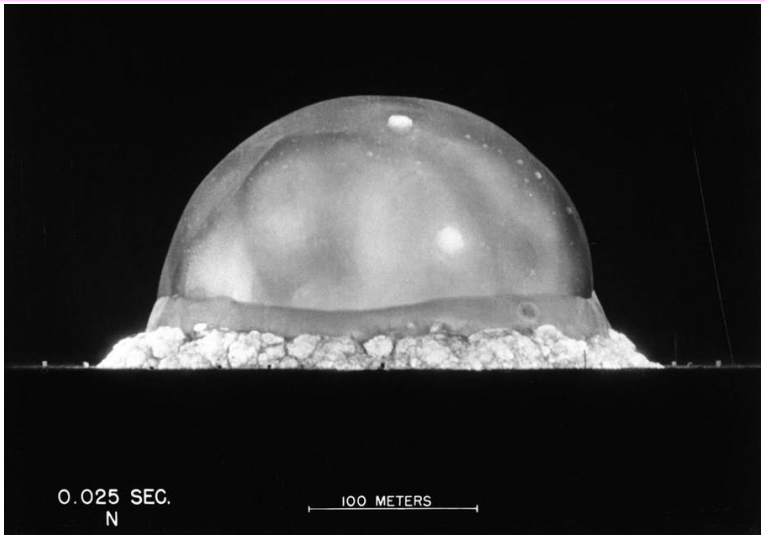

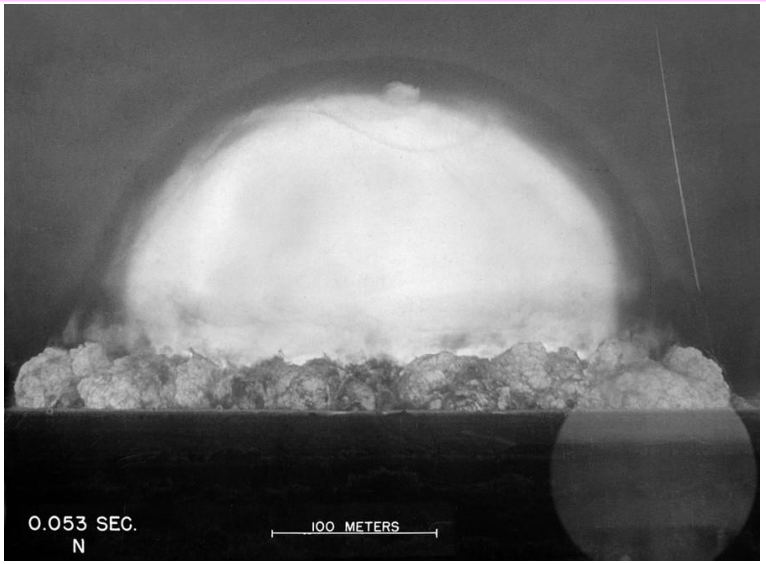

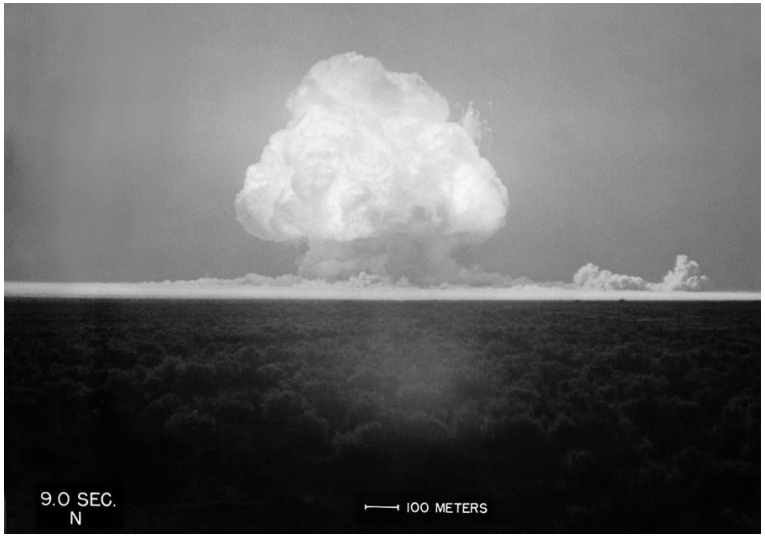

https://www.theatlantic.com/photo/2015/07/70-years-since-trinity-when-we-tested-nuclear-bombs/398735/
https://en.wikipedia.org/wiki/Trinity_%28nuclear_test%29

Hiroshima Bomb – “Little Boy”

Gun Type – Easiest to design and build (Hiroshima bomb was never tested)

About 13 kiloton explosive yield

Talk given by Dr. Charles D. Ferguson, President, Federation of American Scientists, Department of Physics, Colloquium, American University, 2012

Atomic bomb is very destructive

Hiroshima: August 6, 1945

Nagasaki: August 9, 1945

Talk given by Dr. Charles D. Ferguson, President, Federation of American Scientists, Department of Physics, Colloquium, American University, 2012

The fusion process

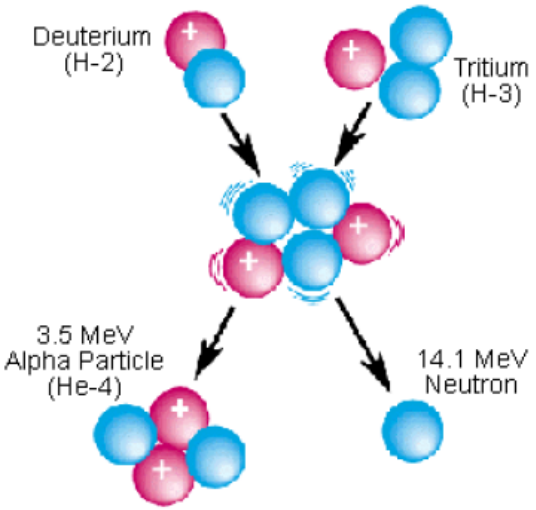

Deuterium-Tritium Fusion Reaction

$^2H+^3H \Rightarrow {}^4He+n+Q \equiv 17.6$ MeV

Energy release Q=17.6 MeV

In comparison

$^2H+^2H \Rightarrow {}^1H+^3H+Q \equiv 4.0$ MeV

$^2H+^2H \Rightarrow {}^3He+n+Q \equiv 3.2$ MeV

$^3H+^3H \Rightarrow {}^4He+2n+Q \equiv 11.3$ MeV

$^{235}U+n \Rightarrow X_A+X_B+3n+Q \approx 200$ MeV

Fusionable Material, deuterium ^2H (D) and tritium ^3H (t):

Deuterium: natural occurrence (heavy water) (0.015%).

Tritium: natural occurrence in atmosphere through cosmic ray bombardment; radioactive with $T_{1/2}$=12.3 y.

“Advantages” of hydrogen bomb

Fusion of $^2H+^3H$: $\frac{Q}{A} = \frac{17.6\ MeV}{(3+2)\ amu} = 3.5\ \frac{MeV}{amu}$

Fission of ^{235}U: $\frac{Q}{A} = \frac{200\ MeV}{236\ amu} = 0.85\ \frac{MeV}{amu}$

Fusion is 4 times more powerful than fission and generates 24 times more neutrons!

Neutron production:

$^2H+^3H: \quad \frac{n}{A} = \frac{1}{5} = 0.2$

$^{235}U + n: \quad \frac{n}{A} = \frac{2}{236} = 0.0085$

https://isnap.nd.edu/Lectures/phys20061/pdf/10.pdf

Hydrogen bomb uses a fission bomb to initiate the fusion reaction

Fuel

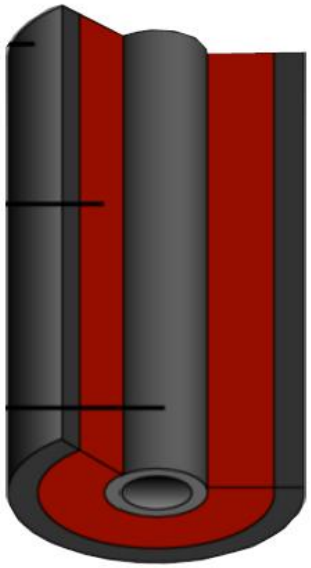

Primary Fission Device

Core: ^{239}Pu, ^{235}U,
plus $^{2}H+^{3}H$ booster

Shell: ^{238}U tamper

High explosive lenses

Secondary Fusion Device

Radiation channel

^{239}Pu sparkplug

^{6}Li, ^{2}H, ^{3}H fusion cell

^{238}U tamper

https://isnap.nd.edu/Lectures/phys20061/pdf/10.pdf

Event sequence

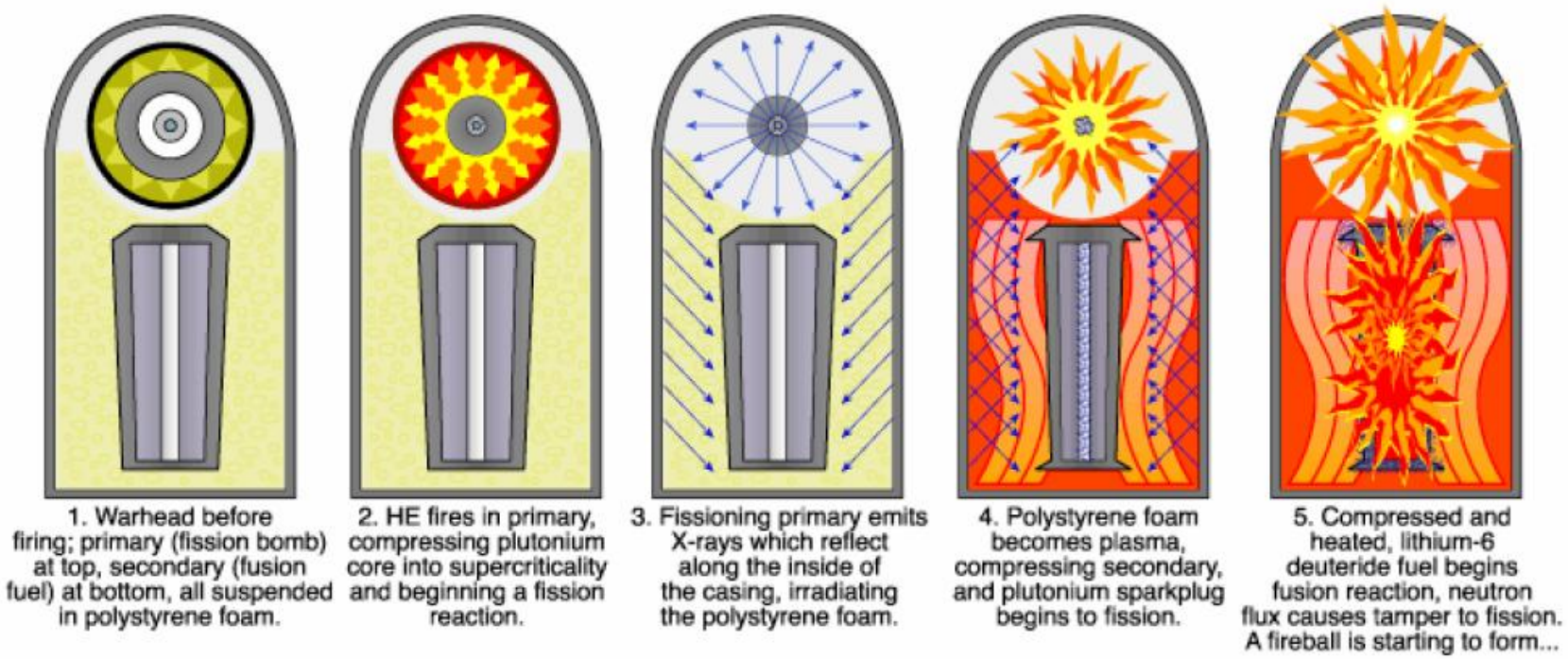

Additional pressure from recoil of exploding shell (ablation)!

https://isnap.nd.edu/Lectures/phys20061/pdf/10.pdf

You don't want to build a hydrogen bomb!

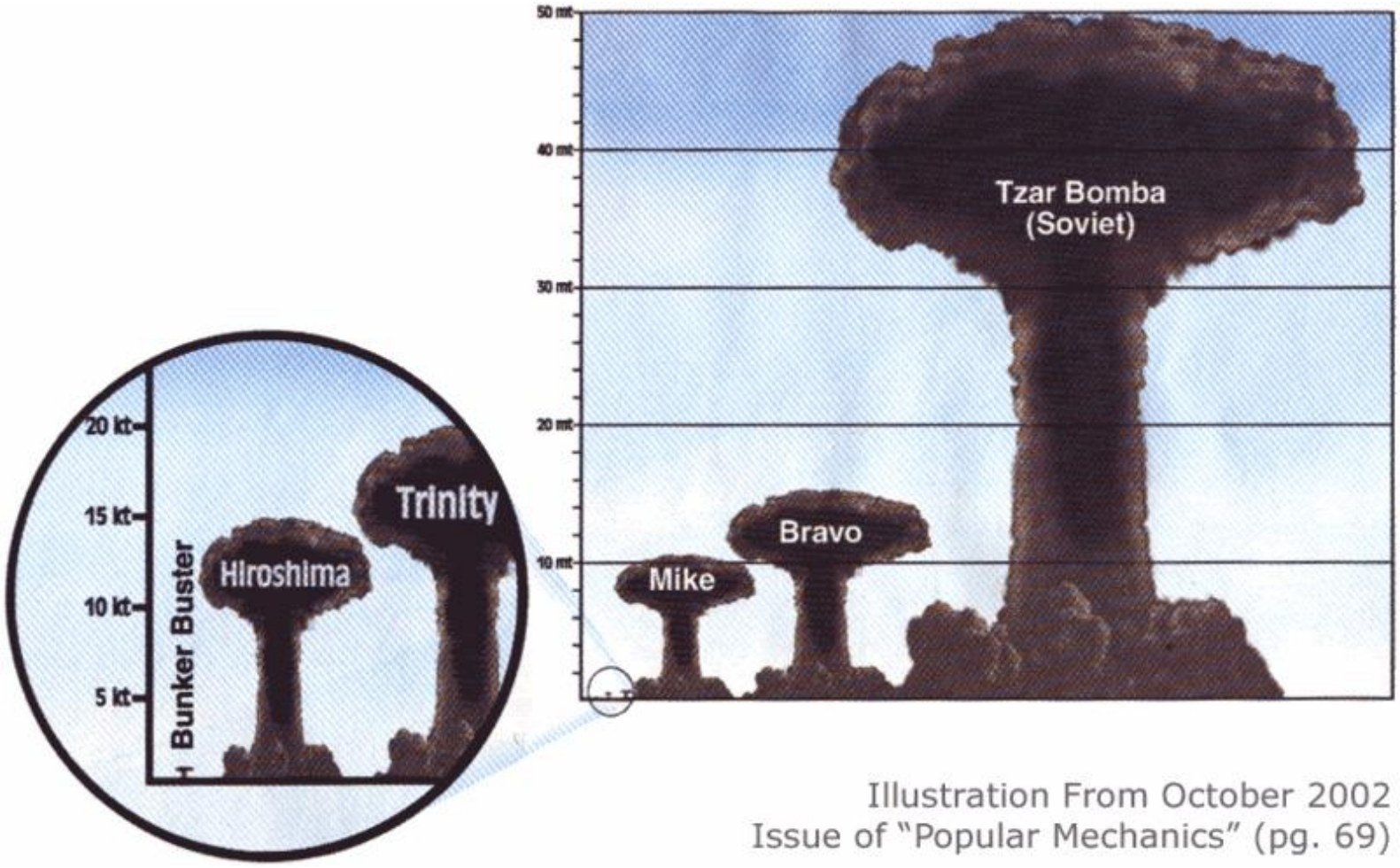

Illustration From October 2002
Issue of "Popular Mechanics" (pg. 69)